Multi-State Density Functional Theory (MS-DFT) and Multi-State Energy Decomposition Analysis (MS-EDA)

A DISSERTATION

SUBMITTED TO THE FACULTY OF THE GRADUATE SCHOOL

OF THE UNIVERSITY OF MINNESOTA

BY

Christian Peter Hettich

IN PARTIAL FULFILLMENT OF THE REQUIREMENTS

FOR THE DEGREE OF

DOCTOR OF PHILOSOPHY

Jiali Gao

May, 2025

Acknowledgements

We stand on the shoulders of Giants. Some do not only lift us up with their accumulated knowledge, but also by inspiring us to thrive for greatness. I am immeasurably grateful to everyone who has inspired me to keep going to where I find myself now.

Abstract

This work presents the theory and application of a multistate energy decomposition analysis (MS-EDA), making use of multistate density functional theory (MSDFT). Through this research, a method has been developed that can be conveniently used to elucidate the energy terms contributing to intermolecular interactions of molecular complexes in electronically excited states. Multistate density functional theory is a novel quantum theory that employs matrix density as the fundamental variable both for the ground state and for excited states. The method goes beyond the Hohenberg-Kohn theorems for one electronic state and treats all electronic states on an equal footing. Chapter 1 reviews the fundamental principles and theorems of MSDFT and introduces the concepts of minimal active space (MAS) and matrix correlation functional. In addition, the computational procedure and approximations of non-orthogonal state interaction (NOSI) are presented, upon which the remainder of the research and calculation is built.

Chapter 2 summarizes the development of a block-localized excitation (BLE) approach for self-consistent-field (SCF) optimization of excited state (non-aufbau) configurations. The BLE method is a form of delta SCF (ΔSCF) procedure using a projection scheme in molecular orbital basis that matches the order and occupation of the initial, predefined electronic configuration. The main novelty of the BLE method is to allow block localization of molecular orbitals on individual molecules in a molecular complex or a subset of atomic orbitals belonging to a given symmetry. Consequently, it is possible to optimize a set of non-orthogonal block-localized molecular orbitals for a system in which one molecule is excited to an excited configuration in the presence of other molecules in the ground state. The individually optimized excited configurations are

used to form a minimal active space for subsequent MSDFT-NOSI calculations to determine the energies of the adiabatic ground and excited state as well as their densities. The BLE method is illustrated in the study of excimer formation for a naphthalene dimer and a preliminary analysis of energy terms of binding interactions was presented. The BLE method was further applied in Chapter 3 to a group of bi-molecular complexes that have low-lying charge transfer states. It was shown that both local covalent and intermolecular charge-transfer excited states can be adequately treated by using MSDFT-NOSI along with MAS in which individual configurations are optimized by the BLE method.The computed excitation energies, including charge-transfer states, from NOSI calculations employing the M06-2X functional to approximate the diagonal terms of the matrix correlation functional along with the cc-pVDZ basis functions are in good accord with results from EOM-CCSDT benchmarks.

Chapters 4 and 5 rigorously formulate the theory, define energy terms for intermolecular interactions in excited states, and present findings from applications of energy decomposition analyses on a range of molecular complexes in excited states. In the present MS-EDA approach, energy terms associated with interactions in the ground state are grouped into a single term called local interaction energy and the focus of the energy decomposition analysis is placed on energy terms unique to excited states. These include the exciton resonance energy due to the electronic coupling interactions among locally excited states of individual monomers, the super-exchange stabilization energy due to forward and backward charge transfer states between two monomers, and orbital and configuration delocalization energy as a result of expanding the molecular orbitals from block-localized states to full molecular orbitals over the entire molecular complex and determinant configurations that specifically included in the MAS. A key feature in the MS-EDA method is that all intermediate states are variationally optimized using the BLE technique. It was found that molecular complexes in excited states can be categorized into three types: (1) encounter excited-state complex, (2) charge-transfer exciplex, and (3) intimate excimer or exciplex. For all examples, MS-EDA's decomposition of the binding energy allows for an unambiguous identification of the excitation character.

Finally, in Chapter A, the bond dissociation process of methyl radical in excited states is summarized, providing insights into the interplay of diabatic states corresponding to different electronic states of the dissociated species. The active space in this chapter has one noteworthy difference from the examples in all other chapters. In all of those examples, the off-diagonal elements of the Hamilton matrix functional have generally small contributions from their WFT-style terms. In this methyl dissociation example however, the NOSI-MSDFT procedures and TDFs that we developed are applied to valence-bond style determinants. This demonstrates that these procedures and TDFs are also applicable to such an active space, which is characterized by strong WFT-style contributions to the interactions between determinants (and by a large overlap between determinants).

In summary, this work illustrates the computational method, accuracy and the wide range of applications of nonorthogonal state interaction in multistate density functional theory. It is hoped that the MS-EDA method will be a useful tool for understanding the nature of intermolecular interactions of excimers and exciplexes.

Contents

List of Tables

List of Figures

Chapter 1

Introduction

Kohn–Sham density functional theory (DFT)[1] has proven remarkably successful across many systems, but it is fundamentally a ground-state theory based on the Hohenberg–Kohn theorems. It inherits the additional restriction that only nondegenerate ground states without strong static correlation can be described accurately. Although several extensions of DFT to excited states have been proposed, the only fully rigorous framework until recently has been linear-response time-dependent DFT (TD-DFT),[2] which - despite its widespread adoption - suffers from well-documented failures for charge-transfer excitations, Rydberg states, and double excitations. To this end, an alternative subspace theory of excited states was formulated by Theophilou[3] who showed that the average density, $\rho_V(r)$, of the lowest N eigenstates uniquely determines the subspace spanned by their wavefunctions and hence fixes the sum of their energies. However, because $\rho_V(r)$ captures only the sum of state densities, this subspace theory cannot yield individual state energies or densities themselves unless those states are already known.

Lu and Gao recently showed[4] that the full matrix density $\mathbf{D}(r)$ - whose diagonal elements are the individual state densities and whose off-diagonal elements are the transition densities - contains the necessary and sufficient information to resolve each state individually. In this formulation, the trace of $\mathbf{D}(r)$, i.e., $tr\mathbf{D}(r) = \rho_V(r)$, defines the exact subspace, while the off-diagonal elements makes it possible to describe state interactions and allows determination of the individual excited states.

This thesis summarizes studies of excited-state processes and intermolecular interactions using this newly formulated density functional theory for all electronic states, namely multistate density functional theory (MSDFT).

1.1 Pre-Existing Methods

The existing methods for quantum mechanically calculating the energy of a system of electrons in an external potential follow two paradigms. The older paradigm is wave function theory (WFT), where the wave function fully and uniquely determines the state of the system and all of its properties. The second paradigm is density functional theory (DFT),[5] . Multistate density functional theory (MSDFT) is fundamentally an extension of the DFT paradigm. But the existing practical implementation also utilizes concepts from wave function theory, most notably from the non-orthogonal configuration interaction (NOCI) method.

The theoretical foundation for ground-state DFT are the 3 Hohenberg-Kohn theorems, which can be simply summarized as follows.

1. The fact that the electron density, Hamiltonian and wave function of the ground state uniquely determine each other;

2. The existence of a universal Hamilton density functional $F[n(r)]$;

3. A variational principle for determining the energy and density of the ground state.

The practical implementation of a DFT method is due to Kohn and Sham[1] has gained status as the standard method within the DFT paradigm. The Kohn-Sham density functional theory (KS-DFT) method splits the energy as a functional of the density $E[n(r)]$ into 3 known (or approximated/ assumed) terms and 1 unknown term:

$$E[n(r)] = E^{\text{ext}}[n(r)] + F[n(r)]E[n(r)] = E^{\text{ee}}[n(r)] + T^{\text{KS}}[n(r)] + E^{\text{xc}}[n(r)] \tag{1.1}$$

The splitting into the influence due to the external potential $E^{\text{ext}}[n(r)] = \int V^{\text{ext}} n(r)dr$ and the universal functional $F[n(r)]$ follows directly from the Hohenberg-Kohn theorems. The terms that Kohn and Sham split the universal functional into are the classically known electron-electron repulsion energy $E^{\text{ee}}[n(r)] \propto \iint \frac{n(r)n(r')}{r-r'}drdr'$ and the (minimal) kinetic energy of a single-determinant state $T^{\text{KS}}[n(r)] = \langle\psi|\hat{T}^{\text{WFT}}|\psi\rangle$ whose wave function matches the required density $n(r) = \langle\psi|\hat{n}(r)|\psi\rangle$. The remaining term is called exchange-correlation functional and, like $F[n(r)]$, its exact functional form is unknown. Its purpose is to add the non-classical part of the electron-electron interaction ("exchange", which technically also includes the usually much smaller self-interaction corrections) and to correct for the deviation of the true ground state from a single determinant ("correlation"). To include these effects, a plethora of xc functionals with continually advancing complexity and accuracy have been developed. They are typically categorized by their input parameters/ dependencies: The local density approximation (LDA) and generalized gradient approximation (GGA) functionals only depend on the electron density (and its gradients), respectively. Hybrid functionals also depend on the total value of the exact Hartree-Fock exchange of the system (typically mixing one quarter to one half of exact exchange with an accordingly reduced amount of functional-based exchange). Double hybrid functionals utilize not only exchange from WFT to augment the functional-based exchange but also correlation corrections based on Møller-Plesset (MP2) perturbation theory to augment the single-determinant based kinetic energy. Meta functionals depend in addition to the electron density also on the kinetic energy density.

In WFT, the parametrization that is used to express the wave function is the only approximation, and the main difference between WFT methods is the employed parametrization. The earliest and simplest WFT method that can truly be called quantum mechanical is the Hartree-Fock method. This method is built on the premise of approximating the wave function as a single Slater determinant. In contrast, CI methods define the wave function to be a linear combination of a certain set of Slater determinants, where the coefficients of this linear combinations are optimized. The "main branch" of the CI family (CIS, CISD, CISDT, ...) uses the Hartree-Fock orbitals from the "ground state" (or reference) Slater determinant for all Slater determinants. And in this branch, the set of included Slater determinants is truncated to those determinants which differ from the "ground state" (or reference) Slater determinant by at most the excitation of one, two, or three, ... electrons. Non-orthogonal configuration interaction (NOCI) drops the requirement that all Slater determinants share a common set of orbitals. Instead all occupied orbitals of all determinants are optimized simultaneously with the weights of the determinants. This causes the Slater determinants to be non-orthogonal to each other, but reduces the number of required Slater determinants.

1.2 Multistate Density Functional Theory

Recently, Lu and Gao proved three fundamental theorems in density functional theory,[4] which can be simply summarized as follows.

1. The existence of a Hamilton matrix density functional for the lowest N eigenstates;

2. The variational principle for determining the multistate energy yielding the energies and densities of the lowest N eigenstates;

3. The representation of the N-dimensional matrix density by at most N^2 Slater determinants.

We consider a system with the Hamiltonian $\hat{H} = \hat{H}^0 + v_{\rm ext}(\vec{r})$ where $\hat{H}^0$ contains the internal electronic interaction and kinetic energy operators, and $v_{\rm ext}(\vec{r})$ represents any external potential. Restricting our attention to the N-dimensional subspace $\mathbb{V}$ spanned by the lowest N eigenstates, we introduce the matrix density $\mathbf{D}(\vec{r})$. Its diagonal entries, $D_{ii}(\vec{r}) = n_i(\vec{r})$ are the individual state densities, while the off-diagonal entries $D_{ij}, i \neq j$ are the transition densities between states i and j.

Then, the three theorems introduced above are stated below:

Theorem 1 (Existence of Hamiltonian matrix functional)**.** *In the subspace $\mathbb{V}$ spanned by the lowest N eigenstates including all degerate states of the highest energy, the Hamilton operator can be expressed as a matrix density functional $\boldsymbol{\mathcal{H}}[\mathbf{D}] = \boldsymbol{\mathcal{F}}[\mathbf{D}] + \int \mathbf{D}(\vec{r}) v_{ext}(\vec{r}) d^3r$ where $\boldsymbol{\mathcal{F}}[\mathbf{D}]$ is a universal functional independent of $v_{ext}(\vec{r})$.*

Theorem 1 establishes a one-to-one correspondence between $\mathbf{D}$ and $\boldsymbol{\mathcal{H}}[\mathbf{D}]$.

Theorem 2 (Variation principle)**.** *For any trial density $\mathbf{D}'(\vec{r})$, the trace of $\boldsymbol{\mathcal{H}}[\mathbf{D}]$, called multistate energy, is greater than or equal to the multistate energy of the matrix density $\mathbf{D}$ belonging to the subspace $\mathbb{V}$ (of the lowest N eigenstates): $\mathrm{tr}\{\boldsymbol{\mathcal{H}}[\mathbf{D}']\} \geq tr\{\boldsymbol{\mathcal{H}}[\mathbf{D}]\}$, where the equal sign is true when the trial density is a matrix density of the subspace $\mathbb{V}$.*

A highly relevant implication of this theorem is that diagonalization of $\boldsymbol{\mathcal{H}}[\mathbf{D}]$ yields the N eigen-energies of $\mathbb{V}$ (the ground state and the $N-1$ lowest excited states).

Theorem 3 (Density representation)**.** *Up to N^2 independent Slater wave functions are sufficient to represent all N^2 elements of the N dimensional matrix density $\mathbf{D}(r)$.*

In the special case $N = 1$, the first two theorems reduce exactly to the Hohenberg-Kohn theorems for ground-state DFT. The third theorem states that a single ($1^2 = 1$) Slater determinant suffices to represent the exact ground-state density as that used in Kohn-Sham DFT. Just as multi-configurational self-consistent-field (MCSCF) methods in wave function theory (such as the complete-active-space self-consistent-field (CASSCF) method) prescribes an iterative optimization of both the determinant expansion and orbitals in each determinant, multistate density functional theory computations aimed at minimizing the multistate energy by optimizing the matrix density should in principle utilize a similar simultaneous optimization. However, these theorems do not prescribe how to choose these determinants. Indeed, because the same matrix density $\mathbf{D}(\vec{r})$ can be generated by different sets of determinants, no unique choice emerges a priori. This non-uniqueness, however, offers flexibility: a variety of practical algorithms and active-space selection strategies can be developed within the MSDFT framework. Finally, just as the exact exchange-correlation functional in Kohn-Sham DFT remains unknown, the precise form of the multistate universal functional $\boldsymbol{\mathcal{F}}[\mathbf{D}(\vec{r})]$ is unknown - underscoring the central challenge of constructing approximations in excited-state calculations.

1.3 Minimal Active Space

Theorem 3 above defines an upper bound in the number of Slater determinants to represent the matrix density for N states. Collectively, they form an "active space", just as that used in wave function theory, to be used to construct a set of N auxiliary multi-configurational wave functions to determine the matrix density $\mathbf{D}(r)$. This active space that has an upper bound is called minimal active space (MAS), which contains $M \leq N^2$ determinants.

First, we write the N^2 Slater determinants ψ, called "primary states", as follows:

$$\psi_i(r_1, ..., r_{n_e}) = \hat{A}\left\{\chi_1^i(r_1)\cdots\chi_{n_e}^i(r_{n_e})\right\} \tag{1.2}$$

(where $\hat{A}$ is the normalized anti-symmetrization operator and χ^i are the molecular orbitals of state i). From a given basis of M primary states, we can construct "secondary", or auxiliary, multi-state wave functions as linear combinations of the "primary states":

$$\Phi_A = \sum_i^M c_{iA}\psi_i \ , \tag{1.3}$$

The $N \times N$ matrix density is built from these N "secondary" states. One would select those N states that minimize the total subspace energy, that is, the sum of the lowest N eigenvalues of the exact Hamiltonian functional. Once identified, these states define the subspace in which the $N \times N$ Hamiltonian matrix functional is constructed. Diagonalizing the Hamiltonian matrix functional then yields the energies of all N eigenstates, each expressed as a linear combination of the original determinants.

In practical implementations, however, two simplifying choices are usually made.[6] First, the full set of M "primary" determinants is optimized and then fixed in advance rather than re-optimized to build the auxiliary wave functions in every step of the energy minimization. In other words, a non-orthogonal configuration interaction (NOCI) scheme is used, in which only the configuration coefficients in equation (1.3) are further optimized. Since dynamic correlation is included in the single determinant optimization, we call this method nonorthogonal state interaction (NOSI). Second, rather than recomputing the Hamiltonian from scratch in the reduced subspace, one obtains the $N \times N$ Hamiltonian simply by projecting the full $M \times M$ Hamiltonian matrix in the primary basis onto the selected secondary basis.

With these two approximations, the workflow becomes straightforward: assemble the Hamiltonian in the primary determinant space, diagonalize it to extract the lowest N eigenstates, and adopt those eigenvalues as the subspace energy. Although this streamlined approach deviates from the full multiconfigurational optimization of both orbital and configuration coefficients, it avoids difficulties to achieve self-consistent-field convergence in a nonorthogonal MCSCF-type of approach and has proven effective in practice.

1.4 The Hamilton Matrix Functional (Correlation Matrix Functional)

The exact matrix-energy functional $\mathcal{F}[\mathbf{D}]$ in multistate DFT remains formally unknown. However, one can construct useful approximations by using wave-function-theory (WFT)-style contributions analogously as the approximation in Kohn–Sham DFT to use a single determinant basis for the ground state. Below, we express all intermediate quantities in the primary determinant basis (indices i, j). The analogous definitions in the secondary basis (indices A, B) follow via the linear transformation of Eq. 1.3. With the minimal active space for a set of multiconfigurational wave functions and the universal matrix functional, we then define a correlation functional

$$\mathcal{E}^{\mathrm{c}}[\mathbf{D}(\vec{r})] = \mathbf{F}[\mathbf{D}] - (\mathbf{T}^{\mathrm{ms}}[\mathbf{D}] + \mathbf{E}^{\mathrm{HFx}}[\mathbf{D}]) \,, \tag{1.4}$$

where $\mathbf{T}^{\mathrm{ms}}[\mathbf{D}]$ is the multi-configurational kinetic energy term for the N auxiliary states and $\mathbf{E}^{\mathrm{HFx}}[\mathbf{D}]$ the Hartree-Fock–exchange contribution constructed from the same determinant set. By subtracting these leading WFT terms, $\mathcal{E}^{\mathrm{c}}[\mathbf{D}]$ captures the remaining many-body correlation effects not already accounted for in $\mathbf{T}^{\mathrm{ms}}[\mathbf{D}]$ and $\mathbf{E}^{\mathrm{HFx}}[\mathbf{D}]$. In short, the matrix elements for the wave function part can be written as

$$\langle\psi_i|\hat{H}^0|\psi_j\rangle = (\mathbf{T}^{\mathrm{ms}})_{ij} + (\mathbf{E}^{\mathrm{HFx}})_{ij} \ . \tag{1.5}$$

Note that, unlike Kohn–Sham DFT, which approximates (parts oll all of) the exchange energy via a local or generalized gradient approximation functional for the exchange, here we include the full exact (wave function theory) Hartree-Fock–exchange contribution explicitly. The remaining correlation functional, $\mathcal{E}^{\mathrm{c}}[\mathbf{D}]$, then represents the residual many-body interactions not accounted for by assembling the N^2 single-determinant primary states into N multi-determinant secondary states or by their mutual interactions.

As a result, the full Hamilton matrix density functional is given as:

$$H_{ij} = (\mathbf{T}^{\mathrm{ms}})_{ij} + (\mathbf{E}^{\mathrm{HFx}})_{ij} + \int D_{ij}(\vec{r})V^{\mathrm{ext}}(\vec{r})d\vec{r} + (\mathcal{E}^{\mathrm{c}}[\mathbf{D}])_{ij} \ . \tag{1.6}$$

The use of the notation $(\mathcal{E}^{\mathrm{c}}[\mathbf{D}])_{ij}$ in this equation instead of the notation $(\mathcal{E}^{\mathrm{c}}[D_{ij}])_{ij}$ emphasizes that the correlation functional generally depends on the whole density matrix $\mathbf{D}(\vec{r})$.[6] There may exist a basis in which there is an element-by-element mapping from D_{ij} to the matrix element $(E_{\mathrm{C}})_{ij}$, but only under extraordinary conditions could there be any hope that such an element-by-element relation happens to hold exactly in either the primary or secondary basis.

Nevertheless, a straightforward way to build a practical approximation is to assume, as noted earlier, that each element of the Hamiltonian matrix in the primary basis depends only on the corresponding element of state density. At first glance, this suggests that the off-diagonal Hamiltonian element $H_{ij}[\mathbf{D}]$ should be treated as a functional of the transition density D_{ij} between determinants i and j, i.e., $H_{ij} = H_{ij}[D_{ij}]$. The transition density is defined as

$$D_{ij}(r) = \langle \psi_i | \hat{n}(r) | \psi_j \rangle \tag{1.7}$$

where $\hat{n}(r)$ is the density operator.

Introducing such a scheme would effectively define a transition density functional (TDF) - a notion that does not exist in Kohn–Sham DFT. To date, practical approximations [7, 8] for off-diagonal Hamiltonian elements have depended on each state's own density D_{ii} and D_{jj} and their wavefunctions ψ_i and ψ_j, rather than on the transition density D_{ij} itself. Nonetheless, the phrase "transition density functional" is sometimes used to describe either the entire off-diagonal contribution or just its correlation correction, despite the absence of any explicit functional depending solely on D_{ij}.

1.5 Procedure and Approximations (Nonorthogonal State Interaction)

The procedure that is used throughout this thesis proceeds in two consecutive steps. The first step is to obtain the basis determinants (in the primary basis). The diagonal elements $\mathcal{F}_{ii}[D_{ii}]$ of the matrix functional $\boldsymbol{\mathcal{F}}[\mathbf{D}]$ lend themselves to be approximated by the universal energy functional of Kohn-Sham DFT F^{KS} (using any of the tested and proven exchange correlation functionals F^{xc}):

$$\mathcal{F}_{ii}[D_{ii}] \approx F^{\mathrm{KS}}[D_{ii}] = T(\psi_i) + E^{\mathrm{coul}}[D_{ii}] + F^{\mathrm{xc}}[D_{ii}]\ . \tag{1.8}$$

I.e. the evaluation of the diagonal elements $\mathcal{H}_{ii}[D_{ii}(\vec{r})]$ of $\boldsymbol{\mathcal{H}}[\mathbf{D}]$ becomes equivalent to evaluating the energy of a given Kohn-Sham determinant $\psi_i(\vec{r})$ with an approximate exchange-correlation functional developed for Kohn-Sham DFT:

$$\mathcal{H}_{ii}[D_{ii}(\vec{r})] = \mathcal{E}^{\text{KS-DFT}}[\psi_i(\vec{r})] \; . \tag{1.9}$$

In multistate DFT, one would ideally select the N linear combinations of determinants ("secondary states") that minimize the sum of the lowest N eigenvalues of the exact Hamiltonian functional and then construct and diagonalize the corresponding $N \times N$ Hamiltonian matrix in that subspace to obtain refined excited state wavefunctions. In practice, each determinant configuration in the MAS is variationally optimized independently. A major challenge in this step is to constrain the orbital optimization on determinants with non-aufbau occupations without falling back to the ground state or a lower energy configuration. Thus, in order to force each diagonal element to converge to a different Slater determinant and obtain a set of linearly independent Slater determinants ($\psi_i(\vec{r}) \neq \psi_j(\vec{r}), i \neq j$), these optimizations have to be carried out subject to a different constraint for each Slater determinant, enforcing linearly independent (and thus non-ground state) configurations.

Three methods for enforcing these non-aufbau occupied configurations have been implemented in the software used to perform MSDFT calculations in this work. The oldest strategy[7] relies on partitioning the basis functions (AOs) into so called "blocks". And it is within these individual blocks instead of the whole system that the occupation is defined and aufbau configurations are constructed. The determinants then differ in the occupation of these blocks (and potentially in which basis AOs are placed into which block).

In the second approach, called block-localized excitation (BLE),[9] a projection operator is used to express the excited state MOs (orbital coefficients $\mathbf{T}$) in the basis of the ground state MOs (orbital coefficients $\mathbf{T}_0$) $(\mathbf{T}_0{}^\dagger \mathbf{F} \mathbf{T}_0)\mathbf{T} = (\mathbf{T}_0{}^\dagger \mathbf{D} \mathbf{T}_0)\mathbf{T}\boldsymbol{\epsilon}^{\text{BLE}}$. This makes the orbital ordering largely unchanged during the SCF iteration and, thus, keep the initial orbital occupation stable.

Finally, the third method that has been developed is the target state optimization (TSO) technique,[10] which places the MOs that are vacated with respect to the ground state configuration into a separate block and only diagonalizes the Fock matrix of the remaining orbitals. The TSO approach is thus constraining the occupied orbitals by removing the degrees of freedom of the ground state MOs that have been blocked off. This inevitably leads to slightly higher energies. But on the other hand the TSO approach is essentially a ground state optimization process, which can not collapse to lower energy states. In practice, both BLE and TSO methods have shown to be highly robust against collapsing to lower energy states.

For the off-diagonal matrix elements, we use an approximation that splits them into a sum of two terms. The first term is given by the WFT-style kinetic and exchange interaction of the Kohn-Sham determinants. The second term uses one of two approximations: Either as the overlap-weighted average of the correlation energies of the two states (i and j)

$$E^{\mathrm{c}}_{ij} \approx S_{ij}\frac{1}{2}(E^{\mathrm{c}}_i + E^{\mathrm{c}}_j) \tag{1.10}$$

or using a scheme that enforces degeneracy among spin triplets or quartets:

$$E(\psi^{\uparrow\downarrow}_{S=1}) \stackrel{!}{=} E(\psi^{\uparrow\uparrow}_{S=1}) = E(\psi^{\downarrow\downarrow}_{S=1}) \tag{1.11a}$$

or, for systems with an odd number of electrons:

$$E(\psi^{\uparrow\uparrow\downarrow}_{S=3/2}) = E(\psi^{\uparrow\downarrow\downarrow}_{S=3/2}) \stackrel{!}{=} E(\psi^{\uparrow\uparrow\uparrow}_{S=3/2}) = E(\psi^{\downarrow\downarrow\downarrow}_{S=3/2}) \tag{1.11b}$$

In the second step, we perform a single diagonalization of the Hamilton matrix, which yields the eigenstates of this matrix. As mentioned above, the sum of the lowest N eigen energies constitutes the lowest possible multi-state energy among any N-dimensional subspace of the space spanned by the basis. And as such, the diagonalization is providing the minimization (within this space).

This workflow - used consistently throughout this thesis - actually predates the formal proof of the three theorems of multistate density functional theory. (A nonorthogonal self-consistent-field (NOSCF) scheme for generating $\mathbf{D}(\vec{r})$ was proposed in Ref. [4], but it has not yet been implemented.) Because each determinant is built from its own set of molecular orbitals, these determinants need not be orthogonal - a feature shared with non-orthogonal configuration interaction (NOCI) in wave-function theory. In MSDFT, however, we go further: we incorporate dynamic correlation into each determinant via an exchange–correlation functional, developed for single-determinant Kohn-Sham theory, before mixing them (in the state interaction step). This ordering - dynamic correlation first, then static correlation - means MSDFT is best described as non-orthogonal state-interaction (NOSI). By Liu and Hoffmann's taxonomy, this "dynamic-then-static" sequence clearly places our method in the corresponding family of multistate correlation techniques.[11]

Chapter 2

Block-Localized Excitation for Excimer Complex and Diabatic Coupling

This chapter is based on the publication [9]. I contributed by running calculations, analyzing results and revising the manuscript.

2.1 Introduction

It is often more convenient to use a diabatic representation of localized initial and final states than the delocalized adiabatic ground and excited states to determine reaction rates and to model solvent reorganization in electron transfer (ET) and excited-state energy transfer (EET) processes.[12, 13] Furthermore, intermolecular interactions of aromatic compounds can have drastic changes in the excited state, sometimes forming stronger excimer complexes than that in the ground state.[14] The subsequent nonadiabatic dynamics of the excimer complexes can undergo radiative emission or conical intersection to return to the ground state.[13] In this case, calculations of nonadiabatic couplings require derivatives of the wave function, and the derivative coupling terms may become singular at the crossing points.[15] In contrast, the potential energy surfaces of diabatic states are smooth.[16] However, diabatic states are not unique,[17] and many computational techniques have been described to approximate diabatic states.[15, 18, 19, 20, 21, 22, 23, 24, 25] To this end, we have proposed a generalized diabatic at construction (GDAC) approach on the basis of an effective valence bond (VB) classification,[26, 27] which maximally constrains these diabatic states in bonding characters to the asymptotic dissociation limit for the processes of interest. GDAC diabatic states are physically interpretable configurations that form an active space to describe the adiabatic potential energy surfaces. Therefore, the validity and adequacy of GDAC diabatic states can be verified by comparison of experimental observables with properties determined from their resulting adiabatic states. In this chapter, we present a block-localized excitation (BLE) method to define locally excited configurations for treating excited energy transfer and for describing intermolecular interactions of excimer complexes.

VB theory naturally has orbital constraints, which can be generalized to represent diabatic states. The large number of configurations in ab initio VB theory prevents its practical use on large and condensed phase systems,[28] though modern approaches are improving its applicability.[29, 30, 31] On the other hand, block-localized wave function (BLW) theory allows for the construction of an effective VB-like configuration using a single determinant.[32] In BLW, a diabatic state is represented in terms of block-localized orbitals (BLO), an effective representation of the ab initio VB configurations within a molecular fragment.[33, 34, 35, 36] The BLOs can be optimized in wave function theory (WFT)[32, 33, 35] and using Kohn-Sham density functional theory (KS-DFT).[37, 7] In this regard, the block-localized Kohn-Sham orbitals are strictly localized on a given fragment by construction that is constrained in orbital space.[33, 36] Related localization methods include that developed by Stoll and coworkers,[38] the self-consistent field for molecular interactions (SCF-MI),[39, 40, 41] locally projected molecular orbitals,[42, 43] absolutely localized molecular orbitals,[44, 45] and gradient methods with respect to orbital coefficients.[38, 46, 47, 48, 49] The BLW configurations can be used in nonorthogonal configuration interaction (NOCI) either in WFT,[50] called mixed molecular orbital and VB theory,[34, 51] or in multistate density functional theory (MSDFT),[7, 52, 8, 53] to yield the adiabatic ground and excited states. MSDFT has been used in a number of applications,[26, 27, 7, 8, 54, 55, 56] including proton-coupled electron transfer (PCET)[57] and singlet fission[58] with approximate local-excitations.

A closely related approach is constrained density functional theory-configuration interaction (CDFT-CI) based on density confinement in a certain spatial domain.[59, 60, 61] CDFT-CI has been used to estimate electronic couplings for ET and EET reactions, but the results heavily depend on basis functions used (refs [62] and [63] and references there in). Recently, non-Aufbau occupation of the orbitals was employed to construct localized singlet excited state in singlet fission.[64] One question here is physically constraining electrons within a spatial region on a property that is in fact distributed in the full space. Consequently, the computation also depends on the particular population method used because it is not a physical observable,[63] and the constrained integration number of electrons actually is a composite from the wave functions from different target states.[65] Another related approach is the Frenkel-Davydov exciton approach using states derived from time-dependent density functional theory calculations for isolated monomers,[66, 67, 68] with which both dipole-coupling and Dexter exchange interactions are directly determined as in the study of singlet fission using MSDFT[58] and PCET.[57] In the latter case, local states are variationally optimized in the presence of the environment through a QM/MM interaction Hamiltonian.[58]

In this chapter, we extended the block-localization method to treat excited states constrained within individual fragments. Similar to previous works for the ground state, the main focus is to obtain BLOs in the excited states. In principle, such calculations can be performed using CASSCF or time-dependent density functional theory (TDDFT) within a fixed molecular fragment.[2] However, a single-determinant representation rather than a multiconfigurational approach is desired to keep spirit of computational efficiency of KS-DFT for the ground state in MSDFT for the excited state. Here, we find a ΔSCF type of models suitable for our aim to construct localized excited states.[69] Of course, the performance of ΔSCF methods is rather system-dependent, encountering optimization collapse to the ground state or to undesired configurations. To resolve these problems, a number of techniques have been developed such as the maximum overlap (MOM),[70] improved MOM,[71] the MOM square methods,[72] and square gradient minimization (SGM).[73] These approaches can be directly adopted to construct diabatic states in the active space for MSDFT. In particular, the present BLE approach is a variation of ΔSCF methods, which is illustrated by the intermolecular interactions of a naphthalene dimer complex both in its first triplet and in two singlet excited states.[74, 75, 76, 77] The latter features an interesting curve crossing of two low-lying singlet states as the two aromatic compounds are in close proximity. This was clearly resolved recently using a DMRG-CASPT2 approach including the full active space of 20 electrons in 20 orbitals, but such a curve crossing is only revealed by adding post-SCF perturbation corrections for dynamic correlation.[76]

The remainder of this chapter is organized as follows. In Section 2.2, we present the theory and computational details of a BLE method to obtain single-determinant representation of excited configurations in the MSDFT active space. An SCF projection method and an MOM of wave function procedure through singular value decomposition are described to ensure ΔSCF convergence. Numerical results on the naphthalene excimer complex are then presented in Section 2.3, where we apply the present method to determine the transfer integrals associated with excited energy transfer both in the lowest singlet and in the triplet states, and binding interactions of excimer formation in these two states. Finally, the chapter is concluded with summary remarks in Section 2.4.

2.2 Theory

2.2.1 BLW Method for the Ground State

For completeness, we begin with a brief review of the BLW method for the ground state, which will be used later to construct diabatic states of locally excited configurations. In BLW, the determinant wave function is written as follows[32, 36]

$$\Psi_{\mathrm{u}} = N_{\mathrm{u}} \hat{A} \left\{ \Phi^1 \Phi^2 ... \Phi^K \right\} \tag{2.1}$$

Where N_{u} is the normalization constant, $\hat{A}$ is the antisymmetrization operator, K is the number of blocks, and Φ^A denotes a product of spin-orbitals of block A, $\Phi^A =$

$\phi_1^A\alpha\phi_1^A\beta...\phi_{nA\alpha}^A\alpha\phi_{nA\beta}^A\beta$, which are localized by construction

$$\boldsymbol{\phi}^A = \chi\mathbf{T}^A \tag{2.2}$$

where $\boldsymbol{\phi}^A$ is a matrix of BLOs in block A and χ a row vector of basis orbitals, and $\mathbf{T}^A$ is a matrix of orbital coefficients. In general, BLOs from different blocks are nonorthogonal.

The total coefficient matrix $\mathbf{T}$ is block-diagonal in the original BLW method when different blocks have different basis orbitals. In this chapter, that restriction has been lifted such that different blocks can share a group of common basis functions. The total density matrix $\mathbf{D}$ is given by[7]

$$\mathbf{T}T^\dagger\mathbf{T}^\dagger\mathbf{D} = \mathbf{T}(\mathbf{T}^\dagger\mathbf{S}\mathbf{T})^{-1}\mathbf{T}^\dagger \tag{2.3}$$

where $\mathbf{S} = \chi^\dagger\chi$ is the overlap matrix of the atomic orbitals. Then, the energy of such a block-constrained system is given by

$$E = \mathrm{Tr}(\mathbf{Dh}) + \frac{1}{2}\mathrm{Tr}(\mathbf{DJD}) + E_{\mathrm{XC}}(\rho) \tag{2.4}$$

where $\mathbf{h}$ and $\mathbf{J}$ are the usual one-electron and Coulomb integral matrices, and $E_{\mathrm{XC}}(\rho)$ is the exchange-correlation energy in standard KS-DFT. The constrained optimization of the BLOs can be achieved using the Broyden-Fletcher-Goldfarb-Shanno updating scheme[78] with the energy gradient given as follows[38, 46, 47, 48, 49]

$$\begin{aligned}\delta E =& 2\,\mathrm{Tr}(\delta\mathbf{D}\cdot\mathbf{J})\\ =& 2\,\mathrm{Tr}\left[(\mathbf{1}-\mathbf{SD}_\alpha)\mathbf{F}_\alpha\mathbf{T}_\alpha(\mathbf{T}_\alpha^\dagger\mathbf{S}\mathbf{T}_\alpha)^{-1}\delta\mathbf{T}_\alpha^\dagger\right.\\ &\left.+(\mathbf{1}-\mathbf{SD}_\beta)\mathbf{F}_\beta\mathbf{T}_\beta(\mathbf{T}_\beta^\dagger\mathbf{S}\mathbf{T}_\beta)^{-1}\delta\mathbf{T}_\beta^\dagger\right]\end{aligned} \tag{2.5}$$

where $\mathbf{F}$ is the Fock matrix.

The gradient optimization method can be applied to closed shell, restricted open shell, and unrestricted open shell cases. Both analytic orbital gradient and numerical orbital Hessian have been implemented in our program, though the latter is time-consuming. The gradient optimization method is used when common basis functions are used in different blocks.[47, 48] Three different forms of SCF equations have been described in the literature.[7, 39, 40, 41, 42, 43, 44, 45, 79] In Appendix B, we provide another direct derivation and highlight the properties of the non-orthogonal block SCF equations. These methods are derived on the basis of zero energy gradient, and their computational costs are essentially the same when the number of the blocks is not large. In this chapter, the approach described in ref [7] is used for the ground state calculations, and is extended to the localized orbitals for excited states (below).

To accelerate the convergence of the SCF, we employ the DIIS (direct inversion in the iterative subspace) method[80] by using energy gradients (Appendix B) as the error vectors and updating the projected Fock matrix and the effective overlap matrix for each block. We have also implemented a DIIS by updating the Fock matrix and coefficients of the whole system. Efficiencies of the two methods are found to be similar for the naphthalene dimer system.

2.2.2 Block-Localized Excitation

In the present study, we are interested in obtaining a computationally efficient representation of locally excited configurations within a given block. Traditional methods for excited states are usually of multiconfigurational nature, even for the simplest excited state approaches such as configuration interaction with single excitations (CIS) and TDDFT. Clearly, a multiconfigurational wave function technique within a fixed block would have not been desirable for a DFT-based method for the intended applications. To this end, we employ a ΔSCF-like approach to represent locally excited configurations.[69] ΔSCF is a single determinant technique, with which the exchange-correlation functional developed for KS-DFT can be directly used, keeping in mind that the present Kohn-Sham determinant using BLO is constrained in the framework presented in Section 2.2.1 In a ΔSCF scheme, the localized orbitals can be optimized in a way that is very similar to the ground state Hartree-Fock-Roothaan equation. However, it is known that the original ΔSCF method often suffers from SCF convergence,[69] and when it converges, an unwanted excited state or the ground state could be obtained.

A number of local excitation ΔSCF methods have been reported,[81, 82, 83, 84, 85, 86, 87, 88, 89, 90, 91, 92, 93, 94] including the MOM method[70] and MOM [72] squared, the SGM,[73] the local SCF method for core-excited states,[82] and a constricted variational DFT (SCF-CV-DFT) by one electron excitation to the virtual orbital space.[83] The single determinant approach can also be achieved by orthogonality constraints on the excited state. The "big shift" method was formulated by setting a large value (more than 1010 au) to the diagonal element of the Fock matrix corresponding to ground state orbitals.[84] Similarly, an asymptotic projection method was suggested by adding an infinite projector to the frozen orbital in the Hamiltonian operator.[85] Yet, another alternative is the guided SCF approach by transformation of the Fock matrix from the atom orbitals (AO) basis to the excited state orbitals basis.[86] Similar to the BLW method, but enforcing orbital orthogonality between the core and the valence is the projection configuration interaction method.[87]

In this chapter, we adopt a ΔSCF approach to represent locally excited non-Aufbau configurations and employ two techniques to ensure SCF convergence. In the first method, we project the ΔSCF equations to the BLO space of the ground state in each iteration to retain the desired order of orbitals for the subsequent SCF iteration. Either the HF or KS-DFT method can be used. The approach in this study can be summarized below, making use of a general case of a single electron excitation from an occupied BLO

j to a virtual BLO b. For clarity, only the α spin is shown.

1. We obtain BLOs of the ground state by solving the generalized secular equation $\mathbf{F}^0\mathbf{T}^0 = \mathbf{S}\mathbf{T}^0\mathbf{E}^0 0$, where the superscript emphasizes ground state orbitals.

2. The initial guess determinant corresponding to the excitation $\phi_j^0(\alpha) \rightarrow \phi_b^0(\alpha)$ is constructed by switching the occupied and virtual BLOs:

$$\Psi_{b0}^{\mathrm{BLE}} = |(\phi_1^0\phi_2^0 \cdots \phi_{j-1}^0\phi_b^0\phi_{j+1}^0 \cdots \phi_n^0)(\phi_{n+1}^0 \cdots \phi_{b-1}^0\phi_j^0\phi_{b+1}^0 \cdots \phi_m^0)\rangle_\alpha$$

   Here, the two pairs of parentheses denote occupied and virtual spaces, and there is no change in the occupation of β electrons.

3. To solve the eigen equation $f|\phi\rangle = |\phi\rangle$, we set $|\phi\rangle = \boldsymbol{\chi}\mathbf{T}^0\mathbf{T}$, and left multiply $\langle\phi^0| = (\boldsymbol{\chi}\mathbf{T}^0)^\dagger$. This has the effect of diagonalizing the Fock-like matrix in the BLO basis of the ground state, $(\mathbf{T}^{0\dagger}\mathbf{F}\mathbf{T}^0)\mathbf{T} = (\mathbf{T}^{0\dagger}\mathbf{S}\mathbf{T}^0)\mathbf{T}^{0\dagger}\mathbf{E}^{\mathrm{BLE}}$, to yield a new set of orbitals $\mathbf{T}$ for the block-localized excited determinant. After diagonalization, it is not needed to resort the eigenvectors according to the energy of each orbital as the order of ground state molecular orbitals is kept.

4. The effective Fock matrix for the BLE configuration can be obtained in the AO basis using the transformation matrix $\mathbf{T}_{\mathrm{new}} = \mathbf{T}^0\mathbf{T}^{\mathrm{BLE}}$ for the next SCF iteration in step 3 until convergence, where $\mathbf{T}^{\mathrm{BLE}}$ is $\mathbf{T}$ with the orbitals $\phi_j(\alpha) \rightarrow \phi_b(\alpha)$ swapped. Usually, good convergence can be obtained by projecting the ground state orbitals. We can also use the orbitals produced in a previous iteration to do the projection. Alternatively, we can use a permuted $\mathbf{T}^0$ to realize the ΔSCF excitation, then follow the process above without eigenvector permutation.

The above procedure is general in that any combinations of α and β excitations, including multiple excitations can be included. We note that the guided SCF method also employs a similar projection method.[86] The determinant that is optimized using the method presented above is not orthogonal to the ground state, but the overlap with the ground-state determinant is usually small. To obtain a localized excited state that is orthogonal to the localized ground state, the particle orbital can be obtained from the projection of unoccupied orbital space after obtaining the hole orbital from a full space projection. The derivation within localized constraint is presented in Appendix B. Furthermore, the adiabatic ground and excited states can be obtained using MSDFT through configuration interaction among these determinant configurations (see Section 2.2.3) such that conical intersection between the ground and first excited states can be obtained.[8]

The second method that we have implemented to improve the ΔSCF convergence is based on the maximum overlap of wave function (MOW) with the initial determinant for the excited configuration, denoted as $\mathbf{T}_{b0}^{\mathrm{BLE}} = (\phi_1^0, ..., \phi_b^0, ..., \phi_n^0)_\alpha$. All steps in the MOW procedure are identical to those outlined above, except step 4 to choose the correct n occupied orbitals of the BLE configuration. Here, at the Ith iteration, the goal is to construct a determinant for a specific BLE configuration that maximizes the overlap with the initial guess Ψ_{b0}^{BLE}: $\underset{max}{\phi}\left\{\langle\Psi_{0b}^{\mathrm{BLE}}|\Psi_{Ib}\rangle = |\mathbf{T}_{0b}^{\mathrm{BLE}^\dagger}|\mathbf{S}\mathbf{T}_{Ib}\right\}$ It would be unfeasible to try out all C_m^n possibilities by brute force. Instead, we choose the n orbitals that maximize its Frobenius norm, $|\mathbf{T}_{0b}^{\mathrm{BLE}^\dagger}|\mathbf{S}\mathbf{T}_{IbF} = \sqrt{\sum_i^n \sum_j^n O_{i^0 I_j}^2}$, which can be easily accomplished by singular value decomposition. This is equivalent to an approach called MOM squared.[70, 72] With the above ΔSCF projection and the MOW method, BLOs for an excited configuration within a given block A can be obtained using the approach described in Subsection 2.2.1 Because the excited determinants are fully localized, there is no charge transfer contribution between different blocks. We have adopted an unrestricted open-shell treatment both in the ΔSCF projection and in the MOW method, which yield identical results at convergence. All results in the examples illustrated below are obtained by using the block-localized ΔSCF projection scheme.

2.2.3 MSDFT and Electronic Coupling of BLE Diabatic States.

The adiabatic ground and excited states of the delocalized system can be obtained using MSDFT through NOCI by solving the generalized secular equation,[34, 7, 51, 52, 53, 95] for which the BLE configurations form a minimal active space (MAS) for the adiabatic excited states of interest

$$\mathbf{HC} = \mathbf{SCE} \tag{2.6}$$

where $\mathbf{E}$ is a diagonal matrix of adiabatic energies, $\mathbf{C}$ is a matrix of the CI-coefficient, $\mathbf{H}$ is the CI-Hamiltonian, and $\mathbf{S}$ is the overlap matrix, which is determined using the separately optimized Kohn-Sham BLE-determinants ($S_{AB} = \langle\Psi_A^{\mathrm{BLE}}|\Psi_B^{\mathrm{BLE}}\rangle$).[34] The adiabatic energies of the ground and excited states are given using[7, 52]

$$\begin{aligned} E_I^{\mathrm{MS}}[\rho_I] = &\sum_A c_{AI}^2 H_{AB}^{\mathrm{BLE}}[\rho_A] \\ &+ 2\sum_{A>B} c_{AI}c_{BI} H_{AB}^{\mathrm{TDF}}[\rho_{AB}, \Psi_A^{\mathrm{BLE}}, \Psi_B^{\mathrm{BLE}}] \end{aligned} \tag{2.7}$$

In MSDFT, the diagonal matrix elements of the CI Hamiltonian $H_A^{\mathrm{BLE}}[\rho_A]$ are the energies determined using the methods described in Section 2.2.1 for the ground state determinant and in Section 2.2.2 for block-localized excited configurations. Each off-diagonal element consists of two terms: a standard interaction term between two nonorthogonal determinants, Ψ_A^{BLE} and Ψ_B^{BLE}, and a transition density functional (TDF) energy[26, 27, 7, 52, 53]

$$H_{AB}^{\mathrm{TDF}} = \langle\Psi_A^{\mathrm{BLE}}|H|\Psi_B^{\mathrm{BLE}}\rangle + E_{AB}^{\mathrm{TDF}}[\rho_{AB}, \Psi_A^{\mathrm{BLE}}, \Psi_B^{\mathrm{BLE}}] \tag{2.8}$$

where E_{AB}^{TDF} is the dynamic correlation contribution to the TDF, or simply, the TDF that depends on the transition density ρ_{AB} as well as the determinant functions Ψ_A^{BLE} and Ψ_B^{BLE}. TDF is a novel class of correlation functional, which does not exist in KS-DFT, accounting for dynamic correlation in electronic coupling and playing a role in removing any double counting of electron correlation in a multiconfigurational representation of DFT.[8] As in KS-DFT, the exact functional form of E_{AB}^{TDF} is not known, but under special conditions, such as the spin coupling of two unpaired electrons forming a pair of spin-adapted singlet and triplet states, the value of E_{AB}^{TDF} can be obtained consistently with a particular KS-DFT functional approximation to the two spin-mixed determinant configurations.[8, 96] This is achieved by enforcing the energy degeneracy of the high ($M_S = 1$) and low ($M_S = 0$) spin projections of the triplet states proposed by Ziegler et al.[69] A related approach is the spin-restricted density functional theory for biradical calcualtions.[97, 98, 99] Here, the correlation energy of the high-spin projection state $E_{\mathrm{c}}^{\mathrm{KS}}[\rho(|1,1\rangle)]$, which can be adequately represented by a single determinant in KS-DFT, along with that of the mixed low-spin determinant $E_{\mathrm{c}}^{\mathrm{KS}}[\rho(|1,0\rangle)]$, is used to define the magnitude of the correlation contribution[8]

$$E_{AB}^{\mathrm{TDF}}[\rho_{AB}, \Psi_A^{\mathrm{BLE}}, \Psi_B^{\mathrm{BLE}}] = E_{\mathrm{c}}^{\mathrm{KS}}[\rho(|1,1\rangle)] - E_{\mathrm{c}}^{\mathrm{KS}}[\rho(|1,0\rangle)] \tag{2.9}$$

In general applications, one possible approximation for $E_{\mathrm{c}}^{\mathrm{TDF}}$ is a determinant-weighted average of correlation energies of the two interacting states[8]

$$E_{AB}^{\mathrm{TDF}} \approx \frac{\langle \Psi_A^{\mathrm{BLE}} | H | \Psi_B^{\mathrm{BLE}} \rangle}{E_A^{\mathrm{HF}}[\Psi_A^{\mathrm{BLE}}] + E_B^{\mathrm{HF}}[\Psi_B^{\mathrm{BLE}}]} \left[E_A^{\mathrm{c}}(\rho_A) + E_B^{\mathrm{c}}(\rho_B) \right] \tag{2.10}$$

where $E_A^{\mathrm{HF}}[\Psi_A^{\mathrm{BLE}}]$ and $E_B^{\mathrm{HF}}[\Psi_B^{\mathrm{BLE}}]$ are HF energies determined by using the KS-determinants for the BLE configurations, and $E_A^{\mathrm{c}}(\rho_A)$ and $E_B^{\mathrm{c}}(\rho_B)$ are the corresponding correlation energies. Alternatively, the TDF energy can be approximated by an overlap scaled average of the correlation energies of the two diabatic states.[7, 52]

$$E_{AB}^{\mathrm{TDF}} \approx \frac{1}{2} M_{AB}^{\mathrm{KS}} \left[E_A^{\mathrm{c}}(\rho_A) + E_B^{\mathrm{c}}(\rho_B) \right] \tag{2.11}$$

where M_{AB}^{KS} is the overlap between two Kohn-Sham determinants. The numerical results from these approximate approaches are similar.

These block-localized configurations may be considered as charge- and energy-localized diabatic states, and their electronic coupling elements are related to the transfer integrals for electron and excited energy transfer applications. Within the MS-DFT framework and CDFT-CI, the ET integral between any two diabatic states can be calculated.[7, 63, 65] Because the BLE configurational states are generally non-orthogonal, the effective coupling term $V_{AB}^{\perp}$ between states A and B can be calculated through Löwdin orthogonalization

$$V^{\perp} = \frac{H_{AB} - M_{AB}(H_A + H_B)/2}{1 - M_{AB}^2} \tag{2.12}$$

where M_{AB}^{KS} is the overlap integral of states A and B.

2.3 Computational Details

The naphthalene monomer structure was optimized with the D_{2h} symmetry using Gaussian-16 at the B3LYP/6-31+G(d) level of theory, following the work of Shirai et al.[76] Then, the monomer structure is kept fixed and is used to construct a face-to-face dimer configuration at various separation distances, ranging from 2.9 to 20 Å. A structure at 50 Å was also built to verify asymptotic energies. It is known that the face-to-face structure of the excimer complex has the lowest energy in both the singlet and triplet states.[74, 75, 76, 77, 100, 101, 102] Further, upon relaxation from the monomer geometry, the Franck-Condon approximation suggests that the diabatic couplings should not change significantly.[75, 77] In BLE calculations, the dimer is separated into two blocks, each containing one naphthalene molecule. Single-point energy calculations are performed using MSDFT, for which a total of 16 block-localized configurations plus the adiabatic ground state have been obtained using block-localized KS-DFT. The PBE0 functional and the cc-pVDZ basis set are used in all calculations.[103] For the excitations on both monomers and with all three combinations of source and target orbitals, the separately optimized open-shell singlet determinants with $\alpha\beta$ and $\beta\alpha$ spin combinations are converged to the same set of BLO, based on which the spin-coupled singlet and triplet states are obtained. This is equivalent to switching α and β electron spins of an open-shell configuration to yield a spin pair. The all-spin up triplet configuration ($M_S = 1$) at each geometry was obtained by separate open-shell calculations. The energy for the $M_S = 1$ state is used to determine the correlation energy term E_{AB}^{TDF} for the TDF of spin-pair coupling (Eq. 2.6). This makes the orbitals not entirely compatible, but the energy difference is less than 0.1 eV, smaller than uncertainties from the method itself, compared with the results obtained using a common set of orbitals. Although this is not a conventional procedure for spin-adapted configurations,[104] it is not without precedents and we have used it in a number of applications.[26, 27, 52, 8] This is also consistent with the use of a single determinant to treat open-shell systems using KS-DFT,[105, 106] yielding lower energy than that adopting a restricted open-shell approach. All other computational details are the same as in other studies.

The potential energies curves for the naphthalene dimer have also been computed using MSDFT with the M06-2X density functional and the cc-pVDZ basis, yielding the same trends with the benefit that additional and empirical dispersion corrections are not needed. The results can be found in the Supporting Information of [9].

The method described in Section 2.2 has been implemented in a locally modified version of the GAMESS-US program,[107] with which all calculations have been performed.

2.4 Results And Discussion

An important application of the present BLE method is to understand dimer interactions of aromatic species in the excited states and to determine the electronic coupling in excitation energy transfer (EET) processes from one part of the molecular system to another.[108] We first apply the BLE method to determine the diabatic and adiabatic potential energy curves for the naphthalene dimer in the face-to-face configuration. This is followed by calculations of the EET couplings both in the singlet and triplet states. This system is chosen because it has been extensively studied and there is a challenging curve-crossing that is only obtained with a method balancing static and dynamic correlation.[74, 75, 76, 77, 100, 101, 102, 109] Here, we chose the face-to-face stacked parallel configuration in our study, corresponding to the minimum-energy configuration in the first singlet and triplet excited states of the dimer complex (excimer).[75, 76, 77, 100, 110, 111, 112]

2.4.1 Excimer Interactions in the Singlet State

Shirai et al.[76] reported a most comprehensive investigation of the naphthalene excimer complex in the singlet state using DMRG-CASPT2 with cc-pVDZ and cc-pVTZ basis functions, which revealed an inversion of the $^1L_a^-$ and $^1L_b^-$ states along the dimer separation path. In that study, the full π electrons in an active space of $[20\,\mathrm{e}, 20\,\mathrm{o}]$ were used. Dynamic correlation is critical for the excimer calculations, without which the qualitative trends of the two low-lying are wrong at the DMRG-CASSCF level.

MSDFT follows a dynamic-then-static (DTS) ansatz, in which dynamic correlation is incorporated in the optimization of BLOs through Kohn-Sham density functionals for each individual determinant configuration.[7, 52] Moreover, each configuration in the active space for MSDFT is separately optimized, further introducing orbital relaxation. Consequently, it is expected that a minimal number of essential configurations would be sufficient to describe the properties of the relevant low-energy states. Following the insights provided by Shirai et al. on the naphthalene excimer complex, we tested the idea of a MAS for the two low-lying excited states of naphthalene excimer by MSDFT (Fig. 2.1) This includes three local singly excited configurations for each monomer (Eqs. 2.13–ł2.20), plus a pair of charge transfer states between two monomers (Eqs. 2.19 and 2.20), which are depicted in Fig. 2.1.

$$\Omega_{A^\star B}^{S_{2\to 3}S_0} = \frac{1}{\sqrt{2}}\left\{\Psi_{A^\star B}({S_2}^{\bar{3}}S_0) - \Psi_{A^\star B}({S_{\bar{2}}}^{3}S_0)\right\} \tag{2.13}$$

$$\Omega_{A^\star B}^{S_{2\to 4}S_0} = \frac{1}{\sqrt{2}}\left\{\Psi_{A^\star B}({S_2}^{\bar{4}}S_0) - \Psi_{A^\star B}({S_{\bar{2}}}^{4}S_0)\right\} \tag{2.14}$$

$$\Omega_{A^\star B}^{S_{1\to 3}S_0} = \frac{1}{\sqrt{2}}\left\{\Psi_{A^\star B}({S_1}^{\bar{3}}S_0) - \Psi_{A^\star B}({S_{\bar{1}}}^{3}S_0)\right\} \tag{2.15}$$

$$\Omega_{AB^\star}^{S_0S_{2\to 3}} = \frac{1}{\sqrt{2}}\left\{\Psi_{AB^\star}(S_0{S_2}^{\bar{3}}) - \Psi_{AB^\star}(S_0{S_{\bar{2}}}^{3})\right\} \tag{2.16}$$

$$\Omega_{AB^\star}^{S_0S_{2\to 4}} = \frac{1}{\sqrt{2}}\left\{\Psi_{AB^\star}(S_0{S_2}^{\bar{4}}) - \Psi_{AB^\star}(S_0{S_{\bar{2}}}^{4})\right\} \tag{2.17}$$

$$\Omega_{AB^\star}^{S_0S_{1\to 3}} = \frac{1}{\sqrt{2}}\left\{\Psi_{AB^\star}(S_0{S_1}^{\bar{3}}) - \Psi_{AB^\star}(S_0{S_{\bar{1}}}^{3})\right\} \tag{2.18}$$

$$\Omega_{A^-B^+} = \frac{1}{\sqrt{2}}\left\{\Psi_{A^-B^+}(D^\alpha D_\beta) - \Psi_{A^-B^+}(D^\beta D_\alpha)\right\} \tag{2.19}$$

$$\Omega_{A^+B^-} = \frac{1}{\sqrt{2}}\left\{\Psi_{A^+B^-}(D_\beta D^\alpha) - \Psi_{A^+B^-}(D_\alpha D^\beta)\right\} \tag{2.20}$$

In Eqs. 2.13–2.20, the notation ${S_i}^{\bar{a}}$ or ${S_{\bar{i}}}^{a}$ denotes a single excitation within a given singlet block in which the β-spin of an electron in the corresponding orbital is represented

Figure 2.1: Schematic depiction of (a) block-locally excited configurations of monomer A⋆ in the presence of monomer B in its ground state, (b) block-locally excited configurations of monomer B⋆ in the presence of monomer A in its ground state, and (c) two charge transfer states between monomers A and B. Each yellow block shows one block-localized determinant configuration of the whole dimer, and the left and right halves within it show the four relevant fragment orbitals of the two monomers, respectively. The four BLOs used in the figure include the two highest occupied fragment orbitals, ϕ_1 and ϕ_2, and the two lowest unoccupied fragment orbitals, ϕ_3 and ϕ_4, of the excited monomer. The locally excited monomer is indicated by a star. Only singlet spin-adapted states are shown, whereas the symmetric (in-phase) combination of two determinants corresponds to a triplet state.

by an over-hat, and D specifies a doublet block with α and β spin of the unpaired electrons in the occupied (subscript) and virtual (superscript) orbitals (with the reference ground-state configuration, S_0). In short, Eqs. 2.13–2.20 represent single excitations in a blocked 4-electron and 4-orbital space minus the largest energy transition, in which each individual determinant is separately optimized using BLE to yield spin-adapted configurational state functions for singlet (as written) and triplet states (symmetric combinations). Note that MAS is not necessarily a black-box selection in that a great deal of insights of the configuration space ought to be known in the first place, such as the naphthalene dimer in the present study. Furthermore, the configurational state functions in MAS are not equivalent to the orthogonal configurations in CASSCF. However, MAS, when verified by comparison of its resulting adiabatic energies with experiment, can be quite useful for interpretation from energy decomposition analysis[36] and for carrying out dynamic simulations of nonadiabatic processes.

We begin with the low-lying excited states of a naphthalene monomer, whose active space in MSDFT can be represented using Eqs. 2.13–2.20 (omitting the orbitals on fragment B). There are two singlet excited states of similar energies, corresponding to ${}^1\mathrm{B}_{3u}({}^1L_b)$ and ${}^1\mathrm{B}_{2u}({}^1L_b)$ symmetry.[113] The latter is of HOMO $\rightarrow$ LUMO character given by Eq. 2.13 (Fig. 2.1a), and the complementary symmetric combination of the two determinants, $\left\{\Psi_{A^\star B}({S_2}^{\bar{3}}S_0)+\Psi_{A^\star B}({S_{\bar{2}}}^{3}S_0)\right\}/\sqrt{2}$, corresponds to the $M_S = 0$ multiplet of the first triplet excited state $|1,0\rangle$. The $M_S = 1$ state of the triplet ($|1,1\rangle$) can be adequately treated by KS-DFT, and a vertical excitation energy of 3.13 eV above the ground state is obtained with PBE0/cc-pVDZ. The value is in accord with experiment (3.0 eV), and is used to define[69] the TDF for spin-coupling interaction (Eq. 2.9).[8] We obtained a vertical excitation energy of 4.52 eV ${}^1L_a$ singlet state (Eq. 2.10) from MSDFT@PBE0, falling in the range of experimental observations (4.45[114, 115] and 4.7 eV).[116]

For the diabatic coupling between the symmetry-allowed spin-adapted states E^{TDF}_{14-15} (Eqs. 2.14 and 2.15), we used the average of the two spin-coupling values determined with Eq. 2.9[114, 115] because the transition energies are nearly degenerate for the HOMO$-1 \rightarrow$ LUMO (4.48 eV) and HOMO $\rightarrow$ LUMO+1 (4.51 eV) single excitations.[76] This yields an energy for ^1L_b of 4.14 eV in comparison with the experimental value of 3.97 eV.[114, 115] The E^{TDF}_{14-15} value for naphthalene is used for the local (monomer) ^1L_b excitation in the dimer complex at all geometries because it is intrinsically a local (monomer) property. For comparison, CASPT2/cc-pVTZ calculations yielded vertical excitation energies of 3.83 and 4.34 eV for the ^1L_b and ^1L_a states,[76] whereas 4.03 and 4.56 eV were obtained by Roos and coworkers using natural atomic orbital basis functions.[117] Overall, we found that with an MAS of three spin-adapted diabatic states in MSDFT, the computed energies of the three low-lying excited states (two singlet and one triplet) are within 0.2 eV of experimental values.[114, 115]

Second, Figure 2.2 shows the potential energy curves for the ground state and three low-lying excited states determined from MSDFT@PBE0 calculations (solid curves), along with the corresponding curves for the singlet states by DMRG-CASPT2 (dashed curves) and DMRG-CASSCF (dotted curves) from ref [76]. Because the energies for the excited states are overestimated by 0.3 to 0.5 eV from DMRG-CASPT2 calculations of the naphthalene monomer, this trend is transferred to the potential energy curves of the dimer complex. At large interfragment separations (ł> 3.5 Å), the two low-lying singlet states of naphthalene in the excimer complex follow the same order in energy as that of the monomer: $^1L_a^-(^1\mathrm{B}_{3g}) >^1 L_a^-(^1\mathrm{B}_{2g})$. However, the charge-transfer (CT) state (Fig. 2.1c and Eqs. 2.19 and 2.20) is strongly mixed in $^1L_a^+$ at short distances (Fig. 2.3), stabilizing intermolecular interactions between two naphthalene molecules in the excimer complex. This leads to an inversion of the $^1L_a^-$ and $^1L_b^-$ energy levels to bring $^1L_a^-$ as the first singlet excited state of the excimer complex. MSDFT calculations

Figure 2.2: Computed potential energy curves of the adiabatic ground and the first triplet (T1) and first two singlet (S1) excited states from MSDFT along with those determined by using DMRG-CASPT2 (DMRG) and DMRG-CASSCF (CAS) with 20 electrons in 20 orbitals for the singlet states (ref [76]).

The PBE0 functional is used in MSDFT calculations.

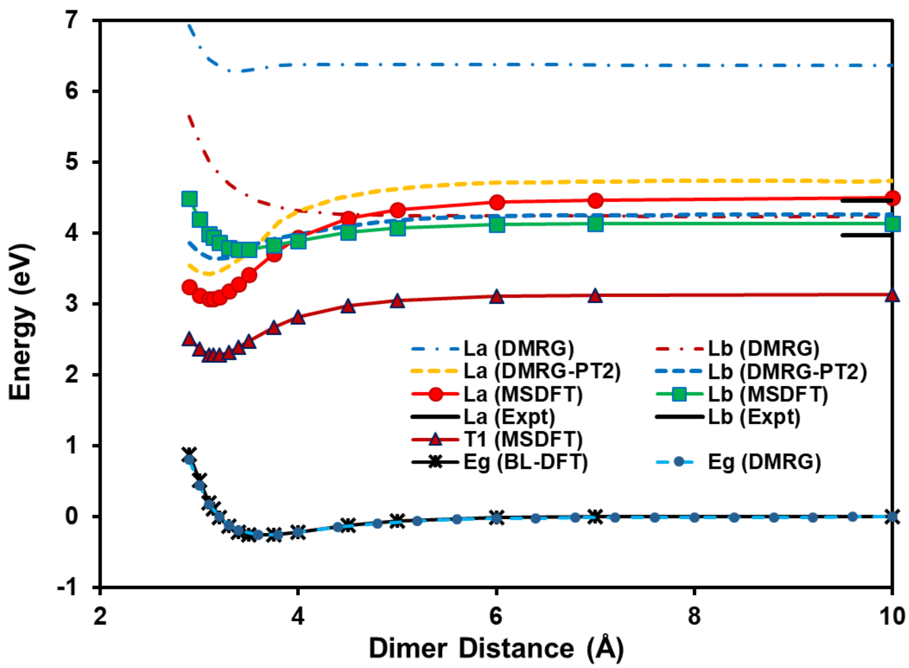

Figure 2.3: Computed adiabatic singlet excited states, along with BLE diabatic states, excitonic resonance (ER) diabatic states, and CT resonance diabatic states. Energies are given relative to the separated naphthalene molecules in the ground state. All computations have been performed using MSDFT with the PBE0 density functional (MSDFT@PBE0) and the cc-pVDZ basis set.

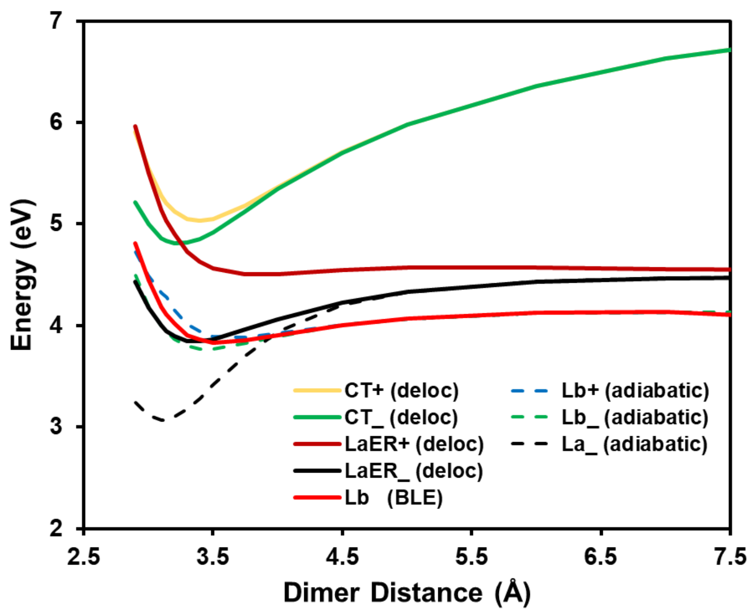

show that the singlet energies are inverted at a distance of about 3.9 Å (Fig. 2.2), somewhat longer than the DMRG-CASPT2 prediction (distances of inversion at 3.26 to 3.62 Å using, respectively, cc-pVDZ and cc-pVTZ basis sets).[76] The qualitative trend of these two low-lying states are critically dependent on the active space used in CASPT2 calculations; the correct order is only obtained when the active space is greater than [12 e, 12 o]. The order of energy levels is not correctly obtained using the single-reference EOM-CCSD/cc-pVTZ method.[76] Furthermore, the work of Shirai et al. demonstrated that dynamic correlation is absolutely necessary for the excimer complex, without which ${}^1L_b^-$ remains the lowest state incorrectly at all separations, below ${}^1L_a^-$ by as much as 1.6 eV using DMRG-CASSCF [20 e, 20 o].

An anonymous referee noted that the energy of the ${}^1L_b^-$ state is more repulsive at short distances than that determined by DMRG-PT2, which may reflect CT effects not included in the small active space used in this study. While CT effects are captured in the ${}^1L_a^-$ state, high-lying CT states at longer separations may indeed become competitive to make contributions at a short interfragment distance, and this has been observed in the study of the photochemical dissociation of LiH.[26]

Third, using the active states defined by Eqs. 2.13–12.20, we obtained vertical emission (fluorescent) energies of 3.0 and 4.0 eV from ${}^1L_a^-$ and ${}^1L_b^-$, respectively, which are similar to DMRG-CASPT2 values of 3.25 and 3.65 eV (Supporting Information, see ref. [76]), and in reasonable accordance with an experimental value of 3.13 eV for the first state.[118] These values are dependent on the structures of the excimer complex, which were not optimized in the present study. We obtained a binding energy of 1.44 eV for the ${}^1L_a^-$ state of the excimer (including Grimme's D3 dispersion correction applied to all states), stronger than that predicted using DMRG-CASPT2 (1.23 and 1.33 eV using cc-pVDZ and cc-pVTZ basis sets) and a value of 0.99 eV using SOS-CIS(D_0)/aug-cc-pVDZ.[77] Basis set superposition errors (BSSE), which decrease the binding energy by

0.33 and 0.17 eV for the two basis sets, have been noted.[76] In principle, the present BLE configurations in MSDFT do not have BSSE by construction, which was pioneered by Gianinetti et al.[39, 40, 41] The binding energy is much weaker for the ${}^1L_a^-$ state at about 0.36 eV from MSDFT, comparable to the DMRG-CASPT2 value (ca. 0.5 eV).[76]

Finally, it is of interest to note that only eight spin-adapted configurational state functions (16 determinants) plus the ground state are used in the present MSDFT calculations, whereas the DMRG study included all π-electron in a $[20\,\mathrm{e}, 20\,\mathrm{o}]$ active space, consisting of more than $3 \cdot 10^{10}$ configurations.[76] Both qualitative trends as well as quantitative results from MSDFT with an MAS are at least of the quality of DMRG-CASPT2. It is sobering to note that without perturbation correction for dynamic correlation, ${}^1L_a^-$ from DMRG-CASSCF $[20\,\mathrm{e}, 20\,\mathrm{o}]$ is more than 2 eV too high than the experimental value at large dimer separation, while the result for ${}^1L_b^-$ is nearly perfect because there is little dynamic correlation (Fig. 2.2). The agreement highlights the usefulness of a DTS approach for balancing dynamic and static correlation in excited state calculations at a cost comparable to KS-DFT for the ground state.

The nature of resonance stabilization of ${}^1L_a^-$ relative to that of ${}^1L_b^-$ is revealed by comparing diabatic states in the two symmetry groups in Fig. 2.3. For ${}^1L_b^-({}^1\mathrm{B}_{2g})$, the BLEs of each naphthalene molecule in the presence of the second monomer are constructed as follows

$$|A^\star B(L_b)\rangle = a^A_{2\to4}\Omega^{S_{2\to4}S_0}_{A^\star B} - a^A_{1\to3}\Omega^{S_{1\to3}S_0}_{A^\star B} \tag{2.21}$$

$$|AB^\star(L_b)\rangle = a^B_{2\to4}\Omega^{S_0 S_{2\to4}}_{AB^\star} - a^B_{1\to3}\Omega^{S_0 S_{1\to3}}_{AB^\star} \tag{2.22}$$

where the coefficients $a_{ia}^{A/B}$ are determined by using MSDFT (Eqs. 2.14 and 2.15 for $|A^\star B\rangle$ and Eqs. 2.17 and 2.18 for $|AB^\star\rangle$). These two diabatic states are completely degenerate shown as a single curve in Fig. 2.3 (red). Interestingly, the presence of the second monomer lowers the BLE state $|A^{\star}B(L_b)\rangle$ by 0.30 eV relative to an isolated naphthalene, largely because of the empirical D3 dispersion term. The resonance delocalization of these two BLEs is weak, resulting in a pair of adiabatic states ${}^1L_b^-$ and ${}^1L_b^+$ (blue dashed curves), whose energy splitting is only 0.17 eV at the minimum of the complex (3.4 Å), gaining only 0.06 eV in binding energy for the lower state ${}^1L_b^-$. This is consistent with the results from DMRG calculations with and without the PT2 correction (Fig. 2.2). In contrast, it is no longer physically meaningful to define a BLE (HOMO $\rightarrow$ LUMO) diabatic state for ${}^1L_a^-(1\,{}^1\mathrm{B}_{3g})$ because CT configurations dominate coupling interactions and it is not a local (monomer) property. Of course, one can nevertheless construct a BLE for the "covalent" diabatic configuration (not shown) similar to Eqs. 2.18 and 2.19, and its energy monotonically decreases as the dimer distance shortens. In this case, we construct two pairs of resonance states from the local HOMO $\rightarrow$ LUMO excited configurations, ER, and from the CT configurations across monomer boundaries, charge-transfer resonance (CR)

$$(L_a^{\pm})_{\mathrm{ER}} = \frac{1}{\sqrt{2}}\left\{\Omega_{A^{\star}B}^{S_{2\rightarrow 4}S_0} \pm \Omega_{AB^{\star}}^{S_0 S_{2\rightarrow 3}}\right\} \tag{2.23}$$

$$(\mathrm{CT})_{\mathrm{CR}}^{\pm} = \frac{1}{\sqrt{2}}\left\{\Omega_{A^-B^+} \pm \Omega_{A^+B^-}\right\} \tag{2.24}$$

Figure 2.3 shows that the resonance splitting (0.88 eV) in $(L_a^{\pm})_{\mathrm{ER}}$ is significantly greater than that in the ${}^1L_b^-$ state, gaining a resonance stabilization energy of 0.65 eV, and the resonance propagates to long dimer separations without vanishing at 10 Å (black and gray curves). The interaction between the CT configurations is less pronounced (green and orange curves). Importantly, electronic coupling of the BLE resonance diabatic state $(L_a^{\pm})_{\mathrm{ER}}$ and that of the CT state $(\mathrm{CT})_{\mathrm{CR}}^{-}$ lowers the complexation energy of the BLE resonance state by 0.79 eV and shifts the minimum of the ER state from 3.3

Figure 2.4: Computed adiabatic triplet excited state (T1) along with BLE diabatic states, ER diabatic states, and CT resonance diabatic states. Energies are given relative to the separated monomers in the ground state. All computations have been performed using MSDFT with the PBE0 density functional (MSDFT@PBE0) and the cc-pVDZ basis set.

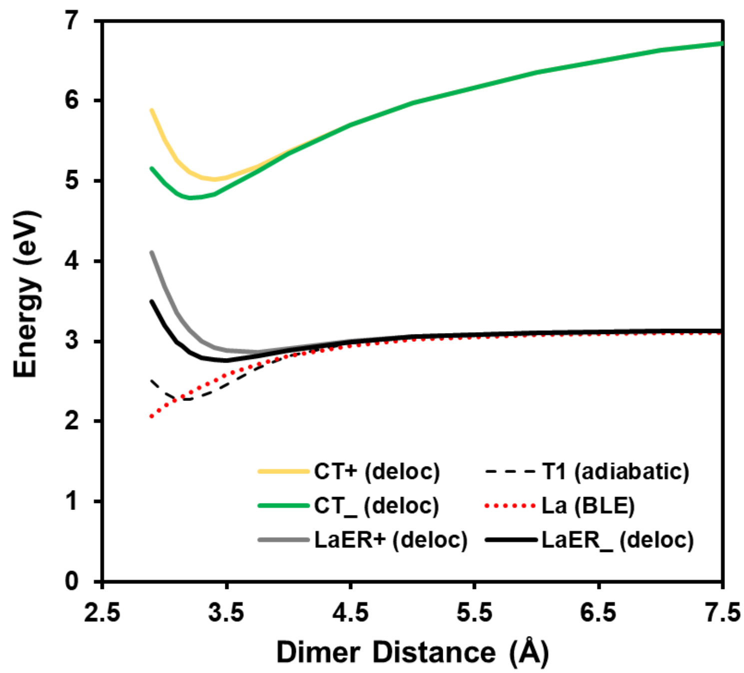

to 3.1 Å (Fig. 2.3). Therefore, both the resonance delocalization of BLE and CT stabilization contributes significantly, with the latter playing a slightly greater role (55 % vs. 45 %) in the total excimer binding energy.

2.4.2 Excimer in the Triplet State

The computed first triplet excited state is shown in Fig. 2.2 and its diabatic state composition is separated in Fig. 2.4. Although a number of higher energy states, both singlet and triplet, can be obtained, other diabatic configurations may or may not be needed to fully characterize these adiabatic states. Because the main goal is to illustrate the BLE optimization method to define configurational states for MSDFT calculations, these states are not further analyzed and shown. Although there has been controversy on the existence of a triplet excimer of naphthalene,[75, 77, 119, 120, 121, 122] the work of Pabst et al. convincingly demonstrated that the triplet state excimer is as important and as stable as that for the singlet configurations.[75] The reason is simple from the present diabatic perspective because the excimer complex in the triplet state $^3L_a^-$ has an equivalent manifold of interactions as that of the excimer complex in the singlet state $^1L_a^-$, except that electronic couplings in the triplet states are somewhat weaker. Consequently, a binding energy of 0.85 eV is obtained for the excimer complex at a separation of 3.2 Å from MSDFT calculations. Thus, the triplet excimer also forms a strong complex. This may be compared with a value of 0.56 eV predicted by Pabst et al. using CC2/cc-pVTZ after the BSSE correction,[75] and values of 0.79 and 0.60 eV with frozen and relaxed monomer structures by Kim.[77] The interfragment distance for the triplet excimer was found to be 3.08 Å in the work of Pablst et al. Another key spectroscopic quantity of interest is the adiabatic phosphorescence energy, which is estimated to be 2.27 eV from MSDFT, in reasonable agreement with the result of Pabst et al. (2.54 eV).[75] Phosphorescence in the present face-to-face configuration is symmetry forbidden, but deviations from the minimum structure could produce emissions and experimental observations of naphthalene triplet excimers show an energy of 2.3 to 2.4 eV in solution.[121, 122]

The present study also yield a singlet – triplet (S – T) energy gap, which is 1.0 eV between ^3L_a and ^1L_b for naphthalene, and 0.79 eV between $^3L_a^-$ and $^1L_a^-$ in the excimer complex. Thus, there is a small red-shift in the energy gap of 0.21 eV between the monomer and excimer complexes. S – T energy gaps of 1.16 and 1.38 eV were obtained by Kim for naphthalene in the ground monomer geometry and relaxed structure, respectively, which are correspondingly red-shifted by 0.2 in the monomer and 0.3 eV in the excimer complex.[77]

2.4.3 Excitonic Coupling Between Singlet Excited States of Naphthalene Molecules

EET plays an important role in many artificial and natural molecular devices such as organic light-emitting diodes, photovoltaics, and the photo-synthetic system.[123, 124] In the weak coupling limit, the EET rate constant can be calculated using the Fermi's golden rule[15]

$$k_{\mathrm{EET}} = \frac{2\pi}{\hbar}|V|^2\delta(E_i - E_f) \tag{2.25}$$

where V is the electronic coupling between the initial state E_i and final state E_f. Therefore, the electronic coupling parameter is a key quantity to determine the EET rate constants.

The excitonic coupling between two locally excited states (covalent configuration) in the ${}^1L_a^-$ state has been determined in the range of 2.5 to 20 Å between dimer separation (Fig. 2.5), which may be considered to associate with singlet excitation energy transfer (SEET) from the initial (Eq. 2.13) to the final (eq. 2.16) states.[109] At distances greater than 6 Å, the excitonic coupling is reciprocally proportional to the cube of the separation distance, indicating that the energy resonance in the excited state is dominated by long-range electrostatic interactions, consistent with a Förster dipole − dipole interaction model.[15] At close proximity, Dexter exchange coupling becomes important and deviation from the linearity of long-range behavior occurs. Figure 2.5 shows that the effect of the basis set size on the computed BLE coupling is small at all distances, suggesting that the present BLE approach is a robust procedure for modeling exciton coupling in the singlet state.

The SEET coupling parameters have also been computed on the basis of locally excited diabatic states constructed using BLOs optimized in the triplet state ($M_S = 1$)

Figure 2.5: Computed transfer integral (V) for the excited energy transfer in the first singlet excited state between two naphthalene molecules as a function of the intermolecular separation. The PBE0 density functional is used in all calculations with different basis sets. Spin-flip using orbitals optimized in the triplet-state (T-SF) with the 6-31G(d) basis set was used; ionic configurations determined by perturbation theory (IC-PT); and IC by solving an eigenvalue equation (IC-EIG). ICs were calculated using the aug-cc-pVDZ basis set. The slopes were fitted using data in the range from 8 to 20 Å.

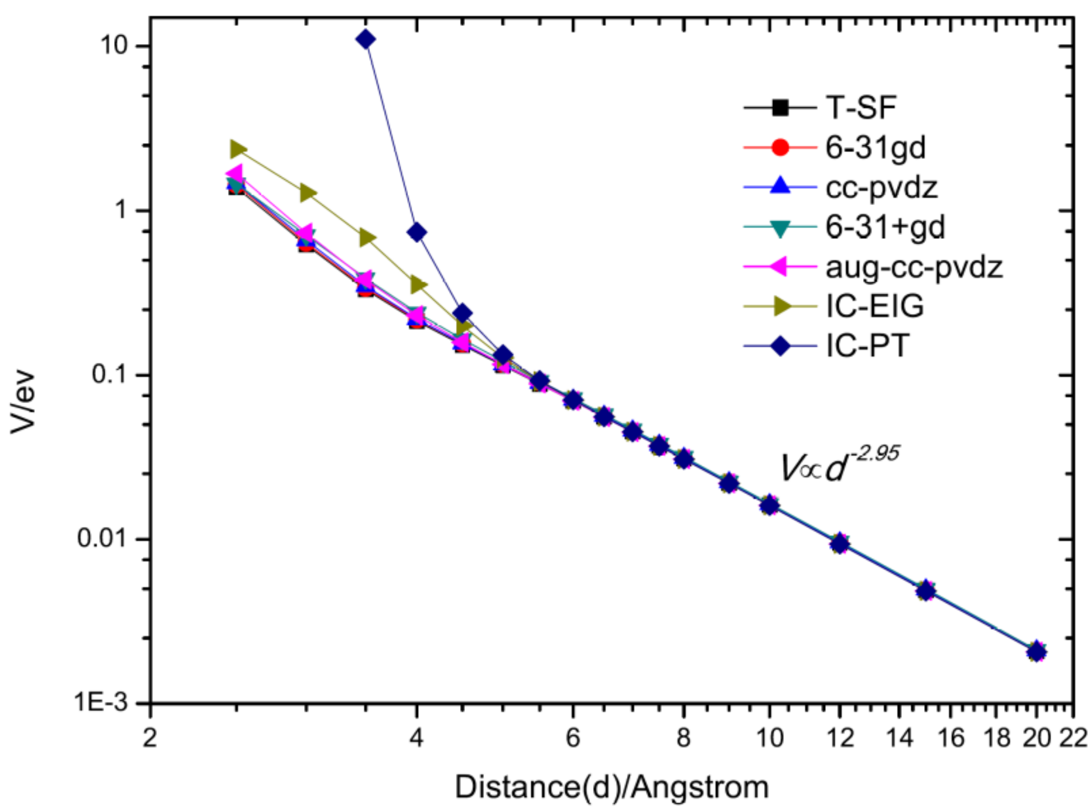

followed by an $\alpha \rightarrow \beta$ spin flip (T-SF). In these calculations, the 6-31G(d) basis set was used. The computed electronic coupling values are not sensitive with respect to orbital optimization in the singlet or triplet states (Fig. 2.5). We further examined the effect of ionic configurations (ICs) given in Eqs. 2.19 and 2.20, which could be important for excited energy transfer through a super-exchange mechanism.[58] Two approaches were used to determine IC contributions. Using a perturbation theory (IC-PT) with the aug-cc-pVDZ basis set,[125] we noticed significant deviations from results obtained using other models at short interchromophore distances. Not surprisingly, perturbation theory is expected to be valid when contributions from ICs are small at long distances. The IC contribution can be determined in the initial (A excitation) and final (B excitation) states using MSDFT (IC-EIG). Figure 2.5 shows that IC contributions cause a modest enhancement to the computed transfer integrals obtained directly using locally excited configurations at short distances, whereas at long ranges this effect diminishes beyond 5 Å.

2.4.4 Excitonic Coupling in the Triplet Excited States

In contrast to the singlet state, excitonic coupling in the triplet excitation energy transfer (TEET) process is dominated by short-range coupling. Using MSDFT, both spin multiplets of the locally excited triplet state can be defined. In particular, the $M_S = 0$ state is defined by two BLE determinants through symmetric combination complementary of the singlet state in Eqs. 2.13 and 2.16.

$$\Omega_{A^\star B}^{T_{2\rightarrow 3}S_0} = \frac{1}{\sqrt{2}}\left\{\Psi_{A^\star B}(S_2{}^{\bar{3}}S_0) + \Psi_{A^\star B}(S_{\bar{2}}{}^{3}S_0)\right\} \tag{2.26}$$

$$\Omega_{AB^\star}^{S_0T_{2\rightarrow 3}} = \frac{1}{\sqrt{2}}\left\{\Psi_{AB^\star}(S_0S_2{}^{\bar{3}}) + \Psi_{AB^\star}(S_0S_{\bar{2}}{}^{3})\right\} \tag{2.27}$$

Of course, the $M_S = 1$ state can be treated by a single determinant. We note that the condition for energy degeneracy of these spin multiplets defines the spin-coupling correlation energy of the TDF along with the PBE0 correlation energy.[8]

The calculated TEET excitonic couplings are shown in Fig. 2.6 for both the $M_S = 0$ and $M_S = 1$ triplet states. We first compare the "$1+1$", "BLW", and "relaxed" methods for $M_S = 1$ states and the BLE method for $M_S = 0$ states with the 6-31G(d) basis set. "$1+1$" means that the localized wave function is composed directly of the wave functions of two blocks. "Relaxed" means that the wave functions are relaxed without any restriction starting from BLW. The couplings of the "relaxed" method are the same starting either from BLW or "$1+1$". The couplings of "$1+1$", "BLW", and BLE methods have small differences because the polarization interaction between two blocks is small for the eclipsed naphthalene molecules at certain distances. The "relaxed" method did not give a smooth curve because the obtained wave function may deviate from the optimized state when the distance is less than 4.5 Å. Therefore, the "relaxed" method may not be stable when the interaction between two blocks is strong.

In contrast to SEET, where the computed transfer integrals do not show dependence on basis functions, Fig. 2.6 reveals that inclusion of diffuse functions in computing the EET coupling is critical. Charge transfer contributions are also important, enhancing the coupling term by a factor of 2 over that without including ICs. Both the perturbation approach and eigenvalue solution yielded similar results except at distances shorter than 3 Å. The coupling values obtained with diffuse functions decay exponentially, $V_{\mathrm{TEET}}\ e^{-\beta r}$, with β values of 2.48 $\mathrm{\AA}^{-1}$ without ICs, and 2.60 $\mathrm{\AA}^{-1}$ with the inclusion of ICs. These observations are consistent with the results reported in refs [109, 125, 126, 127, 128].

The exponential decay of the TEET coupling is similar to ET coupling because the TEET can be viewed as two electron exchanges with different spins.[15] We further calculated the couplings of ET and hole transfer (HT) at the aug-cc-pVDZ level from

Figure 2.6: Computed electronic coupling vs. monomer separation distance between two stacked locally excited naphthalene molecules in the first triplet state, both in the $M_S = 0$ and $M_S = 1$ spin-projection states. In all calculations, the hybrid PBE0 functional is used with basis functions indicated in the figure or in the text. T-SF with the 6-31G(d) basis set was used; IC-PT; IC-EIG; "1 + 1": localized state directly composed of fragment orbitals for the monomers in the triplet state; and "relax": variationally optimized locally excited states using the 6-31G(d) basis set. ICs were calculated using the aug-cc-pVDZ basis set. The exponential parameters in the figures are 2.60 Å^{-1} obtained using IC-EIG at distances of 3.5 to 7 Å and 2.48 Å^{-1} without ICs at distances of 2.5 to 7 Å.

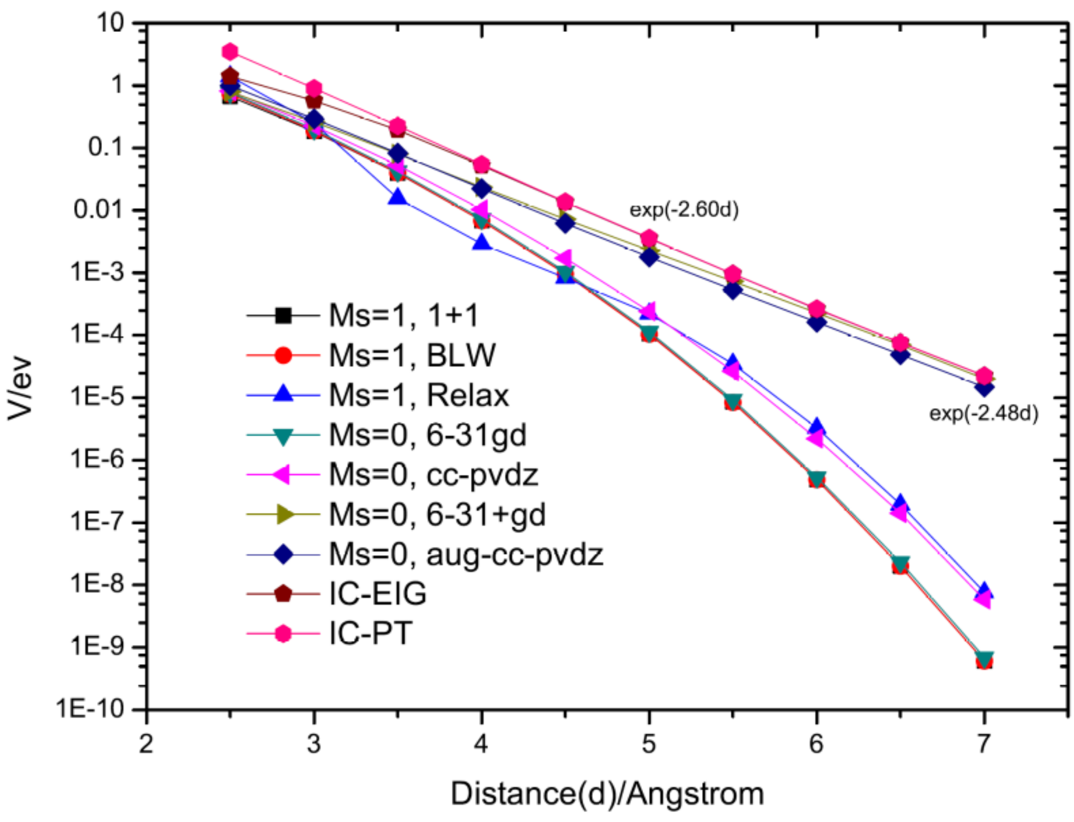

3.5 to 7 Å using MSDDFT for two naphthalene molecules. The β values of ET and HT are 1.00 and 1.45 Å^{-1}, respectively. Thus, the β value of TEET is almost the sum of the β values of ET and HT.

Equation 2.8 shows that the computed electronic coupling is proportional to the overlap of the two diabatic states when the overlap is small and orbital variations can be ignored.

$$V_{AB} = \frac{M_{AB}}{1 - M_{AB}^2}(F_{AB} - H_{AA}/2 - H_{BB}/2) \approx M_{AB}C_{AB} \tag{2.28}$$

The approximation $V_{AB} = CM_{AB}$, where M_{AB} is the overlap integral between determinants A and B, has been applied to ET.[129] This trend is indeed reproduced using MSDFT along with BLE states in Fig. 2.7, in which all methods exhibit nearly perfect linear regression ($R^2 > 0.99$ from exponential root-mean-square logarithmic error analysis).[129, 130]

2.5 Conclusions

In this chapter, we describe a BLE method on the basis of fragment-block localization and ΔSCF optimization such that a single-determinant representation for excited diabatic states can be approximated using density functional theory. We examined two optimization approaches to ensure the convergence of the block-localized molecular orbitals for a BLE, including a ΔSCF projection and an MOW technique. Within the framework of MSDFT, the use of the present BLE method in the construction of an effective, MAS is illustrated by the excimer complex formation of two naphthalene molecules both in the singlet and triplet states. Furthermore, excited energy transfer integrals in the singlet (SEET) and triplet (TEET) excited states of the naphthalene dimer are determined using block-localized excited diabatic states.

Numerical results show that the BLE method can provide a reasonable description

Figure 2.7: Correlations between the coupling constants and the wavefunction overlaps for TEET. The labels for all the curves are the same as those in Fig. 2.6.

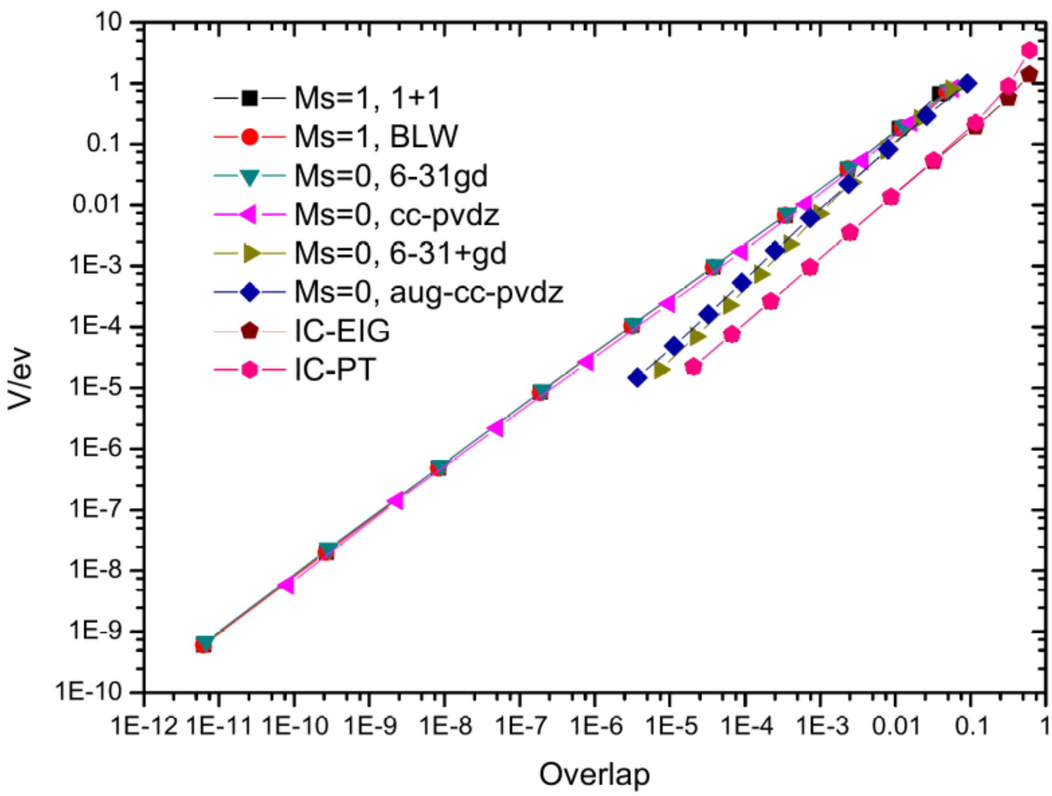

of the transfer integrals associated with excited energy transfer in the singlet and triplet states. Using an MAS of eight spin-adapted configurations, the present MSDFT method correctly produced qualitatively and quantitatively the trends of an energy-level inversion involving the two lowest singlet excited states $^1L_a^-$ and $^1L_b^-$, in good accordance with the DMRG-CASPT2 results. The latter approach used a large, complete active space of all 20 π electrons in 20 orbitals, consisting of more than $3 \cdot 10^{10}$ configurations. Yet, without perturbation correction, it was still not possible to produce the correct order, with the $^1L_b^-$ state below that of $^1L_a^-$ by as much as 1.6 eV for the excimer complex. Dynamic correlation proved to be absolutely critical to bring $^1L_a^-$ below $^1L_b^-$ in DMRG-CASPT2. The good performance of MAS-MSDFT in comparison with DMRG-CASPT2 illustrates the effectiveness of a DTS ansatz to reduce the size of the active space in excited state calculations. It should be reminded that the choice of an MAS is not necessarily a black-box approach and an understanding of the nature of the relevant excited states is required. The benefits of this representation include physical insights gained from a diabatic perspective and its connection to classical theories such as the Marcus theory for ET. Although the calculations were illustrated on a model system of two identical monomers, the method can certainly be applied to heterodimers and complex molecular blocks in photo-receptor proteins.[55, 56]

Chapter 3

Minimal-Active-Space Multistate Density Functional Theory for Excitation Energy involving Local and Charge Transfer States

This chapter is based on the publication [131]. I contributed by performing computations, analaying results and revising the manuscript.

3.1 Abstract

Multistate density functional theory (MSDFT) employing a minimum active space (MAS) is presented to determine charge transfer (CT) and local excited states of bimolecular complexes. MSDFT is a hybrid wave function theory (WFT) and density functional theory, in which dynamic correlation is first incorporated in individual determinant configurations using a Kohn–Sham exchange-correlation functional. Then, nonorthogonal configuration-state interaction is performed to treat static correlation. Because molecular orbitals are optimized separately for each determinant by including Kohn–Sham dynamic correlation, a minimal number of configurations in the active space, essential to representing low-lying excited and CT states of interest, is sufficient to yield the adiabatic states. We found that the present MAS-MSDFT method provides a good description of covalent and CT excited states in comparison with experiments and high-level computational results. Because of the simplicity and interpretive capability through diabatic configuration weights, the method may be useful in dynamic simulations of CT and nonadiabatic processes.

3.2 Introduction

Charge transfer (CT) states are electronically excited states which are of fundamental importance in materials and chemical processes, including those in photosynthesis, photoreceptor proteins, catalysis, and photovoltaic devices. Two questions are intertwined and need to be considered together:[132] (1) an accurate description of the electronic excitation of CT states and (2) an efficient and chemically intuitive representation of the potential energy surfaces for the subsequent nuclear dynamic simulations. In principle, high-level quantum-chemical methods can be used; however, in practice, it is often difficult to find an approach that can satisfy both requirements simultaneously. Furthermore, most computational models for excited states are based on multi-configuration self-consistent-field (MCSCF) approaches such as the complete-active-space self-consistent-field (CASSCF) method. Even at the simplest level of single-excitation configuration interaction (CIS) and linear-response time-dependent density functional theory (TDDFT), which is known to perform poorly on CT states, the large number of configurations included in these calculations makes the interpretation of CT states difficult.[133, 134, 135, 136] CT states are long-ranged and highly sensitive to donor-acceptor distance, typically having intersections with all local states in the form of both conical intersections and avoided curve crossings. Thus, the assignment of CT states can be difficult as shown in a recent study of bimolecular complexes that include inter-fragment CT interactions.[133, 137, 138] In this chapter, we present an approach that employs a minimal active space (MAS) in multistate density functional theory (MS-DFT) to treat CT states as well as local valence excitations on a range of bimolecular complexes. Importantly, the present method provides a straightforward interpretation of results.

For large chromophores of materials interest, TDDFT is a desired approach to model excited states and charge separation processes,[134, 139, 140, 141] and a number of developments have made these methods more reliable for treating CT states,[142, 143] including double hybrid functionals[144, 145] and range-separated techniques[146, 147] along with the optimization of the separation parameter specifically for a given system.[148, 149] Recent studies showed that restricted open-shell Kohn-Sham DFT and exciton models may present other ways of modeling CT states.[73, 66, 67, 68] Nevertheless, the performance of TDDFT on CT states is often system and functional-dependent,[134, 139, 141, 143, 147, 150] and it is not clear if a double hybrid functional is viable for treating large chromophores in photosystems.[145] It was pointed out that the uncertainties in TDDFT calculations demand benchmark tests to calibrate economic approaches for CT states.[133] To this end, a set of two-component molecular complexes that include local valence excitations and CT states has been investigated at the EOM-CCSDT (equation of motion coupled cluster with singles, doubles, and triples) and EOM-CCSDT-3 (iterative EOM-CCSDT) levels of theory.[133] Subsequently, the performance of a family of lower-cost CC models was evaluated, including EOM-CCSD (equation of motion coupled cluster with singles and doubles), CC2 (second-order approximations to CCSD), and ADC(2) (second-order algebraic diagrammatic construction) along with the third-order CC3 and non-iterative EOM-CCSD(T)(a)* alternatives.[133, 137] The test was further extended to the spin-component-scaled (SCS) CC2 and ADC(2), showing significant reduction in error over the original CC2 and ADC(2) calculations.[138]

MSDFT was developed for treating CT reactions such as proton-coupled electron transfer[57] and singlet fission of pentacene monolayer materials,[58] in which a balanced treatment of dynamic and static correlation is important.[7, 52, 8, 56] Our aim is to use a small set of localized configurations with well-defined physical properties, called diabatic states such as those in Marcus theory for electron transfer, to represent CT and excited states of molecular complexes.[9, 151] Consequently, charge-localized and locally excited diabatic states can be defined to form an active space of basis configurations.[26, 27] In addition, the method can be used as an interpretive tool in energy decomposition analysis to quantify CT energy and exciton coupling.[36, 152] MSDFT is a hybrid wave function theory (WFT) and DFT, in which dynamic correlation is modeled through a Kohn-Sham density functional at the level of each individual determinant.[7, 52] As a result, dynamic correlation is incorporated in each determinant configuration, and the energies of the adiabatic states are obtained by a “dynamic-then-static”[153, 154, 155] type of nonorthogonal state interaction (NOSI).[156, 157, 51, 34, 95] Coupled with separate optimizations of the orbitals in all determinant configurations, we anticipate that only a minimal number of basic configurations, essential to the problem of interest, is needed in MSDFT to treat low-lying valence and CT excited states. This expectation is confirmed in the present investigation.

For comparison, there has been much recent progress in the development of ensemble DFT (EDFT) based on a variational principle of statistical ensembles of ground and excited states,[158, 159, 160, 161, 162] where the excitation energies can be extracted. Although the use of an exact exchange approximation brings hope to model CT excitations,[163] practical applications have so far been scarce.[164] EDFT treats a collection of adiabatic states within the realm of KS-DFT without consideration of state interactions. On the other hand, adiabatic ground and excited states are obtained in MSDFT by NOSI in which dynamic contributions are introduced into electronic coupling.[52] To this end, a spin-restricted EDFT has been described, effectively introducing coupling by optimizing fractional occupations,[97, 165] and a DFT/MRCI method has been reported, which employs empirically scaled two-electron integrals.[166] There have also been a number of multiconfigurational DFT (MC-DFT) models in the literature.[167, 168, 169, 170, 171, 172] Among the early works of this category are those by Savin and coworkers, who used the on-top pair density to treat multi-determinant states[173] and introduced a local measure of density aimed at removing the fraction of correlation energy from the DFT functional that has already been expressed in the MCSCF wave function.[174] The latter approach has been extended to open-shell systems and multi-reference perturbation theory.[167, 168, 169] In this regard, MC-DFT also follows the KS approximation and, in practice, makes use of KS functionals with transformed densities. Common to all these methods is the use of a common set of orbitals for all states. In contrast, in MSDFT, the orbitals of each determinant state are separately optimized.

3.3 Results and Discussion

3.3.1 Theoretical Method

The energy density functional of MSDFT for the adiabatic ground and excited states is given by[7, 52]

$$E_I^{\mathrm{MS}}[\rho_I] = \sum_A c_{AI}^2 H_A[\rho_A] + 2\sum_{A>B} c_{AI}c_{BI}H_{AB}^{\mathrm{TDF}}[\rho_{AB}, \Psi_A, \Psi_B] \tag{3.1}$$

where $E_I^{\mathrm{MS}}[\rho_I]$ is the energy of adiabatic state I, $H_A[\rho_A]$ is the Kohn-Sham DFT energy for block-localized determinant A in the active space, corresponding to a diagonal matrix element of the NOSI Hamiltonian, $H_{AB}^{\mathrm{TDF}}[\rho_{AB}, \Psi_A, \Psi_B]$ is a transition density functional (TDF) of the off-diagonal matrix element, defining electronic coupling between states A and B, and the coefficients $\{c\}$ are obtained by solving the generalized secular equation $\mathbf{HC} = \mathbf{SCE}$. Formally, the determinant state Ψ_A is strictly defined by a constrained KS-DFT[175] whose constraining potential forces the KS-state to reproduce the energy of a contracted state of the full configuration interaction (FCI) wave function through singular value decomposition (SVD).[52] In the present study, $H_A[\rho_A]$ is approximated using block-local excited KS-DFT,[7] with the slight complication that nonorthogonal orbitals are employed.

The TDF of the off-diagonal matrix elements of the NOSI Hamiltonian H is new (absent in KS-DFT). Specifically, TDF can be separated into two terms: a wave function contribution between nonorthogonal KS-determinants Ψ_A and Ψ_B,[51, 34] and a TDF correlation energy E_{AB}^{TDF},[7, 52, 26, 27, 53]

$$H_{AB}^{\mathrm{TDF}} = \left\langle \Psi_A^{\mathrm{BLE}} \middle| \hat{H} \middle| \Psi_B^{\mathrm{BLE}} \right\rangle + E_{AB}^{\mathrm{TDF}}[\rho_{AB}, \Psi_A^{\mathrm{BLE}}, \Psi_B^{\mathrm{BLE}}] \tag{3.2}$$

where $\hat{H}$ is the electronic Hamiltonian, and ρ_{AB} is the transition density of determinants

Ψ_A and Ψ_B. E_{AB}^{TDF} has the formal definition as the difference between the electronic coupling of two SVD-contracted FCI states, denoted by $H_{AB}^{\mathrm{FCI-SVD}}$, and that of two constrained KS-determinants ($\left\langle \Psi_A^{\mathrm{BLE}} \left| H \right| \Psi_B^{\mathrm{BLE}} \right\rangle$).[52] Therefore, the MSDFT eigenstates in Eq. 3.1 would be exact in the sense that they would reproduce the FCI energies, had the exact constraining potential been known for each determinant.

In practical applications, the exact functional form of E_{AB}^{TDF}, just as the exchange-correlation functional in Kohn-Sham DFT, is unknown and an explicit approximate functional has not yet been developed. However, under special situations such as the present CT and local excitations involving spin coupling interactions, its value can be consistently determined with the Kohn-Sham exchange-correlation functional used to optimize the block-localized (a form of constrained) Kohn-Sham determinants Ψ_A and Ψ_B, avoiding or minimizing any double counting of electron correlation.[8, 96, 176] In particular, for spin-pairing interactions between two unpaired electrons, the TDF energy can be obtained by enforcing the degeneracy condition of spin components of the triplet states as proposed by Ziegler et al.,[176, 69]

$$E_{AB}^{\mathrm{TDF}}\left[\rho_{AB}, \Psi_{\uparrow\downarrow}, \Psi_{\downarrow\uparrow}\right] = E_c^{\mathrm{KS}}\left[\rho(\Psi_{\uparrow\uparrow})\right] - E_c^{\mathrm{KS}}\left[\rho(\Psi_{\downarrow\uparrow})\right] \tag{3.3}$$

where $\Psi_{\uparrow\downarrow}$ and $\Psi_{\downarrow\uparrow}$ are the determinants (A and B) of different spin combinations of two unpaired electrons,$E_c^{\mathrm{KS}}[\rho(\Psi_{\uparrow\uparrow})]$ and $E_c^{\mathrm{KS}}[\rho(\Psi_{\downarrow\uparrow})]$ are, respectively, the correlation energies of KS-DFT using the determinant for the high-spin (both spins up) determinant $\Psi_{\uparrow\uparrow}$ and a mixed-spin determinant $\Psi_{\downarrow\uparrow}$ (equally $\Psi_{\uparrow\downarrow}$).[8] This approach has been generalized to any spin coupling cases.[176] An example using a triplet reference for singlet-triplet splitting may be found in the spin-restricted density functional theory for biradicals.[97, 99] For other situations in this chapter, we used the overlap-scaled correlation energy to approximate the TDF energy for electronic coupling:

$$E_{AB}^{\mathrm{TDF}} = \frac{1}{2} S_{AB}^{\mathrm{KS}} \left[E_c^{\mathrm{KS}} \left(\rho_A \right) + E_c^{\mathrm{KS}} \left(\rho_B \right) \right] \tag{3.4}$$

where $S_{AB}^{\mathrm{KS}} = \langle \Psi_A | \Psi_B \rangle$, the overlap between two Kohn-Sham determinants.[7, 52] Throughout this study, we employed the Minnesota M06-2X functional,[177] denoted as MSDFT@M06-2X, and cc-pVDZ basis sets, which was used to match that in the work of Kozma et al. for comparison.[133, 138]

3.3.2 Charge Transfer Resonance States

Recently, we investigated the significance of CT stabilization of valence excited states on the naphthalene excimer complex using MSDFT[9] and introduced a block-localized excitation (BLE) technique to form the MAS. Here, we extend that study to the excimer complex of anthracene molecules and examine the effect of orbital overlap on CT resonance coupling by sliding a monomer along the direction of the long molecular axis (x-axis). First, there are two characteristic $\pi \rightarrow \pi^{\star}$ singlet excited states of linear polyacenes, corresponding to the L_a state (Platt notation or ${}^1\mathrm{B}_{2u}$),[178, 179, 180] predominantly of HOMO $\rightarrow$ LUMO character with a transition density from the ground state that is polarized along the short y-axis, and the L_b (${}^1\mathrm{B}_{3u}$) states, which is a mixture of HOMO $\rightarrow$ LUMO $+ 1$ and HOMO $- 1 \rightarrow$ LUMO transitions. For benzene and naphthalene, the L_b state is lower than L_a, but the order is reversed for anthracene and larger polyacenes.[179, 181] Similar to the naphthalene excimer,[9] we include three (3) locally excited configurational state functions (CSF) for each monomer, corresponding to HOMO $\rightarrow$ LUMO, HOMO $\rightarrow$ LUMO $+ 1$, and HOMO $- 1 \rightarrow$ LUMO excitations, and a pair of inter-fragment CT states to describe the low-energy states.[182] Thus, the present MAS in MSDFT calculations consists of eight spin-adapted CSFs plus the

Figure 3.1: Computed potential energy curves for the anthracene excimer. Shown are the adiabatic ground state (E_g), the in-phase and out-phase combinations of locally excited singlet (L_a^+ and L_a^-) and triplet (T^+ and T^-) states, stabilized by mixing with the resonance states of forward and backward charge transfer states. Vertical gray lines indicate the position of the shown structures on the abscissa. Energies are given in electron volts relative to the separated monomers in the ground state.

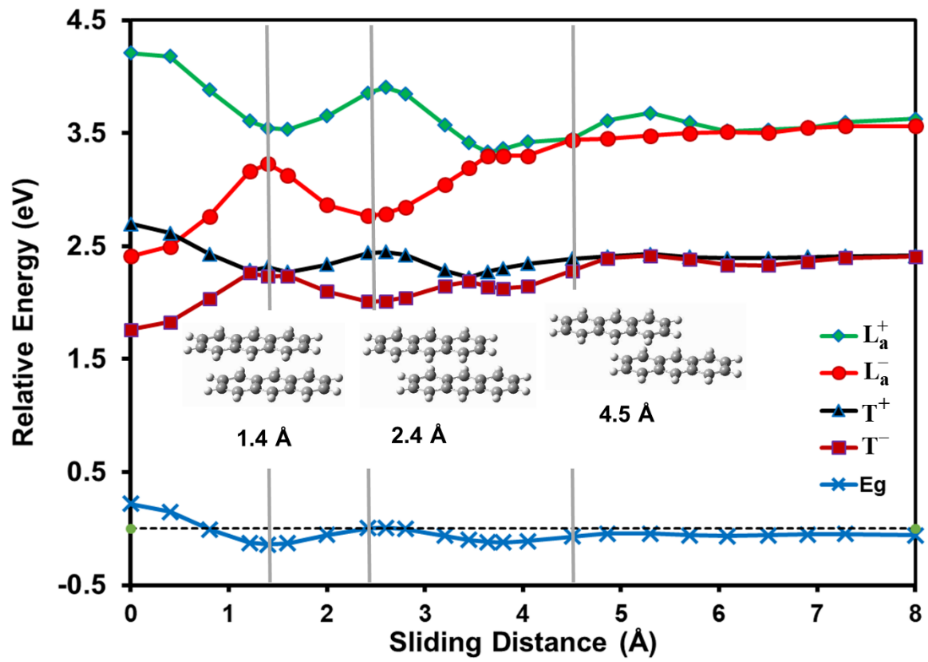

Kohn-Sham ground state. The monomer geometry in the ground state, optimized using B3LYP/aug-cc-pVTZ, is used and the monomers are placed at the face-to-face configuration at a separation of 3.2 Å, close to the minimum distance of the first singlet excimer complex.[77] Since L_b is little affected by the CT states,[9] we focus on the singlet L_a and triplet states in the discussion of anthracene excimer.

Depicted in Fig. 3.1 are the potential energy curves along the x-axis for the singlet (L_a^- and L_a^+) and triplet (T^- and T^+) states of anthracene dimer, corresponding to the out-phase and in-phase combinations of the monomer singlet L_a and triplet states. First, the computed vertical excitation energies of anthracene are 3.66 eV for the singlet

L_a state and 2.47 eV for the triplet state. A recent quantum Monte Carlo calculation yielded vertical excitation energy of 3.64 eV for the L_a state.[183] The computed adiabatic transitions are 3.40 and 2.06 eV, respectively, which may be compared with the corresponding experimental values of 3.43 and 1.85 eV.[184, 185] Clearly, the adiabatic triplet state is sensitive to geometry relaxation, suggesting that the energy curves of the triplet states may be overestimated by about 0.4 eV in Fig. 3.1.[184, 185]

The minimum-energy arrangement of both the singlet and triplet state of the anthracene excimer is in the face-to-face configuration (Fig. 3.1). The two local (monomer) $^1B_{2u}(L_a)$ states and two triplet states respectively interact to yield a pair of in-phase (L_a^+ and T^+) and of out-phase (L_a^- and T^-) exciton combinations. Importantly, the forward and backward CT resonance states are strongly mixed with the valence exciton states, leading to a binding energy of -1.25 eV for the L_a^- state and of -0.58 eV for the T^- state. Without including CT stabilization, the exciton coupling of two local $^1B_{2u}$ states only produces resonance energy of just -0.38 eV (30 %) in the singlet state and the coupling between two local triplet states results in a net repulsive interaction by 0.08 eV, consistent with the findings in the naphthalene excimer.[9] For comparison, binding energies of 1.72 and 1.09 eV, respectively, for the singlet and triplet excimers have been reported from a scaled-opposite-spin (SOS) CIS(D_0) calculation.[77] The importance of CT states has been attributed to account for the ultrafast conversion of singlet fission in pentacene monolayer materials.[58]

Figure 3.1 reveals that the anthracene excimer has a singlet-triplet energy gap of 0.65 eV between the L_a^- and T^- states, which is in good accord with a computational value of 0.63 eV using the SOS-CIS(D_0) method.[77] The singlet-triplet energy gap is significantly reduced in the excimer complex relative to that of the monomer (1.19 eV) because the CT resonance states strongly enhance exciton coupling of local excitations, stabilizing the L_a^- state and giving rise to a large energy separation between L_a^- and

L_a^+ On the other hand, CT stabilization of the triplet state is smaller than that of the L_a state, leading to a differential singlet-triplet energy gap. The effect of orbital phase-matching on the singlet-triplet gap is illustrated in Fig. 3.1 as the two monomers are slid along the x-axis. At a sliding distance of 1.4 Å relative to the face-to-face configuration (Fig. 3.1), the overlap between the two locally excited states reaches a minimum, at which point the exciton coupling has weak interactions, reducing L_a^- L_a^+ splitting to only 0.32 eV. This represents a net reduction by 1.48 eV relative to the exciton coupling (1.80 eV) in the face-to-face configuration. The origin of the large variation of exciton coupling along the molecular long axis can be attributed to reduced CT mixing with the local valence states from the analysis of structure weight. It is interesting to note that the singlet-triplet gap increases at this distance as a result of the opposite trend between L_a^- and T^+ (Fig. 3.1).Three periods of oscillations are clearly seen in the L_a^- and L_a^+ coupling, corresponding to maximum overlaps of three, two, and one aromatic rings. Exciton coupling diminishes beyond about 6 Å, about half-ring left in dimer overlap, which is in good accord with a study of substituted anthracene excimers using TDDFT.[186] Note that although the T^- state oscillates synchronously with the L_a^- state, the variation of the T^+ state follows reciprocally, leading to a curve crossing with L_a^- at about 0.9 Å.

An understanding of electronic coupling in terms of phase-matching of conjugated molecular fragments can be useful in developing materials that exhibit singlet fission and thermally activated delayed fluorescence (TADF) for applications in highly efficient organic light-emitting diodes (OLEDs).[187, 188] Overall, this example illustrates the effectiveness of a dynamic-then-static ansatz[27] coupled with NOSI for a balanced treatment of dynamic and static correlation involving CT states.[7, 52] Furthermore, the M06-2X density functional is adequate to describe both local valence and inter-fragment CT states as well as their interactions.

3.3.3 Charge Transfer States of Aryl-Tetracyanoethene Complexes

To further validate the performance of MAS-MSDFT@M06-2X, we examine the computed excitation energies of five bimolecular complexes that have a CT state as the lowest singlet excited state. These bimolecular complexes consist of one tetracyanoethene (TCNE) molecule and one aryl donor: benzene, toluene, *o*-xylene, naphthalene, and anthracene. This set of compounds has been used by Baer and coworkers to illustrate the optimization of system-specific range-separation parameters to improve the performance of TDDFT for CT states,[148] and by others to validate the performance of new density functionals.[189] In MSDFT, each bimolecular complex is partitioned into two monomer fragments, and the MAS includes a total of five local (monomer) valence excitations (four single excitations of the aromatic compounds involving HOMO, HOMO - 1, LUMO, and LUMO + 1, plus one local $\pi \rightarrow \pi^{\star}$ excitation of TCNE) and three CT states (HOMO and HOMO - 1 of the aryl molecules to the LUMO of TCNE and one backward CT from TCNE to an aryl compound), along with the ground state. Although local valence excitations are included in the present calculation, there is little mixing with CT states, except in the narrow regions of (avoided) curve crossings along the direction of inter-fragment separation, if the inter-fragment distance is varied (not shown). Since we are not aware of prior computational results nor experimental data available for these valence excitations of the excimer complexes, both TDDFT and MSDFT results are given in Supplementary Table 1 of Ref. [131]. Further, for these complexes, we have also used the hybrid PBE0 and B3LYP functionals with the cc-pVDZ and cc-pVTZ basis sets, and the results are given in Supplementary Table 3 of Ref. [131], which show similar performance as the M06-2X model. The molecular geometries used in the work of Stein et al. are adopted here,[148] and the BLE approach was used to optimize the fragmental block-localized Kohn-Sham orbitals of each configuration.[9]

The computed excitation energies are listed in Table 3.1, along with TDDFT results

Table 3.1: Computed first and second excitation energies (in eV) of aryl$\cdots$tetracyanoethene complexes in the gas phase along with experimental data.

Aryl-TCNE-complex	M06-2X	BNL[a]	BNL(γopt)[a]	CAM-QTP-02[b]	MSDFT @M06-2X	Expt.[c]
Benzene	2.99, 3.04	4.4	3.8	3.85	3.66, 3.74	3.59 (3.67)
Toluene	2.74, 2.94	4.0	3.4	3.50	3.28, 3.63	3.36 (3.35)
o-Xylene	2.48, 2.78	3.7	3.0	3.25	3.07, 3.32	3.15 (3.15)
Naphthalene	1.94, 2.73	3.3	2.7	2.80, 3.57	2.69, 3.43	2.60, 3.23
Anthracene	1.89, 2.94	2.6	2.1		1.62, 2.90, 3.73[d]	1.73, 2.79[e]

[a]ref. [148].
[b]ref. [189].
[c]ref. [190] and data in parentheses from ref. [191].
[d]Values reduced by 0.3 eV for solvent effects estimated in ref. [148].
[e]in CH_2Cl_2 solution, ref. [192].

from the M06-2X and the CAM-QTP-02 functionals,[189] and the default and optimized range-separated (γopt) BNL functional[148] for comparison with experimental data.[190, 191, 192] Each of the aromatic compounds consists of two orbitals, HOMO and HOMO - 1, close in energy (degenerate in benzene), resulting in two close-lying CT states from MSDFT and TDDFT calculations. In most complexes, only one broad peak was observed experimentally, but in some cases, two distinctively resolved peaks can be detected.[190, 191, 192] Thus, the average values of the two CT states are compared with experiments with a single resolvable peak, whereas two excited states in the naphthalene and anthracene complexes are used since they were resolved experimentally. Standard Kohn-Sham functionals severely underestimate the excitation energies of inter-fragment CT states, although the M06-2X functional exhibits smaller errors than B3LYP.[148] The default parameter for range-separation in the BNL functional overestimates the first CT excitation energies. However, after this parameter was specifically optimized for each complex to treat CT states, a good agreement with experiments ($\pm$0.2 eV) was obtained.[148] In the present study, by virtue of block-localization in MSDFT,[9, 26, 27] the limits of ionization potentials (IP) and electron affinities (EA) of each monomer at long inter-fragment separation are rigorously maintained - an important criterion for properly describing CT states. The performance of MSDFT on CT states for the molecular complexes is deemed sufficient because of a root-mean-square deviation (RMSD) of 0.12 eV and a mean signed error (MSE) of 0.08 eV between MSDFT@M06-2X/cc-pVDZ calculations and experiments for the seven resolvable CT states (Table 3.1). The use of a cc-pVTZ basis shows similar trends, but the energies are underestimated by about 0.1 to 0.2 eV (Supplementary Table ł1). For comparison, TDDFT calculations using the latest version of ionization potential-fitted CAM-QTP-02 functional with the cc-pVTZ basis set gave MSE and RMSD errors of 0.21 and 0.34 eV for these compounds (without anthracene).[189]

In the anthracene-TCNE complex, a second absorption peak was found in the UV range with transition energy of 2.79 eV in dichloromethane solution; however, its origin was uncertain and it was assumed to be due to CT from the HOMO - 1 of anthracene to TCNE.[192] We found that the HOMO $- 1 \rightarrow$ TCNE CT transition occurs at a higher energy of 4.03 eV in the gas phase, which is separated from the first CT excitation by two local valence excitations (3.20 and 3.61 eV) of the anthracene molecule in the bimolecular complex. Even with the inclusion of solvent effects, estimated to be about 0.3 eV,[148] the reduction of the excitation energy is not sufficient to bring the second CT excitation down below 3 eV. Further, TDDFT using the M06-2X functional works very well for this complex, yielding CT energies of 1.89 and 3.55 eV, along with two valence excitations at 2.94 and 3.52 eV, consistent with MSDFT results (Supplementary Table ł1). Therefore, the near UV band of the anthracene-TCNE complex observed experimentally[192] can be assigned to a local valence excitation of the complex. Overall, the good agreement between MSDFT@M06-2X and experimental results suggests that the present MAS configurations are adequate for modeling CT states, which is further evaluated both on valence and CT states of the bimolecular complexes benchmark.[133]

3.3.4 Local and Charge Transfer States of Bimolecular Complexes

Table 3.2: Excitation energies (eV) of local ($1 \rightarrow 1$ or $2 \rightarrow 2$) and charge transfer ($1 \rightarrow 2$ or $2 \rightarrow 1$) states computed using EOM-CCSDT (EOM-CCSDT-3 for acetone-nitromethane and pyrrole-pyrazine complexes) and MAS-MSDFT using the M06-2X functional, along with charge character (ω_{CT}) determined at the EOM-CCSD level and Chirgwin-Coulson structure weight (W_{CT}) of charge transfer configuration from MSDFT.

Complex ($1 \cdots 2$) and CT state[a]		excitation[b]	State[c]	EOM-CCSDT[d]	MSDFT	ω_{CT}[e]	W_{CT}
$H_3N \cdots F_2$		$2 \rightarrow 2$	$1\,^1$E	3.97	4.31		
	CT1	$1 \rightarrow 2(1)$	$2\,^1A_1$	6.64	6.37	0.76	0.96
		$2 \rightarrow 2$	$2\,^1$E	NA	7.22		
		$1 \rightarrow 1$	$3\,^1A_1$	7.98	7.82		
		$2 \rightarrow 1$	BCT		15.7		1.00
$Me_2CO \cdots F_2$		$1 \rightarrow 1$	$2A''$	4.39	4.30		
		$2 \rightarrow 2$	$2A'$	4.18	4.42		
		$2 \rightarrow 2$	$1A''$	4.19	4.43		
	CT2	$1 \rightarrow 2$	$3A''$	5.85	5.83	0.96	1.00
		$2 \rightarrow 1$	BCT		14.1		1.00

Table 3.2: (continued)

Complex ($1 \cdots 2$) and CT state[a]	excitation[b]	State[c]	EOM-CCSDT[d]	MSDFT	ω_{CT}[e]	W_{CT}
Pyrazine $\cdots F_2$	$2 \rightarrow 2$	$2A_1$	4.16	4.41		
	$2 \rightarrow 2$	$2B_1$	4.19	4.42		
	$1 \rightarrow 1$	$3A_1$	4.28	4.28		
	$1 \rightarrow 1$	$2B_1$	4.99	4.48		
	$1 \rightarrow 1$	$1A_2$	5.04	5.26		
	$1 \rightarrow 1$	$1B_2$	5.81	5.69		
CT3	$1 \rightarrow 2$	$2B_2$	6.28	6.27	0.98	1.00
CT4	$2 \rightarrow 1(2)$	$2A_2$	6.45	6.32	0.64	0.97
$H_3N \cdots OF_2$	$2 \rightarrow 2$	$2A'$	4.20	3.42		
	$2 \rightarrow 2$	$1A''$	4.93	4.85		
	$2 \rightarrow 2$	$2A''$	6.64	5.01		
	$2 \rightarrow 2$	$3A'$	6.83	5.36		
CT5	$1 \rightarrow 2(1)$	$4A'$	7.04	7.07	0.86	0.92
	$2 \rightarrow 2$	$3A''$	7.11	7.97		
	$1 \rightarrow 1(2)$	$5A'$	7.96	7.62	0.04	0.08
	$2 \rightarrow 1$	BCT		13.6		1.00
$Me_2CO \cdots MeNO_2$	$2 \rightarrow 2$	2A	4.04	4.18		
	$1 \rightarrow 1$	3A	4.42	4.48		
	$2 \rightarrow 2$	4A	4.43	5.05		
CT6	$1(2) \rightarrow 2$	5A	6.42	6.51	0.80	0.94
	$2(1) \rightarrow 2$	6A	6.58	6.33	0.20	0.06
	$2 \rightarrow 1$	BCT		9.48		

Table 3.2: (continued)

Complex $(1 \cdots 2)$ and CT state[a]	excitation[b]	State[c]	EOM-CCSDT[d]	MSDFT	ω_{CT}[e]	W_{CT}
Pyrazine $\cdots NH_3$	$1 \rightarrow 1$	$2A'$	4.35	4.26		
	$1 \rightarrow 1$	$1A''$	4.99	4.56		
	$1 \rightarrow 1$	$2A''$	5.08	5.30		
	$1 \rightarrow 1$	$3A'$	5.88	5.68		
	$1 \rightarrow 1$	$3A''$	6.83	6.49		
	$1 \rightarrow 1$	$4A'$	7.04	7.03		
CT7	$2 \rightarrow 1(2)$	$5A'$	7.49	7.72	0.63	0.71
	$2 \rightarrow 2(1)$	$6A'$	7.80	7.32	0.27	0.29
	$2 \rightarrow 1(L+1)$	CT		8.37		1.00
	$1 \rightarrow 2$	BCT		9.89		1.00
H-bonded Pyrrole-pyrazine	$2 \rightarrow 2$	$1B_2$	4.38	4.38		
	$2 \rightarrow 2$	$1B_1$	5.01	4.59		
	$2 \rightarrow 2$	$1A_2$	5.22	5.42		
CT8	$1 \rightarrow 2$	$2B_1$	5.27	5.53	1.00	1.00
CT9	$1 \rightarrow 2$	$2A_1$	6.00	6.39	0.97	1.00
	$2 \rightarrow 2$	$2B_2$	6.01	5.74		
CT10	$1 \rightarrow 2$	$3A_1$	6.17	6.42	0.99	1.00
	$1 \rightarrow 1$	$4A_1$	6.50	6.70		
	$2 \rightarrow 1$	BCT		11.3		1.00

Table 3.2: (continued)

Complex (1 ⋯ 2) and CT state[a]		excitation[b]	State[c]	EOM-CCSDT[d]	MSDFT	ω_{CT}[e]	W_{CT}
Stacked Pyrrole-pyrazine		$2 \rightarrow 2$	2A′	4.33	4.25		
		$2 \rightarrow 2$	3A′	4.98	4.49		
		$2 \rightarrow 2$	1A″	5.09	5.22		
	CT11	$1(2) \rightarrow 2$	2A″	5.48	5.33	0.84	0.76
		$2(1) \rightarrow 2$	3A″	5.90	5.83	0.23	
	CT12	$1(2) \rightarrow 2(1)$	4A′	6.07	6.19	0.66	0.86, 0.09
	CT13	$2(1) \rightarrow 1(2)$	5A′	6.34	6.55	0.61	0.87, 0.09
TFE ⋯ ethene (5 Å)		$1(2) \rightarrow 1(2)$	$1B_2$	7.43	7.60		
		$2(1) \rightarrow 2(1)$	$1B_1$	8.61	8.14		
	CT14	$1 \rightarrow 2$	$5B_1$	10.57	10.40	0.99	1.00
		$2 \rightarrow 1$	BCT		10.68		1.00

[a]The set of 14 CT states in reference [133] are specifically indicated in the first column.
[b]The parentheses in the "excitation" column denote *minor* contributions from the other monomer to the initial and/or final orbitals for states of mixed local and CT character.
[c]BCT is the backward charge transfer relative to the direction of CT states labeled in the first column.
[d]Excitation energies were determined for all complexes using EOM-CCSDT, except acetone-nitromethane and pyrrole-pyrazine complexes for which EOM-CCSDT-3 was used.[133]
[e]Determined at the EOM-CCSD level of theory.

We next turn to a set of two-component molecular complexes that have been established using EOM-CCSDT or EOM-CCSDT-3 in ref. [133] (Table 3.2). In this dataset, each bimolecular complex is comprised of two different compounds from a list of nine molecules: F_2, NH_3, OF_2, $CH_2 = CH_2$, $CF_2 = CH_2$, $(CH_3)_2C = O$, CH_3NO_2, pyrrole, and pyrazine. In MSDFT calculations, each bimolecular complex is divided into two monomer blocks as in the aryl-TCNE complexes. A MAS of locally excited and inter-fragment CT configurations is defined as follows: only single excitations involving key frontier orbitals (Supplementary Computational Procedureł) of each monomer ($1 \rightarrow 1$ and $2 \rightarrow 2$), called local excitations, are included along with one forward ($1 \rightarrow 2$) and one backward ($2 \rightarrow 1$) CT state. In particular, for NH_3, $CH_2 = CH_2$, $CF_2 = CH_2$, and pyrrole, we include only HOMO $\rightarrow$ LUMO excitations, whereas both $n \rightarrow \pi^\star$, and $\pi \rightarrow \pi^\star$ excitations are selected in acetone and nitromethane, noting that there are two $\pi \rightarrow \pi^\star$ configurations in nitromethane from the in-phase and out-phase combinations of the oxygen lone pairs. For F_2, all four π $(\pi_x, \pi_y, \pi_x^\star, \text{and}\, \pi_y^\star) \rightarrow \sigma^\star$ excitations are used, and we adopted eight CSF for both pyrazine and OF_2, due to excitations from two π and two lone pair orbitals, respectively, to two $\pi^\star$ orbitals, and to two $\sigma^\star$ orbitals. For the $H_3N \cdots F_2$ complex, we also examined the effect of two double excitations of F_2, but they only have a minimal effect (about 0.1 eV) on the computed excitation energies (Supplementary Tableł 2). These locally excited configurations are chosen to correspond to the valence states in the dataset of Kozma et al.[133, 137, 138] Therefore, the largest number of excited configurations in the present MAS-MSDFT calculations is 14 for the pyrazine-F_2 complex. All states in an MAS are spin adapted in this study. A full list of orbitals used to define these local single-excitations of all compounds are given in the Supplementary Computational Procedure.

Overall, for the fourteen CT states (Table 3.2) of the Kozma dataset, the mean error of MAS-MSDFT using the M06-2X functional is 0.06 eV and the RMSD is 0.19 eV relative to values determined by CCSDT(CCSDT-3). The excitation energies of CT states are slightly overestimated using MAS-MSDFT, but the overall agreement with results at the CCSDT level is good. Table 3.2 also includes 39 of the 41 local valence excited states in that dataset,[133] omitting two high-energy local excitations of TFE $\cdots$ ethene that are not represented in an MAS with just four configurations in the present study. In comparison with EOM-CCSDT and EOM-CCSDT-3 results, the mean error for the local excitations of the bimolecular complexes is -0.12 eV and the RMSD is 0.48 eV.

The somewhat large statistical error is clearly due to a systematic underestimate of the valence excitation energies of one compound, OF_2 (Table 3.2).[133] This deviation is due to the functional used which may be related to the particular optimization of the density functional. Without this complex, the mean and RMSD errors from the CCSDT (CCSDT-3) dataset are reduced to -0.04 and $0.29\,\text{eV}$, respectively. This agreement with EOM-CCSDT results is reasonable considering the simplicity of a small active space used in MSDFT calculations, and considering that this, in turn, enables a straightforward interpretation of adiabatic energies directly from its diabatic origin using Chirgwin-Coulson configuration weight.

3.3.5 Significance of Coupling Between Charge Transfer and Valence Excited States

A major difficulty in the study of CT states[133, 137, 138] was its assignment from multi-configurational calculations. Often, visual inspection of natural orbitals of the difference density is made, but a set of numerical descriptors have recently been introduced on the basis of one-electron transition density.[135, 136] In the latter analysis, the descriptor ω_{CT} specifies CT character in terms of the weight of contributions with charge separation in some predefined fragments. A ω_{CT} value of 0 corresponds to a local excitation, whereas a CT state is indicated by a value close to 1. ω_{CT} is very effective in cases where CT states can be clearly identified; however, about one third of the complexes in the benchmark set have strong mixing between a CT state and local excitations, making classification of CT state difficult.[133, 137] Two bimolecular complexes, $NH_3 \cdots F_2$ and $CF_2 = CF_2 \cdots CH_2 = CH_2$, were especially highlighted in the work of Kozma et al.[133, 137] In the former complex, we included a second local excitation that was not listed in the original dataset (Table 3.1). In the latter complex, an inter-fragment separation of 5 Å (rather than its optimal geometry at 3.5 Å) was used to clearly separate

Figure 3.2: Potential energy curves of the adiabatic ground state, the first three singlet valence excited states, and the NH_3 to F_2 charge transfer state as a function of $N-F$ distance (Å) of the $NH_3 \cdots F_2$ complex. All calculations are performed using MSDFT with the M06-2X functional and cc-pVDZ basis set and energies are given relative to the fully separated monomers. The first two excited states consist of two degenerate states and adiabatic states are labeled corresponding to those at long inter-fragment distances, which are different at short distances.

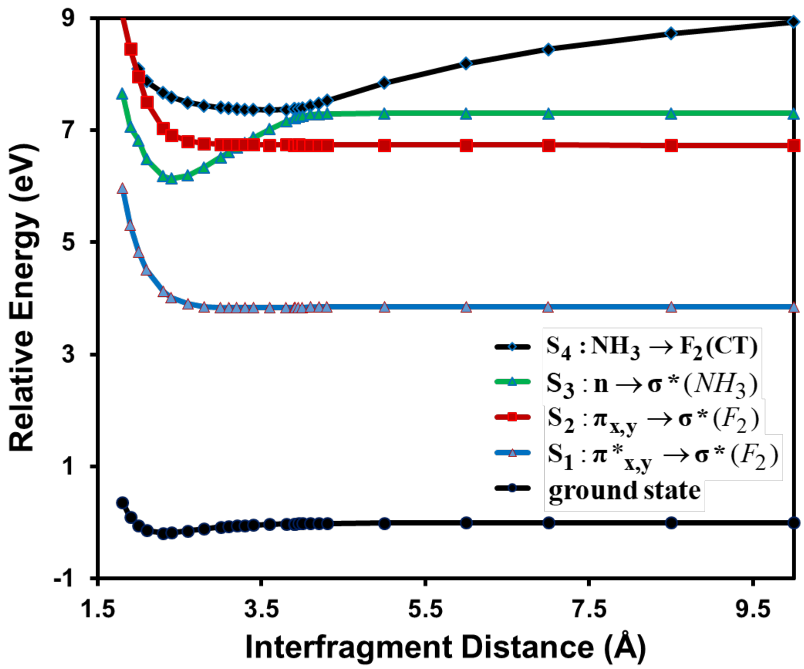

ionic and covalent states. In these cases, the geometries at which avoided crossings occur and their energy gaps are sensitive to the level of theory used.[137]

In MSDFT, the basic configurations in the MAS are strictly localized diabatic and effective valence-bond (VB) states by construction,[52, 26, 27] whose contributions to an adiabatic state can be determined by Chirgwin-Coulson structural weights,[51, 34, 193] and the position of the diabatic state crossing point can be used to define the geometry of an avoided crossing between two interacting adiabatic states.[57, 194] Figure 3.2 shows the potential energy curves of the ground and the first four singlets excited states

Figure 3.3: Potential energy curves of adiabatic (solid curves) and diabatic states (dotted curves) of $NH_3 \rightarrow F_2$. The curve crossing region in Fig. 3.2 is displayed. Diabatic states are determined by using the generalized diabatic at construction (GDAC) method for the $NH_3 \rightarrow F_2$ charge transfer and local transitions of $n \rightarrow \sigma^\star$ in NH_3 and the ${}^1\Pi_g$ state $(\pi_x, \pi_y \rightarrow \sigma^\star)$ in F_2. Three adiabatic potential energy curves are shown as a function of $N - F$ distance in the $NH_3 \cdots F_2$ complex.

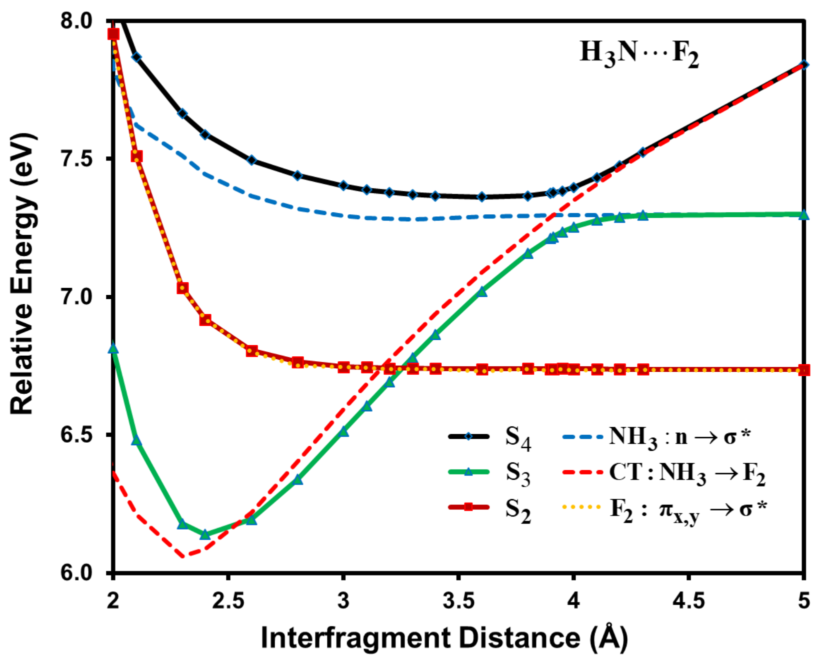

of $NH_3 \cdots F_2$ as a function of $N-F$ distance. A clear feature of a CT state corresponding to NH_3 to F_2 transition can be observed by its strong dependence on inter-fragment separation, consistent with that reported previously.[137] In the region between 3 and 4 Å, the CT state crosses the $2\,{}^1E$ state, a doubly degenerate local F_2 excitation, and the $2\,{}^1A_1$ state, a local excitation of ammonia, resulting in an allowed crossing at 3.3 Å and one avoided crossing of an energy gap of 0.14 eV. The corresponding orthogonalized diabatic states determined by the generalized diabatic at construction (GDAC) method,[27] along with the adiabatic curves, in the avoid crossing regions are depicted in Fig. 3.3, revealing the rapidly switching character of ionic and valence excited states. Interestingly, the N − F distance at the crossing point between the diabatic states corresponding to the CT state and the NH_3 local excited state is located at 3.9 Å, slightly shorter than that (4.0 Å) of the smallest energy gap between the adiabatic curves. This may be compared with a value of about 3.75 Å determined using EOM-CCSDT.[137] Kozma et al. found that the second-order CC2 method yielded an unusually long crossing distance at about 5.3 Å with a tiny energy gap, while the non-iterative CCSD(T)(a)* method gives the same geometry as that of CCSDT, but the energy gap was underestimated for lack of a proper diagonalization.[137]

For the CT state of the $NH_3 \cdots F_2$ complex (CT1) at the optimal structure, the excitation energy of 6.64 eV (6.28 eV with cc-pVTZ basis) was assigned based on charge character analysis using CCSD results.[133] For comparison, the present MSDFT calculations yielded a value of 6.36 eV with a dominant CT structural weight of 0.96. The energy of the $^1\Pi_g$ state of F_2 (a $\pi \rightarrow \sigma^\star$ excitation) determined by using MSDFT@M06-2X is about 1 eV higher than that using CCSDT (ca. 5.7 eV), placing the CT state below that of the $2\,^1$E valence state. However, due to the mixing between CT and locally excited states in this case, the classification of a CT state is ambiguous, and the $2\,^1$E state was not listed in the dataset of Kozma et al.[133] The lower energy value from CCSDT calculations was attributed to contributions from double excitation. However, the inclusion of HOMO to LUMO double excitations has little effects in the present MSDFT calculation (Supplementary Tableł 2). Nevertheless, a previous MRSDCI calculation predicted a value of 7.24 eV for this state, similar to the present calculation, and was assigned to a broadband of 6.5 to 7.5 eV from experiment.[195] This difference further highlights the sensitivity of state assignments; there is little uncertainty in assigning CT states in the present MSDFT approach since CT diabatic states are defined by construction in the MAS and they have well-defined configuration weights in each adiabatic state.[193]

Figure 3.4: Chirgwin–Coulson structure weights of locally excited and charge transfer (CT) configurations. Shown in the top panel are the two lowest singlet valence excited states and the bottom figures exhibit two charge transfer states as a function of inter-fragment distance (Å) between tetrafluoroethene (1) and ethene (2). The M06-2X density functional and cc-pVTZ basis set are used in MSDFT calculations, including four configuration state functions.

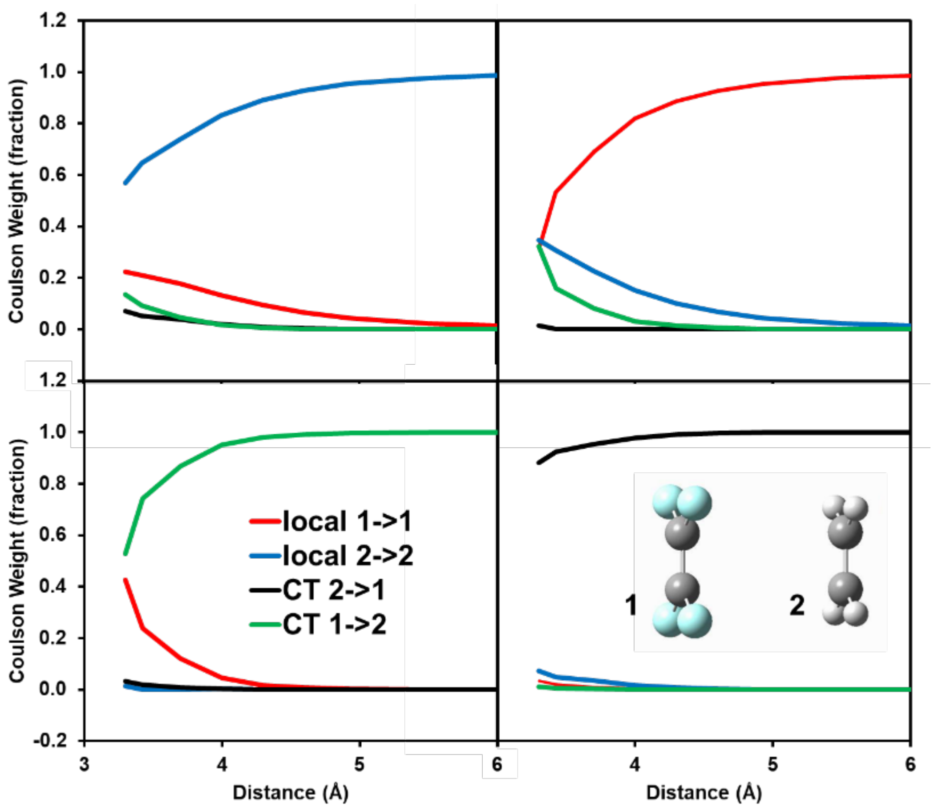

For the tetrafluoroethene (TFE) $\cdots$ ethene complex, which was used as a test case for CT states in a number of previous studies,[142, 143, 147, 150, 189] It was not possible to clearly isolate the CT state in the optimal geometry since local excited states and CT states are strongly coupled.[133] Consequently, a structure at an inter-fragment separation of 5 Å was used, which shows a ω_{CT} value of 0.99. Figure 3.4 displays the Chirgwin-Coulson structure weights for the two lowest singlet states and the forward (ethene to TFE) and backward (TFE to ethene) CT states. The decrease of the dominant weight towards short distances in each of the four states shows a strong coupling between the locally excited $\pi \rightarrow \pi^{\star}$ resonance state and the ethene to TFE CT state at short distances. Strong mixing between local and CT states close to the optimal dimer geometry illustrates the difficulty to clearly assign a CT state using these structures.[133] Coupling interactions to CT states vary quickly with the change of inter-fragment distance; however, resonance delocalization interactions between the two $\pi \rightarrow \pi^{\star}$ states can persist at much longer separations (see the top row of graphs in Fig. 3.4). For the monomer species, we obtained vertical excitation energy of 8.2 and 7.5 eV for ethene and TFE (complex structure), which may be compared, respectively, with previous computational results of 8.4 eV from EOM-CCSDT-3[196] and 7.0 eV from SAC-CI,[197] indicating that the present MAS is sufficient to model these low-lying states.[73, 9]

It is of interest to comment on the three CT states of the pyrrole $\cdots$ pyrazine complexes. For the side-by-side hydrogen-bonded structure, the computed Chirgwin-Coulson structure weights provide a clear identification of the three CT states, CT8, CT9, and CT10 in Table 3.2, corresponding to nearly 100 % contributions due to specifically HOMO(pyrrole) $\rightarrow$ LUMO(Pyrazine), HOMO(pyrrole) $\rightarrow$ LUMO + 1(Pyrazine), and HOMO $-$ 1(pyrrole) $\rightarrow$ LUMO(Pyrazine) CT. Similarly, the ω_{CT} values were found in the range of 0.97 to 1.00 for these states.[133, 138] However, in the π-π stacked configuration, strong resonance couplings among the CT states as well as covalent excited configurations are involved. The lowest ionic state CT11 (Table 3.2) is mixed with 24 % of local $n \rightarrow \pi^{\star}$ valence excitations of pyrazine, and the CT component itself is a mixture between HOMO(pyrrole) $\rightarrow$ LUMO + 1(Pyrazine) and HOMO $-$ 1(pyrrole) $\rightarrow$ LUMO(Pyrazine) transitions. The next (local valence) excitation contains 23 % ionic character. For comparison, the CT11 state has a ω_{CT} value of 0.84 from analysis of the EOM-CCSD results. The difference between the structure weight and ω_{CT} value could be due to a slight shift in geometry that has the largest coupling with CT state by different methods (MSDFT vs. CCSD) or could be the difference is the analysis method itself. MSDFT calculations show that CT12 and CT13 states are CT resonance states between HOMO(pyrrole) $\rightarrow$ LUMO + 1(Pyrazine) and HOMO − 1(pyrrole) $\rightarrow$ LUMO(Pyrazine) configurations, plus a small amount of about 5 % of local excitations. These two states are more than 95 % CT character according to their Chirgwin-Coulson structure weights. However, transition density indices are ambiguous, showing just 61 to 66 % of ionic character.[133, 138]

In summary, the performance of MSDFT employing a MAS on local excited and inter-fragment CT states has been examined on a series of bimolecular complexes. MSDFT is a hybrid WFT and DFT, which follows a dynamic-then-static ansatz.[153, 154, 155] In MSDFT, dynamic correlation is first included via block-localized KS-DFT, and the orbitals are separately optimized for each determinant configuration. This is followed by a NOSI calculation to incorporate static correlation and to yield the adiabatic states.[52] Because of these two factors, it is expected that a small number of configurations would be sufficient to model low-lying local excited states and CT states.[9, 151] In this chapter, we used a MAS consisting of singly excited configurations of key frontier orbitals plus forward and backward CT configurations. Using the Minnesota M06-2X density functional for each determinant configuration, we found that the present MAS-MSDFT method can provide a good description of CT states as well as the exciton resonance of local excited states. The computational cost of MSDFT is comparable to M separate KS-DFT optimizations (M is the number of determinants in an MAS), which can be performed independently in parallel, plus evaluation of the nonorthogonal off-diagonal matrix elements. Although the examples illustrated in this study featured separate monomers, a procedure similar to the projected hybrid orbital method for combined QM/MM calculations can be extended to treat fragments separated by covalent bonds. Due to the simplicity and interpretive power through energy decomposition analysis and determination of configuration weights,[36] the present method may be useful for direct dynamic simulations of nonadiabatic processes, and analyses of CT contributions to exciton coupling can be useful in the study of materials exhibiting TADF in future applications.

3.4 Methods

3.4.1 Computational Details

The anthracene monomer structure was optimized with the $D_{2\mathrm{h}}$ symmetry using Gaussian 16 at the B3LYP/aug-cc-pVTZ level of theory. Then, the monomer structure was kept fixed and used to construct face-to-face dimer configurations at a separation of 3.2 Å. Then, one monomer was slid along the long molecular axis up to 8 Å. Single-point energy calculations were performed using MSDFT, for which a total of 16 block-localized configurations (to form eight CSFs) plus the adiabatic ground state have been obtained using block-localized Kohn-Sham DFT. Geometries for the aryl-TCNE complexes were adopted from ref. [148, 149] and the structures for the remaining bimolecular complexes are taken directly from the work of Kozma et al.[133]

The computational procedure of MSDFT consists of two steps. First, a set of individually optimized determinant states are obtained to form a spin-adapted active space. Then, in the second step, NOSI is performed to yield the adiabatic ground and excited state energies. Here, we emphasize "state interaction" because on top of each determinant configuration, dynamic correlation is included via block-localized (constrained) KS-DFT. An analogy in WFT is a class of perturb-then-diagonalize methods. In particular, for local excitations of each monomer in a complex, the separately optimized open-shell singlet determinants with $\alpha\beta$ and $\alpha\beta$ spin combinations were checked to converge to the same set of block-localized orbitals, and the orbitals were optimized using the method described in ref. [9]. The spin-coupled singlet and triplet states ($M_S = 0$) were obtained by switching the α and β electron spins of an open-shell configuration to yield a pair of spin-coupled determinants. The all-spin up triplet configuration ($M_S = 1$) at each geometry was then obtained by a separate open-shell calculation. The energies for the $M_S = 1$ and $M_S = 0$ states were matched to yield the transition correlation energy contribution E_{AB}^{TDF} (the TDF correlation) in spin-pair coupling interactions according to Eq. 3.3.[8, 176]

The energies for the diabatic states were determined using the GDAC method.[27] The Minnesota M06-2X density functional along with the cc-pVDZ basis functions are used in all calculations except that for the aryl-TCNE complexes where the PBE0 and B3LYP functionals and the cc-pVTZ basis set were also used. Additional details are summarized in the Supplementary Information.

The MSDFT method described in this chapter has been implemented in a locally modified version of the GAMESS-US program,[107] with which all calculations have been performed.

Chapter 4

Excimer Energies

This chapter is based on the publication [198]. I contributed by running calculations, analyzing results and revising the manuscript.

4.1 introduction

Energy decomposition analysis (EDA) is a useful tool for understanding intermolecular interactions.[199, 36, 200] Although methods for molecular complexes in the ground state have been thoroughly developed,[201, 202, 203, 204, 205, 206, 207, 208, 209, 210, 211, 212, 213, 214, 215, 216, 217, 218, 219, 220, 221, 44, 222, 223, 33, 224, 225, 226, 227, 228, 229, 230, 175, 231, 232, 233, 234, 235, 236, 237, 238, 239, 240, 241, 242, 243, 244, 245, 246, 247, 248, 249] few approaches are currently available for analyzing energy terms of excimers and exciplexes – molecular aggregates formed in the electronic excited states. One exception is a study by Ge et al.,[250, 251] who used the same energy terms in ground-state EDA,[36, 243] including frozen (froz), polarization (pol), and charge transfer (CT) terms, to describe intermolecular interactions (int) in the excited states $\Delta E^{\star}_{\text{int}} = \Delta E^{\star}_{\text{froz}} + \Delta E^{\star}_{\text{pol}} + \Delta E^{\star}_{\text{CT}}$. The method was introduced on the basis of configuration interaction with singly excitations (CIS), in principle, extendable to time-dependent density functional theory (TDDFT) for excited-state calculations. In particular, the frozen excitation energy was obtained with the use of fixed orbitals of each isolated fragment along with its excitation amplitudes, and frozen interactions were modeled through the merged Fock matrix. Similarly, polarization contribution was determined with the relaxed, fragment block-localized molecular orbitals (BLMO) also called absolutely localized MOs.[221, 44, 223, 33, 38] The CT term was simply the difference between the excitation energy of the full complex and the other two terms. The study was extended to excimers with the addition of an exciton splitting term between the frozen excited states.[252] That work provided an analysis of excited-state interactions from a ground-state analogy. On the other hand, it is of interest to define variationally optimizable diabatic states,[35, 26, 27] such as the local excitations of individual chromophores in the presence of other molecules in the ground state. Electronic coupling interaction among local states can be used to determine the rates of excited-state energy transfer such as light-harvesting in photosynthesis and perception,[55, 56, 253, 254] photoexcitation-induced oxidation-reduction reactions, and processes in photovoltaic devices and fuel cells.[58] In this chapter, we introduce an alternative, multistate energy-decomposition analysis (MS-EDA) for an excimer complex-excited-state complex formed between the same chemical species. We focus on energy terms unique to excited states, including local excitation, exciton excitation ΔE_{Ex}, resonance stabilization due to superexchange ΔE_{SE}, and orbital and configuration-state delocalization ΔE_{OCD}. The method is illustrated on the acetone and pentacene excimers, relevant to chemiluminescence and singlet fission in materials for solar cells.[58, 255]

4.2 Theory

Considering the following photochemical process of excimer formation,

$$X + Y \xrightarrow{h\nu^K} X + Y^\star \xrightarrow{\Delta E_b^K} (XY)^\star \tag{4.1}$$

we define the total formation energy, or binding energy, of the excimer $(XY)^\star$ in its Kth excited-state relative to that of two separate molecules in the ground state (Eq. 4.1) as follows:

$$\Delta E_b^K = E_{(XY)^\star}^K[\Psi_{(XY)^\star}^K] - E_X^0[\Psi_X^0] - E_Y^0[\Psi_Y^0] - h\nu^K \tag{4.2}$$

where the superscript "0" denotes the energy and wave function of a molecule in the ground state, $E_{(XY)^\star}^K$ is the energy of the Kth excited state of the excimer $(XY)^\star$, characterized by the wave function $\Psi_{(XY)^\star}^0$, and $h\nu^K$ is the external photoenergy of chromophore excitation. Although the main goal of this study is concerned with excimers, we nevertheless use different symbols X and Y to denote the two interacting molecules for convenience of discussion. Thus, the theory is generally applicable to exciplexes in which $X \neq Y$. Also, the method can easily be generalized to any number of molecules, suitable for the treatment of delocalized, exciton-resonance excitation of extended materials and biological light-harvesting systems.

4.3 Multistate Energy Decomposition Analysis (MS-EDA)

We partition the total binding interaction energy of an excimer complex (Eq. 4.2) in its Kth excited state into the following terms:

$$\begin{aligned}\Delta E_b^K =& \Delta E_{\text{Lint}}[(X \bullet Y)] - h\nu_{\text{ex}}^K + \Delta E_{\text{Ex}}^K[(X \bullet Y)^\star] \\ &+ \Delta\Delta E_{\text{SE}}^K[(X^\pm \bullet Y^\mp)^\star] + \Delta\Delta E_{\text{OCD}}^K[(XY)^\star]\end{aligned} \tag{4.3}$$

where $E_{\text{Lint}}[(X \bullet Y)]$ denotes the local interaction energy between monomers X and Y in the ground state, $\Delta E_{\text{Ex}}^K[(X \bullet Y)^\star]$ is the excitation energy of the Kth exciton state (Ex) due to resonance delocalization of local, monomer excitations, $\Delta\Delta E_{\text{SE}}^K[(X^\pm \bullet Y^\mp)^\star]$ specifies the effect of interfragment charge-transfer configurations called superexchange stabilization (SE), and $\Delta\Delta E_{\text{OCD}}^K[(XY)^\star]$ represents the energy change due to orbital and configuration-state delocalization (OCD) by expansion from monomer BLMOs to the full molecular space. The sequence of intermediate states (Eq. 4.3) depicted in Scheme 4.2 have well-defined wave functions (or Kohn-Sham states) which can be variationally optimized, and the decomposed energy terms sum up exactly to the definition of Eq. 4.2.

Figure 4.1: Scheme detailing the Multistate Energy Decomposition Analysis (MS-EDA) of the Excimer Binding Energy ΔE_b The top row corresponds to the physical process of excimer formation (Eq. 4.2). The remaining illustration highlights each energy term defined by Eq. 4.3 and their progressive change in MS-EDA. The shapes of objects represent molecular geometries, while different colors depict the corresponding wave functions with boundaries shown for block-localization. All wave functions can be variationally optimized. The local excited in pink (Lex) and charge transfer diabatic states in light yellow background denote the minimum active space (MAS) for the exciton and super-exchange states. The energy changes are defined by Eq. 4.4 for the local interaction energy ΔE_{Lint}, Eq. 4.6for the exciton excitation energy ΔE_{Ex}, Eq. 4.9 for the super-exchange stabilization energy ΔE_{SE}, and Eq. 4.10 for the orbital and configuration delocalization effects ΔE_{OCD}. The definition of the respective wave functions can also be found in these equations.

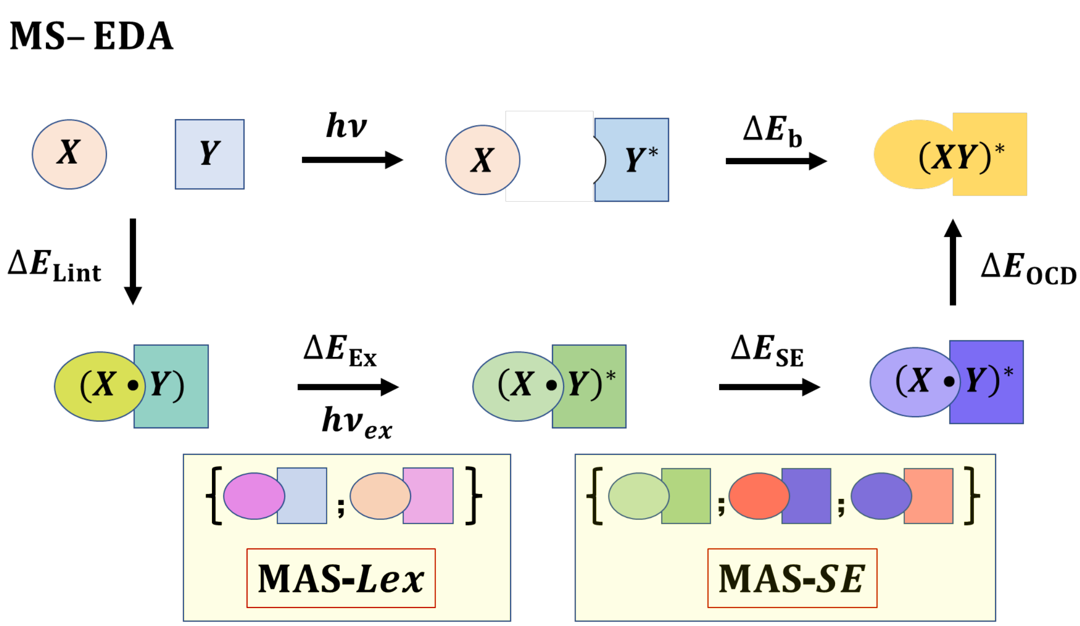

4.3.1 Local Interaction Energy in the Ground State

For analysis of excited-state energies in MS-EDA, we focus on the energy terms that are directly related to the excimer complex. Therefore, all energy contributions that can be associated with intermolecular interactions between monomers X and Y in the ground state are grouped into a single term called local interaction (Lint) energy in MS-EDA.

$$\Delta E_{\mathrm{Lint}}[(X \bullet Y)] = E_{(X \bullet Y)}[\Psi_{(X \bullet Y)}] - E_X^0[\Xi_X^0] - E_Y^0[\Xi_Y^0] \tag{4.4}$$

where Ξ_X^0 and Ξ_Y^0 are Kohn-Sham determinants for molecules X and Y in isolation in their equilibrium geometries, the notation $(X \bullet Y)$ separating monomers X and Y by the symbol "•" represents a block-localized bimolecular complex, and the parentheses indicate that the product wave function of the monomers (ground or excited states) is antisymmetrized, e.g., $\Psi_{(X \bullet Y)} = \hat{A}\Psi_X \Psi_Y$. This convention is used throughout this chapter. We note that the molecular geometry used to determine $E_{(X \bullet Y)}[\Psi_{(X \bullet Y)}]$ is that of the excimer complex, not the structure optimized for the ground state.

The term "block-local" refers to the strict localization of molecular orbitals (block-localized molecular orbital "BLMO")[33] in WFT or Kohn-Sham orbitals in DFT (block-localized Kohn-Sham "BLKS") in the complex $(X \bullet Y)$.[7] They are strictly localized within the two individual molecular fragments because BLMOs are expanded over basis orbitals on the atoms in each monomer.[33] $\Delta E_{\mathrm{Lint}}[(X \bullet Y)]$ includes classical Coulomb interaction, quantum-mechanical exchange-repulsion, and polarization energies, plus the energy change from the equilibrium geometries of isolated monomers to that in the excimer. This classification follows exactly the convention used in the BLW-ED analysis, similar to other ground-state EDA models.[36, 33, 243] It is identical to the total binding energy of the complex (XY), at the given geometry, without the charge-transfer term.[36] Since these are ground-state properties which have been thoroughly explored in the past,[36, 200, 215, 221] we do not further separate and discuss them in this chapter. Specific details may be found in references [36, 33, 243].

4.3.2 Exciton Excitation Energy

According to Frenkel exciton model,[256] the resonance excitation (exciton) of an extended system (excimer in this chapter) results from the interaction of locally (monomer) excited states. The wave function for this intermediate state, or simply an exciton state, denoted as $(X \bullet Y)^{\star}$, is determined by nonorthogonal state interaction (NOSI)[176, 131] in multistate density functional theory (MSDFT):[257, 258]

$$\Psi^{K}_{(X\bullet Y)^{\star}} = a_{1K}\Psi^{K_X}_{(X^{\star}\bullet Y)} + a_{2K}\Psi^{K_Y}_{(X\bullet Y^{\star})} \tag{4.5}$$

where the superscript specifies the Kth excited state of the exciton, $\Psi^{K_X}_{(X^{\star}\bullet Y)}$ and $\Psi^{K_Y}_{(X\bullet Y^{\star})}$ represent, respectively, the wave functions of the two locally excited monomers in the presence of the other species in the ground state $\Psi^{K_X}_{(X^{\star}\bullet Y)} = |\Phi_{X^{\star}}\Theta_Y\rangle$ and $\Psi^{K_Y}_{(X\bullet Y^{\star})} = |\Phi_X\Theta_{Y^{\star}}\rangle$, and a_{1K} and a_{2K} are the state coefficients. The states K_X and K_Y of $\Psi^{K_X}_{(X^{\star}\bullet Y)}$ and $\Psi^{K_Y}_{(X\bullet Y^{\star})}$ correspond to those that contribute to the exciton state K. Note that $\Psi^{K_X}_{(X^{\star}\bullet Y)}$ and $\Psi^{K_Y}_{(X\bullet Y^{\star})}$ themselves, in fact, are generally multiconfigurational wave functions, and more than one state from each monomer may contribute.

The energy difference between the exciton state and the block-localized molecular complex, i.e., the exciton-excitation energy $\Delta E^{K}_{\mathrm{Ex}}$, corresponds to the transition from the ground state of the monomer complex $(X\bullet Y)$ to the exciton resonance state $(X\bullet Y)^{\star}$:

$$\Delta E^{K}_{\mathrm{Ex}} = E^{K}_{(X\bullet Y)^{\star}} - E_{(X\bullet Y)} \tag{4.6}$$

where $E^{K}_{(X\bullet Y)^{\star}}$ and $E_{(X\bullet Y)}$ are the energies of the Kth exciton state $\Psi^{K}_{\mathrm{Ex}} \equiv \Psi^{K}_{(X\bullet Y)^{\star}}$ and the ground state $\Psi_{(X\bullet Y)}$, respectively.

The wave function for the exciton state (Eq. 4.5) can be variationally optimized by using a multiconfiguration self-consistent-field (MCSCF) approach or configuration interaction such as CIS and nonorthogonal configuration interaction (NOCI), also called mixed molecular orbital and valence bond (MOVB) in WFT.[51, 34] Alternatively, the energies can be obtained from multistate SCF (MS-SCF)[6] and NOSI methods in MSDFT. NOSI is used in the present study, in which we first determine the locally excited states for monomer $X^\star$ in the presence of Y in its ground state and monomer $Y^\star$ in X, respectively, using the block-localized excitation (BLE) method to variationally optimize $\Psi^{K_X}_{(X^\star \bullet Y)}$ and $\Psi^{K_Y}_{(X \bullet Y^\star)}$ along with the M06-2X functional.[9, 151, 177] Then, we construct the Hamiltonian matrix functional, and the state coefficients a_{1K} and a_{2K} in Eq. 4.5 are obtained by diagonalizing the NOSI Hamiltonian matrix.[7]

Importantly, the structure weight for each of the locally excited states in the resonance exciton state can be evaluated according to the Chirgwin-Coulson scheme:[193]

$$W^K_{X^\star} = a^2_{1K} + a_{1K}a_{2K}S_{12} \tag{4.7a}$$

$$W^K_{Y^\star} = a^2_{2K} + a_{1K}a_{2K}S_{12} \tag{4.7b}$$

where S_{12} is the overlap integral between the two locally excited states:

$$S_{12} = S_{21} = \int dr \Psi^{K_X}_{(X^\star \bullet Y)} \Psi^{K_Y}_{(X \bullet Y^\star)}$$

4.3.3 Charge Transfer States and Superexchange Energy

The exciton states above from state interactions among locally excited monomers do not explicitly account for charge-transfer (CT) delocalization in the full system. Often, the energies of CT states between monomers X and Y are high relative to valent excitations, but they, nevertheless, play an important role in stabilizing the excited complex. If the two monomers are symmetrically equivalent, there is no net charge transfer, but the stabilization energy due to the resonance between CT configurations can still be significant. Such a resonance effect is also called a superexchange (SE) interaction in electron transfer theory,[259] which is adopted here. The charge-resonance SE states are given by $\Psi_{\mathrm{SE}} = b_2'|X^+ \bullet Y^-\rangle \pm b_3'|X^- \bullet Y^+\rangle$, or simply denoted by $\Psi_{\mathrm{SE}} = b_2'\Psi_{\mathrm{FCT}} \pm b_3'\Psi_{\mathrm{BCT}}$ between the $X \to Y$ forward (FCT) and $Y \to X$ backward (BCT) CT states.

Here, we define the SE-stabilized intermediate state by the wave function

$$\Psi_{\mathrm{SE}}^{K} = b_1\Psi_{(X\bullet Y)^\star}^{K} + b_2\Psi_{\mathrm{FCT}} \pm b_3\Psi_{\mathrm{BCT}} \tag{4.8}$$

where different coefficients for the two CT states have been used in case $X \neq Y$, in which a single, directional CT state may dominate in an exciplex complex. In this regard, it is of interest to distinguish the term charge transfer, representing a specific, directional CT diabatic state, from superexchange which describes a physical property, a resonance-stabilization interaction of the intermediate state. In Eq. 4.8, we have assumed that the order of excited states has not changed due to mixing with the CT states. This assumption is purposely for the convenience of expression; in practice, the correct state must be matched at different decomposition steps.

The net stabilization energy due to the admixture between the exciton and SE states is called the superexchange energy $\Delta E_{\mathrm{SE}}^{K}$:

$$\Delta\Delta E_{\mathrm{SE}}^{K} = E_{\mathrm{SE}}^{K}[\Psi_{\mathrm{SE}}^{K}] - E_{\mathrm{Ex}}^{K}[\Psi_{(X\bullet Y)^\star}^{K}] \tag{4.9}$$

Analogous to the exciton intermediate state, $\Psi_{\mathrm{Ex}}^{K} = \Psi_{(X\bullet Y)^\star}^{K}$ and its energy can be obtained from NOCI in WFT and NOSI in MSDFT.[257, 6] In principle, TDDFT and an MCSCF method could be used in both exciton and superexchange steps, but it can be rather complicated with nonorthogonal orbitals between different fragment blocks. This is easily accomplished in MSDFT employing NOSI.[9, 151]

4.3.4 Orbital Delocalization

So far, the wave functions (or Kohn-Sham determinants) for the intermediate states have been constructed on the basis of fragmental BLMOs. Although incorporation of the SE effects introduces charge delocalization, the charge density is generally not sufficiently relaxed. Furthermore, the intermediate states decomposed at this point may have not included all configurational state functions used to determine the energies of the adiabatic excimer complex $(X \bullet Y)^\star$. Therefore, in the final step of the MS-EDA method, we release the monomeric block-localization constraints and use the fully delocalized molecular orbitals to obtain the energies of the excited states for the excimer complex. These states are denoted as $\Psi^K_{(XY)\star}$ without the dot "•" separating monomers X and Y. The energy change in this step is called orbital and configuration-state delocalization (OCD) energy, analogous to, but different from, the CT energy term in ground-state EDA models since additional configurational state functions may also be included in the final step.

$$\Delta E^K_{\mathrm{OCD}} = E^K_{(XY)\star}[\Psi^K_{(XY)\star}] - E^K_{\mathrm{SE}}[\Psi^K_{\mathrm{SE}}] \tag{4.10}$$

The present MS-EDA method includes three computational steps: (1) the calculation of excitation energies of monomers, (2) the determination of the reference states for energy analysis for block-localized intermediate states, and (3) the evaluation of excitation energies of the fully delocalized dimer complex. The results from both steps (1) and (3) can be validated by comparison with results from TDDFT or MCSCF calculations as well as experimental data. TDDFT is adopted in this chapter to determine the excitation energies of the excimers. Thus, MS-EDA may be regarded as an analytical tool to interpret the numerical results from TDDFT calculations.

The adiabatic ground and excited states as well as all intermediate states for energy analysis are obtained from NOSI in multistate density functional theory. NOSI differs from nonorthogonal CI (NOCI) in that dynamic correlation is included in the basis states in the first place. Lu and Gao proved that the Hamiltonian in the subspace spanned by the lowest N eigenstates is a matrix functional $\boldsymbol{\mathcal{H}}[\mathbf{D}(\mathbf{r})]$ of the multistate density $\mathbf{D}(\mathbf{r})$,[257] extending Hohenberg-Kohn theorems for the ground state to any number of N states in MSDFT. Significantly, it was proven that $\mathbf{D}(\mathbf{r})$ can be represented by no more than N^2 determinants, defining an upper bound for the number of determinants in an active space,[257] i.e., a minimal active space (MAS),[176, 131, 6] in excited-state DFT calculations. $\mathbf{D}(\mathbf{r})$ can be variationally optimized by minimizing the trace of $\boldsymbol{\mathcal{H}}[\mathbf{D}(\mathbf{r})]$. Then, diagonalization of $\mathcal{H}$ yields the exact energies for all N adiabatic ground and excited states, provided that the exact correlation matrix functional is known (the Lu-Gao theorems established its existence).[257] As in Kohn-Sham DFT, approximate correlation matrix functionals must be used in MSDFT calculations. The accuracy of the present MSDFT-NOSI method can be validated by comparison with results from TDDFT on systems that it is adequate as in the present case, employing the same correlation density functional.[176, 131]

We focus on the lowest excited states of a monomer species and their interactions in the excimer complex. For the monomers and block-localized excitations in dimers in this chapter, we found that it is sufficient to just include 5 spin-adapted configurations in the MAS, consisting of the reference (ground) state from KS-DFT and four singly excited configurations from the two highest occupied KS orbitals (HOMO) to the two lowest unoccupied KS orbitals (LUMO). Each of the singly excited KS-determinants is optimized using the BLE technique, a form of ΔSCF method capable of block-localized constraints on the orbitals in the dimer case.[9, 151]

Before presenting the MS-EDA results, we outline the procedure for determining the elements of the Hamiltonian matrix functional $\boldsymbol{\mathcal{H}}[\mathbf{D}(\mathbf{r})]$. In particular, the diagonal elements $\mathcal{H}_{AA}[\mathbf{D}(\mathbf{r})]$ are given by the KS-DFT energies of the corresponding determinants for the block-localized, excited configurations as well as that of the Kohn-Sham ground state.

$$\mathcal{H}_{AA} = E_A^{\mathrm{KS}}(\Xi_A) \tag{4.11}$$

where Ξ_A is a determinant constrained to a given orbital occupation, including both the ground-state and excited configuration. Specifically, the constrained BLKS-determinant wave function for the block-localized dimeric configuration $(X \bullet Y)$ is written as follows:

$$\Xi_{(X\bullet Y)}^{\mathrm{KS}} = \hat{A}\left\{(\xi_1^X \cdots \xi_{N_X}^X) \bullet (\xi_1^Y \cdots \xi_{N_Y}^Y)\right\} \tag{4.12}$$

where $\hat{A}$ is the antisymmetrizer and ξ_j^U is the jth block-localized spin-orbital of fragment $U(U \in \{X, Y\}$, and N_U is the number of electrons. For the four singly excited states in the MAS, one of the two highest occupied orbitals is replaced by one of the two lowest unoccupied orbitals, and Ξ_A is optimized individually using the BLE method for the nonaufbau configurations.[9] Note that "state" in this chapter refers to a spin-adapted wave function representing the exact density by incorporating dynamic correlation with BLKS-DFT; it is different from a determinant configuration.

The transition density functional (TDF),[52] i.e., the correlation energies for the off-diagonal matrix elements of $\boldsymbol{\mathcal{H}}[\mathbf{D}(\mathbf{r})]$, can be determined rigorously among spin-complement configurations to yield the spin-adapted states. For example, the TDF correlation energy for the spin-adapted singlet state is obtained in an NOSI calculation with the constraint that the energy of the triplet state $|1, 0\rangle$ is identical to that of the $|1, 1\rangle$ state.[176, 8, 96] Notice that the latter can be adequately represented by a single determinant, exact in KS-DFT if the KS exchange-correlation functional is exact. Thus, given an approximate density functional approximation used for $\mathcal{H}_{AA}[\Xi_A^{\uparrow\downarrow}]$ and $\mathcal{H}_{BB}[\Xi_B^{\uparrow\downarrow}]$ where the arrows indicate the spin of the coupled electrons, the electronic coupling $\mathcal{H}_{AA}[\rho_{AB}]$ to yield the singlet spin-adapted state is uniquely determined by

$$\begin{aligned}\mathcal{H}_{AA}[\rho_{AB}] =& \langle \Xi_A^{\uparrow\downarrow}|\hat{H}|\Xi_B^{\downarrow\uparrow}\rangle \\ &+\frac{1}{2}\Big\{E_{\mathrm{c}}^{\mathrm{KS}}[\rho_T(\Xi_T^{\uparrow\uparrow})] - E_{\mathrm{c}}^{\mathrm{KS}}[\rho_A(\Xi_A^{\uparrow\downarrow})]\Big\}\end{aligned} \tag{4.13}$$

where $E_{\mathrm{c}}^{\mathrm{KS}}[\rho_T(\Xi_T^{\uparrow\uparrow})]$ and $E_{\mathrm{c}}^{\mathrm{KS}}[\rho_A(\Xi_A^{\uparrow\downarrow})]$ are the correlation energies from KS-DFT using the spin-up triplet determinant $\Xi_T^{\uparrow\uparrow}$, and the spin-mixed determinant $\Xi_A^{\uparrow\downarrow}$ (equivalent with $\Xi_B^{\downarrow\uparrow}$ here).

For the remaining off-diagonal matrix elements, an approximate TDF is needed to account for the dynamic correlation in the electronic coupling between two interacting states. Unlike KS-DFT, an approximate TDF is currently not yet available. In this study, we use an overlap-weighted average correlation energy from KS-DFT for the two individual states Ξ_A and Ξ_B to approximate the TDF correlation term:[7]

$$\begin{aligned}\mathcal{H}_{AA}[\mathbf{D}(\mathbf{r})] =& \langle \Xi_A^{\mathrm{KS}}|\hat{H}|\Xi_B^{\mathrm{KS}}\rangle \\ &+\frac{1}{2}S_{AB}^{\mathrm{KS}}\Big\{E_{\mathrm{c}}^{A}[\rho_A(\Xi_A^{\mathrm{KS}})] + E_{\mathrm{c}}^{B}[\rho_B(\Xi_B^{\mathrm{KS}})]\Big\}\end{aligned} \tag{4.14}$$

where $\langle \Xi_A^{\mathrm{KS}}|\hat{H}|\Xi_B^{\mathrm{KS}}\rangle$ is obtained using the two BLKS determinant wave functions,[51, 34, 260] Ξ_A^{KS} and Ξ_B^{KS}, for configurations A and B, S_{AB}^{KS} is their overlap integral, and $E_{\mathrm{c}}^{A}[\rho_A]$ and $E_{\mathrm{c}}^{B}[\rho_B]$ are the corresponding correlation energies from the KS approximate density functional. The approximation of Eq. 4.14 is the main source of error in MS-EDA.

4.4 Computational Details

The MS-EDA method has been implemented in the Qbics program in our laboratories[261] and a separate BLW-ED program[36] interfaced with the GAMESS-US package.[107] The method and energy terms are illustrated by two excimer complexes: the asymmetric excimer complex of two acetone molecules (Fig. 4.2A), and the pentacene dimer in three different geometry arrangements, including the optimized S_1 excimer, the stacked configuration of two pentacene monomers separated by 3.3 Å, each in the ground-state geometry, and the fishbone configuration in the crystal used in an application to singlet fission (Fig. 4.2B).[58] MSDFT-NOSI and TDDFT calculations were carried out using the Minnesota M06-2X density functional[177] along with the cc-pVDZ

Figure 4.2: Structures and orbital of excimer complexes. (A). Shown are the optimized structure and the highest singly occupied orbital for the acetone S1 excimer. (B). Three configurations of pentacene dimer are used in the study, corresponding to the optimized S1 excimer structure, the on-top stacked configuration of two ground-state pentacene molecules, and a fishbone relative orientation from a pentacene crystal structure.

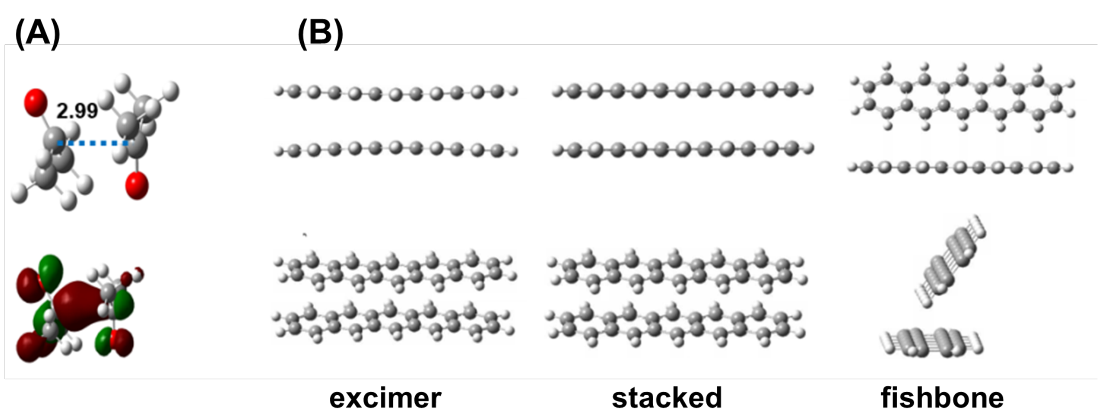

basis set for the pentacene excimer and cc-pVTZ for the acetone dimer.[262] Geometries were optimized using Gaussian16.[263] Throughout this chapter, we use electron volts (eV) as the energy unit to relate with electronic spectroscopy.

4.5 Results

Table 4.1: Computed energies (eV) for the ground state and the $n \to \pi^\star$ excited state of an acetone molecule.[a]

geometry[b]	MSDFT/NOSI		TDDFT
	$\Delta E(S_0)$	$\Delta E(S_1)$	$\Delta E(S_1)$
S_0	-0.02	4.43	4.28
S_1	0.84	3.78	3.79
$(S_0)_{\mathrm{DM}}$	-0.02	4.39	4.25
$(S_1)_{\mathrm{DM}}$	0.75	3.80	3.79
Excimer[c]	0.0	2.93, 4.16	2.91, 3.98

[a]Geometries used include the monomer structure in the ground state (S_0) and the first excited state (S_1), along with the monomers in the optimized dimeric excimer (DM), resembling the ground and excited state. Energies are determined using nonorthogonal state interaction (NOSI) and time-dependent density functional theory (TDDFT). The Minnesota M06-2X density functional along with the cc-pVTZ basis set is used.
[b]Acetone monomer geometries in different states used in energy calculations. Monomer energies are relative to that determined using M06-2X/cc-pVTZ.
[c]Excimer excitation energies relative to the ground-state energy using the excimer structure.

Table 4.1 lists the energies of the ground state and the $n \to \pi$ excited state from MSDFT-NOSI and TDDFT calculations relative to that from KS-DFT for acetone. The results for the $L_a(S_1)$ and $L_b(S_2)$ states of pentacene are given in Table 4.2. The performance of NOSI and possible double counting of electron correlation in a multi-state DFT can be validated by comparison of the ground-state energies with that from KS-DFT calculations.[52] We find that the difference in ground-state energy between MSDFT and KS-DFT is generally small, with the largest deviation being just $-0.02\,\mathrm{eV}$ for acetone. Note that the KS-DFT state is included in the active space in all NOSI calculations. This observation indicates that there is little double-counting of correlation in NOSI for the present systems using the M06-2X functional. Importantly, the inclusion of the Kohn-Sham ground state ensures orthogonality of the computed excited states to the ground state. Listed in Tables 4.1 and 4.2 are relative energies for the

Table 4.2: Computed ground-state and excitation energies (eV) for pentacene using NOSI and TDDFT.[a]

geometry[b]	MSDFT/NOSI			TDDFT	
	S_0	$L_a(S_1)$	$L_b(S_2)$	$L_a(S_1)$	$L_b(S_2)$
S_0	0.0	2.39	3.35	2.35	3.63
S_1	0.21	2.06	3.11	2.10	3.54
$(S_1)_{\mathrm{DM}}^{\mathrm{monomer}}$	0.09	2.10	3.14	2.06	3.44
Excimer[c]	0.0	0.88,	2.33,	0.87,	2.14,
	0.0	1.87	2.49	2.04	2.42

[a]Optimized geometries for the ground state (S_0) and the first excited state (S_1 also labeled as L_a), and the monomer geometry in the optimized excimer $(S_1)_{\mathrm{DM}}^{\mathrm{monomer}}$ are used. The Minnesota M06-2X density functional along with the cc-pVDZ basis set is used.
[b]Acetone monomer geometries in different states used in energy calculations. Monomer energies are relative to that determined using M06-2X/cc-pVDZ.
[c]Excimer excitation energies relative to the ground-state energy using the excimer structure.

ground and excited states from NOSI and TDDFT calculations employing monomer geometries optimized for S_0 and S_1 states and monomers in the optimized monomer structure. In addition, we included the computed excitation energies of the excimer complexes. The agreement between NOSI and the linear-response theory is good with a root-mean-square deviation (RMSD) of 0.22 eV, which is largely due to the somewhat greater differences between NOSI and TDDFT for the L_b state of pentacene using M06-2X. If only L_a states of pentacene are included, the RMSD error is less than 0.01 eV. Experimental absorption and fluorescence energies for acetone are 4.5 and 2.8 eV in the gas phase,[264] and an acetone excimer fluorescence energy of 3.06 eV has been reported;[265] these results are in good accord with NOSI and TDDFT results in Table 4.1. The results in Table 4.1 demonstrate that the MAS used in NOSI for these chromophores is sufficient to represent these states, demonstrating that MS-EDA can be applied to analyze interaction energies of excited-state complexes.

4.5.1 Asymmetric Acetone Excimer

For MS-EDA, we first consider the asymmetric acetone excimer, which was optimized for the S_1 state of the complex using TDDFT with the M06-2X functional. We obtained a structure that is best characterized as the local excitation of one monomer that is distorted at the carbonyl carbon from sp^2 hybridization (Fig. 4.2A), forming a tail-to-tail dimer with an in-phase combination of the distorted $\pi^\star$ orbital of the two acetone molecules as the highest singly occupied orbital. The vastly different monomer structures here turn out to be equivalent to a general exciplex complex if the two compounds were different. Interestingly, the distorted acetone monomer in the excimer complex, $(AA)_{S_1}$, is somewhat less deformed by about 0.1 eV (2.4 kcal/mol) than the optimized geometry, $(A)_{S_1}$, in isolation, but the adiabatic excitation energies (3.8 eV) are essentially the same (Table 4.1). The agreement between NOSI and TDDFT calculations is good for the four geometries considered (Table 4.1).

Figure 4.3 shows the progressive change of energies for the ground state and excited states for the terms defined by Eq. 4.3. First, there is a weak binding interaction in the ground state with a ΔE_{Lint} value of -0.24 eV (-5.5 kcal/mol), giving rise to local excitation energies of 3.00 and 4.39 eV in the bimolecular complex, essentially the same as the isolated monomers in the equilibrium S_1 and S_0 geometries at 2.95 and 4.45 eV, respectively (Table 4.1). Excitation energies for the monomer-in-excimer geometries are also similar (3.05 and 4.41 eV). Thus, there is a small polarization effect of less than 0.05 eV that stabilizes the excited states due to local excitation. Interestingly, state interaction among the locally excited states has little effect on the exciton states, with identical first and second excitation energies as the two locally excited states. For this excimer structure, the net exciton resonance energy is zero. Superexchange due to mutual charge transfer does contribute to state stabilization, lowering the first and the second excited-state energy by 0.06 and 0.12 eV, respectively. The magnitudes of SE

Figure 4.3: Computed ground and excited-state energies (eV) for the acetone monomer (A) and the excimer complex (AA) and the intermediate energy terms from multi-state energy-decomposition analysis (MS-EDA). The energies for the fully delocalized excimer are determined using TDDFT/M06-2X. States shown in the light-yellow background are determined using nonorthogonal state interaction (NOSI) with the excimer geometry, and the excited species are indicated in red. The notations $(A)_0$ and $(A)_1$ denote the optimized structures for the ground and first excited state of acetone. Energies are given relative to that of acetone in the ground state.

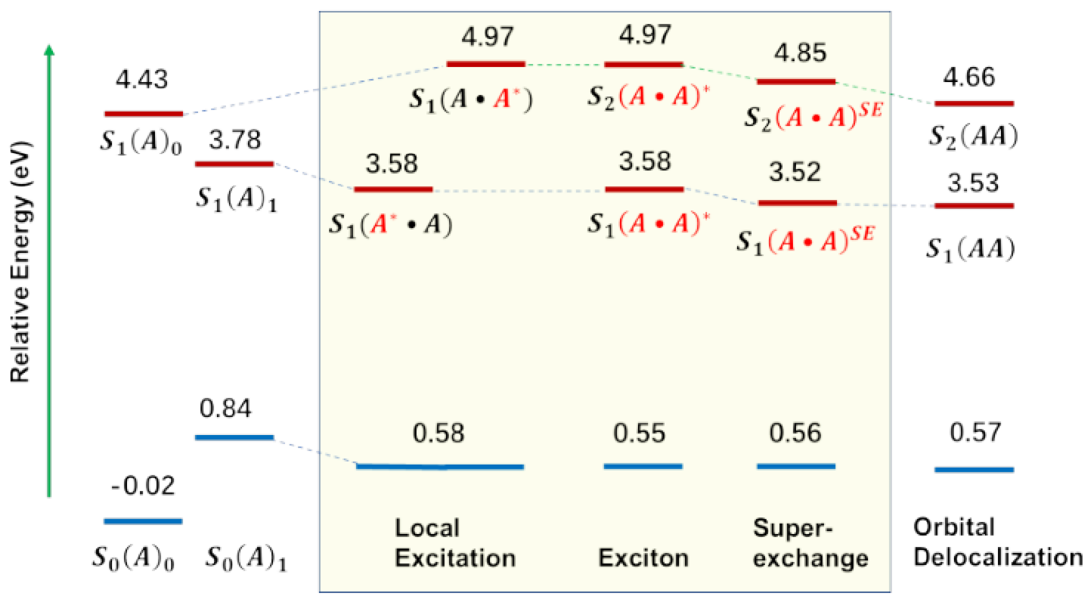

stabilization in these two states are mirrored by the corresponding structural weights for the nonequivalent CT directions, amounting to 2.56 % and 0.06 % for the BCT (monomer 2 $\rightarrow$ monomer 1) and FCT states in the first excited state and 0.02 % and 7.54 % in the second excited state. Notice the different directions of CT contributions for the two states. Finally, we found that orbital delocalization and configuration-space expansion in TDDFT calculations have little effect on the ground state (not surprisingly) and the first excited state; however, a noticeable stabilization to the second excited state of the excimer, by 0.19 eV, is obtained (Fig. 4.3). Overall, a net binding energy of -0.23 eV (-5.3 kcal/mol) for the acetone excimer is obtained from both NOSI and TDDFT calculations.

4.5.2 Pentacene Excimer

We now turn to the case of the pentacene excimer, which exhibits different behaviors in comparison with that in the asymmetric acetone excimer. Listed in Table 4.3 are the computed energy terms, including local excitation ΔE_{Lex}, exciton excitation states ΔE_{Ex}, superexchange stabilization ΔE_{SE}, and the orbital and configuration delocalization energies ΔE_{OCD} for the excimer complex, associated with the excimer states of pentacene in three different geometrical arrangements. The first geometry corresponds to a fully optimized structure of the S_1 excimer ($D_{2\mathrm{h}}$ symmetry) with the shortest interfragment separation at 3.15 Å, the second configuration is an on-top stacked construction with the ground-state monomer geometry at 3.3 Å, and the third is derived from the pentacene crystal in a fishbone relationship used previously (Fig. 4.2B).[58] These structures are of interest by their own rights, but the fishbone relationship is directly relevant to pentacene monolayer materials used in solar cell research.[58] However, we shall not address the mechanism of singlet fission in the present MS-EDA study; interested readers may find conclusions in an early study using MSDFT.[58]

Table 4.3: Computed excitation energies (eV) and energy components from multistate energy decomposition analysis (MS-EDA) for pentacene dimers in the excimer, stacked, and fishbone geometries.[a]

Energy term	Excimer		Stacked		Fishbone[c]	
	L_a	L_b	L_a	L_b	L_a	L_b
$\Delta E_{\mathrm{Lint}}[\Psi(X \bullet Y)]^{\mathrm{b}}$	0.03		0.05		−0.33	
$\Delta E_{\mathrm{Lex}}[\Psi^{K_X}_{(X^\star \bullet Y)}]$	1.89	3.04	2.10	3.28	2.00	2.92
$\Delta E_{\mathrm{Lex}}[\Psi^{K_Y}_{(X \bullet Y^\star)}]$	1.89	3.04	2.10	3.28	1.98	2.92
$\Delta E_{\mathrm{Ex}}[\Psi^{K}_{(X \bullet Y)^\star}]$	1.33	2.70	1.74	2.80	1.97	2.92
$\Delta E_{\mathrm{Ex}}[\Psi^{K\prime}_{(X \bullet Y)^\star}]$	2.46	3.38	2.58	3.47	2.02	2.93
$\Delta E_{\mathrm{SE}}[\Psi^{K}_{(X \bullet Y)^\star_\pm}]$	0.62	2.70	1.02	2.80	1.88	2.92
$\Delta E_{\mathrm{SE}}[\Psi^{K\prime}_{(X \bullet Y)^\star_\pm}]$	2.30	3.38	2.54	3.47	1.97	2.93
$\Delta E^{K}_{\mathrm{OCD}}$	0.87	2.42	1.24	2.58	2.03	2.98
$\Delta E^{K}_{\mathrm{OCD}}{}'$	2.04	2.80	2.35	3.02	2.24	NA[d]

[a]Excitation energies are relative to that of the adiabatic ground state of isolated pentacene(s). The M06-2X density functional is used. See caption of Table 4.2.

[b]The ground-state binding energy for the delocalized dimers are −0.05, +0.03, and −0.47 eV for the excimer, stacked, and fishbone geometries, respectively. Binding energies for the first excited-state complexes are −1.52, −1.15, and −0.36 eV in the three corresponding geometries. Much of the excited-state binding energy for the fishbone configuration originates from ground-state binding.

[c]The HOMO − 1 → LUMO + 1 configuration was not included in NOSI calculations.

[d]Several mixed states have close energies, not assigned to the L_b state.

Figure 4.4: Computed ground and excited-state energies for pentacene excimer from multistate energy-decomposition analysis (MS-EDA). States shown in light-yellow background are determined using nonorthogonal state interaction (NOSI) in MS-EDA analysis with the excimer geometry, in which excited species are indicated in red. The M06-2X density functional is used in all calculations.

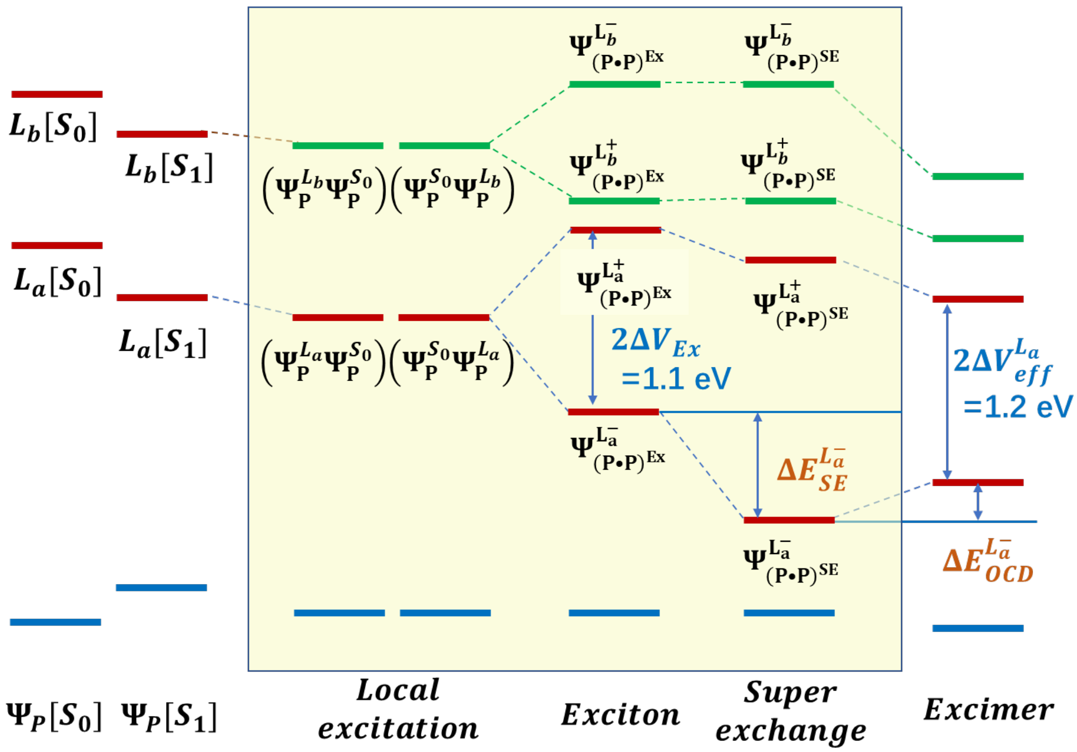

First, mutual polarization induced by local excitation of one monomer introduces modest effects relative to the adiabatic energies of an isolated monomer, stabilizing the L_a and L_b states of the excimer by 0.17 (2.06 vs. 1.89) and 0.07 (3.11 vs 3.04) eV (Tables 4.2 and 4.3), respectively. This is significant in view of the nonpolar nature of the hydrogen carbon system, although there is also a slight change from structural variations from the monomer to the excimer. The most striking finding from Table 4.3 and also in Fig. 4.4 is the large exciton coupling energies and the resulting energy splitting for both the L_a and L_b states in the excimer and stacked structures, giving rise to exciton splitting energies $|2\Delta V_{\mathrm{Ex}}|$ of 1.13 and 0.84 eV for the L_a states and 0.68 and 0.67 eV for

Table 4.4: Computed exciton coupling (energy-splitting) $|\Delta V_{\mathrm{Ex}}|$ and resonance energies associated with super-exchange stabilization $\Delta E_{\mathrm{SE}}^{\mathrm{res}}$ and orbital and configuration delocalization $\Delta E_{\mathrm{OCD}}^{\mathrm{ad}}$ (energies in electronvolts (eV))[a]

Relative energy	Excimer		Stacked		Fishbone	
	L_a	L_b	L_a	L_b	L_a	L_b
$\|2\Delta V_{\mathrm{Ex}}\|$	1.13	0.52	0.84	0.67	0.05	0.01
$\Delta\Delta E_{\mathrm{SE}}^{\mathrm{res},\pm}$	−0.71	0.00	−0.72	0.00	−0.09	0.00
$\Delta\Delta E_{\mathrm{SE}}^{\mathrm{res},\mp}$	−0.16	0.00	−0.04	0.00	−0.05	0.00
$\Delta\Delta E_{\mathrm{OCD}}^{\mathrm{ad},\pm}$	+0.15	−0.28	+0.22	−0.22	+0.15	0.06
$\Delta\Delta E_{\mathrm{OCD}}^{\mathrm{ad},\mp}$	+0.26	−0.58	−0.19	−0.45	+0.27	NA

the L_b states (Table 4.4). Interestingly, the computed exciton coupling (energy splitting) between locally excited states is fortuitously nearly identical to that determined as the energy difference between the two adiabatic states (Table 4.2, Fig. 4.4).In comparison with the "solar-cell relevant" fishbone structure, the computed exciton coupling is only 0.05 eV for the L_a state and 0.01 eV for the L_b state. Phase matching of the two chromophore wave functions in the dimer (excimer) complex is critical for the strength of their interaction and can have a major impact on the energy levels.[131] This effect is clearly reflected in the tilted monomers in the fishbone complex. Thus, a small adjustment to better align the overlap of monomer wave functions may significantly enhance electronic coupling for energy and charge transfer. A major stabilizing factor of the excimer energies comes from superexchange. Formally, superexchange originates from the mutual charge transfer, $|\Psi_X^+ \bullet \Psi_Y^-\rangle$ and $|\Psi_X^- \bullet \Psi_Y^+\rangle$, between two monomers. However, there is no net charge transfer in the excimer complex of pentacene nor in the stacked configuration of pentacene dimer because of symmetry. Superexchange refers to the resonance stabilization of these two CT states by mixing with the exciton states. This necessarily lowers the excimer energy relative to the corresponding exciton state because of the variational principle, which is clearly confirmed by the numerical results in Table 4.3. In the pentacene dimers, superexchange stabilizes the L_a state significantly by -0.7 eV in the excimer and stacked dimer configurations, but to a much smaller extent (-0.09 eV) in the fishbone arrangement (Table 4.4). Thus, phase matching of the wave functions favoring strong overlap is important to resonance mixing of interfragment charge transfer. In all cases, superexchange produced no effect on the stability of the L_b state, but it does stabilize the ground state to a much smaller extent than the L_a excited states.

Finally, we comment on the effects of orbital delocalization and expansion of the configuration space in excited-state calculations to yield the adiabatic ground and excited states. Unlike ground-state EDA, where orbital delocalization necessarily stabilizes the ground-state energy, the energies of the excited energies also depend on the "active space" used, which could increase or decrease the energies of a particular excited state. In principle, Hohenberg-Kohn-Sham DFT gives the exact energy of the ground state, but linear response theory introduces additional approximations. The Lu-Gao theorems of MSDFT establishes a foundation for exact excited-state calculations as does that of Hohenberg-Kohn theorems for the ground state.[257, 5] As in Kohn-Sham theory,[1] an approximate matrix correlation functional is needed. In a range of studies, we have found that the approximations used in the present MS-EDA analysis yield good results for excited-state calculations. The computed excitation energies for the present system are within 0.2 eV of the TDDFT values (see Tables 4.1 and 4.2), and it is not clear which is more accurate without a thorough analysis. In view of the widespread use of the linear response theory, we have adopted the TDDFT values for the final adiabatic energies to determine the ΔE_{OCD} term in MS-EDA. For the pentacene excimer, the OCD contribution raises the energy of the first excited state but lowers those for the higher states. Currently, we have not separated the effects from orbital and configuration expansions, which would be of interest in future studies.

An anonymous referee noted the abnormal energy increase in the ΔE_{OCD} term for the $S_1(L_a^-)$ state. We attribute this observation to overstabilization by superexchange in the present analysis, leading to an energy too low for the SE state. This issue originates from the approximate TDF energy using Eq. 4.14. MSDFT-NOSI calculations of the delocalized excimer complex show an energy splitting of 1.0 eV, in fact, slightly smaller than the value from TDDFT (1.2 eV) in Table 4.2 (Fig. 4.4). In view of the $\Delta E_{\mathrm{SE}}[\Psi^K_{(X\bullet Y)^\star_\pm}]$ energy term (0.62 eV) in Table 4.3, it is likely that the SE effect is overestimated at least by 0.2 eV. This highlights the need to systematically develop a matrix correlation functional for both the ground and excited states.

4.6 Conclusion

In summary, a multistate energy decomposition analysis (MS-EDA) method is introduced to dissect the energy components in excimer complexes. Ground-state EDA, which has been extensively explored in the past, remains an active area of research. However, the development of methods for analysis of intermolecular interactions in the excited states has lagged partially because it is difficult to introduce well-defined intermediate states at higher energy levels, not to mention that the computation of excited-state energies itself is challenging. Akin to an energy decomposition analysis for the ground state, the present MS-EDA provides a clear separation of energy terms that can be variationally optimized for excited-state complexes. MSDFT based on the Lu-Gao theorems provides a straightforward classification of exciton coupling, super-exchange resonance and orbital-configuration expansion. Critical to this analysis is to account for state interaction. As demonstrated in the present study, state interaction provides key insights into an understanding of excitonic coupling and superexchange stabilization. These quantities, directly computed from the basis states of the MAS for MSDFT, rather than a *post priori* transformation, are of fundamental importance to determining the rates of electron transfer and excited-state energy transfer and in applications to design light-emitting materials. The examples highlight the roles of state energy-matching and wave function phase-matching to the magnitude of exciton coupling and superexchange stabilization from a perspective of well-defined diabatic states. Further, MS-EDA provides a useful tool for interpreting excited-state energies from delocalized calculations.

Chapter 5

Multistate Energy Decomposition Analysis of Molecular Excited States

This chapter is based on the publication [266]. I contributed by running calculations, analysing results and revising the manuscript.

5.1 Introduction

Energy decomposition analysis (EDA) is widely used and plays an important role in the understanding of intermolecular interactions in molecular systems.[200, 267, 36, 222, 198, 243] These studies provide insights into the interplay of Pauli exclusion, polarization and charge transfer effects that contribute to intermolecular forces. In turn, the information gained from these investigations can be useful to designing and optimizing empirical potential energy functions for condensed-phase and biomolecular simulations.[268, 269] A large number of EDA models have been proposed, but they are almost exclusively limited to molecular complexes in the ground state.[222, 243, 201, 204, 205, 208, 209, 210, 211, 212, 213, 214, 215, 216, 217, 218, 219, 220, 221, 223, 33, 227, 228, 229, 230, 175, 231, 232, 233, 234, 235, 236, 237, 238, 239, 240, 242, 244, 245, 246, 247, 248, 249] On the other hand, a major current frontier of theoretical chemistry is to study chemical processes taking place in electronically excited states in areas such as photochemistry, photovoltaic devices,[58] photosynthesis and photoreception in biology,[55, 56, 253, 254] catalysis, and even reactions in fuel cells and at the electrodes.[270] Electronic coupling among local states in these systems can be used to determine the rate of excited-state energy transfer. Unfortunately, little attention has been paid to energy decomposition analysis of intermolecular interactions in excited states,[198, 252, 250, 74] although several studies of energy components of excited states have been reported.[136, 135] Moreover, it is not always clear if the intuitive terms for the ground state can be adapted to molecular systems in the excited states. In this chapter, we present a multistate energy decomposition analysis (MS-EDA) introduced in a recent preliminary report[198] to define the energy terms relevant to intermolecular interactions in excited states. This is now possible following the development of multistate density functional theory (MSDFT) to treat the ground state, excited states and diabatic states on an equal footing with the inclusion of electron correlation.[257, 258, 6, 7]

Energy decomposition analysis was first introduced by Morokuma and Kitaura on the basis of Hartree-Fock theory in the 1970s,[201, 202] who defined intuitive terms such as electrostatic, exchange repulsion, polarization and charge transfer energies, which are intimately related to concepts used in chemical research. The method was an instant success and has become extremely popular in computational chemistry.[203] Subsequently, a wide range of models have been proposed, attacking the energy components from different perspectives for different situations. Roughly speaking, these methods may be grouped into three categories: (1) physical approaches, either based on a formal perturbation theory or by intuitive construction and modification of the interaction terms; (2) variational methods, developed by constructing well-defined intermediate molecular wave functions that can be variationally optimized; and (3) perturbation theories using quantum chemical methods or classical electrostatics theory.

The original Kitaura-Morokuma EDA belongs to the first category through a gradual annihilation of the Fock and overlap matrix elements relevant to intermolecular interactions.[202] Other models that partition the energy terms through an electron density formulation such as the interacting quantum atom (IQA) method according to zero-flux density surfaces,[271] and the natural energy decomposition analysis (NEDA) by making use of natural bond orbitals.[209, 272] EDA models that do not include variational energy minimization of the intermediate states can lead to an overestimation of the resonance energy and charge transfer effects.[273, 274, 275]

EDA models belonging to the second category were developed with certain elements of variational optimization of key reference intermediate states for energy partition. In Mo's block-localized wave function (BLW)[32] approach and the absolutely localized molecular orbital analysis,[243, 221] the strictly block-localized orbitals for every intermediate in the EDA are fully variationally optimized, providing a set of well-defined diabatic intermediate states for interpretation of the resonance energies of aromaticity, anomeric effects and forward-and-backward bonding interactions.[36, 246, 226] Other illustrative examples include the early constrained space orbital variations (CSOV) method by successively mixing occupied and virtual orbitals of different molecules,[205, 206, 207] and the reduced variational space self-consistent-field (RVS-SCF) model in which the orbitals of one fragment is optimized in the presence of the frozen orbitals of other fragments.[208] Another class of EDA theory features the extended transition state (ETS) scheme,[229, 276, 277] along with natural orbitals for chemical valence (NOCV) theory, in which not only noncovalent intermolecular interactions are decomposed, but also the energy of a chemical bond can be separated into unpaired electron contributions.[220, 228] The ETS-NOCV method allows the analysis of bonding characteristics such as σ, π, δ bond types.[277]

In category three,[233] perhaps the best known example is the popular symmetry-adapted perturbation theory (SAPT), which can be applied both to wave function theory and density functional theory.[234, 278] The SAPT method relies on a series of monomer Fock, perturbation and interaction operators. The first order polarization and exchange corrections are assigned to electrostatic and exchange energies, and higher order terms result in induction and dispersion terms. However, separation of charge-transfer energy can be challenging in perturbation approaches.[279, 280, 225]

Energy decomposition analysis for molecular complexes in the excited states is rare. Methods exist to extract local information and charge transfer contribution in excited states by analyzing density difference and transition density matrices.[74, 136, 135, 281, 282, 283, 284, 285] In principle, EDA methods for the ground state can be adapted to describe interactions in the excited states. One application was recently reported by Ge et al., who transferred the corresponding energy terms in the ground-state EDA to excited complexes.[250, 251] In particular, the interaction energy for an exciplex (int) is separated into frozen (froz), polarization (pol) and charge transfer (CT) terms, similar to that in the ground state: $\Delta E^{\star}_{\text{int}} = \Delta E^{\star}_{\text{froz}} + \Delta E^{\star}_{\text{pol}} + \Delta E^{\star}_{\text{CT}}$.[252] To obtain "frozen" excitations, the orbitals for each isolated monomer and its excitation amplitudes are combined to construct a supramolecular operator. Later, an excitation splitting term was incorporated to describe interactions between degenerate monomer states in a symmetric excimer.[252] While this excited-state decomposition scheme revealed interesting information in the lens of a ground-state microscope, the intermediate states cannot be variationally optimized because interfragment interactions were reconstructed from separate monomer terms. Yet, there is an interest in defining intermediate diabatic states which can be used to represent excitations localized on individual monomers to understand the reaction rates of excited-state energy transfer and excitation induced oxidation-reduction reactions.[286] Recently, we introduced a multistate approach,[198] making use of multistate density functional theory (MSDFT),[257] to define variationally optimizable intermediate states to interpret properties associated with excited-state processes,[26, 27] including local excitation, exciton resonance, superexchange, and orbital-and-configuration delocalization. This chapter further expands that work in several fronts. In addition to understanding intermolecular interactions in excited-state complexes, the energy terms and the associated diabatic states in this analysis can be used to investigate ultrafast photo-chemical reactions.[58, 55, 254]

In the following, we first present the theory of multistate energy decomposition analysis (MS-EDA), and the fundamental principles and computational algorithms of MSDFT. Then, we illustrate the MS-EDA method with a set of applications to excited-state complexes which can be loosely classified as encounter exciplex, excitation-induced charge-transfer complex, and intimate excimer and exciplex. We validate the computational procedure by comparison with results from time-dependent density functional theory (TDDFT) that works well for most of these exciplexes and their monomers as well as with available experimental data. In some cases, the computational MS-EDA results shed light on experimental findings with new interpretations. It is hoped that the new MS-EDA method shall stimulate further analysis and interpretation of computational results on excited states from delocalized wave function theories and TDDFT.

5.2 Theory

We aim at developing a method for energy analysis of molecular complexes in an excited state. For the photo-chemical reaction producing the exciplex $(XY)^\star$ between compounds X and Y

$$X + Y \xrightarrow{h\bar{\nu}_0^K} X + Y^\star \xrightarrow{\Delta E_b^K} (XY)^\star \tag{5.1}$$

we define the binding energy of $(XY)^\star$ in its Kth excited state as

$$\Delta E_b^K = E^K_{(XY)^\star}[\Psi^K_{(XY)^\star}] - E^0_X[\Psi^0_X] - E^0_Y[\Psi^0_Y] - h\bar{\nu}_0^K \tag{5.2}$$

where the superscript "0" denotes the energy and wave function of a molecule in the ground state, and $E^K_{(XY)^\star}$ is the energy of the Kth excited state of the exciplex $(XY)^\star$ associated with the wave function $\Psi^K_{(XY)^\star}$, and $h\bar{\nu}_0^K$ is the energy for chromophore excitation whose definition will be addressed next (not necessarily Y alone as indicated).

Before we discuss the energy components, we first take a closer look at the meaning of "binding energy" ΔE_b^K of an exciplex. It turns out that it is not as straightforward as that of a bimolecular complex in the ground state. From a viewpoint of the physical process, the external energy supplied (i.e., photoexcitation) to initiate the formation of an excited-state complex from two isolated molecules in their ground state is the vertical transition of one relevant monomer (or more) to the Franck-Condon region. Then, the excited species can quickly relax to its equilibrium geometry of a specific excited state (e.g., K), which in turn binds to another monomer and together relaxes

Figure 5.1: Explanation of the treatment of the excimer formation process. The top row corresponds to the physical process of exciplex formation (Eq. 5.2). The remaining illustration highlights the energy terms defined by Eq. 5.4. The shapes of objects represent molecular geometries, while different colors depict the polarized wave functions under different conditions. Blocks with boundaries denote fragment-localized wave functions, all of which can be variationally optimized. The lower panels in light-yellow shade specify the minimal active space (MAS) in nonorthogonal state interacion (NOSI) calculations, respectively, for the exciton state, derived from local excited states (Lex) shown in pink, and for the super-exchange (SE) contribution due to charge transfer diabatic states. Adapted with modifications from ref [198]. Copyright 2023 American Chemical Society.

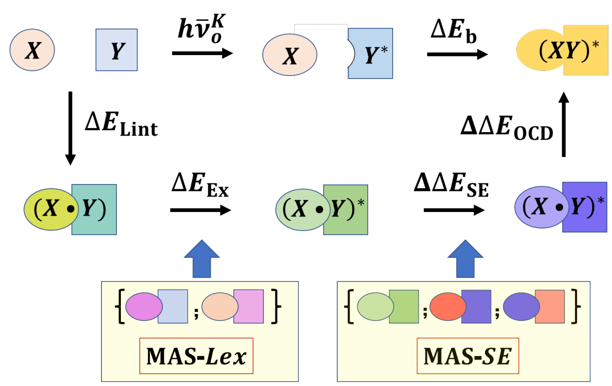

to the equilibrium exciplex (Scheme 5.3). Alternatively, two molecules form a ground-state complex, the dimer absorbs a photon and gets excited into an exciplex, which then directly relaxes to its final geometry. The precise mechanism is not always known exactly, but the final state is well-defined (Eq. 5.1), and its energy can be related to the emission spectrum of the exciplex. However, the energy difference between the final exciplex and the vertical excitation energy is not ΔE_b^K since some of the vertical excitation energy may have dissipated (without discussing its possible mechanisms) into the environment in the relaxation process. Furthermore, it is not always clear if one, two or a fraction of each monomer are excited in the first place, e.g., in the case of a symmetric or nearly symmetric excimer where the excited state is delocalized over both monomers. Therefore, we need to define an effective external energy $h\bar{\nu}_0^K$ to produce the unbound monomers to form the corresponding exciplex in the Kth excited state.

Here, we define $h\bar{\nu}_0^K$ in Eq. 5.1 as the minimum excitation energy associated with the formation of the exciplex in the Kth excited state, which is the weighted sum of the adiabatic excitation energies (ν_{ad}) of the monomers at their geometries in the exciplex complex. It is related to the "vertical" emission energies (ν_{em}) of the monomers in the exciplex geometries and the geometrical distortion energy in going from the equilibrium structures of the ground-state monomers to the distorted geometries ($X[S_K^{\mathrm{EC}}]$ and $Y[S_K^{\mathrm{EC}}]$) in the excited complex.

$$\begin{aligned} h\bar{\nu}_0^K =& h\left\{w_X^{(K)}\nu_{\mathrm{ad}}^{(K)}(X[S_K^{\mathrm{EC}}]) + w_Y^{(K)}\nu_{\mathrm{ad}}^{(K)}(Y[S_K^{\mathrm{EC}}])\right\} \\ =& \Delta E_{\mathrm{dist}}(X[S_K^{\mathrm{EC}}]) + \Delta E_{\mathrm{dist}}(Y[S_K^{\mathrm{EC}}]) \\ &+ h\left\{w_X^{(K)}\nu_{\mathrm{em}}^{(K)}(X[S_K^{\mathrm{EC}}]) + w_Y^{(K)}\nu_{\mathrm{em}}^{(K)}(Y[S_K^{\mathrm{EC}}])\right\} \end{aligned} \tag{5.3}$$

where $w_X^{(K)}$ and $w_Y^{(K)}$ are the structure weights of monomer excited states in the exciton complex defined in Section 5.2.2. Thus, $h\bar{\nu}_0^K$ is the effective external energy used to deform the monomer geometries and to excite them to the corresponding states at the fractions found in the exciton complex. Clearly, $h\bar{\nu}_0^K$ is state-specific. Then, the energy change in going from the isolated, "fractionally" excited monomers to the final complex is the exciplex binding energy ΔE_b^K.

5.2.1 Multistate Energy Decomposition Analysis (MS-EDA)

In MS-EDA, on the basis of the thermodynamic cycle in Scheme 5.3, we separate the binding energy of an exciplex in Eq. 5.2 into the following terms:

$$\begin{aligned} \Delta E_b^K =& \Delta E_{\mathrm{Lint}}[(X \bullet Y)] + \Delta E_{\mathrm{Ex}}^K[(X \bullet Y)^\star] - h\bar{\nu}_0^K \\ &+ \Delta\Delta E_{\mathrm{SE}}^K[(X^\pm \bullet Y^\mp)^\star] + \Delta\Delta E_{\mathrm{OCD}}^K[(XY)^\star] \end{aligned} \tag{5.4}$$

Figure 5.2: Visual explanation of the energies and energy differences that the excimer formation energy is decomposed into. $[S_0]$ and $[S_1^{EC}]$ indicate geometries of X and Y in the respective equilibrium ground state and that in optimized exciplex complex (EC) in the first excited state. Blue lines are monomer compounds, and maroon lines denote dimer structures. Energies that can be observed spectroscopically are indicated by $h\nu$, except for local excitations given in relative energies. Resonance and delocalization energies are given in brown. Energy changes in light yellow shade are associated with the exciplex binding energy.

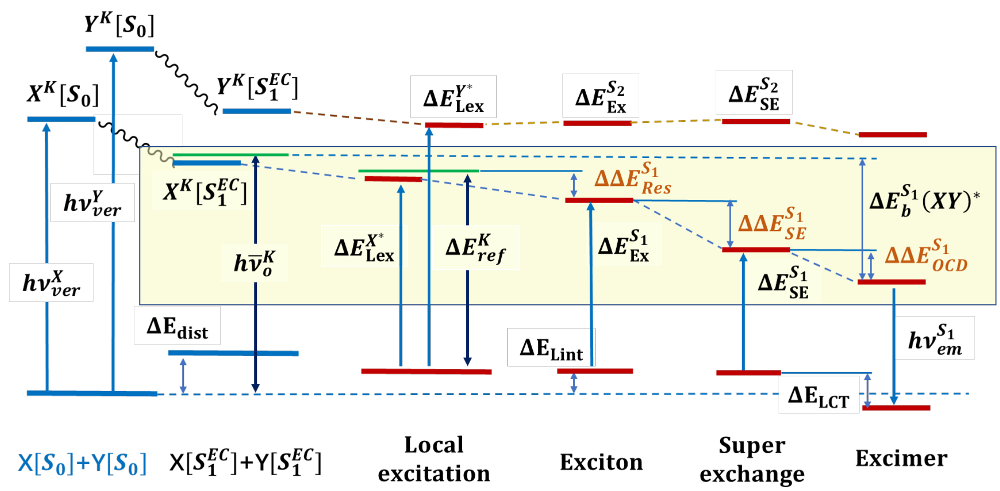

where $E_{\text{Lint}}[(X \bullet Y)]$ denotes the local interaction energy between monomers X and Y in the ground state, $\Delta E_{\text{Ex}}^K[(X \bullet Y)^\star]$ is the excitation energy of the Kth exciton (Ex) state and $h\bar{\nu}_0^K$ is defined in Eq. 5.3, $\Delta\Delta E_{\text{SE}}^K[(X^\pm \bullet Y^\mp)^\star]$ specifies superexchange stabilization (SE), and $\Delta\Delta E_{\text{OCD}}^K[(XY)^\star]$ represents the energy change due to orbital and configuration-state delocalization (OCD). The progressive energy terms in the MS-EDA procedure are schematically illustrated in Scheme 5.4 with a sequence of intermediate states leading to the final exciplex formation. Each state depicted in Scheme 5.3 has a well-defined wave function (or MSDFT configuration states) that can be variationally optimized.

Although the binding energy of an excited-state complex is state-dependent, we will sometimes omit the superscript K for simplicity, but one needs to keep in mind that the intermediate states and energy terms in MS-EDA correspond to the same Kth state of the exciplex (not necessarily in the same order) and they must be matched in the analysis. Often, the lowest excited state of a given spin is of particular interest, although symmetry allowed and avoided curve crossings can take place and the order of states may differ at different stages of the MS-EDA scheme, in which case, analysis of more than one state is necessary.

The individual energy components in Eq. 5.4 can be further decomposed into more specific terms to gain insights into the intricacy of intermolecular interactions in an excited state. Some of these energy terms can be directly measured experimentally or extracted from experimental data. In this section, we define the interaction energy terms. In the next section, we analyze the additional components that constitute some of these terms in the exciplex.

Throughout this chapter, we use Ψ and Φ to denote a physical adiabatic state or an intermediate diabatic state with further specification indicated by a subscript and the particular excited state specified by a superscript. Ψ and Φ are typically multistate wave functions, which are also used to represent the matrix density. The Greek letter Ξ is used to specify a single Slater determinant wave function for a given electronic configuration, typically monomer-block localized, to represent the corresponding electron density in block-localized excitation (BLE) and target state optimized density functional theory (TSO-DFT) calculations.[10, 9] Occupied Kohn-Sham molecular spin orbitals, typically block localized, are denoted by $\xi_i, \xi_j, ...$, and unoccupied (virtual) orbitals are given as $\xi_a, \xi_b, ...$. In the present MS-EDA method, we use the monomer block-localized Kohn-Sham (BLKS) determinant, $\Xi(X \bullet Y)^K S$, as a reference state, which is used to generate the initial guess for singly excited configurations Ξ_i^a, all of which are variationally optimized individually using BLE and TSO-DFT for block-localized excitation.[10, 9] Together, these variationally optimized determinants states form a minimum active space denoted by a single subscript $\Xi_A; A = 1, ...$

5.2.1.1 Ground-State Interaction Energy

The formation of a molecular aggregate in an excited state has energy contributions both from binding interactions in the ground state and from energy terms induced by photoexcitation (Scheme 5.3), keeping in mind that in many situations an exciplex is only stable in the excited state (thus, the ground-state effect could be repulsive). Since EDA has been thoroughly investigated for molecular interactions in the ground state, we separate ground-state and excited-state energies in the present multistate analysis. Consequently, the energy components leading to the monomer block-localized complex in the ground state are grouped into a single term called local interaction (Lint) energy in MS-EDA.

$$\Delta E_{\text{Lint}}[(X \bullet Y)] = E_{(X \bullet Y)}[\Psi_{(X \bullet Y)}] - E_X^0[\Xi_X^0] - E_Y^0[\Xi_Y^0] \tag{5.5}$$

where Ξ_X^0 and Ξ_Y^0 are Kohn-Sham determinants for molecules X and Y in isolation in their equilibrium geometries (Fig. 5.3), the notation $(X \bullet Y)$ denotes a bimolecular complex whose wave function is block-localized, indicated by the symbol $\bullet$, the parentheses specify an antisymmetrized product wave function from the monomers $\Psi_{(X \bullet Y)} = \hat{A}\{\Omega_X \Omega_Y\}$ with Ω_X and Ω_Y denoting products of BLKS orbitals. This convention is used throughout this chapter. Here, the mutual polarization between the two monomers are naturally included in $\Psi_{(X \bullet Y)}$ as a result of variational optimization of the wave function; $\Psi_{(X \bullet Y)}$ can be a multistate wave function in which case it is replaced by a linear combination of configuration state functions in the active space. Note that an energy deformation term has been included in ΔE_{Lint} because the molecular geometry of the exciplex is used to determine $E_{(X \bullet Y)}[\Psi_{(X \bullet Y)}]$ in eq 5.

Figure 5.3: Reference state (dashed lines in red) for local excitations (lines black) and exciton-resonance stabilization energy (blue arrows). Local and exciton excitation energies relative to the block-localized complex are indicated by red arrows.

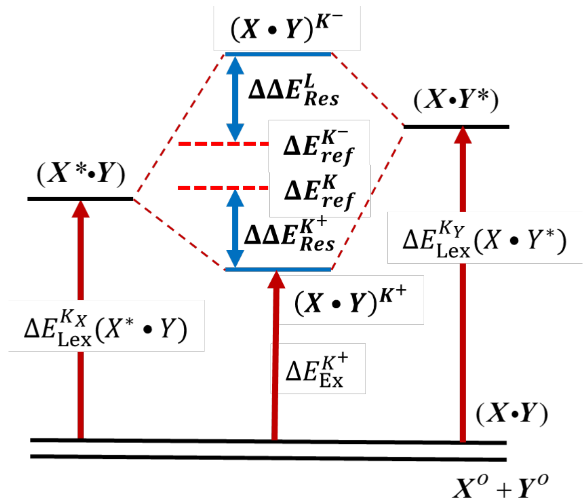

$\Delta E_{\text{Lint}}[(X \bullet Y)]$ is called local-interaction energy because molecular orbitals are not globally delocalized over the full complex. In addition to the structural deformation energy, it includes an electrostatic term called Heitler-London energy, $\Psi^0_{(X \bullet Y)} = \hat{A}\{\Omega^0_X \Omega^0_Y\}$, and a polarization energy in the variationally optimized state $\Psi_{(X \bullet Y)} = \hat{A}\{\Omega_X \Omega_Y\}$.[36, 33] Note that $\Delta E_{\text{Lint}}[(X \bullet Y)]$ is not the binding energy of the bimolecular complex (XY) in the ground state because charge-transfer delocalization is not included. Additional details for ground-state analysis can be found in references [200, 267, 36, 243].

5.2.1.2 Exciton Excitation Energy

In MS-EDA, we first define an exciton state, denoted by $(X \bullet Y)^\star$ (Scheme 5.3). Then, the energy difference between the exciton state and the ground state of the block-localized complex is called the exciton-excitation energy ΔE^K_{Ex}.

$$\Delta E^K_{\text{Ex}} = E^K_{(X \bullet Y)^\star} - E_{(X \bullet Y)} \tag{5.6}$$

where $E^K_{(X \bullet Y)^\star}$ and $E_{(X \bullet Y)}$ are the energies of the Kth exciton state and the ground state, respectively, corresponding to the wave functions $\Psi^K_{(X \bullet Y)^\star}$ and $\Psi_{(X \bullet Y)}$ (Eq. 5.5). According to the Frenkel exciton model,[256] the wave function of the exciton state is expressed as follows.

$$\Psi^K_{(X \bullet Y)^\star} = a_{1K} \Psi^{K_X}_{(X^\star \bullet Y)} + a_{2K} \Psi^{K_Y}_{(X \bullet Y^\star)} \tag{5.7}$$

where $\Psi^{K_X}_{(X^\star \bullet Y)}$ and $\Psi^{K_Y}_{(X \bullet Y^\star)}$ are the spin-adapted, configuration state functions of the two locally excited monomers (MAS-*Lex* in Scheme 5.3), and a_{1K} and a_{2K} are the state coefficients. The superscripts K_X and K_Y specify, respectively, the states of the locally excited states of monomers X and Y that contribute to the exciton state K (again, the subscripts or even K are typically omitted without causing confusion). In general, both $\Psi^{K_X}_{(X^\star \bullet Y)}$ and $\Psi^{K_Y}_{(X \bullet Y^\star)}$ are multiconfigurational wave functions, and more than one state from each monomer may be included.

Obviously, Eq. 5.7 can be extended to any number of monomers in an aggregate of n monomers or to condensed phases:

$$\Psi^K_{\text{Ex}} = \sum_{A=1}^{n} a_A \Psi^{K_A}_{(X_1 \cdots X_A^\star \cdots X_n)}$$

where $\Psi^{K_A}_{(X_1 \cdots X_A^\star \cdots X_n)}$ denotes the local excitation to the K_Ath state of monomer $X_A^\star$ in the presence of the rest of the $n-1$ monomers in the ground state. In solution, the local excitation energy of the chromophore includes a solvatochromic shift in comparison with the excitation energy of the isolated monomer. To limit the scope of this chapter, we shall not further discuss condensed-phase properties including exciton delocalization in general situations.

5.2.1.3 Charge Transfer States and Superexchange Energy

The exciton state above from the interactions among strictly localized monomer states includes the mutual polarization induced by chromophore excitation, but charge transfer (CT) contributions are excluded by construction (i.e., monomer localization). In the second step of MS-EDA, we introduce CT resonance states by combining the forward and backward CT states:

$$\Psi_{\mathrm{SE}} = b_2'|X^+ \bullet Y^-\rangle \pm b_3'|X^- \bullet Y^+\rangle \tag{5.8}$$

We note that for a symmetrical excimer the amount of forward and backward CT is the same, leaving a net zero "CT". Nevertheless, charge-transfer resonance in Eq. 5.8 can still stabilize the excimer complex significantly. On the other hand, in asymmetrical exciplexes, the significance of CT resonance strongly depends on the relative energies of the two directions of CT. Then, the CT state in the direction with the lower energy typically plays a dominant role, whereas the effect in the opposite direction of CT can be ignored. To encompass both scenarios, we borrow a term from electron transfer theory,[58, 259] giving the name superexchange (SE) stabilization to the decrease in energy when superexchange states (Eq. 5.8) are admixed to the exciton states (Eq. 5.7).

$$\Delta\Delta E_{\mathrm{SE}}^K = E_{\mathrm{SE}}^K[\Psi_{\mathrm{SE}}^K] - E_{\mathrm{Ex}}^K[\Psi_{(X\bullet Y)^\star}^K] \tag{5.9}$$

where the wave function for the superexchange intermediate state in MS-EDA is given by

$$\Psi_{\mathrm{SE}}^{K} = b_1 \Psi_{(X \bullet Y)^\star}^{K} + b_2 |X^+ \bullet Y^-\rangle \pm b_3 |X^- \bullet Y^+\rangle \tag{5.10}$$

It should be emphasized that the notation $|X^+ \bullet Y^-\rangle$ and $|X^- \bullet Y^+\rangle$ defines a spin-adapted state obtained from MSDFT-NOSI for the spin-pairing interactions between the two spin-mixed determinants with single-electron transfer in α or β spin (MAS-SE in Scheme 5.3). The two resulting eigenstates correspond to a singlet state and a triplet component with $M_S = 0$ (see below).

5.2.1.4 Orbital and Configuration-State Delocalization

In the final step of MS-EDA, we relax the strictly localized BLKS orbitals to the fully delocalized molecular (or Kohn-Sham) orbitals over the entire exciplex system. In addition, the number of basis configurations used to define the intermediate states in the exciton and superexchange step is relatively small, which is useful for interpretation of excited-state energies. Thus, the difference between excited-state energies from TDDFT calculations for the delocalized exciplex and MSDFT-NOSI in analysis is also included. We denote the Kth adiabatic excited state of the exciplex as $\Psi_{(XY)^\star}^{K}$ where the removal of the dot "$\bullet$" emphasizes spatial delocalization of the orbitals and configuration space. The energy change in this step is called orbital and configuration-state delocalization (OCD) energy.

$$\Delta\Delta E_{\mathrm{OCD}}^{K} = E_{(XY)^\star}^{K}[\Psi_{(XY)^\star}^{K}] - E_{\mathrm{SE}}^{K}[\Psi_{\mathrm{SE}}^{K}] \tag{5.11}$$

In principle, SE and OCD energies can be combined as the overall CT effects, similar to that in ground-state EDA, but it is useful to make the distinction and separation here in view of the difference in the number of basis configuration state functions to treat the intermediate states and the adiabatic states of the exciplex.

The $\Delta\Delta E^{K}_{\mathrm{OCD}}$ term is defined in terms of excited-state energies (Eq. 5.11), but, in fact, it also includes ground-state effects, corresponding to the charge-transfer energy term in ground-state EDA, denoted by ΔE_{LCT} (Scheme 5.2). It can be extracted as the difference between the energy of the (XY) complex in the ground state and the local binding state $(X \bullet Y)$. Thus, the contribution to exciplex binding from the total ground-state effect is $\Delta E_{\mathrm{Lb}} = \Delta E_{\mathrm{Lint}} + \Delta E_{\mathrm{LCT}}$. Then, the OCD effect on the excited state is $\Delta\Delta E^{(K)}_{\mathrm{OCD}} = \Delta\Delta E^{K}_{\mathrm{OCD}} - \Delta E_{\mathrm{Lb}}$. In this chapter, we do not further separate these two OCD terms, except in $E^{(K)}_{\mathrm{OCD}}$. In some specific cases, we comment on the numerical results of these terms.

On computation of the excited-state energy of an exciplex, multiconfiguration self-consistent-field (MCSCF) or configuration interaction-based approaches such as multireference configuration interaction (MRCI) in wave function theory can be used to determine the energies and excited-state wave functions $\Psi^{K}_{(XY)^\star}$. Alternatively, MS-DFT and linear-response TDDFT method can be used to obtain $E^{K}_{(XY)^\star}$ and $\rho^{K}_{(XY)^\star}$ in density functional theory. Given that MSDFT is a new variational DFT method and the development of approximate matrix correlation functionals hat not yet advanced to a level as that in KS-DFT, we employ TDDFT for estimating the excited state energies of the final exciplexes. Nevertheless, the accuracy of MSDFT in the MS-EDA analysis can be validated by comparison of the computed excitation energies for the monomer states with those obtained using TDDFT, employing a common approximate KS density functional and the same basis set. In this regard, the present MS-EDA method can also be viewed and used as an interpretative tool to dissect and understand the energies from TDDFT calculations.

5.2.2 Block-Localized Excited States

In the above MS-EDA, the exciton state is viewed as the resonance delocalization among monomer-localized excitations of individual chromophores.[256] Of interest is the relative contributions of locally excited states and the overall resonance energy in exciton formation (Eq. 5.7). In this regard, the term *local excitation* refers to the excited state of an individual monomer chromophore in the presence of other compounds in their ground state. This is achieved in TSO-DFT calculations by using the BLMO (in WFT) or BLKS orbitals (in MSDFT) that are strictly localized within each monomer by construction. These BLKS orbitals are clearly different from localized orbitals obtained through a particular symmetry orthogonal transformation.[287, 288] Local excitation has a physical interpretation that can be directly related to experimental solvatochromic shifts induced by solvation (though this important physical property will not be addressed here in view of space). In this section, we further decompose $\Delta E^{K}_{\mathrm{Ex}}$ into specific components related to local excitation and resonance delocalization. This analysis also provides meaning to the structure weights used in the definition of $h\bar{\nu}^{K}_{0}$ in Eqs. 5.2 and 5.3.

5.2.2.1 Local Excitation and Polarization Effects

The excitation energy of a locally excited state of monomer X is given by $\Delta E^{K_X}_{\mathrm{Lex}}(X^{\star}\bullet Y)$:

$$\Delta E^{K_X}_{\mathrm{Lex}}(X^{\star}\bullet Y) \equiv h\nu^{K_X}_{\mathrm{Lex}}(X^{\star}\bullet Y) = \quad E^{K_X}_{(X^{\star}\bullet Y)}[\Psi^{K_X}_{(X^{\star}\bullet Y)}] - E_{(X\bullet Y)}[\Psi_{(X\bullet Y)}] \tag{5.12}$$

where $\nu^{K_X}_{\mathrm{Lex}}(X^{\star}\bullet Y)$ is the excitation frequency of X if one considers Y as an environmental bath such as a solvent or simply another molecule in the present analysis (Scheme 5.4). The introduction of a frequency notation emphasizes the possibility that this quantity may be compared with the experimental absorption spectrum of a chromophore in solution or in a matrix of cluster molecules. Then, the solvatochromic shift of chromophore X in the presence of monomer Y (or in solution) relative to that in isolation (or in another reference solvent denoted by the subscript o), $\nu_{\mathrm{o}}^{K_X}(X^\star)$, is given by

$$\Delta\nu^{K_X}(X^\star \bullet Y) = \nu_{\mathrm{Lex}}^{K_X}(X^\star \bullet Y) - \nu_{\mathrm{o}}^{K_X}(X^\star) \tag{5.13}$$

$\nu_{\mathrm{o}}^{K_X}(X^\star)$ can have the same energy as that of the $h\bar{\nu}_0^K$ term in Eqs. 5.1 and 5.2 for a single chromophore in special cases such as a symmetrical excimer.

Local excitation of monomer X changes its electrostatic field which polarizes the charge distribution of the other monomer Y in the ground state (or solvent). In turn, the reaction field of the ground state of Y further affects the energy of the excited monomer. The equilibrium state $\Psi_{(X^\star \bullet Y)}^{K_X}$ is a result of their mutual polarization, and an understanding of its magnitude is of interest in MS-EDA. In fact, the local excitation energy of $X^\star$ in the block-localized complex $(X \bullet Y)$ (eq 12) may be considered as photoexcitation of X in the hypothetic state $([X_o^\star] \bullet Y)$ without interacting with Y in the complex i.e., the gas-phase adiabatic excitation energy $h\nu_{\mathrm{o}}^{K_X}(X^\star)$, followed by the mutual polarization of $X^\star$ with its environment Y to the local excited state,

$$\Delta E_{\mathrm{Lex}}^{K_X}(X^\star \bullet Y) = h\nu_{\mathrm{o}}^{K_X}(X^\star) + \Delta E_{\mathrm{Lpol}}^{K_X}(X^\star \bullet Y) \tag{5.14}$$

corresponding to the following two steps (see also Scheme 5.3):

$$(X \bullet Y) \xrightarrow{h\nu_{\mathrm{o}}^{K_X}(X^\star)} ([X_o^\star] \bullet Y) \xrightarrow{\Delta E_{\mathrm{Lpol}}^{K_X}(X^\star \bullet Y)} (X^\star \bullet Y)$$

Consequently, the polarization energy arising from local excitation $\Delta E_{\mathrm{Lpol}}^{K_X}(X^\star \bullet Y)$ is identical to the observable spectral shift:

$$\Delta E_{\text{Lpol}}^{K_X}(X^\star \bullet Y) = h\Delta\nu^{K_X}(X^\star \bullet Y) \tag{5.15}$$

For a symmetric dimeric excimer, the polarization energies for the two local excitations are identical. In this case, the block-localized excited states $(X^\star \bullet Y)$ and $(X \bullet Y^\star)$ are strongly correlated between two degenerate states, each corresponding to a *diabatic state*, which is also of interest in the study of excited-state energy transfer and exciton delocalization. The emission spectrum of the resonance state of the excimer may be used to determine the magnitude of the resonance energy relative to the variationally optimized diabatic states.[35] Note that the energies expressed in Eq. 5.14 can indeed be determined variationally by using the block-localized excitation (BLE) method,[9] or the targeted state optimization (TSO) approach.[151]

5.2.2.2 Exciton Resonance Energy

To determine the resonance energy of an exciton state, a variationally optimizable reference state in the absence of resonance (delocalized) excitation must be defined for comparison. For a perfectly symmetric excimer, it is straightforward simply to use the energy of one of the local excitation energies since both local excitations contribute equally. However, in the case of an asymmetric excimer or an exciplex of different monomers in which the two monomers contribute differently, a clear definition of the reference state is needed. Here, we introduce a structure-weighted reference state for estimating the resonance energy in an exciton state.

$$\Delta E_{\text{ref}}^{K} = w_X^K \Delta E_{\text{Lex}}^{K_X}[\Psi_{(X^\star \bullet Y)}^{K_X}] + w_Y^K \Delta E_{\text{Lex}}^{K_Y}[\Psi_{(X \bullet Y^\star)}^{K_Y}] \tag{5.16}$$

where the energies of the locally excited states $\Psi^{K_X}_{(X^\star \bullet Y)}$ and $\Psi^{K_Y}_{(X \bullet Y^\star)}$ are variationally minimized, and w^K_X and w^K_Y are the Chirgwin-Coulson configuration weights[193] of the Kth exciton state in Eq. 5.7.

The structure weights for locally excited states, $\Psi^{K_X}_{(X^\star \bullet Y)}$ and $\Psi^{K_Y}_{(X \bullet Y^\star)}$, in the resonance exciton state (Eq. 5.7) can be determined according to the Chirgwin-Coulson partition:

$$w^K_X = a^2_{1K} + a_{1K} a_{2K} S_{12} \tag{5.17a}$$

$$w^K_Y = a^2_{2K} + a_{1K} a_{2K} S_{12} \tag{5.17b}$$

where S_{12} is the overlap integral between the two locally excited states:

$$S_{12} = S_{21} = \int dr \Psi^{K_X}_{(X^\star \bullet Y)} \Psi^{K_Y}_{(X \bullet Y^\star)}$$

Here, an exciton-state specific reference is defined because each locally excited state has different contributions in different exciton states. This is illustrated in Fig. 5.3 in which two locally excited states in an exciplex interact to produce two exciton states, corresponding to the in-phase and out-phase combinations of $\Psi^{K_X}_{(X^\star \bullet Y)}$ and $\Psi^{K_Y}_{(X \bullet Y^\star)}$. It would have been unfair if the energy of any individual state or the average energy of both states were used as the reference to determine exciton-resonance (ER) energy because the former does not consider the contribution from the other state, and the latter does not truly reflect the relative significance of individual states in the exciton state (Eq. 5.17a). The reference defined in Eq. 5.16 provides an adequate consideration of these factors. In the limit of an identical excimer, the weighted reference state is the same as the energy of one locally excited monomer.

With the same analogy, the structural weights determined at the exciton state are used to define a weighted adiabatic excitation energy for exciplex formation (Eqs. 5.2

and 5.3).

Having defined a reference energy, the exciton resonance energy (Fig. 5.3) due to locally excited state-interaction is easily determined:

$$\Delta\Delta E^K_{\mathrm{Res}} = \Delta E^K_{\mathrm{Ex}} - \Delta E^K_{\mathrm{ref}} \tag{5.18}$$

The use of Eq. 5.18 implies that the sum of the resonance energies for the resonance-stabilized and destabilized exciton states is not exactly the resonance splitting of the delocalized states (Fig. 5.3). We further remark on the use of a weighted local-excitation energy as the reference state. First, the local excitations of all monomers contribute to the resonance-delocalized exciton state. Figure 5.3 highlights schematically the relative energies of the individual energy terms, including the weighted local-excitation energy (reference state), and the resonance stabilization energy for a given exciton state in the complex. In the case where monomers X and Y are asymmetric, the reference states for the in-phase and out-phase combinations of the locally excited states are different. In the former combination, the lower energy state (state K^+ in Fig. 5.3) is stabilized, whereas the higher energy exciton state (state $L(K^-)$ in Fig. 5.3) is destabilized. Since the stabilization and destabilization effects are relative contributions from all locally excited states, the state-specific, weighted local-excitation energy takes into account the relative significance to resonance energy and antiresonance energy. For an excimer complex, since both local-excitation energies are the same, a single reference state is naturally used for both resonance and antiresonance effects.

5.2.3 Multistate Density Functional Theory

Multistate density functional theory (MSDFT) is used to determine the intermediate states in multistate energy-decomposition analysis. Here, we summarize the fundamental theorems of MSDFT,[257, 258] the definition of a Hamiltonian matrix density functional and the nonorthogonal state interaction (NOSI) method.[7, 52, 131] NOSI distinguishes from nonorthogonal configuration interaction (NOCI) in that the former includes dynamic correlation in each excited basis state in an active space, whereas the latter configuration space generally requires expensive corrections for dynamic correlation to yield quantitative results.[6]

5.2.3.1 Fundamental Theorems

Although MSDFT has been used in a range of applications in the past,[7, 52] it was in 2021 that Lu and Gao proved three fundamental theorems, establishing MSDFT as a rigorous density functional theory of quantum mechanics for any number of N states.[257] For a system described by the Hamiltonian $\hat{H} = \hat{H}^0 + v_{\text{ext}}(\mathbf{r})$, where $\hat{H}$ consists of kinetic energies and electronic interaction energies, and $v_{\text{ext}}(\mathbf{r})$ is the local external potential, the first theorem establishes the correspondence of the Hamiltonian and the N-dimensional multistate matrix density $\mathbf{D}(\mathbf{r})$. Theorem 2 is a variational principle, resulting in the energies and densities of all N eigenstates. Theorem 3 defines the representation of an N-dimensional multistate matrix density, enabling the design of different practical algorithms and procedures for computation.

1. Given the subspace $\mathbb{V}$ spanned by the lowest N eigenstates of a molecular system described by $\hat{H}$, the Hamiltonian $\hat{H}^0$ is a universal *matrix functional* of the N-dimensional multistate density $\mathbf{D}(\mathbf{r})$, $H^0 = \mathcal{F}[\mathbf{D}]$, independent of the external potential $v_{\text{ext}}(\mathbf{r})$. Then, the total Hamiltonian *matrix density functional* (HMDF)

is

$$\mathcal{H}[\mathbf{D}] = \mathcal{F}[\mathbf{D}] + \int \mathbf{D}(\mathbf{r}) v_{\text{ext}}(\mathbf{r}) d\mathbf{r}$$

Here, the multistate density $\mathbf{D}(\mathbf{r})$ is a matrix of electron densities $\rho_i(\mathbf{r}) \equiv \rho_{ii}(\mathbf{r})$; $i = 1, ..., N$ and transition densities between any two basis states $\rho_{ij}(\mathbf{r}); i \neq j$; $i, j = 1, ..., N$. In other words, Theorem 1 establishes a one-to-one correspondence between $\mathbf{D}$ and $\mathcal{H}$.

$$\begin{pmatrix} \rho_1(\mathbf{r}) & \cdots & \rho_{N1}(\mathbf{r}) \\ \vdots & \ddots & \vdots \\ \rho_{1N}(\mathbf{r}) & \cdots & \rho_N(\mathbf{r}) \end{pmatrix} \Leftrightarrow \begin{pmatrix} \mathcal{H}_{11}[\mathbf{D}] & \cdots & \mathcal{H}_{N1}[\mathbf{D}] \\ \vdots & \ddots & \vdots \\ \mathcal{H}_{1N}[\mathbf{D}] & \cdots & \mathcal{H}_{NN}[\mathbf{D}] \end{pmatrix}$$

2. For any N-dimensional trial matrix density $\mathbf{D}'(\mathbf{r})$, the trace of $\mathcal{H}[\mathbf{D}'(\mathbf{r})]$, defined as the multistate energy $E_{\text{MS}}[\mathbf{D}'(\mathbf{r})] = \sum_i H'_{ii}$, is greater than or equal to the multistate energy $E_{\text{MS}}[\mathbf{D}]$ of the subspace $\mathbb{V}$:

$$E_{\text{MS}}[\mathbf{D}'(\mathbf{r})] \geq E_{\text{MS}}[\mathbf{D}(\mathbf{r})] \tag{5.19}$$

   The equal sign holds true if the trial density is a matrix density of the subspace $\mathbb{V}$, i.e., $\mathbf{D}'(\mathbf{r}) = \mathbf{D}(\mathbf{r})$. Then, diagonalization of the Hamiltonian matrix $\mathcal{H}[\mathbf{D}]$ yields exactly all N eigenstate energies (and densities), including the ground state and $N - 1$ excited states.

3. The N-dimensional multistate matrix density $\mathbf{D}(\mathbf{r})$ can be sufficiently represented by N^2 independent Slater determinant wave functions.

It is straightforward to see that the Hohenberg-Kohn theorem is a special case of Theorem 1 for the ground state, where $N = 1$. In this case, the HMDF $\mathbf{H} = \mathcal{H}[\mathbf{D}(\mathbf{r})]$ reduces to a 1×1 matrix for one state, the ground state, becoming a scalar energy density functional of the ground state density $\rho_0(\mathbf{r})$: $E_0 = E[\rho_0(\mathbf{r})]$. Then, according to Theorem 3, the density $\mathbf{D}(\mathbf{r}) \equiv \rho_0(\mathbf{r})$ can be represented by a single Slater determinant, as in the Kohn-Sham formulation of HK-DFT.

A major departure, however, from the HKS-DFT is that state interaction is essential to representing the multistate density and determining the energies of excited states, rather than using a noninteracting KS reference system to represent the electron density of the ground state. Importantly, the implication of Theorem 3 is that for a given number of N states of interest, a finite number of N^2 determinant wave functions is sufficient to represent exactly the multistate density $\mathbf{D}(\mathbf{r})$. Consequently, it defines an upper bound of basis configurational states, i.e., a minimal active space (MAS), in MS-DFT. Obviously, the number of determinants (N^2) to exactly represent the multistate density $\mathbf{D}(\mathbf{r})$ is significantly smaller than that needed to represent the corresponding wave functions as in a full CI treatment or even in an approximate method employing a complete active space (CAS).

5.2.3.2 Correlation Matrix Functional

We next introduce the correlation matrix functional, leading to a method for optimizing the multistate matrix density via one-electron orbitals. Given the basis determinants Ξ_A of a MAS, representing exactly the multistate matrix density $\mathbf{D}(\mathbf{r})$ for the N states of interest $\Psi^K; K = 1, ..., N$, the Hamiltonian matrix density functional is written as

$$\mathcal{H}[\mathbf{D}(\mathbf{r})] = \mathbf{T}_{\text{ms}} + \mathbf{E}_{\text{HFx}} + \int \mathbf{D}(\mathbf{r}) v_{\text{ext}}(\mathbf{r}) d\mathbf{r} + \mathcal{E}_{\text{c}}[\mathbf{D}(\mathbf{r})] \qquad (5.20)$$

where the four terms on the right-hand side of the equation are, respectively, the *matrix density functionals* for the kinetic, Hartree-Fock-exchange, external potential, and correlation energies. The matrix elements for the first three terms in Eq. 5.20 are determined from the corresponding Slater determinants,

$$\langle \Xi_A | \hat{H} | \Xi_B \rangle = (T_{\mathrm{ms}})_{AB} + (E_{\mathrm{HFx}})_{AB} + \int D_{AB}(\mathbf{r}) v_{\mathrm{ext}}(\mathbf{r}) d\mathbf{r}$$

The correlation matrix functional $\mathcal{E}_{\mathrm{c}}[\mathbf{D}(\mathbf{r})]$ is formally defined as follows according to Theorem 1,[257]

$$\mathcal{E}_{\mathrm{c}}[\mathbf{D}(\mathbf{r})] = \mathcal{F}[\mathbf{D}(\mathbf{r})] - (\mathbf{T}_{\mathrm{ms}} + \mathbf{E}_{\mathrm{HFx}}) \tag{5.21}$$

Note that for the ground state, i.e., $N = 1$, Eq. 5.21 is equivalent to the exchange-correlation functional in KS-DFT,

$$E_{\mathrm{xc}}^{\mathrm{KS}}[\rho_o(\mathbf{r})] = F[\rho_o(\mathbf{r})] - T_{\mathrm{s}} - \frac{1}{2} \int d\mathbf{r} d\mathbf{r}' \frac{\rho_0(\mathbf{r})\rho_0(\mathbf{r}')}{|\mathbf{r} - \mathbf{r}'|}$$

However, a difference from KS-DFT is that $\mathcal{E}_{\mathrm{c}}[\mathbf{D}]$ defines the part of correlation energy not explicitly included in the minimal active space used to represent $\mathbf{D}(\mathbf{r})$.[6]

5.2.3.3 Nonorthogonal State Interaction

The adiabatic ground and intermediate states in the present MS-EDA analysis are written as linear combinations of determinant basis states Ξ_A that form a minimal active space (MAS), consisting of the Kohn-Sham reference and singly excited configurations,

$$\Psi_{(X\bullet Y)}^{\mathrm{L}} = c_0 \Xi_{(X\bullet Y)}^{\mathrm{KS}} + \sum_{i,a} c_i^a \Xi_i^a \tag{5.22}$$

where $\Xi_{(X\bullet Y)}^{\mathrm{KS}}$ is the reference BLKS determinant for the block-localized complex (Eq. 5.5), Ξ_i^a is a singly excited configuration, and c are configuration coefficients determined by NOSI by diagonalizing the Hamiltonian matrix functional $\mathcal{H}[\mathbf{D}]$. Although orbitals and c can be optimized simultaneously, in NOSI,[6] the determinant states

$\Xi^{\mathrm{KS}}_{(X\bullet Y)}$ and in Eq. 5.22 are variationally optimized first using the block-localized excitation (BLE) method.[10, 9, 151] In particular, each constrained BLKS-determinant wave function is written

$$\Xi_i^a = \hat{A}\left\{(\xi_1^X \cdots \xi_{i-1}^X \xi_a^X \xi_{i+1}^X \cdots \xi_{N_X}^X) \bullet (\xi_1^Y \cdots \xi_{N_Y}^Y)\right\} \tag{5.23}$$

where ξ_j^U is the jth block-localized spin-orbital that is expanded over the basis functions located on atoms of monomer $U(U \in \{X,Y\}$, N_U is the number of electrons, and ξ_a^X indicates that the ith occupied spinorbital of monomer X in the BLKS reference $\Xi^{\mathrm{KS}}_{(X\bullet Y)}$ is replaced by the ath virtual orbital. In MSDFT, we include all spin-complement configurations in the MAS, all of which are together labeled by a single index Ξ_A.

Subsequently, the matrix elements of the Hamiltonian matrix functional $\mathcal{H}[\mathbf{D}]$ in the basis of Ξ_A are determined by

$$\mathcal{H}_{AB} = \langle \Xi_A | \hat{H} | \Xi_B \rangle + \mathcal{E}_{\mathrm{c}}[\mathbf{D}]_{AB} \tag{5.24}$$

where the first term can be evaluated by a standard method for nonorthogonal matrix elements.[260, 51, 34] For the diagonal elements $\mathcal{E}_{\mathrm{c}}[\mathbf{D}]_{AA}$ of the correlation matrix functional, the approximate density functional energy developed for KS-DFT is used,

$$\mathcal{E}_{\mathrm{c}}[\mathbf{D}]_{AB} = E_{\mathrm{xc}}^{\mathrm{KS}}[\rho_A(\mathbf{r})] \tag{5.25}$$

keeping in mind that $\rho_A(\mathbf{r})$ is obtained from a block-localized determinant Ξ_A with non-aufbau occupations for locally excited state.

The off-diagonal element $\mathcal{E}_{\mathrm{c}}[\mathbf{D}]_{AB}$ called transition density functional (TDF)[52] is new, and does not exist in KS-DFT; currently, an explicit approximate TDF has not yet been developed. Thus, further approximations are needed. For spin coupling interactions between determinants that yield a pair of singlet and triplet ($M_S = 0$) states, the value of the TDF energy can be obtained consistently by enforcing the energy degeneracy among the components of a triplet state,[69, 8, 176, 96] corresponding to a KS density functional used for the diagonal terms:

$$(\mathcal{E}_{\mathrm{c}})^{\mathrm{sp}}_{AB} = \frac{1}{2}\left\{E^{\mathrm{KS}}_{\mathrm{xc}}[\rho^{\uparrow\uparrow}_{AB}(\mathbf{r})] - E^{\mathrm{KS}}_{\mathrm{xc}}[\rho^{\uparrow\downarrow}_{A}(\mathbf{r})]\right\} \tag{5.26}$$

where $E^{\mathrm{KS}}_{\mathrm{xc}}[\rho^{\uparrow\uparrow}_{AB}(\mathbf{r})]$ is the "Kohn-Sham" correlation energy with the electron density $\rho^{\uparrow\uparrow}_{AB}(\mathbf{r})$ of the spin-up triplet state $\Xi^{\uparrow\uparrow}_{AB}$, and $E^{\mathrm{KS}}_{\mathrm{xc}}[\rho^{\uparrow\downarrow}_{A}(\mathbf{r})]$ is the KS correlation energy using $\rho^{\uparrow\downarrow}_{A}(\mathbf{r})$ (equivalently with $\rho^{\downarrow\uparrow}_{B}(\mathbf{r})$) corresponding to the spin-mixed determinant state. The superscript sp in Eq. 5.26 indicates spin-pairing interactions. The subscript AB in $\rho^{\uparrow\uparrow}_{AB}(\mathbf{r})$ is used to indicate that the determinant $\Xi^{\uparrow\uparrow}_{AB}$ refers to the triplet state with respect to the two spin complement determinants $\Xi^{\uparrow\downarrow}_{A}$ and $\Xi^{\downarrow\uparrow}_{B}$. Applying the TDF term in Eq. 5.26 in NOSI yields a pair of singlet and triplet states ($M_S = 0$), thereby, the singlet-triplet energy gap without spin contamination. For all other situations, we use the overlap-weighted average correlation energy of the two interacting states to approximate their TDF:[7]

$$(\mathcal{E}_{\mathrm{c}})_{AB} = \frac{1}{2}S^{\mathrm{KS}}_{AB}\left\{E^{A}_{\mathrm{xc}}[\rho_A(\mathbf{r})] + E^{B}_{\mathrm{xc}}[\rho_B(\mathbf{r})]\right\} \tag{5.27}$$

We note that the use of a standard exchange-correlation functional or a hybrid density functional for the diagonal terms typically yields more accurate results than employing a correlation-only functional. In this case, the corresponding exchange term is reciprocally removed in the first term of Eq. 5.24. In other words, standard KS-DFT energies are used for the diagonal terms except that the determinant is block-localized nonaufbau occupation constrained.

5.3 Computational Details

Monomer and exciplex structures have been optimized using KS-DFT or TDDFT with the Minnesota M06-2X density functional[177] and the cc-pVTZ and cc-pVDZ basis sets.[262] The Gaussian16 program is used in these calculations.[263] For the present multistate energy decomposition analysis, the MSDFT-NOSI method has been implemented into the Qbics program developed in our laboratories[261] and a separate program for BLW-ED analysis interfaced with the GAMESS-US program for electronic integrals.[107] In NOSI calculations, we used a fine grid consisting of 96 radial shells and 302 angular points. In addition, EOM-CCSD, FIC-NEVPT2, and MRCI were performed with two basis sets for comparison in the Supporting Information of [266]. Throughout this chapter, energies are given in electron volts (eV), widely used in spectroscopy of excited states.

5.4 Results and Discussion

Based on the nature of stabilizing forces in exciplex formation, we roughly group the excited-state complexes into three categories: (1) encounter excited-state complex, (2) charge-transfer exciplex, and (3) intimate excimer or exciplex. Excited-state complexes in Category 1 originate dominantly from the same type of intermolecular forces as that in the ground state, in which one molecule is in an excited state and the geometry of the other molecule in the complex remains in the ground state with only a minor geometrical deformation induced by (nonphotochemical) intermolecular interactions. The excimer complex between two acetone molecules and the exciplex between acetone and methyl vinyl ether belong to this category, in which one acetone molecule is excited to its $n \to \pi^\star$ state that is loosely bound to the second molecule. In Category 2, interfragment charge-transfer excitation has a lower energy than or similar to that of valence excitations of

Figure 5.4: Comparison of vertical excitation energies obtained using multistate density functional theory (MSDFT) and time-dependent density functional theory (TDDFT). The Minnesota M06-2X functional is used.

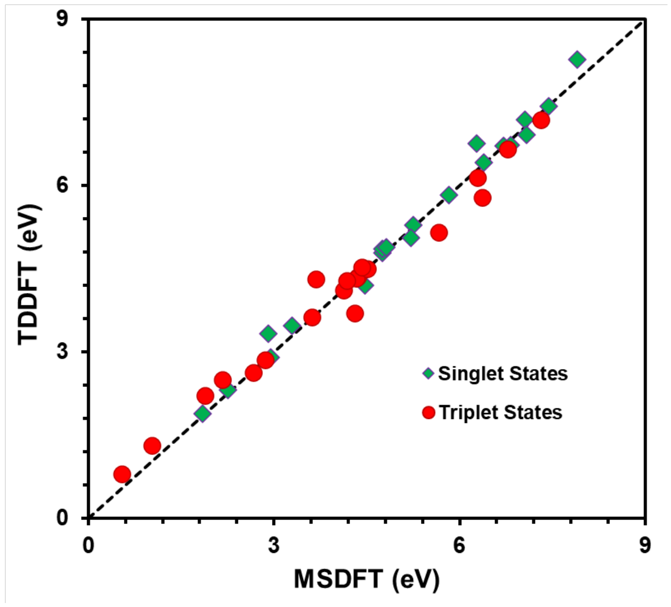

either species in a bimolecular complex. The driving force for exciplex formation is electrostatic Coulomb interaction. Examples include complexes involving the strong electron acceptor tetracyanoethylene (TCNE). Category 3 complexes are produced as a result of the resonant excitation of all individual species in the complex. The pentacene excimer complex in the S_1 state is a vivid illustration.

We first discuss the performance of nonorthogonal state interaction (NOSI) method of MSDFT by comparison with results from TDDFT calculations employing the same approximate density functional (M06-2X). Then, we present findings from MS-EDA analysis of the three categories of excited-state complexes.

5.4.1 Excitation Energies and Validation of Method

The performance of the MSDFT-NOSI method along with a small MAS is validated on the computed excitation energies (Fig. 5.4). Since intermediate reference states in the EDA procedure are electronic diabatic states, which are not direct observable experimentally, we focus on comparison of the

excitation energies of the monomer compounds. Table 5.1 lists the total energies of the ground state and the vertical excitation energies of the first two singlet excited states from MSDFT-NOSI calculations for the monomer compounds considered in this chapter and related molecules. In addition, included in Table 5.1 are the emission energies using the optimized structures of acetone and pentacene in the first excited states. The NOSI results are compared with TDDFT values along with experimental data. For these simple organic chromophores, TDDFT is known to perform well in benchmark studies,[289] providing a good reference for comparison with the NOSI method employing the same approximate density functional and basis set. Table 5.1 shows that the agreement between results from the two computational methods is excellent with a root-mean-square deviation (RMSD) of 0.11 eV for the S_1 states, 0.25 eV for the S_2 states, and 0.19 eV for all vertical excitation energies. A further indicator is the mean-signed-average (MSA) and mean-unsigned-error (MUE), which are -0.06 and 0.14 eV, exhibiting no systematic errors for the singlet excited states. We anticipate that this trend will be carried over to the energies of intermediate states in MS-EDA.

Another important finding is revealed in Table 5.1 by comparing the total ground-state energies from NOSI with those by KS-DFT calculations (Fig. 5.4). The former method is a multistate, multiconfigurational DFT in which *state interaction* is key in determining both the ground state and excited state energies, whereas the latter employs a non-interacting system consisting of a single determinant wave function purely for representing the ground-state density. One lingering question in multiconfigurational

Table 5.1: Computed total energies (au) for the ground state and excitation energies (eV).[a]

molecule [b]	S_0 (au)		S_1			S_1		
	MSDFT	ΔE_{KS}	MSDFT	TDDFT	exp[c]	MSDFT	TDDFT	exp[c]
naphthalene	−385.76533	0.00000	4.75	4.78	4.7	4.81	4.89	3.97
pentacene	−846.54223	0.00000	2.25	2.32	2.3	3.29	3.47	
PCA	−845.54485	−0.00007	5.25	5.29	5.08	5.83	5.83	6.41
TCNE	−447.41678	0.00000	4.75	4.85	4.75, 4.84	5.21	5.06	5.67
t-DME	−307.51100	−0.00015	6.71	6.71	6.2	7.08	6.91	
c-DME	−307.50997	−0.00028	6.39	6.42	6.16	6.82	6.73	
MVE	−193.03249	−0.00043	7.06	7.19	6.48	7.44	7.42	9.6
$Me_2C=O$	−193.07551	−0.00055	4.47	4.20	4.38	7.90	8.27	6.35
$Me_2C=O$ (S_1)	−193.04394	−0.00197	2.94	2.90	3.06	6.27	6.75	
pentacene (S_1)	−846.53459	0.00000	1.85	1.89		2.91	3.33	

[a]The Minnesota M06-2X density functional is used both in NOSI and TDDFT calculations. Relative energy given in electron volts (eV) between results from MSDFT-NOSI and KS-DFT, $\Delta E_{\mathrm{KS}} = E_{\mathrm{NOSI}} - E_{\mathrm{KSDFT}}$. This is a reasonable indicator of possible double counting of electron correlation for single-reference molecules.
[b]PCA: para-chloromethyl anisole, TCNE: tetracyanoethylene, MVE: methyl vinyl ether, DME: 1,2- dimethoxyethene.
[c]References [113, 292, 293, 294, 295, 296]

Table 5.2: Computed total triplet-state energies (au) and excitation energies (eV) for the first two triplet states relative to the singlet ground state.[a]

molecule[b]	$T_1(X)$ MSDFT	$T_1(X)$ ΔE_{KS}	T_1 MSDFT	T_1 TDDFT	T_1 exp[c]	T_2 MSDFT	T_2 TDDFT	T_2 exp
naphthalene	−385.63259	−0.00050	3.61	3.63	3.0	4.18	4.28	3.9
pentacene	−846.50452	−0.01088	1.03	1.32	0.86	2.17	2.50	> 2.0
PCA[c]	−845.40970	−0.03489	3.68	4.32		4.42	4.53	
TCNE	−447.31172	0.00000	2.86	2.86		5.66	5.16	
t-DME	−307.35069	−0.00004	4.36	4.36		6.77	6.65	
c-DME	−307.35079	−0.00026	4.33	4.33		6.29	6.14	
MVE	−192.86691	0.00000	4.51	4.50	4.2	7.31	7.19	8.8
$Me_2C = O$	−192.92376	0.00000	4.13	4.11	4.18	6.36	5.78	5.88
$Me_2C = O$ (S_1)	−192.94603	−0.00001	2.66	2.63		4.30	3.70	
pentacene (S_1)	−846.51462	−0.00923	0.54	0.80		1.88	2.22	

[a]The Minnesota M06-2X density functional is used.
[b]PCA: para-chloromethyl anisole, TCNE: tetracyanoethylene, MVE: methyl vinyl ether, DME: 1,2- dimethoxyethene.
[c]References [296, 297, 298, 299, 300].

DFT (MC-DFT) has been double counting of electron correlation since KS-DFT, in principle, includes all electron correlation, which is added to an MCSCF energy.[52, 131, 290, 291, 169] MSDFT differs from other MC-DFT models in that the total electron density from a MCSCF wave function is not directly used in KS-DFT correlation energy evaluations. Rather, the MSDFT correlation functional is an implicit functional of the multistate density and the correlation functional developed for KS-DFT is used solely to approximate the correlation energy of a determinant state (diagonal terms) of the Hamiltonian matrix density functional $\mathcal{H}[\mathbf{D}]$. Consequently, we find that the difference in the ground-state energy between MSDFT and KS-DFT is negligibly small, even though the KS-DFT state is included as one member of the MAS in all NOSI calculations. Acetone exhibits a small amount of multistate stabilization of 0.55 meV (0.01 kcal/mol) in the ground-state geometry and ca. 2 meV (0.05 kcal/mol) using the S_1 state geometry, while multistate effects as compared to KS-DFT are generally less than 0.5 meV for other compounds. The data in Table 5.1 demonstrate that there is little double-counting of correlation in these systems when an approximate density functional developed for KS-DFT is directly used for the determinant states in MSDFT.

The computed triplet state energies are given in Table 5.2. For the lowest triplet T_1 state, KS-DFT is typically sufficient, whereas the T_2 states are obtained using TDDFT based on this reference. Table 5.2 shows that the accord between NOSI and TDDFT (KS-DFT) results is also reasonably good. In particular, the RMSD errors are 0.25 eV for T_1 states, 0.35 eV for T_2 states, and 0.31 eV overall. Further, the MSE and MUE are, respectively, 0.00 and 0.20 eV for all triplet states. However, the NOSI T_1 energies of pentacene (both in the S_0 and S_1 structures) and para-chloromethyl anisole (PCA) have somewhat greater deviations from KS-DFT values than other cases. We attribute the increased deviation to multiconfiguration characteristics in the T_1 triplet states for these two aromatic compounds, which is confirmed by the Chirgwin-Coulson structure

Figure 5.5: Optimized structures in the first singlet excited states of the acetone excimer and acetone $\cdots$ methyl vinyl ether exciplex.

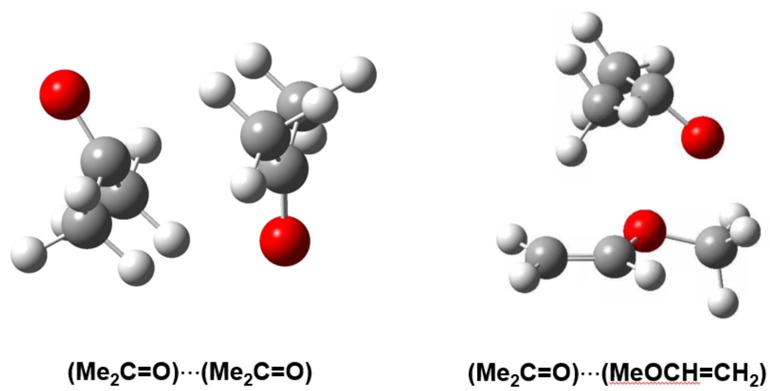

weights, having values of 0.92 and 0.94 for the dominant configuration in the two (S_0 and S_1) pentacene structures, and a value of only 0.65 for the dominant configuration in PCA. Thus, the use of a single determinant in KS-DFT for the T_1 state may be questionable for these compounds and could indeed have large errors. In this regard, the results from MSDFT-NOSI may be more reliable. This is reflected in the computed T_1 energies, where NOSI yields a lower value than KS-DFT.

5.4.2 Encounter Excited State Complexes

The optimized structures (Fig. 5.5) of the excimer complex of two acetone molecules and the exciplex between acetone and methyl vinyl ether in their first excited state using TDDFT/ M06-2X/cc-pVTZ reveal that they are characterized as a single acetone excitation to its $n \rightarrow \pi^\star$ state with a bent geometry interacting with its binding partner in the ground state. This is clearly reflected by the geometrical distortion energies of 0.75 and 0.82 eV for the photochemically excited acetone in the two complexes (Table 5.3), respectively, corresponding to the change from the ground state in equilibrium to that found in the excited-state complexes. For the other partners in the complexes the energy

Table 5.3: Excitation energies of adiabatic, diabatic, and intermediate states in the lowest singlet and triplet excited states associated with the acetone dimeric and acetone $\cdots$ methyl vinyl ether (MVE) exciplex complexes. [a]

$X \cdots Y$ energy terms		$(\mathrm{Me_2C=O}) \cdots (\mathrm{Me_2C=O})$ singlet	triplet	$(\mathrm{Me_2C=O}) \cdots (\mathrm{MVE})$ singlet	triplet
$h\nu_{\mathrm{ad}}$	$X^{\star}[EC]$	3.80	3.53	3.79	3.53
	$Y^{\star}[EC]$	4.39	4.08	6.80	4.39
ΔE_{dist}	$X[EC]$	0.75	0.75	0.82	0.82
	$Y[EC]$	−0.02	−0.02	−0.01	−0.01
E_{Lex}	$(X^{\star} \bullet Y)$	3.58	3.31	3.64	3.38
	$(X \bullet Y^{\star})$	4.97	4.67	7.46	5.04
E_{Ex}	$(X \bullet Y)^{\star}_{+}$	3.58	3.31	3.64	3.38
	$(X \bullet Y)^{\star}_{-}$	4.97	4.67	7.34	5.04
E_{SE}	$(X \bullet Y)^{\mathrm{SE}}_{+}$	3.52	3.26	3.64	3.38
	$(X \bullet Y)^{\mathrm{SE}}_{-}$	4.85	4.55	6.31 (CT),[b] 7.38	5.04
$E_{(XY)}$	$(XY)^{\star}_{1}$	3.53	3.22	3.63	3.39
	$(XY)^{\star}_{2}$	4.66	4.46	5.76 (CT),[b] 7.27	4.51

[a] All energies are given in electron volts (eV), relative to the ground state energies of a monomer, $X[S_0]$ and $Y[S_0]$, or two separate molecules at their optimized structures, i.e., adiabatic ground-state energies are set equal to zero. Square brackets indicate optimized geometry used in energy calculations with S_0 for the ground state and EC as exciplex complex. All calculations for bimolecular complexes adopt the [EC] structure. The M06-2X density functional and the cc-pVTZ basis set are used in NOSI calculations. The energies terms may be compared with the illustration of Scheme 5.3.

[b] Charge transfer (CT) state.

changes are negligible (the small negative values are probably due to multistate effects). Table 5.3lists the adiabatic and intermediate excited-state energies of the monomer and dimer species, all of which are given relative to that at the equilibrium ground state for direct comparison (Scheme 5.3). Therefore, the adiabatic excitation energies of acetone are about 3.8 eV in both complexes, significantly smaller than the vertical excitation energy of 4.47 eV (Table 5.1),but the vertical emission ($h\nu_{ad} - \Delta E_{\text{dist}}$) energies of 3.05 and 2.97 eV of the excited acetone in the exciplex geometries in the two complexes are similar to that (2.94 eV) of the optimized S_1 structure of acetone (Table 5.1) from MSDFT-NOSI calculations. On the other hand, the "adiabatic" excitation energies of the second monomers in the two exciplexes are, respectively, 4.39 and 6.80 eV, close to the vertical excitation energies of the isolated monomers (4.47 and 7.06 eV). Thus, these two exciplexes are best described as dipolar van der Waals complexes.

The triplet state energies are also shown in Table 5.3, exhibiting similar trends, but they are obtained using the same monomer and excimer geometries optimized for the singlet states. Thus, they are not further discussed nor listed for these complexes or any of the other systems below.

The local excitation energies of the excited acetone and its binding partner in both complexes exhibit different trends (Tables 5.1 and 5.2), with a large Stokes shift of 0.84 eV (3.80 eV excitation and 2.96 eV emission) in the acetone excimer and 0.79 eV (3.79 eV excitation and 3.00 eV emission) in the acetone-MVE exciplex for the excited acetone molecule, but with essentially no spectral change for the second monomer in the complex as it largely remains in the ground-state geometry. A relevant quantity is the exciton polarization energy, $\Delta E^{K}_{\text{Lpol}}$, corresponding to the vertical excitation energy difference of the chromophore (acetone) in the same geometry with and without the presence of the second binding partner molecule, which is -0.09 eV (2.96 eV-3.05 eV) for the

Figure 5.6: Ground and excited-state energies (eV) for the first singlet exciplex of acetone and methyl vinyl ether in multistate energy decomposition analysis. The energies of adiabatic ground state of isolated monomers in equilibrium geometries have been set equal to zero. The effective adiabatic excitation energies of the separate monomers in the exciplex geometries are given in red. Singlet (maroon) and triplet (green) states are labeled on the far right for exciplex complex. Energy levels are not drawn in scale. Energies corresponds to excitation and resonance terms defined in Scheme 5.2.

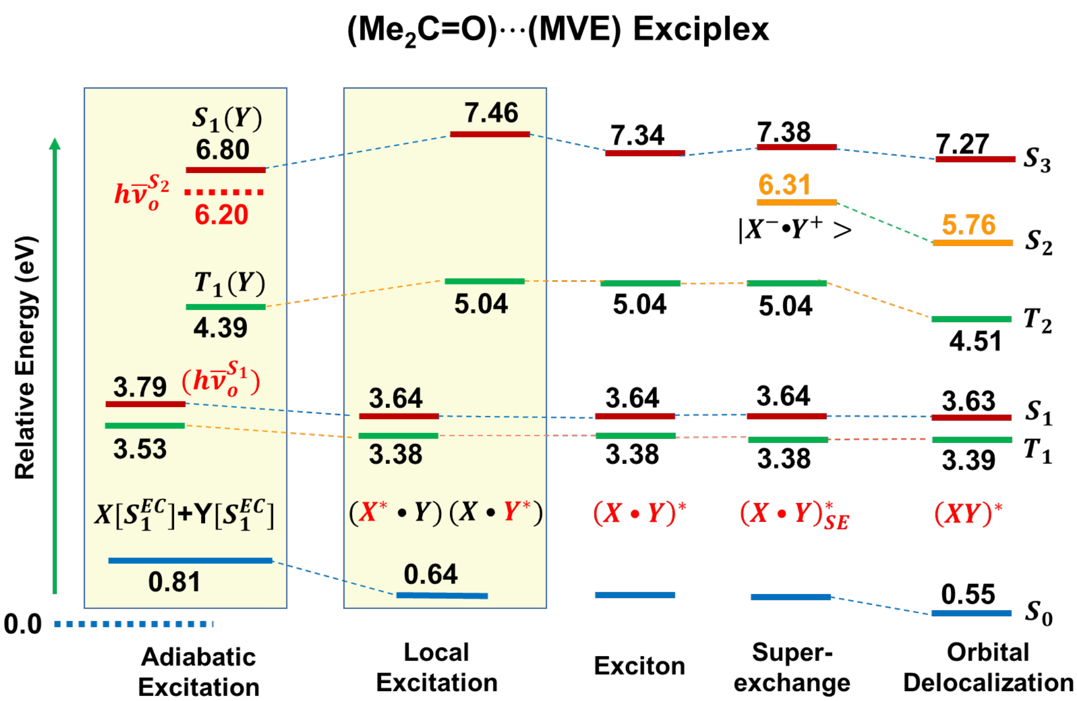

acetone excimer, and +0.03 eVł (3.00 eV-2.97 eV) in the acetone-MVE exciplex. The polarization effects are small for the ground-state monomers, with energy changes of +0.06 and +0.01 eV in the two complexes, respectively. Note that the seemingly positive energy changes are compensated for by the binding energy of the isolated, distorted monomers to form the local complexes (−0.11 and −0.17 eV, respectively). The excited-state energies and relative energies in Table 5.4 are displayed in Fig. 5.6 for the acetone-MVE exciplex, corresponding to the energy terms defined in Scheme 5.4, whereas results for the acetone excimer can be found in ref [198]. Fluorescence quenching by alkyl vinyl ethers

Table 5.4: Relative energies (eV) in multistate energy decomposition analysis of the lowest singlet and triplet excited states in the acetone excimer and acetone $\cdots$ methyl vinyl ether (MVE) exciplex.[a]

$X \cdots Y$	$(\mathrm{Me_2C=O}) \cdots (\mathrm{Me_2C=O})$				$(\mathrm{Me_2C=O}) \cdots (\mathrm{MVE})$			
energy terms	S_1	S_2	T_1	T_2	S_1	S_2	T_1	T_2
$h\bar{\nu}_0^K$	3.80	4.39	3.53	4.08	3.79	6.20	3.53	4.39
$\Delta E_{\mathrm{ref}}^K$	2.96	4.35	2.69	4.05	3.00	6.70	2.74	4.40
ΔE_{Lint}	0.62	0.62	0.62	0.62	0.64	0.64	0.64	0.64
ΔE_{Ex}^K	2.96	4.35	2.69	4.05	3.00	6.70	2.74	4.40
$\Delta\Delta E_{\mathrm{Res}}^K$	0.00	0.00	0.00	0.00	0.00	0.00	0.00	0.00
$\Delta\Delta E_{\mathrm{SE}}^K$	−0.06	−0.12	−0.05	−0.12	0.00	-1.03,[b] 0.04	0.00	0.00
$\Delta\Delta E_{\mathrm{OCD}}^K$	0.01	−0.19	−0.04	−0.09	−0.01	-0.55,[b] -0.11	0.01	−0.53
$\Delta\Delta E_{\mathrm{LCT}}^{S_0}$	−0.07	−0.07	−0.07	−0.07	−0.09	−0.09	−0.09	−0.09
ΔE_b	−0.27	0.27	−0.41	0.38	−0.16	-0.44,[b] 1.07	−0.14	0.12

[a] See Scheme 5.3 and the footnote of Table 5.3.
[b] Charge transfer state, energy given relative to the S_2 exciton state.

has been reported by Schore and Turro who attributed the observed quenching rates to the formation of acetone $\cdots$ ether exciplexes with charge transfer playing a role.[301] A correlation to the observed spectral shift of tetracyanoethylene $\cdots$ alkyl vinyl ethers discussed next was found.

The remainder of the energy terms for the two loosely associated excimer complexes are largely unremarkable except the second excited state of the acetone-MVE exciplex (recall that geometry is optimized for the S_1 state), where a charge transfer state emerges to be lower than the covalent excitation of MVE (state in brown in the superexchange intermediate in Fig. 5.6). Thus, relative to the S_2 exciton state, corresponding to the first local excited state of MVE in the dimer complex, the superexchange stabilization is $-1.03\,\text{eV}$, which is further lowered by $-0.55\,\text{eV}$ by orbital and configuration-state delocalization (OCD term). Therefore, the net binding energy of the S_2 exciplex state (S_1 state geometry) is $-0.44\,\text{eV}$, relative to MVE reference valence excitation ($h\bar{\nu}_o^{S_2}$). For the S_1 exciplexes of acetone dimer and acetone-MVEł, the net binding energies (Eq. 5.4) are -0.27 and $-0.33\,\text{eV}$, with a net ground-state contribution of $0.55\,\text{eV}$ in both systems to overcome the large structural distortion energies.

5.4.3 Charge-Transfer Complexes

Tetracyanoethylene (TCNE) can form rather stable complexes (Fig. 5.7) with methyl vinyl ether (MVE) and naphthalene (Naph) in the ground state with binding energies of $-0.51\,\text{eV}$ and $-0.28\,\text{eV}$ (-11.8 and $-6.5\,\text{kcal/mol}$), respectively (Table 5.5).However, at the S_1 exciplex geometries, the binding energies in the ground state (ΔE_{Lb}) are repulsive ($+0.41\,\text{eV}$) in the MVE structure and barely associative ($-0.03\,\text{eV}$) for the naphthalene complex, indicating significant monomer structure distortion in the exciplex. In both exciplexes, the lowest excited state is of charge transfer character from the electron rich monomers to TCNE. In fact, the three lowest excited states in the TCNE-Naph exciplex

Table 5.5: Relative energies (eV) of adiabatic, diabatic, and intermediate states in the lowest singlet excited states of tetracyanoethylene (TCNE) $\cdots$ methyl vinyl ether and TCNE $\cdots$ naphthalene exciplex.[a]

$X \cdots Y$ energy terms		(TCNE) $\cdots$ ($MeOCH = CH_2$) $[S_0]$ geom	$[S_1]$ geom	(TCNE) $\cdots$ (naphtalene)[b,c] $[S_0]$ geom	$[S_1]$ geom
$h\nu_{\mathrm{ab}}^{\mathrm{ad}}$	$X^{\star}$[EC]	4.68	4.41	4.58	4.44
	$Y^{\star}$[EC]	6.81	6.49	4.61[b]	4.65[b]
				4.69[c]	4.50[c]
ΔE_{dist}	X[EC]	0.00	0.17	0.02	0.22
	Y[EC]	−0.02	−0.03	−0.02	0.12
E_{Lex}	$(X^{\star} \bullet Y)$	4.55	4.67	4.35	4.27
	$(X \bullet Y^{\star})$	6.60	7.04	4.40[b]	4.56[b]
				4.48[c]	4.42[c]
E_{Ex}	$(X \bullet Y)_{+}^{\star}$	4.46	4.58	4.10	3.87
	$(X \bullet Y)_{-}^{\star}$	6.69	7.10	4.40[b]	4.56[b]
				4.69[c]	4.76[c]
E_{SE}	$(X \bullet Y)_{+}^{\mathrm{SE}}$	3.04 (CT)	1.90 (CT)	2.42 (CT)[d]	1.77 (CT)[d]
		4.42	4.69	3.16 (CT)[d]	2.81 (CT)[d]
				4.12[c]	3.98[c]
				4.53 (CT)[d]	4.13 (CT)[d]
	$(X \bullet Y)_{-}^{\mathrm{SE}}$	6.65	7.10	4.41[b]	4.61[b]
				4.69[c]	4.81[c]
$E_{(XY)}$	$(XY)_{1}^{\star}$	2.62 (CT)	1.19 (CT)	1.67 (CT)[d]	1.15 (CT)[d]
		4.29	4.63	2.46 (CT)[d]	2.29 (CT)[d]
				3.77 (CT)[d]	3.45 (CT)[d]
				4.32	4.12
	$(XY)_{2}^{\star}$	NA[e]	NA[e]	4.40[b]	4.38[b]
				4.51[c]	4.53[c]

[a]All energies are given relative to the adiabatic ground state energies of monomers. The M06-2X density functional and the cc-pVDZ basis set are used. The energy terms may be compared with the illustration of Scheme 5.3.
[b,c]Two close-lying states are given for naphthalene.
[b] L_b state.
[c] L_a state.
[d]Charge transfer (CT) states, respectively from HOMO, HOMO − 1, and HOMO − 2 of naphthalene to the LUMO of TCNE.
[e]Not assigned.

Figure 5.7: Optimized bimolecular complex structures (side view on top, and top or tilt views in the bottom) for tetracyanoethylene (TCNE) $\cdots$ methyl vinyl ether, TCNE $\cdots$ naphthalene, and pentacene dimer in the optimized ground state $(XY)S_0$ (crystal structure for pentacene) and first singlet excited state $(XY)S_1$. M06-2X density functional and the cc-pVDZ basis set are used.

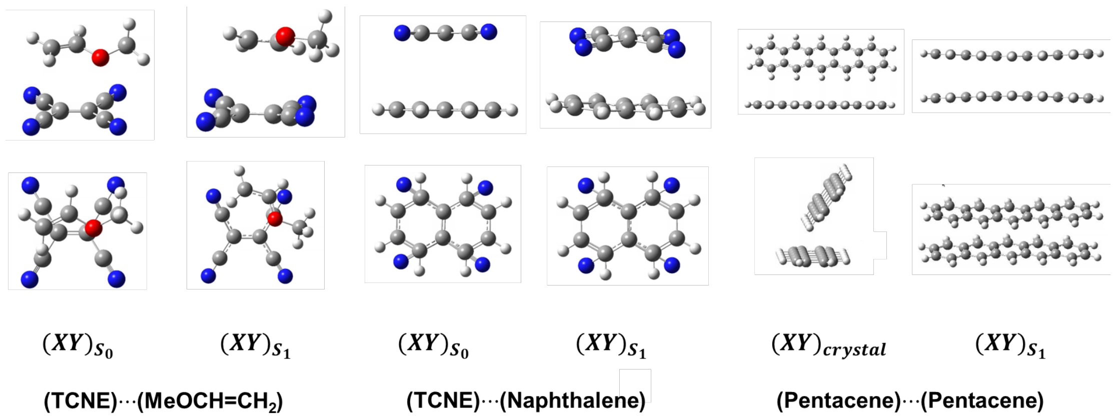

are CT states, corresponding to the transfer of one electron from the HOMO, HOMO -1, and HOMO -2 orbitals of naphthalene to the LUMO of TCNE (Table 5.5 and Fig. 5.8), in both the optimized complex structures of the ground state (S_0) and the first excited state (S_1). In the exciplex complex, the electron acceptor TCNE is noticeably distorted with a bent butterfly like geometry, having a geometrical distortion energy ΔE_{dist} of 0.17 eV in the MVE complex and 0.22 eV in the naphthalene state. Interestingly, covalent vertical excitation energies for both monomers in the two exciplex complexes are not significantly different in the S_0 and S_1 complex structures. Exciton delocalization only lowers the excited-state energies modestly by about 0.1 eV in the TCNE-MVE exciton state, and somewhat greater at 0.25 to 0.40 eV for the TCNE-Naph complex.

Not surprisingly, the greatest energy contribution in the MS-EDA analysis come from charge transfer (CT) effects in the direction from MVE or Naph to TCNE. For the TCNE-MVE complex, the charge-transfer superexchange stabilization is estimated to be 1.42 eV using the ground-state structure of the bimolecular complex, and 2.68 eV

Figure 5.8: Ground (blue) and excited-state (maroon) energies (eV) for the singlet exciplex of tetracyanoethylene (TCNE) and naphthalene in multistate energy decomposition analysis. The S_0 complex geometry is used. The energies are given relative to that of adiabatic ground state of isolated monomers in equilibrium geometry. Three charge transfer states (in brown) appear at the superexchange stage of MS-EDA. The effective adiabatic excitation energies of the separate monomers in the exciplex geometries are 4.62, 4.61, and 4.65 eV for the first, second, and third exciton states, originating dominantly from the $\pi \rightarrow \pi^\star$ state of TCNE, and the L_b and L_a states of naphthalene. Energies corresponding to excitation and resonance terms defined in Scheme 5.2.

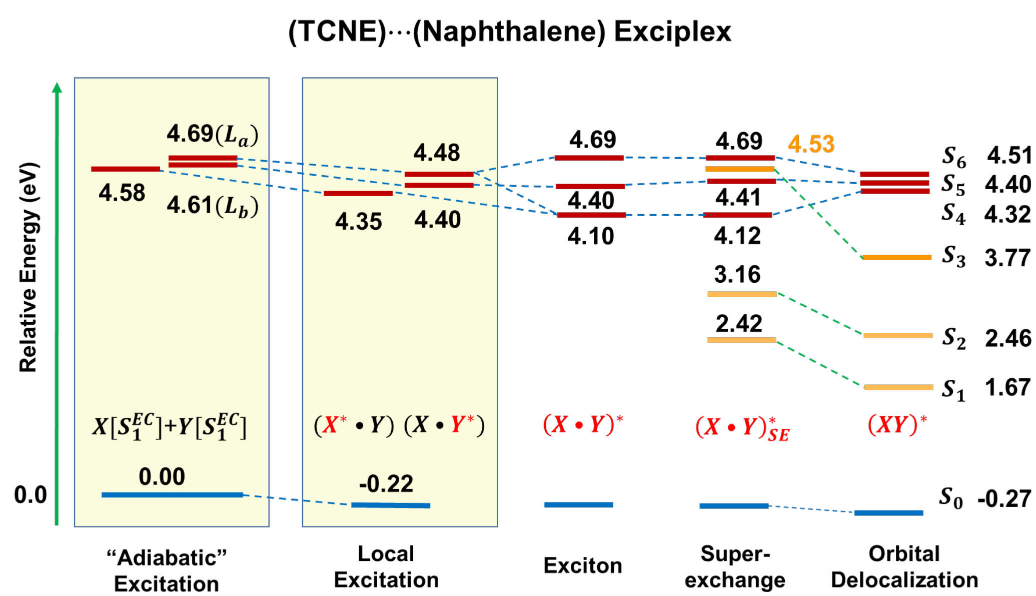

in the S_1 exciplex geometry. Similarly, for the TCNE-Naph exciplex, we found a CT stabilization of 1.68 eV in the S_0 complex geometry (Fig. 5.8), and 2.10 eV in the S_1 exciplex structure. Orbital delocalization also significantly lowers the excitation energies of the exciplexes, contributing -0.42 and -0.71 eV in the two structures of TCNE-MVE exciplex, and -0.75 and -0.62 eV for the TCNE-Naph complexes. However, the charge delocalization effects from TDDFT calculations are likely overestimated due to delocalization errors on charge-transfer excitations.[190]

For a CT exciplex, its binding energy is not directly related to covalent excitation of either monomer. Nevertheless, we can still consider the CT complex formation through an initial formation of the exciton complex, followed by an interfragment charge transfer as in the MS-EDA steps. Then, the definition of binding energy of Eq. 5.3 can still be used. Thus, for TCNE $\cdots$ MVE, the binding energies at geometries of the ground-state complex and the optimized S_1 exciplex are -2.15 and -3.28 eV, and for TCNE $\cdots$ Naph, they are -2.94 and -3.30 eV, respectively.

On the other hand, if one considers the starting reference state as the equilibrium geometry of the bimolecular complex in the ground state, the exciplex binding energy may be defined by the following photochemical process:

$$(XY)[S_0]^{S_0} \xrightarrow{h\nu^{\mathrm{CT}}_{(XY)}} (XY)[S_0]^{S_1} \xrightarrow{\Delta E_{\mathrm{b}}^{\mathrm{CT}}} (XY)[S_1]^{S_1} \tag{5.28}$$

Equation 5.28 shows that for a CT exciplex, the binding energy of the exciplex may be assigned to the energy change from the vertical charge-transfer absorption complex in the equilibrium ground-state geometry to the equilibrium exciplex geometry. From the data in Table 5.6, we immediately obtain a $\Delta E_{\mathrm{b}}^{\mathrm{CT}}$ of -1.13 eV in the TCNE $\cdots$ MVE exciplex and -0.36 eV in TCNE $\cdots$ Naph, as a result of structural relaxation induced by CT excitation. Then, the energy components will be the term-by-term difference in

Table 5.6: Relative energies (eV) in multistate energy decomposition analysis of the lowest singlet states in tetracyanoethylene (TCNE)$\cdots$methyl vinyl ether and TCNE$\cdots$naphthalene exciplex.[a]

$X \cdots Y$	(TCNE)$\cdots$(MeOCH $=$ CH$_2$)				(TCNE)$\cdots$(naphtalene) [b]			
geometry	$[S_0]$ geom		$[S_1]$ geom		$[S_0]$ geom		$[S_1]$ geom	
energy terms	$[S_1]$	$[S_2]$	$[S_1]$	$[S_2]$	$[S_1]$	L_b/L_a	$[S_1]$	L_a/L_b
hnu_o^K	4.77	6.72	4.47	6.37	4.62	4.61/4.65	4.45	4.47/4.65
ΔE_{Lint}	−0.23	−0.23	0.54	0.54	−0.22	-0.22	0.08	0.08
$\Delta E_{\mathrm{ref}}^K$	4.86	6.75	4.18	6.46	4.62	4.62/4.65	4.24	4.27/4.48
ΔE_{Ex}^K	4.69	6.92	4.04	6.66	4.33	4.62/4.91	3.79	4.48/4.68
$\Delta\Delta E_{\mathrm{Res}}^K$	−0.17	0.17	−0.18	0.20	−0.29	0.00/0.26	−0.45	0.21/0.20
$\Delta\Delta E_{\mathrm{SE}}^K$	(−1.42)	−0.04	(−2.68)	0.11	(−1.68)	0.01	(−2.10)	0.05
					(−0.94)	0.00	(−1.06)	0.05
					(0.43)		(0.26)	
					0.02		0.11	
$\Delta\Delta E_{\mathrm{OCD}}^K$	(−0.42)	−0.13	(−0.71)	−0.06	(−0.75)	-0.02	(−0.62)	-0.28
					(−0.70)	-0.18	(−0.52)	-0.23
					(−0.76)		(−0.68)	
					0.20		0.14	
$\Delta E_{\mathrm{LCT}}^{S_0}$	−0.28	−0.28	−0.13	−0.13	−0.05	-0.05	−0.11	-0.11
$\Delta E_{\mathrm{Lb}}^{S_0}$	−0.51		0.41		−0.27	-0.27	−0.03	-0.03
ΔE_{b}^K	(−2.15)		−3.28		(−2.94)	-0.22	(−3.30)	-0.14
covalent					−0.29	-0.14	−0.33	-0.07

[a]Charge transfer (CT) states are shown in parentheses. See Scheme 5.3for energy definition and the footnote of Table 5.3.
[b]Only binding energy for the lowest charge transfer state is shown.

Table 5.5 obtained between the optimized geometries in the ground state $(XY)[S_0]$ and the excited state of the exciplex $(XY)[S_1]$. The details of these energy differences are not further discussed here.

Experimentally, a charge-transfer absorption spectrum for the TCNE $\cdots$ MVE complex has been reported with a maximum absorption wavelength of 401 nm (3.09 eV) in 90 % cyclohexane and 10 % CH_2Cl_2 solution.[302] With the ground-state bimolecular complex structure, the computed values are 3.27 eV (3.04 - (-0.23)) at the superexchange stage using NOSI and 3.13 (2.62 - (-0.51)) eV, without considering solvent effects. The value for the exciplex geometry appears too low. In comparison with previous calculations using an optimized range-separated functional[148, 189] and experimental data,[190] the excitation energies of the TCNE $\cdots$ Naph complex for the first two exciplex states (2.64 and 3.38 eV) using the S_0 structure from the present MS-EDA using NOSI at the superexchange stage are in good accord with experimental results (2.60 and 3.23 eV for S_1 and S_2)[190] and with specifically optimized range-separated TDDFT calculations (2.7 eV for S_1)[148] and the CAM-QTP-02 functional (2.80 and 3.57 eV).[189]

5.4.4 Intimate Excimers

For the third category of excited-state complexes, in which the electronic excitation is fully delocalized over the monomers in the exciplex, we illustrate the energy components of the anthracene dimer system in two geometry arrangements: the optimized S_1

Table 5.7: Computed excitation energies (eV) and energy components from multistate energy decomposition analysis (MS-EDA) for pentacene excimer and a pentacene dimer fishbone configuration.[a]

	excimer		fishbone[b]	
energy term	L_a	L_b	L_a	L_b
$h\bar{\nu}_o^K$	2.10	3.14	2.21	3.24
ΔE_{dist}	0.18	0.18	0.03	0.03
$E_{\text{Lex}}[(X^\star \bullet Y)^K]$	1.89	3.04	1.99/1.98	2.92/2.92
$E_{\text{Ex}}[(X \bullet Y)^{K-}]$	1.46	2.92	1.97	2.92
$E_{\text{Ex}}[(X \bullet Y)^{K+}]$	2.40	3.03	2.02	2.93
$E_{\text{SE}}[(X \bullet Y)^{K-}_{\text{CT}}]$	0.62	2.70	1.88	2.92
$E_{\text{SE}}[(X \bullet Y)^{K+}_{\text{CT}}]$	2.30 (CT), 2.47	3.38	1.97, 2.23 (CT)	2.93
$E^{K-}_{(XY)}$	0.94	2.49	1.71	3.07
$E^{K+}_{(XY)}$	2.11	2.87	1.92	3.10

[a]All excitation energies are given relative to that of the adiabatic ground state of isolated pentacene. The M06-2X density functional is used along with the cc-pVDZ basis set. Adapted from ref [198]. Copyright 2023 American Chemical Society.
[b]The HOMO $-$ 1 $\rightarrow$ LUMO $+$ 1 configuration was not included.

excimer, and a fishbone configuration corresponding to that found in a crystal structure of anthracene (Table 5.7). This system has been described in a preliminary report on the MS-EDA methodology, although a different reference state was used in binding energy calculations. Here, we list the binding energy relative to the reference energy for the unbound species defined in Eq. 5.3 and the locally excited reference state for exciton resonance energies in Table 5.8. We highlight the key contrasting features of the intimate excimer in comparison with conformation dependence of the anthracene dimer itself, and the other two categories of exciplexes. An energy correlation diagram

Table 5.8: Relative energies (eV) in multistate energy decomposition analysis of singlet states of pentacene excimer and pentacene dimer in a fishbone configuration.[a]

geometry	excimer				fishbone[b]			
energy term	L_a^-	L_a^+	L_b^-	L_b^+	L_a^-	L_a^+	L_b^-	L_b^+
$h\bar{\nu}_o^K$	2.10	2.10	3.14	3.14	2.21	2.21	3.24	3.24
$\Delta E_{\mathrm{ref}}^K$	1.89	1.89	3.04	3.04	2.32	2.31	3.25	3.25
ΔE_{Lint}	0.07	0.07	0.07	0.07	−0.33	−0.33	−0.33	−0.33
ΔE_{Ex}^K	1.33	2.46	2.70	3.38	2.30	2.35	3.25	3.26
$\Delta\Delta E_{\mathrm{Res}}^K$	−0.56	0.57	−0.34	+0.34	−0.02	0.04	0.00	0.01
$\Delta\Delta E_{\mathrm{SE}}^K$	−0.84	(-0.10) 0.07	−0.22	0.35	−0.09	-0.05 (0.21)	0.00	0.00
$\Delta\Delta E_{\mathrm{OCD}}^K$	0.32	−0.19	−0.21	−0.51	−0.17	−0.05	0.05	0.07
$\Delta E_{\mathrm{LCT}}^{S_0}$	−0.13	−0.13	−0.13	−0.13	−0.14	−0.14	−0.14	−0.14
$\Delta E_{\mathrm{Lb}}^{S_0}$	−0.05	−0.05	−0.05	−0.05	−0.47	−0.47	−0.47	−0.47
ΔE_{b}^K	−1.22	(0.14)	−0.80	0.15	−0.50	−0.29	−0.27	−0.24

[a]Charge transfer (CT) states are shown in parentheses. Definition of energy terms can be found in Scheme 5.3. The M06-2X density functional is used along with the cc-pVDZ basis set.

for the excimer complex of pentacene dimer can be found in reference [198].

As other polyaromatic acenes, anthracene has two close-lying excited singlet states termed as the $L_a(S_1)$ and $L_b(S_2)$ states. The dimeric excimer of anthracene molecules was optimized to a symmetric geometry using TDDFT with M06-2X/cc-pVDZ, whereas the two monomers in the fishbone configuration in the crystal structure are not fully equivalent. In the latter case the HOMO $-$ 1 to LUMO $+$ 1 excited configuration was not fully converged and thus not included in the calculation, which would affect the L_a energy slightly. In the excimer geometry it has a rather small contribution to the L_a state using the excimer structure with a structure weight of 0.06 (0.94 for the HOMO $\rightarrow$ LUMO configuration). The anthracene dimer as a category 3 excimer is distinguished from the other two classes of exciplexes by strong exciton resonance interaction in all excimer states between the two locally excited monomers, resulting in large energy splitting $|\Delta V_{AB}|$ in the L_a and in the L_b state. Table 5.8 shows that the $L_a^{\pm}$ and $L_b^{\pm}$ energy differences are 1.13 and 0.68 eV for the excimer, and that $|\Delta V_{AB}|$ is highly sensitive to the distance and relative orientation (overlap) between the monomers, reducing to values of 0.05 and 0.01 eV for the two pairs of states in the fishbone configuration. In the excimer complex, the charge-delocalization state lies between the L_a^- and L_a^+ states, stabilizing the former by -0.84 eV, but increasing the energy of L_a^+ by 0.07 eV in a three-state interaction scheme. On the other hand, at the fishbone configuration, the charge-delocalization state is higher in energy than the L_a states, thereby, lowering the energies of both L_a^- and L_a^+ states by -0.09 and -0.05 eV. Surprisingly, superexchange stabilization is also highly dependent on the overlap between the two monomer states. Not surprisingly, the excimer complex has a strong binding energy of -1.16 eV, whereas for the fishbone configuration found in pentacene crystal it is only -0.50 eV, significant, but -0.47 eV comes from ground-state effect using the M06-2X density functional (Table 5.8).

5.4.5 Structure Weights

We finally comment on the computed structure weights of local states in the exciton and superexchange intermediates. In Table 5.9, we list the structure weights of three representative complexes, namely, the acetone $\cdots$ MVE and TCNE $\cdots$ naphthalene exciplex, and the anthracene excimer. In MS-EDA, the structure weights for the exciton states have been used to determine the corresponding weighted adiabatic excitation energy of the isolated molecules ($h\bar{\nu}_o^K$), and the reference energy for the locally excited states (ΔE_{ref}^K) to determine exciton resonance energy. Further examination of the data in Table 5.9 reveals an interesting trend. For the intimate excimer complexes, strong state interactions are found among the symmetry allowed local states. Even though the exciton resonance stabilization is severely reduced in the tilted pentacene orientation of the fishbone structure, exciton delocalization is observed. However, the tilting effect clearly results in a preference for a directional charge transfer in the superexchange complex, with structural weights of 0.28, 0.02, and 0.70 for the L_a^- exciton state and the $|P^- \bullet P^+\rangle$ and $|P^+ \bullet P^-\rangle$ charge transfer states, respectively. For comparison, this state (S_2) in the symmetric excimer complex has an equal forward and backward charge transfer contributions, resulting in a net zero charge transfer in the complex. The implication of this finding could be significant toward an understanding of the mechanism of directional multiexciton formation in singlet fission in pentacene monolayer materials.[58]

For class 2 and 3 exciplexes, although exciton state interactions can be strong in a particular state, they are generally not present for the remaining states. For example, in the acetone $\cdots$ MVE exciplex, the lowest singlet state is 100 % of $n \rightarrow \pi^\star$ local excitation of acetone, whereas in the second S_2 state, dominantly charge transfer from methyl vinyl ether to acetone is mixed with the local $n \rightarrow \pi^\star$ state at 9 % in structure weight. Furthermore, the local acetone $n \rightarrow \pi^\star$ state is strongly mixed with the MVE $\pi \rightarrow \pi^\star$ state, having structure weights of 20 % and 80 %, respectively. Yet, the contribution

Table 5.9: Structure weights of local excited states and individual charge transfer (CT) states in the exciton and superexchange intermediates in multistate energy decomposition analysis (MS-EDA). [a]

exciplex state	exciton $(X \bullet Y)^\star$		superexchange $(X \bullet Y)^{\mathrm{SE}}$		
	$(X^\star \bullet Y)$	$(X \bullet Y^\star)$	$(X \bullet Y)^\star$	$(X^- \bullet Y^+)$	$(X^+ \bullet Y^-)$
$(\mathrm{Me_2C=O}) \cdots$ MVE exciplex					
$(n \to \pi^\star)_X$	1.00	0.00	1.00	0.00	0.00
CT			0.09	0.91	0.00
$(\pi \to \pi^\star)_Y$	0.20	0.80	0.98	0.02	0.00
TCNE $\cdots$ Naphthalene exciplex					
$(CT)_{\mathrm{H}}$[b]			0.02	0.98	0.00
$(CT)_{\mathrm{H-1}}$[b]			0.11	0.89	0.00
$(\pi \to \pi^\star)_X$	0.61	0.39	0.92	0.08	0.00
$(CT)_{\mathrm{H-2}}$[b]			0.0	1.00	0.00
$(L_b)_Y$	0.0	1.00	0.98	0.02	0.00
$(L_a)_Y$	0.36	0.64	0.92	0.08	0.00
(pentacene)$_2$ excimer					
${}^1L_a^-$	0.43	0.57	0.64	0.18	0.18
(CT)			0.10	0.45	0.45
${}^1L_a^+$	0.58	0.42	0.90	0.05	0.05
${}^1L_b^-$	0.17	0.83	1.00	0.00	0.00
${}^1L_b^+$	0.92	0.08	1.00	0.00	0.00
(pentacene)$_2$ fishbone configuration					
${}^1L_a^-$	0.60	0.40	0.68	0.02	0.30
${}^1L_a^+$	0.40	0.60	1.00	0.00	0.00
(CT)			0.28	0.02	0.70
${}^1L_b^-$	0.57	0.43	1.00	0.00	0.00
${}^1L_b^+$	0.43	0.57	0.98	0.02	0.00

[a] States are listed in order of increasing energy of the exciplex, labeled by characteristic transitions of X (the first molecule in a $(X \bullet Y)$ complex) and Y (the second compound).
[b] HOMO, HOMO − 1 and HOMO − 2

of the $\pi \rightarrow \pi^\star$ state of MVE to acetone $n \rightarrow \pi^\star$ excitation is negligible. This is also seen in the TCNE$\cdots$naphthalene exciplex, in which the $\pi \rightarrow \pi^\star$ local state of TCNE is strongly coupled to the L_b state of the aromatic compound, but the L_a state is a pure local excitation. In all asymmetrical exciplexes, only one direction of charge transfer is dominant, rather than a charge-transfer resonance found in the symmetric pentacene excimer.

5.5 Conclusion

In this chapter, we present a multistate energy decomposition analysis (MS-EDA) to dissect the energy components in molecular complexes in excited states. In particular, the total binding energy of an excimer or an exciplex is partitioned into a ground-state effect called local interaction energy ΔE_{Lint}, an exciton excitation energy ΔE^K_{Ex} resulting from the resonance state interaction of individual monomer excited states $|\Psi^\star_X \bullet \Psi^{S_0}_Y\rangle$ and $|\Psi^{S_0}_X \bullet \Psi^\star_Y\rangle$, a superexchange stabilization energy $\Delta\Delta E^K_{\mathrm{SE}}$ due to intermolecular charge transfer $|\Psi^+_X \bullet \Psi^-_Y\rangle$ and $|\Psi^-_X \bullet \Psi^+_Y\rangle$, and an orbital and configuration-state delocalization energy $\Delta\Delta E^K_{\mathrm{OCD}}$ as a result of a stepwise progression from monomer block-localized Kohn-Sham orbitals to the fully delocalized molecular orbitals. To determine the exciton resonance energy $\Delta\Delta E^K_{\mathrm{Res}}$, we have defined a local excitation energy via the structure-weighted reference state without excited-state interaction. Similarly, a structure-weighted adiabatic excitation energy, corresponding to the minimum (photoexcitation) energy needed to produce an exciplex (or excimer) complex, has been introduced to give a well-defined energy term for binding of the exciplex or excimer complex in the excited state.

An important feature of the present MS-EDA method is that key intermediate states associated with different energy terms can be variationally optimized, providing quantitative insights into widely used physical concepts such as exciton delocalization and charge transfer effects in excited states. Although local molecular excitation to a particular state K in the presence of other molecules in the ground state, $\Delta E_{\text{Lex}}^{K}\left[|\Psi_X^{\star} \bullet \Psi_Y^{S_0}\rangle\right]$, is used as a reference state for the exciton resonance energy term, it also has a well-defined physical interpretation and the mutual polarization energy induced by such a local excitation can be related to experimental solvatochromic shifts of the excited chromophore in condensed phases or in molecular clusters. Furthermore, the electronic coupling matrix elements among locally excited states can also be used to determine the rates of excited-state energy transfer and photoexcitation-induced electron transfer. The availability of these diabatic states is made possible in the framework of multi-state density functional theory (MSDFT), a rigorous variational DFT of excited states recently proved by Lu and Gao.[257]

Through MS-EDA analysis, it was shown that molecular complexes in the excited states can be broadly classified into three main categories: (1) encounter excited-state complex, (2) charge-transfer exciplex, and (3) intimate excimer or exciplex. Excited-state complexes in Category 1 are species produced dominantly using the same type of intermolecular forces as that in the ground state, with one molecule happening to be in an excited state. Category 2 exciplexes are formed through intermolecular charge-transfer excitation, which typically has a lower energy than the valence excitations of individual monomers. Clearly, the driving force of exciplex formation here is electrostatic interaction. Intimate excited-state complexes in Category 3 are often, but not limited to, excimers consisting of identical monomers. In this category, exciton delocalization is the main force to produce a fully delocalized excited state. In light of lack of a correlation matrix functional, charge transfer states in some cases such as that in the pentacene excimer are sometimes overestimated in the present analysis. Nevertheless, the illustrative examples presented in this chapter highlight the interplay of local excitation polarization, exciton resonance and superexchange charge-transfer effects in molecular excited states. It is hoped that MS-EDA will become a useful tool for understanding photochemical and photobiological processes.

References

[1] W Kohn and L J Sham. Self-consistent equations including exchange and correlation effects. *Phys. Rev.*, 140:A1133, 1965.

[2] E Runge and E K U Gross. Density-functional theory for time-dependent systems. *Phys. Rev. Lett.*, 52:997, 1984.

[3] A K Theophilou. The energy density functional formalism for excited states. *Journal of Physics C: Solid State Physics*, 12(24):5419, dec 1979.

[4] Yangyi Lu and Jiali Gao. Multistate density functional theory of excited states. *The Journal of Physical Chemistry Letters*, 13(33):7762–7769, 2022, https://doi.org/10.1021/acs.jpclett.2c02088. PMID: 35969514.

[5] P Hohenberg and W Kohn. Inhomogeneous electron gas. *Phys. Rev.*, 136:B864, 1964.

[6] Y Y Lu, R Q Zhao, J Zhang, M Y Liu, and J L Gao. Minimal active space: NOSCF and NOSI in multistate density functional theory. *J. Chem. Theory Comput.*, 18:6407, 2022.

[7] A Cembran, L Song, Y Mo, and J Gao. Block-localized density functional theory (BLDFT), diabatic coupling, and its use in valence bond theory for representing reactive potential energy surfaces. *J. Chem. Theory Comput.*, 5:2702, 2009.

[8] Adam Grofe, Xin Chen, Wenjian Liu, and Jiali Gao. Spin-multiplet components and energy splittings by multistate density functional theory. *J. Phys. Chem. Lett.*, 8(19):4838–4845, 2017, https://doi.org/10.1021/acs.jpclett.7b02202. PMID: 28914545.

[9] Peng Bao, Christian P Hettich, Qiang Shi, and Jiali Gao. Block-Localized excitation for excimer complex and diabatic coupling. *J. Chem. Theory Comput.*, 17(1):240–254, January 2021.

[10] J Zhang, Z Tang, X Zhang, H Zhu, R Zhao, Y Lu, and J Gao. Target state optimized density functional theory for electronic excited and diabatic states. *J. Chem. Theory Comput.*, 19:1777, 2023.

[11] Wenjian Liu and Mark R. Hoffmann. ici: Iterative ci toward full ci. *Journal of Chemical Theory and Computation*, 12(3):1169–1178, 2016, https://doi.org/10.1021/acs.jctc.5b01099. PMID: 26765279.

[12] M Baer. *Beyond Born–Oppenheimer: Electronic Nonadiabatic Coupling Terms and Conical Intersections.* 2006.

[13] V May and O Kühn. *Charge and Energy Transfer Dynamics in Molecular Systems.* 2011.

[14] H Saigusa and E C Lim. Excimer formation in van der waals dimers and clusters of aromatic molecules. *Acc. Chem. Res.*, 29:171, 1996.

[15] C-P Hsu. The electronic couplings in electron transfer and excitation energy transfer. *Acc. Chem. Res.*, 42:509, 2009.

[16] H Koppel, W Domcke, D R Yarkony, and H Koppel. *Conical Intersections: Electronic Structure, Dynamics and Spectroscopy.* 2004.

[17] C A Mead and D G Truhlar. Conditions for the definition of a strictly diabatic electronic basis for molecular systems. *J. Chem. Phys.*, 77:6090, 1982.

[18] J E Subotnik, S Yeganeh, R J Cave, and M A Ratner. Constructing diabatic states from adiabatic states: Extending generalized Mulliken-Hush to multiple charge centers with boys localization. *J. Chem. Phys.*, 129:244101, 2008.

[19] A-J Zhang, P-Y Zhang, T-S Chu, K-L Han, and G-Z He. Quantum dynamical study of the electronic nonadiabaticity in the D+DBr Br(Br*)+D2 reaction on new diabatic potential energy surfaces. *J. Chem. Phys.*, 137:194305, 2012.

[20] Q Ou, G D Bellchambers, F Furche, and J E Subotnik. First-order derivative couplings between excited states from adiabatic TDDFT response theory. *J. Chem. Phys.*, 142:064114, 2015.

[21] X Zhu and D R Yarkony. Constructing diabatic representations using adiabatic and approximate diabatic data - coping with diabolical singularities. *J. Chem. Phys.*, 144:044104, 2016.

[22] H Nakamura and D G Truhlar. Extension of the fourfold way for calculation of global diabatic potential energy surfaces of complex, multiarrangement, non-Born-Oppenheimer systems: Application to HNCO(S-0,S-1). *J. Chem. Phys.*, 118:6816, 2003.

[23] C E Hoyer, K Parker, L Gagliardi, and D G Truhlar. The DQ and DQ phi electronic structure diabatization methods: Validation for general applications. *J. Chem. Phys.*, 144:194101, 2016.

[24] W Domcke and D R Yarkony. Role of conical intersections in molecular spectroscopy and photoinduced chemical dynamics. *Annu. Rev. Phys. Chem.*, 63:325, 2012.

[25] S L Li, D G Truhlar, M W Schmidt, and M S Gordon. Model space diabatization for quantum photochemistry. *J. Chem. Phys.*, 142:064106, 2015.

[26] Adam Grofe, Zexing Qu, Donald G. Truhlar, Hui Li, and Jiali Gao. Diabatic-at-construction method for diabatic and adiabatic ground and excited states based on multistate density functional theory. *Journal of Chemical Theory and Computation*, 13(3):1176–1187, 2017, https://doi.org/10.1021/acs.jctc.6b01176. PMID: 28135420.

[27] M Liu, X Chen, A Grofe, and J Gao. Diabatic states at construction (DAC) through generalized singular value decomposition. *J. Phys. Chem. Lett.*, 9:6038, 2018.

[28] J Gerratt, D L Cooper, P B Karadakov, and M Raimondi. Modern valence bond theory. *Chem. Soc. Rev.*, 26:87, 1997.

[29] W Wu, P Su, S Shaik, and P C Hiberty. Classical valence bond approach by modern methods. *Chem. Rev.*, 111:7557, 2011.

[30] D W Small, K V Lawler, and M Head-Gordon. Coupled cluster valence bond method: Efficient computer implementation and application to multiple bond dissociations and strong correlations in the acenes. *J. Chem. Theory Comput.*, 10:2027, 2014.

[31] J Lee, D W Small, and M Head-Gordon. Open-shell coupled-cluster valence-bond theory augmented with an independent amplitude approximation for three-pair correlations: Application to a model oxygen-evolving complex and single molecular magnet. *J. Chem. Phys.*, 149:244121, 2018.

[32] Y Mo and S D Peyerimhoff. Theoretical analysis of electronic delocalization. *J. Chem. Phys.*, 109:1687, 1998.

[33] Y Mo, J Gao, and S D Peyerimhoff. Energy decomposition analysis of intermolecular interactions using a block-localized wave function approach. *J. Chem. Phys.*, 112:5530, 2000.

[34] Y Mo and J Gao. An ab initio molecular Orbital-Valence bond (MOVB) method for simulating chemical reactions in solution. *J. Phys. Chem. A*, 104:3012, 2000.

[35] L Song and J Gao. On the construction of diabatic and adiabatic potential energy surfaces based on ab initio valence bond theory. *J. Phys. Chem. A*, 112:12925, 2008.

[36] Y Mo, P Bao, and J Gao. Energy decomposition analysis based on a block-localized wavefunction and multistate density functional theory. *Phys. Chem. Chem. Phys.*, 13:6760, 2011.

[37] Y Mo, L Song, and Y Lin. Block-Localized wavefunction (BLW) method at the density functional theory (DFT) level. *J. Phys. Chem. A*, 111:8291, 2007.

[38] H Stoll, G Wagenblast, and H Preuss. On the use of local basis sets for localized molecular orbitals. *Theor. Chim. Acta*, 57:169, 1980.

[39] E Gianinetti, M Raimondi, and E Tornaghi. Modification of the roothaan equations to exclude BSSE from molecular interactions calculations. *Int. J. Quantum Chem.*, 60:157, 1996.

[40] E Gianinetti, I Vandoni, A Famulari, and M Raimondi. Extension of the SCF-MI method to the case of K fragments one of which is an open-shell system. *Adv. Quantum Chem.*, 31:251, 1998.

[41] M Raimondi, A Famulari, R Specchio, M Sironi, F Moroni, and E Gianinetti. Ab initio non-orthogonal approaches to the computation of weak interactions and of localized molecular orbitals for QM/MM procedures. *Theochem*, 573:25, 2001.

[42] T Nagata, O Takahashi, K Saito, and S Iwata. Basis set superposition error free self-consistent field method for molecular interaction in multi-component systems: Projection operator formalism. *J. Chem. Phys.*, 115:3553, 2001.

[43] G G Ferenczy and W H Adams. Optimization of selected molecular orbitals in group basis sets. *J. Chem. Phys.*, 130:134108, 2009.

[44] R Z Khaliullin, M Head-Gordon, and A T Bell. An efficient self-consistent field method for large systems of weakly interacting components. *J. Chem. Phys.*, 124:204105, 2006.

[45] R Z Khaliullin, M Head-Gordon, and A T Bell. Theoretical study of solvent effects on the thermodynamics of Iron(III) [tetrakis(pentafluorophenyl)]porphyrin chloride dissociation. *J. Phys. Chem. B*, 111:10992, 2007.

[46] G F Smits and C Altona. Calculation and properties of Non-Orthogonal, strictly local Molecular-Orbitals. *Theor. Chim. Acta*, 67:461, 1985.

[47] M Couty, C A Bayse, and M B Hall. Extremely localized molecular orbitals (ELMO): a non-orthogonal Hartree-Fock method. *Theor. Chem. Acc.*, 97:96, 1997.

[48] K Sorakubo, T Yanai, K Nakayama, M Kamiya, H Nakano, and K Hirao. A non-orthogonal Kohn-Sham method using partially fixed molecular orbitals. *Theor. Chem. Acc.*, 110:328, 2003.

[49] L Song, J Song, Y Mo, and W Wu. An efficient algorithm for energy gradients and orbital optimization in valence bond theory. *J. Comput. Chem.*, 30:399, 2009.

[50] E J Sundstrom and M Head-Gordon. Non-orthogonal configuration interaction for the calculation of multielectron excited states. *J. Chem. Phys.*, 140:114103, 2014.

[51] Y Mo and J Gao. Ab initio QM/MM simulations with a molecular orbital-valence bond (MOVB) method: application to an SN2 reaction in water. *J. Comput. Chem.*, 21:1458, 2000.

[52] Jiali Gao, Adam Grofe, Haisheng Ren, and Peng Bao. Beyond Kohn–Sham approximation: Hybrid multistate wave function and density functional theory. *The Journal of Physical Chemistry Letters*, 7(24):5143–5149, 2016, https://doi.org/10.1021/acs.jpclett.6b02455. PMID: 27973892.

[53] X Chen and J Gao. Fragment exchange potential for realizing pauli deformation of interfragment interactions. *J. Phys. Chem. Lett.*, 11:4008, 2020.

[54] P Asgari, Y Hua, A Bokka, C Thiamsiri, W Prasitwatcharakorn, A Karedath, X Chen, S Sardar, K Yum, G Leem, B S Pierce, K Nam, J Gao, and J Jeon. Catalytic hydrogen atom transfer from hydrosilanes to vinylarenes for hydrosilylation and polymerization. *Nat. Catal.*, 2:164, 2019.

[55] H Li, Y J Wang, M P Ye, S S Li, D Y Li, H S Ren, M Wang, L C Du, H Li, G Veglia, J L Gao, and Y X Weng. Dynamical and allosteric regulation of photoprotection in light harvesting complex II. *Sci. China Chem.*, 63:1121, 2020.

[56] X Li, H Ren, M Kundu, Z Liu, F W Zhong, L Wang, J Gao, and D Zhong. A leap in quantum efficiency through light harvesting in photoreceptor UVR8. *Nat. Commun.*, 11:4316, 2020.

[57] Alessandro Cembran, Makenzie R. Provorse, Changwei Wang, Wei Wu, and Jiali Gao. The third dimension of a more O'Ferrall-Jencks diagram for hydrogen atom

transfer in the isoelectronic hydrogen exchange reactions of (PhX)(2)H-center dot with X = o, NH, and CH2. *Journal of Chemical Theory and Computation*, 8(11):4347–4358, 2012, https://doi.org/10.1021/ct3004595. PMID: 23226989.

[58] W-L Chan, T C Berkelbach, M R Provorse, N R Monahan, J R Tritsch, M S Hybertsen, D R Reichman, J Gao, and X-Y Zhu. The quantum coherent mechanism for singlet fission: Experiment and theory. *Acc. Chem. Res.*, 46:1321, 2013.

[59] Q Wu and T Van Voorhis. Constrained density functional theory and its application in Long-Range electron transfer. *J. Chem. Theory Comput.*, 2:765, 2006.

[60] Q Wu, C-L Cheng, and T Van Voorhis. Configuration interaction based on constrained density functional theory: A multireference method. *J. Chem. Phys.*, 127:164119, 2007.

[61] T Van Voorhis, T Kowalczyk, B Kaduk, L-P Wang, C-L Cheng, and Q Wu. The diabatic picture of electron transfer, reaction barriers, and molecular dynamics. *Annu. Rev. Phys. Chem.*, 61:149, 2010.

[62] B Kaduk, T Kowalczyk, and T Van Voorhis. Constrained density functional theory. *Chem. Rev.*, 112:321, 2012.

[63] M G Mavros and T Van Voorhis. Communication: CDFT-CI couplings can be unreliable when there is fractional charge transfer. *J. Chem. Phys.*, 143:231102, 2015.

[64] S R Yost, J Lee, M W B Wilson, T Wu, D P McMahon, R R Parkhurst, N J Thompson, D N Congreve, A Rao, K Johnson, M Y Sfeir, M G Bawendi, T M Swager, R H Friend, M A Baldo, and T Van Voorhis. A transferable model for singlet-fission kinetics. *Nat. Chem.*, 6:492, 2014.

[65] H Ren, M R Provorse, P Bao, Z Qu, and J Gao. Multistate density functional theory for effective diabatic electronic coupling. *J. Phys. Chem. Lett.*, 7:2286, 2016.

[66] A F Morrison, Z-Q You, and J M Herbert. Ab initio implementation of the Frenkel-Davydov exciton model: A naturally parallelizable approach to computing collective excitations in crystals and aggregates. *J. Chem. Theory Comput.*, 10:5366, 2014.

[67] A F Morrison and J M Herbert. Low-Scaling quantum chemistry approach to Excited-State properties via an ab initio exciton model: Application to excitation energy transfer in a Self-Assembled nanotube. *J. Phys. Chem. Lett.*, 6:4390, 2015.

[68] J M Herbert, X Zhang, A F Morrison, and J Liu. Beyond Time-Dependent density functional theory using only single excitations: Methods for computational studies of excited states in complex systems. *Acc. Chem. Res.*, 49:931, 2016.

[69] T Ziegler, A Rauk, and E J Baerends. Calculation of multiplet energies by Hartree-Fock-Slater method. *Theor. Chim. Acta*, 43:261, 1977.

[70] A T B Gilbert, N A Besley, and P M W Gill. Self-Consistent field calculations of excited states using the maximum overlap method (MOM). *J. Phys. Chem. A*, 112:13164, 2008.

[71] G M J Barca, A T B Gilbert, and P M W Gill. Simple models for difficult electronic excitations. *J. Chem. Theory Comput.*, 14:1501, 2018.

[72] J Liu, Y Zhang, and W Liu. Photoexcitation of Light-Harvesting C-P-C-60 triads: A FLMO-TD-DFT study. *J. Chem. Theory Comput.*, 10:2436, 2014.

[73] D Hait and M Head-Gordon. Excited state orbital optimization via minimizing the square of the gradient: General approach and application to singly and doubly excited states via density functional theory. *J. Chem. Theory Comput.*, 16:1699, 2020.

[74] A L L East and E C Lim. Naphthalene dimer: Electronic states, excimers, and triplet decay. *J. Chem. Phys.*, 113:8981, 2000.

[75] M Pabst, B Lunkenheimer, and A Köhn. The triplet excimer of naphthalene: A model system for Triplet-Triplet interactions and its spectral properties. *J. Phys. Chem. C*, 115:8335, 2011.

[76] S Shirai, Y Kurashige, and T Yanai. Computational evidence of inversion of l-1(a) and L-1(b)-Derived excited states in naphthalene excimer formation from ab initio multireference theory with large active space: DMRG-CASPT2 study. *J. Chem. Theory Comput.*, 12:2366, 2016.

[77] D Kim. Effects of intermolecular interactions on the Singlet-Triplet energy difference: A theoretical study of the formation of excimers in acene molecules. *J. Phys. Chem. C*, 119:12690, 2015.

[78] D C Liu and J Nocedal. On the limited memory bfgs method for Large-Scale optimization. *Math Program*, 45:503, 1989.

[79] T Nagata and S Iwata. Perturbation expansion theory corrected from basis set superposition error. i. locally projected excited orbitals and single excitations. *J. Chem. Phys.*, 120:3555, 2004.

[80] A Famulari, G Calderoni, F Moroni, M Raimondi, and P B Karadakov. Application of the DIIS technique to improve the convergence properties of the SCF-MI algorithm. *Theochem*, 549:95, 2001.

[81] N Ferré and X Assfeld. Application of the local self-consistent-field method to core-ionized and core-excited molecules, polymers, and proteins: True orthogonality between ground and excited states. *J. Chem. Phys.*, 117:4119, 2002.

[82] J Gavnholt, T Olsen, M Engelund, and J Schiotz. Delta self-consistent field method to obtain potential energy surfaces of excited molecules on surfaces. *Phys. Rev. B: Condens. Matter Mater. Phys.*, 78:075441, 2008.

[83] T Ziegler, M Seth, M Krykunov, J Autschbach, and F Wang. On the relation between time-dependent and variational density functional theory approaches for the determination of excitation energies and transition moments. *J. Chem. Phys.*, 130:154102, 2009.

[84] P C a De Mello, M Hehenberger, and M C Zernert. Converging SCF calculations on Excited-States. *Int. J. Quantum Chem.*, 21:251, 1982.

[85] V N Glushkov, N I Gidopoulos, and S Wilson. Alternative technique for the constrained variational problem based on an asymptotic projection method: I. basics. *Front. Quantum Syst. Chem. Phys.*, 18:429, 2008.

[86] B Pen, B E Van Kuiken, F Z Ding, and X S Li. A guided Self-Consistent-Field method for Excited-State wave function optimization: Applications to Ligand-Field transitions in Transition-Metal complexes. *J. Chem. Theory Comput.*, 9:3933, 2013.

[87] P R Surján. Orthogonality constrained excited states. *Chem. Phys. Lett.*, 325:120, 2000.

[88] V N Glushkov and X Assfeld. Orthogonality-constrained Hartree-Fock and perturbation theory for high-spin open-shell excited states. *Theor. Chem. Acc.*, 135:3, 2016.

[89] F A Evangelista, P Shushkov, and J C Tully. Orthogonality constrained density functional theory for electronic excited states. *J. Phys. Chem. A*, 117:7378, 2013.

[90] W D Derricotte and F A Evangelista. Simulation of x-ray absorption spectra with orthogonality constrained density functional theory. *Phys. Chem. Chem. Phys.*, 17:14360, 2015.

[91] M Tassi, I Theophilou, and S Thanos. Hartree-Fock calculation for excited states. *Int. J. Quantum Chem.*, 113:690, 2013.

[92] M Tassi, I Theophilou, and S Thanos. Double excitations from modified hartree fock subsequent minimization scheme. *J. Chem. Phys.*, 138:124107, 2013.

[93] I Theophilou, M Tassi, and S Thanos. Charge transfer excitations from excited state Hartree-Fock subsequent minimization scheme. *J. Chem. Phys.*, 140:164102, 2014.

[94] K Carter-Fenk and J M Herbert. State-Targeted energy projection: A simple and robust approach to orbital relaxation of Non-Aufbau Self-Consistent field solutions. *J. Chem. Theory Comput.*, 16:5067, 2020.

[95] A Cembran, A Payaka, Y-L Lin, W Xie, Y Mo, L Song, and J Gao. A Non-Orthogonal Block-Localized effective hamiltonian approach for chemical and enzymatic reactions. *J. Chem. Theory Comput.*, 6:2242, 2010.

[96] L K Yang, A Grofe, J Reimers, and J Gao. Multistate density functional theory applied with 3 unpaired electrons in 3 orbitals: The singdoublet and tripdoublet states of the ethylene cation. *Chem. Phys. Lett.*, 736:136803, 2019.

[97] M Filatov and S Shaik. Spin-restricted density functional approach to the open-shell problem. *Chem. Phys. Lett.*, 288:689, 1998.

[98] M Filatov and S Shaik. A spin-restricted ensemble-referenced Kohn-Sham method and its application to diradicaloid situations. *Chem. Phys. Lett.*, 304:429, 1999.

[99] M Filatov and S Shaik. Diradicaloids: Description by the spin-restricted, ensemble-referenced Kohn-Sham density functional method. *J. Phys. Chem. A*, 104:6628, 2000.

[100] N O Dubinets, A A Safonov, and A A Bagaturyants. Structures and binding energies of the naphthalene dimer in its ground and excited states. *J. Phys. Chem. A*, 120:2779, 2016.

[101] C Climent, M Barbatti, M O Wolf, C J Bardeen, and D Casanova. The photophysics of naphthalene dimers controlled by sulfur bridge oxidation. *Chem. Sci.*, 8:4941, 2017.

[102] S Tretiak, W M Zhang, V Chernyak, and S Mukamel. Excitonic couplings and electronic coherence in bridged naphthalene dimers. *Proc. Natl. Acad. Sci. U.S.A.*, 96:13003, 1999.

[103] J P Perdew, K Burke, and M Ernzerhof. Generalized gradient approximation made simple. *Phys. Rev. Lett.*, 77:3865, 1996.

[104] P Pokhilko, D Izmodenov, and A I Krylov. Extension of frozen natural orbital approximation to open-shell references: Theory, implementation, and application to single-molecule magnets. *J. Chem. Phys.*, 152:034105, 2020.

[105] J A Pople, P M W Gill, and N C Handy. Spin-Unrestricted character of Kohn-Sham orbitals for Open-Shell systems. *Int. J. Quantum Chem.*, 56:303, 1995.

[106] D H Ess and T C Cook. Unrestricted prescriptions for Open-Shell singlet diradicals: Using economical ab initio and density functional theory to calculate

Singlet-Triplet gaps and bond dissociation curves. *J. Phys. Chem. A*, 116:4922, 2012.

[107] Michael W. Schmidt, Kim K. Baldridge, Jerry A. Boatz, Steven T. Elbert, Mark S. Gordon, Jan H. Jensen, Shiro Koseki, Nikita Matsunaga, Kiet A. Nguyen, Shujun Su, Theresa L. Windus, Michel Dupuis, and John A. Montgomery Jr. General atomic and molecular electronic structure system. *Journal of Computational Chemistry*, 14(11):1347–1363, 1993, https://onlinelibrary.wiley.com/doi/pdf/10.1002/jcc.540141112.

[108] S Speiser. Photophysics and mechanisms of intramolecular electronic energy transfer in bichromophoric molecular systems: Solution and supersonic jet studies. *Chem. Rev.*, 96:1953, 1996.

[109] C-P Hsu, Z-Q You, and H-C Chen. Characterization of the short-range couplings in excitation energy transfer. *J. Phys. Chem. C*, 112:1204, 2008.

[110] A K Chandra and E C Lim. Semiempirical theory of excimer luminescence. *J. Chem. Phys.*, 48:2589, 1968.

[111] M Kołaski, C R Arunkumar, and K S Kim. Aromatic excimers: Ab initio and TD-DFT study. *J. Chem. Theory Comput.*, 9:847, 2013.

[112] S Shirai, S Iwata, T Tani, and S Inagaki. Ab initio studies of aromatic excimers using multiconfiguration Quasi-Degenerate perturbation theory. *J. Phys. Chem. A*, 115:7687, 2011.

[113] M Schreiber, M R Silva-Junior, S P A Sauer, and W Thiel. Benchmarks for electronically excited states: CASPT2, CC2, CCSD, and CC3. *J. Chem. Phys.*, 128:134110, 2008.

[114] G A George and G C Morris. Intensity of absorption of naphthalene from 30 000 cm-1 to 53 000 cm-1. *J. Mol. Spectrosc.*, 26:67, 1968.

[115] R H Huebner, S R Meilczarek, and C E Kuyatt. Electron Energy-Loss spectroscopy of naphthalene vapor. *Chem. Phys. Lett.*, 16:464, 1972.

[116] J W Mcconkey, S Trajmar, K F Man, and J M Ratliff. Excitation of naphthalene by Electron-Impact. *J. Phys. B: At., Mol. Opt. Phys.*, 25:2197, 1992.

[117] J Matos, B O Matos, and B O Roos. A CASSCF study of the singlet singlet and triplet triplet spectroscopy of naphthalene. *Theor. Chim. Acta*, 74:363, 1988.

[118] T Azumi and S P Mcglynn. Energy of excimer luminescence .i. reconsideration of excimer processes. *J. Chem. Phys.*, 41:3131, 1964.

[119] E C Lim. Molecular triplet excimers. *Acc. Chem. Res.*, 20:8, 1987.

[120] A K Chandra and E C Lim. Semiempirical theory of excimer luminescence .2. comparison with previous theories and consideration of transition probability and stability of excimer triplet state. *J. Chem. Phys.*, 49:5066, 1968.

[121] J Langelaar, R P H Rettschnick, A M F Lambooy, and G J Hoytink. Monomer and excimer phosphorescence of phenanthrene and naphthalene in solution. *Chem. Phys. Lett.*, 1:609, 1968.

[122] T Takemura, M Aikawa, H Baba, and Y Shindo. Kinetic study of triplet excimer formation in fluid solution by means of phosphorimetry. *J. Am. Chem. Soc.*, 98:2205, 1976.

[123] D Holten, D F Bocian, and J S Lindsey. Probing electronic communication in covalently linked multiporphyrin arrays. a guide to the rational design of molecular photonic devices. *Acc. Chem. Res.*, 35:57, 2002.

[124] G R Fleming and R van Grondelle. Femtosecond spectroscopy of photosynthetic light-harvesting systems. *Curr. Opin. Struct. Biol.*, 7:738, 1997.

[125] B Shi, F Gao, and W Liang. A simplified approach for the coupling of excitation energy transfer. *Chem. Phys.*, 394:56, 2012.

[126] R D Harcourt, G D Scholes, and K P Ghiggino. Rate expressions for excitation transfer .2. electronic considerations of direct and through-configuration exciton resonance interactions. *J. Chem. Phys.*, 101:10521, 1994.

[127] G D Scholes, R D Harcourt, and K P Ghiggino. Rate expressions for excitation transfer .3. an Ab-Initio study of electronic factors in excitation transfer and exciton resonance interactions. *J. Chem. Phys.*, 102:9574, 1995.

[128] Z-Q You and C P Hsu. The fragment spin difference scheme for triplet-triplet energy transfer coupling. *J. Chem. Phys.*, 133:074105, 2010.

[129] F Gajdos, S Valner, F Hoffmann, J Spencer, M Breuer, A Kubas, M Dupuis, and J Blumberger. Ultrafast estimation of electronic couplings for electron transfer between pi-conjugated organic molecules. *J. Chem. Theory Comput.*, 10:4653, 2014.

[130] A Kubas, F Gajdos, A Heck, H Oberhofer, M Elstner, and J Blumberger. Electronic couplings for molecular charge transfer: benchmarking CDFT, FODFT and FODFTB against high-level ab initio calculations. II. *Phys. Chem. Chem. Phys.*, 17:14342, 2015.

[131] R Q Zhao, C P Hettich, X Chen, and J L Gao. Minimal-active-space multistate density functional theory for excitation energy involving local and charge transfer states. *NPJ. Comput. Mater.*, 7:148, 2021.

[132] C A Rozzi. Quantum coherence controls the charge separation in a prototypical artificial light-harvesting system. *Nat. Commun.*, 4, 2013.

[133] B Kozma. A new benchmark set for excitation energy of charge transfer states: systematic investigation of coupled cluster type methods. *J. Chem. Theory Comput.*, 16, 2020.

[134] N T Maitra. Charge transfer in time-dependent density functional theory. *J. Phys. Cond. Matter*, 29, 2017.

[135] F Plasser and H Lischka. Analysis of excitonic and charge transfer interactions from quantum chemical calculations. *J. Chem. Theory Comput.*, 8:2777, 2012.

[136] F Plasser. TheoDORE: A toolbox for a detailed and automated analysis of electronic excited state computations. *J. Chem. Phys.*, 152:084108, 2020.

[137] B Kozma, R Berraud-Pache, A Tajti, and P G Szalay. Potential energy surfaces of charge transfer states. *Mol. Phys.*, 118, 2020.

[138] A Tajti, B Kozma, and P G Szalay. Improved description of charge-transfer potential energy surfaces via spin-component-scaled CC2 and ADC(2) methods. *J. Chem. Theory Comput.*, 17, 2021.

[139] J Autschbach. Charge-transfer excitations and time-dependent density functional theory: problems and some proposed solutions. *Chemphyschem*, 10, 2009.

[140] J I Fuks. Time-dependent density functional theory for charge-transfer dynamics: review of the causes of failure and success. *Eur. Phys. J. B*, 89, 2016.

[141] S Kummel. Charge-transfer excitations: a challenge for time-dependent density functional theory that has been met. *Adv. Energy Mat.*, 7, 2017.

[142] A Dreuw, J L Weisman, and M Head-Gordon. Long-range charge-transfer excited states in time-dependent density functional theory require non-local exchange. *J. Chem. Phys.*, 119, 2003.

[143] Y Zhao and D G Truhlar. Density functional for spectroscopy: no long-range self-interaction error, good performance for rydberg and charge-transfer states, and better performance on average than B3LYP for ground states. *J. Phys. Chem. A*, 110, 2006.

[144] S Grimme and F Neese. Double-hybrid density functional theory for excited electronic states of molecules. *J. Chem. Phys.*, 127, 2007.

[145] A Ottochian. Double hybrids and time-dependent density functional theory: an implementation and benchmark on charge transfer excited states. *J. Comput. Chem.*, 41, 2020.

[146] A. Savin. *Recent Development and Applications of Modern Density Functional Theory*, volume 4. Elsevier, 1996. (ed Seminario, J. M.).

[147] Y Tawada, T Tsuneda, S Yanagisawa, T Yanai, and K Hirao. A long-range-corrected time-dependent density functional theory. *J. Chem. Phys.*, 120, 2004.

[148] T Stein, L Kronik, and R Baer. Reliable prediction of charge transfer excitations in molecular complexes using Time-Dependent density functional theory. *J. Am. Chem. Soc.*, 131:2818, 2009.

[149] R Baer, E Livshits, and U Salzner. Tuned range-separated hybrids in density functional theory. *Annu. Rev. Phys. Chem.*, 61, 2010.

[150] A Dreuw and M Head-Gordon. Single-reference ab initio methods for the calculation of excited states of large molecules. *Chem. Rev.*, 105, 2005.

[151] A Grofe, R Zhao, A Wildman, T F Stetina, X Li, P Bao, and J Gao. Generalization of Block-Localized wave function for constrained optimization of excited determinants. *J. Chem. Theory Comput.*, 17:277, 2021.

[152] M Garcia-Viloca, D G Truhlar, and J Gao. Importance of substrate and cofactor polarization in the active site of dihydrofolate reductase. *J. Mol. Biol.*, 327, 2003.

[153] W Liu and M R Hoffmann. SDS: the 'static-dynamic-static' framework for strongly correlated electrons. *Theor. Chem. Acc.*, 133, 2014.

[154] N Zhang, W J Liu, and M R Hoffmann. Iterative configuration interaction with selection. *J. Chem. Theory Comput.*, 16, 2020.

[155] N Zhang, W Liu, and M R Hoffman. Further development of iCIPT2 for strongly correlated electrons. *J. Chem. Theory Comput.*, 17, 2021.

[156] A J W Thom and M Head-Gordon. Hartree-Fock solutions as a quasidiabatic basis for nonorthogonal configuration interaction. *J. Chem. Phys.*, 131, 2009.

[157] T Voorhis and M Head-Gordon. A nonorthogonal approach to perfect pairing. *J. Chem. Phys.*, 112, 2000.

[158] N D Mermin. Thermal properties of the inhomogeneous electron gas. *Phys. Rev.*, 137, 1965.

[159] E K U Gross, L N Oliveira, and W Kohn. Density-functional theory for ensembles of fractionally occupied states .1. basic formalism. *Phys. Rev. A*, 37, 1988.

[160] E K U Gross, L N Oliveira, and W Kohn. Rayleigh-Ritz variational principle for ensembles of fractionally occupied states. *Phys. Rev. A*, 37, 1988.

[161] T Gould and S Pittalis. Density-driven correlations in many-electron ensembles: theory and application for excited states. *Phys. Rev. Lett.*, 123, 2019.

[162] E Fromager. Individual correlations in ensemble density functional theory: state- and density-driven decompositions without additional Kohn-Sham systems. *Phys. Rev. Lett.*, 124, 2020.

[163] T Gould and S Pittalis. Hartree and exchange in ensemble density functional theory: avoiding the nonuniqueness ddisaster. *Phys. Rev. Lett.*, 119, 2017.

[164] T Gould, L Kronik, and S Pittalis. Charge transfer excitations from exact and approximate ensemble Kohn-Sham theory. *J. Chem. Phys.*, 148, 2018.

[165] M Filatov. Spin-restricted ensemble-referenced Kohn-Sham method: basic principles and application to strongly correlated ground and excited states of molecules. *WIREs Comput. Mol. Sci.*, 5, 2015.

[166] S Grimme and M Waletzke. A combination of Kohn-Sham density functional theory and multi-reference configuration interaction methods. *J. Chem. Phys.*, 111, 1999.

[167] S Yamanaka, K Nakata, T Ukai, T Takada, and K Yamaguchi. Multireference density functional theory with orbital-dependent correlation corrections. *Int. J. Quant. Chem.*, 106, 2006.

[168] T Ukai, K Nakata, S Yamanaka, T Takada, and K Yamaguchi. A CAS-DFT study of fundamental degenerate and nearly degenerate systems. *Mol. Phys.*, 105, 2007.

[169] J Grafenstein and D Cremer. The self-interaction error and the description of non-dynamic electron correlation in density functional theory. *Theor. Chem. Acc.*, 123:171, 2009.

[170] F Moscardo and E Sanfabian. Density-functional formalism and the 2-body problem. *Phys. Rev. A*, 44, 1991.

[171] A Savin. A combined density functional and configuration-interaction method. *Int. J. Quant. Chem.*, S22, 1988.

[172] P Sharma, J J Bao, D G Truhlar, and L Gagliardi. Multiconfiguration pair-density functional theory. *Annu. Rev. Phys. Chem.*, 72, 2021.

[173] A D Becke, A Savin, and H Stoll. Extension of the local-spin-density exchange-correlation approximation to multiplet states. *Theor. Chim. Acta*, 91, 1995.

[174] B Miehlich, H Stoll, and A Savin. A correlation-energy density functional for multideterminantal wavefunctions. *Mol. Phys.*, 91, 1997.

[175] P H Dederichs, S Bluegel, R Zeller, and H Akai. Ground states of constrained systems: application to cerium impurities. *Phys. Rev. Lett.*, 53:2512, 1984.

[176] Ruoqi Zhao, Adam Grofe, Zikuan Wang, Peng Bao, Xin Chen, Wenjian Liu, and Jiali Gao. Dynamic-then-static approach for core excitations of open-shell molecules. *The Journal of Physical Chemistry Letters*, 12(31):7409–7417, 2021, https://doi.org/10.1021/acs.jpclett.1c02039. PMID: 34328742.

[177] Y Zhao and D G Truhlar. M06 DFT functionals. *Theor. Chem. Acc.*, 120:215, 2008.

[178] J R Platt. Classification of spectra of cata-condensed hydrocarbons. *J. Chem. Phys.*, 17, 1949.

[179] S Grimme and M Parac. Substantial errors from time-dependent density functional theory for the calculation of excited states of large pi systems. *Chemphyschem*, 4, 2003.

[180] C M Marian and N Gilka. Performance of the density functional theory/multireference configuration interaction method on electronic excitation of extended pi-systems. *J. Chem. Theory Comput.*, 4, 2008.

[181] D Biermann and W Schmidt. Diels-Alder reactivity of polycyclic aromatic-hydrocarbons .1. acenes and benzologs. *J. Am. Chem. Soc.*, 102, 1980.

[182] C Adamo and V Barone. Toward reliable density functional methods without adjustable parameters: the PBE0 model. *J. Chem. Phys.*, 110, 1999.

[183] N Dupuy, S Bouaouli, F Mauri, S Sorella, and M Casula. Vertical and adiabatic excitations in anthracene from quantum monte carlo: constrained energy minimization for structural and electronic excited-state properties in the JAGP ansatz. *J. Chem. Phys.*, 142, 2015.

[184] M Baba. Structure and excited-state dynamics of anthracene: ultrahigh-resolution spectroscopy and theoretical calculation. *J. Chem. Phys.*, 130, 2009.

[185] M R Padhye, S P Mcglynn, and M Kasha. Lowest triplet state of anthracene. *J. Chem. Phys.*, 24, 1956.

[186] Y Gao. Excimer formation and evolution of excited state properties in discrete dimeric stacking of an anthracene derivative: a computational investigation. *Phys. Chem. Chem. Phys.*, 20, 2018.

[187] J Eng and T J Penfold. Understanding and designing thermally activated delayed fluorescence emitters: beyond the energy gap approximation. *Chem. Rec.*, 20, 2020.

[188] S Y Lin, Q Ou, Y Wang, Q Peng, and Z G Shuai. Aggregation-enhanced thermally activated delayed fluorescence efficiency for two-coordinate carbene-metal-amide complexes: a QM/MM study. *J. Phys. Chem. Lett.*, 12, 2021.

[189] R L A Haiduke and R J Bartlett. Non-empirical exchange-correlation parameterizations based on exact conditions from correlated orbital theory. *J. Chem. Phys.*, 148:184106, 2018.

[190] I Hanazaki. Vapor-Phase electron Donor-Acceptor complexes of tetracyanoethylene and of Sulfur-Dioxide. *J. Phys. Chem.*, 76:1982, 1972.

[191] M Kroll. Molecular complexes and their spectra. XX. gas-phase electron donor-acceptor complexes. *J. Am. Chem. Soc.*, 90, 1968.

[192] J M Masnovi, E A Seddon, and J K Kochi. Electron-transfer from anthracenes - comparison of photoionization, charge-transfer excitation and electrochemical oxidation. *Can. J. Chem.*, 62, 1984.

[193] H B Chirgwin and C A Coulson. The electronic structure of conjugated systems. VI. *Proc. R. Soc. London Ser. A*, 201:196, 1950.

[194] X Guo, Z Qu, and J Gao. The charger transfer electronic coupling in diabatic perspective: a multi-state density functional theory study. *Chem. Phys. Lett.*, 691, 2018.

[195] H Moriyama, Y Wasada-Tsutsui, M Sekiya, and H Tatewaki. The singlet electronic excited states of the F-2 molecule. *J. Chem. Phys.*, 118, 2003.

[196] J D Watts, S R Gwaltney, and R J Bartlett. Coupled-cluster calculations of the excitation energies of ethylene, butadiene, and cyclopentadiene. *J. Chem. Phys.*, 105, 1996.

[197] S Arulmozhiraja, M Ehara, and H Nakatsuji. Electronic excitations of fluoroethylenes. *J. Chem. Phys.*, 126, 2007.

[198] Ruoqi Zhao, Christian Hettich, Jun Zhang, Meiyi Liu, and Jiali Gao. Excimer energies. *J. Phys. Chem. Lett.*, 14(12):2917–2926, March 2023.

[199] J Gao and X Xia. A prior evaluation of aqueous polarization effects through monte carlo QM-MM simulations. *Science*, 258:631, 1992.

[200] L L Zhao, M von Hopffgarten, D M Andrada, and G Frenking. Energy decomposition analysis. *WIREs Comput. Mol. Sci.*, 8:e1345, 2018.

[201] K Morokuma. Molecular orbital studies of hydrogen bonds. 3. C=O H-O hydrogen bond in h2co h2o and h2co 2h2o. *J. Chem. Phys.*, 55:1236, 1971.

[202] K Kitaura and K Morokuma. New energy decomposition scheme for Molecular-Interactions within Hartree-Fock approximation. *Int. J. Quantum Chem.*, 10:325, 1976.

[203] K Morokuma. Why do molecules interact - origin of electron Donor-Acceptor complexes, Hydrogen-Bonding, and proton affinity. *Acc. Chem. Res.*, 10:294, 1977.

[204] T Ziegler and A Rauk. Calculation of bonding energies by Hartree-Fock slater method. 1. Transition-State method. *Theor. Chim. Acta*, 46:1, 1977.

[205] P S Bagus, K Hermann, and C W Bauschlicher. A new analysis of Charge-Transfer and polarization for Ligand-Metal bonding - model studies of al4co and al4nh3. *J. Chem. Phys.*, 80:4378, 1984.

[206] P S Bagus, K Hermann, and C W Bauschlicher. On the nature of the bonding of lone pair ligands to a Transition-Metal. *J. Chem. Phys.*, 81:1966, 1984.

[207] P S Bagus and F Illas. Decomposition of the chemisorption bond by constrained variations - order of the variations and construction of the variational spaces. *J. Chem. Phys.*, 96:8962, 1992.

[208] W J Stevens and W H Fink. Frozen fragment reduced variational space analysis of hydrogen bonding interactions. application ot the water dimer. *Chem. Phys. Lett.*, 139:15, 1987.

[209] E D Glendening and F Weinhold. Natural resonance theory: I. general formalism. *J. Comput. Chem.*, 19:593, 1998.

[210] M S Gordon and J H Jensen. Understanding the hydrogen bond using quantum chemistry. *Acc. Chem. Res.*, 29:536, 1996.

[211] W Chen and M S Gordon. Energy decomposition analyses for many-body interaction and applications to water complexes. *J. Phys. Chem.*, 100:14316, 1996.

[212] M S Gordon, L Slipchenko, H Li, and J H Jensen. The effective fragment potential: a general method for predicting intermolecular interactions. *Ann. Rep. Comput. Chem.*, 3:177, 2007.

[213] P Reinhardt, J-P Piquemal, and A Savin. Fragment-Localized Kohn-Sham orbitals via a singles Configuration-Interaction procedure and application to local properties and intermolecular energy decomposition analysis. *J. Chem. Theory Comput.*, 4:2020, 2008.

[214] Q Wu, P W Ayers, and Y K Zhang. Density-based energy decomposition analysis for intermolecular interactions with variationally determined intermediate state energies. *J. Chem. Phys.*, 131:164112, 2009.

[215] P F Su and H Li. Energy decomposition analysis of covalent bonds and intermolecular interactions. *J. Chem. Phys.*, 131:014102, 2009.

[216] J P Piquemal, A Marquez, O Parisel, and C Giessner-Prettre. A CSOV study of the difference between HF and DFT intermolecular interaction energy values: The importance of the charge transfer contribution. *J. Comput. Chem.*, 26:1052, 2005.

[217] C Gourlaouen, J P Piquemal, T Saue, and O Parisel. Revisiting the geometry of nd(10) (n+1)s(0) [M(H2O)](P+) complexes using four-component relativistic DFT calculations and scalar relativistic correlated CSOV energy decompositions (MP+=Cu+, zn2+, ag+, cd2+, au+, hg2+). *J. Comput. Chem.*, 27:142, 2006.

[218] F M Bickelhaupt, E J Baerends, K B Lipkowitz, and D B Boyd. *Reviews in Computational Chemistry*, volume 15. 1999.

[219] C Fonseca Guerra, F M Bickelhaupt, J G Snijders, and E J Baerends. The nature of the hydrogen bond in DNA base pairs: The role of charge transfer and resonance assistance. *Chem.-Eur. J.*, 5:3581, 1999.

[220] F M Bickelhaupt and E J Baerends. The case for steric repulsion causing the staggered conformation of ethane. *Angew. Chem., Int. Ed.*, 42:4183, 2003.

[221] R Z Khaliullin, E A Cobar, R C Lochan, A T Bell, and M Head-Gordon. Unravelling the origin of intermolecular interactions using absolutely localized molecular orbitals. *J. Phys. Chem. A*, 111:8753, 2007.

[222] J Andres, P W Ayers, R A Boto, R Carbo-Dorca, H Chermette, J Cioslowski, J Contreras-Garcia, D L Cooper, G Frenking, C Gatti, F Heidar-Zadeh, L Joubert, A M Pendas, E Matito, I Mayer, A J Misquitta, Y R Mo, J Pilme, P L A Popelier, M Rahm, E RamosCordoba, P Salvador, W H E Schwarz, S Shahbazian, B Silvi,

M Sola, K Szalewicz, V Tognetti, F Weinhold, and E L Zins. Nine questions on energy decomposition analysis. *J. Comput. Chem.*, 40:2248, 2019.

[223] Y Mo, Y Zhang, and J Gao. A simple electrostatic model for trisilylamine: Theoretical examinations of the n.fwdarw..sigma. negative hyperconjugation, p.pi..fwdarw.d.pi. bonding, and stereoelectronic interaction. *J. Am. Chem. Soc.*, 121:5737, 1999.

[224] Y Mo, P v R Schleyer, W Wu, M Lin, Q Zhang, and J Gao. Importance of electronic delocalization on the C-N bond rotation in HCX(NH2) (x = o, NH, CH2, s, and se). *J. Phys. Chem. A*, 107:10011, 2003.

[225] Y Mo and J Gao. Polarization and Charge-Transfer effects in aqueous solution via ab initio QM/MM simulations. *J. Phys. Chem. B*, 110:2976, 2006.

[226] Y R Mo. Computational evidence that hyperconjugative interactions are not responsible for the anomeric effect. *Nat. Chem.*, 2:666, 2010.

[227] G Frenking, C Loschen, A Krapp, S Fau, and S H Strauss. Electronic structure of CO - an exercise in modern chemical bonding theory. *J. Comput. Chem.*, 28:117, 2007.

[228] G Frenking and N Frohlich. The nature of the bonding in transition-metal compounds. *Chem. Rev.*, 100:717, 2000.

[229] A Michalak, M Mitoraj, and T Ziegler. Bond orbitals from chemical valence theory. *J. Phys. Chem. A*, 112:1933, 2008.

[230] R Kurczab, M P Mitoraj, A Michalak, and T Ziegler. Theoretical analysis of the resonance assisted hydrogen bond based on the combined extended transition

state method and natural orbitals for chemical valence scheme. *J. Phys. Chem. A*, 114:8581, 2010.

[231] E Francisco, A M Pendas, and M A Blanco. A molecular energy decomposition scheme for atoms in molecules. *J. Chem. Theory Comput.*, 2:90, 2006.

[232] S N Liu, N Govind, and L G Pedersen. Exploring the origin of the internal rotational barrier for molecules with one rotatable dihedral angle. *J. Chem. Phys.*, 129:094104, 2008.

[233] A J Stone. *The Theory of Intermolecular Forces.* 1996.

[234] B Jeziorski, R Moszynski, and K Szalewicz. Perturbation theory approach to intermolecular potential energy surfaces of van der waals complexes. *Chem. Rev.*, 94:1887, 1994.

[235] A J Misquitta and K Szalewicz. Symmetry-adapted perturbation-theory calculations of intermolecular forces employing density-functional description of monomers. *J. Chem. Phys.*, 122:214109, 2005.

[236] M Shahbaz and K Szalewicz. Dispersion energy from local polarizability density. *Phys. Rev. Lett.*, 122:213001, 2019.

[237] S S Xantheas. On the importance of the fragment relaxation energy terms in the estimation of the basis set superposition error correction to the intermolecular interaction energy. *J. Chem. Phys.*, 104:8821, 1996.

[238] C Angeli, R Cimiraglia, and J P Malrieu. On the relative merits of non-orthogonal and orthogonal valence bond methods illustrated on the hydrogen molecule. *J. Chem. Educ.*, 85:150, 2008.

[239] W B Schneider, G Bistoni, M Sparta, M Saitow, C Riplinger, A A Auer, and F Neese. Decomposition of intermolecular interaction energies within the local pair natural orbital coupled cluster framework. *J. Chem. Theory Comput.*, 12:4778, 2016.

[240] A Altun, M Saitow, F Neese, and G Bistoni. Local energy decomposition of Open-Shell molecular systems in the Domain-Based local pair natural orbital coupled cluster framework. *J. Chem. Theory Comput.*, 15:1616, 2019.

[241] P R Horn, Y Z Mao, and M Head-Gordon. Probing non-covalent interactions with a second generation energy decomposition analysis using absolutely localized molecular orbitals. *Phys. Chem. Chem. Phys.*, 18:23067, 2016.

[242] D S Levine, P R Horn, Y Z Mao, and M Head-Gordon. Variational energy decomposition analysis of chemical bonding. 1. Spin-Pure analysis of single bonds. *J. Chem. Theory Comput.*, 12:4812, 2016.

[243] Y Z Mao, M Loipersberger, P R Horn, A Das, O Demerdash, D S Levine, S P Veccham, T Head-Gordon, and M Head-Gordon. From intermolecular interaction energies and observable shifts to component contributions and back again: A tale of variational energy decomposition analysis. *Annu. Rev. Phys. Chem.*, 72:641, 2021.

[244] S P Veccham, J Lee, Y Z Mao, P R Horn, and M Head-Gordon. A non-perturbative pairwise-additive analysis of charge transfer contributions to intermolecular interaction energies. *Phys. Chem. Chem. Phys.*, 23:928, 2021.

[245] H Y Shen, Z L Wang, and M Head-Gordon. Generalization of ETS-NOCV and ALMO-COVP energy decomposition analysis to connect any two electronic states and comparative assessment. *J. Chem. Theory Comput.*, 18:7428, 2022.

[246] J T Han, A Grofe, and J L Gao. Variational energy decomposition analysis of Charge-Transfer interactions between metals and ligands in carbonyl complexes. *Inorg. Chem.*, 60:14060, 2021.

[247] P T Mathew and F Z Fang. Periodic energy decomposition analysis for electronic transport studies as a tool for atomic scale device manufacturing. *Int. J. Extr. Manufact.*, 2:015401, 2020.

[248] Y Xu, S Zhang, E Lindahl, R Friedman, W Wu, and P F Su. A general tight-binding based energy decomposition analysis scheme for intermolecular interactions in large molecules. *J. Chem. Phys.*, 157:034104, 2022.

[249] H Chen and C K Skylaris. Energy decomposition analysis method for metallic systems. *Phys. Chem. Chem. Phys.*, 24:1702, 2022.

[250] Q H Ge, Y Z Mao, and M Head-Gordon. Energy decomposition analysis for exciplexes using absolutely localized molecular orbitals. *J. Chem. Phys.*, 148:064105, 2018.

[251] K D Closser, Q H Ge, Y Z Mao, Y H Shao, and M Head-Gordon. Superposition of fragment excitations for excited states of large clusters with application to helium clusters. *J. Chem. Theory Comput.*, 11:5791, 2015.

[252] Q H Ge and M Head-Gordon. Energy decomposition analysis for excimers using absolutely localized molecular orbitals within Time-Dependent density functional theory and configuration interaction with single excitations. *J. Chem. Theory Comput.*, 14:5156, 2018.

[253] X K Li, Z Y Liu, H S Ren, M Kundu, L J Wang, J L Gao, and D P Zhong. Dynamics and mechanism of light harvesting in UV photoreceptor UVR8. *Chem. Sci.*, 11:12553, 2020.

[254] X K Li, Z Y Liu, H S Ren, M Kundu, F W Zhong, L J Wang, J L Gao, and D P Zhong. Dynamics and mechanism of dimer dissociation of photoreceptor UVR8. *Nature Commun.*, 13:93, 2022.

[255] L Yue and Y J Liu. Conical intersection in chemiluminescence of cyclic peroxides. *J. Phys. Chem. Lett.*, 13:10671, 2022.

[256] J Frenkel. On the transformation of light into heat in solids. I. *Phys. Rev.*, 37:17, 1931.

[257] Y Y Lu and J L Gao. Multistate density functional theory of excited states. *J. Phys. Chem. Lett.*, 13:7762, 2022.

[258] Y Y Lu and J L Gao. Fundamental variable and density representation in multistate DFT for excited states. *J. Chem. Theory Comput.*, 18:7403, 2022.

[259] M Zarea, D Powell, N Renaud, M R Wasielewski, and M A Ratner. Decoherence and quantum interference in a Four-Site model system: Mechanisms and turnovers. *J. Phys. Chem. B*, 117:1010, 2013.

[260] H F King, R E Staton, H Kim, R E Wyatt, and R G Parr. Corresponding orbitals and the nonorthogonality problems in molecular quantum mechanics. *J. Chem. Phys.*, 47:1936, 1967.

[261] J Zhang, Z Pan, R Zhao, X Hou, X Zhang, Z Tang, Y Zhang, Y Wu, W Liu, and J Gao. *Qbics - Quantum biology, informatics and chemistry server.* Shenzhen Bay Laboratory: Shenzhen, China, 2023.

[262] T H Dunning. Gaussian basis sets for use in correlated molecular calculations. i. the atoms boron through neon and hydrogen. *J. Chem. Phys.*, 90:1007, 1989.

[263] M J Frisch, G W Trucks, H B Schlegel, G E Scuseria, M A Robb, J R Cheeseman, G Scalmani, V Barone, G A Petersson, H Nakatsuji, X Li, M Caricato, A V Marenich, J Bloino, B G Janesko, R Gomperts, B Mennucci, H P Hratchian, J V Ortiz, A F Izmaylov, J L Sonnenberg, D F Williams, F Lipparini, F Egidi, J Goings, B Peng, A Petrone, T Henderson, D Ranasinghe, V G Zakrzewski, J Gao, N Rega, G Zheng, W Liang, M Hada, M Ehara, K Toyota, R Fukuda, J Hasegawa, M Ishida, T Nakajima, Y Honda, O Kitao, H Nakai, T Vreven, K Throssell, J A Montgomery, J E Peralta, F Ogliaro, M J Bearpark, J J Heyd, E N Brothers, K N Kudin, V N Staroverov, T A Keith, R Kobayashi, J Normand, K Raghavachari, A P Rendell, J C Burant, S S Iyengar, J Tomasi, M Cossi, J M Millam, M Klene, C Adamo, R Cammi, J W Ochterski, R L Martin, K Morokuma, O Farkas, J B Foresman, and D J Fox. *Gaussian 16.* 2016.

[264] K Aidas, K V Mikkelsen, B Mennucci, and J Kongsted. Fluorescence and phosphorescence of acetone in neat liquid and aqueous solution studied by QM/MM and PCM approaches. *Int. J. Quantum Chem.*, 111:1511, 2011.

[265] M O'Sullivan and A C Testa. Monomer and excimer emission of acetone. *J. Am. Chem. Soc.*, 90:6245, 1968.

[266] Christian P Hettich, Xiaoyong Zhang, David Kemper, Ruoqi Zhao, Shaoyuan Zhou, Yangyi Lu, Jiali Gao, Jun Zhang, and Meiyi Liu. Multistate energy decomposition analysis of molecular excited states. *JACS Au*, 3(7):1800–1819, July 2023.

[267] P F Su, Z Tang, and W Wu. Generalized Kohn-Sham energy decomposition analysis and its applications. *WIREs-Comput. Mol. Sci.*, 10:e1460, 2020.

[268] J Gao, J J Pavelites, and D Habibollazadeh. Simulation of liquid amides using a polarizable intermolecular potential function. *J. Phys. Chem.*, 100:2689, 1996.

[269] W Xie, J Pu, A D MacKerell, and J Gao. Development of a polarizable intermolecular potential function (PIPF) for liquid amides and alkanes. *J. Chem. Theory Comput.*, 3:1878, 2007.

[270] C Curutchet and B Mennucci. Quantum chemical studies of light harvesting. *Chem. Rev.*, 117:294, 2017.

[271] M A Blanco, A M Pendas, and E Francisco. Interacting quantum atoms: A correlated energy decomposition scheme based on the quantum theory of atoms in molecules. *J. Chem. Theory Comput.*, 1:1096, 2005.

[272] E D Glendening and A Streitwieser. Natural energy decomposition analysis - an energy partitioning procedure for Molecular-Interactions with application to weak Hydrogen-Bonding, strong ionic, and moderate Donor-Acceptor interactions. *J. Chem. Phys.*, 100:2900, 1994.

[273] V Pophristic and L Goodman. Hyperconjugation not steric repulsion leads to the staggered structure of ethane. *Nature*, 411:565, 2001.

[274] Y Mo and J Gao. Theoretical analysis of the rotational barrier of ethane. *Acc. Chem. Res.*, 40:113, 2007.

[275] Y Mo, W Wu, L Song, M Lin, Q Zhang, and J Gao. The magnitude of hyperconjugation in ethane: a perspective from ab initio valence bond theory. *Angew. Chem., Int. Ed.*, 43:1986, 2004.

[276] G te Velde, F M Bickelhaupt, E J Baerends, C F Guerra, S J A Van Gisbergen, J G Snijders, and T Ziegler. Chemistry with ADF. *J. Comput. Chem.*, 22:931, 2001.

[277] M P Mitoraj, A Michalak, and T Ziegler. A combined charge and energy decomposition scheme for bond analysis. *J. Chem. Theory Comput.*, 5:962, 2009.

[278] K Szalewicz and B Jeziorski. Symmetry-Adapted Double-Perturbation analysis of Intra-Molecular correlation effects in weak Inter-Molecular interactions - He-He interaction. *Mol. Phys.*, 38:191, 1979.

[279] A J Misquitta. Charge transfer from regularized Symmetry-Adapted perturbation theory. *J. Chem. Theory Comput.*, 9:5313, 2013.

[280] Y Mo and J Gao. Polarization and Charge-Transfer effects in lewis Acid-Base complexes. *J. Phys. Chem. A*, 105:6530, 2001.

[281] Z Pei, J J Yang, J H Deng, Y Z Mao, Q Wu, Z B Yang, B Wang, C M Aikens, W Z Liang, and Y H Shao. Analysis and visualization of energy densities. II. insights from linear-response time-dependent density functional theory calculations. *Phys. Chem. Chem. Phys.*, 22:26852, 2020.

[282] Y S Wang, O Haze, J P Dinnocenzo, S Farid, R S Farid, and I R Gould. Bonded exciplexes. a new concept in photochemical reactions. *J. Org. Chem.*, 72:6970, 2007.

[283] V A Spata and S Matsika. Role of excitonic coupling and Charge-Transfer states in the absorption and CD spectra of Adenine-Based oligonucleotides investigated through QM/MM simulations. *J. Phys. Chem. A*, 118:12021, 2014.

[284] F Plasser and H Lischka. Electronic excitation and structural relaxation of the adenine dinucleotide in gas phase and solution. *Photochem. Photobio. Sci.*, 12:1440, 2013.

[285] A I Krylov. From orbitals to observables and back. *J. Chem. Phys.*, 153:080901, 2020.

[286] M B Smith and J Michl. Singlet fission. *Chem. Rev.*, 110:6891, 2010.

[287] S F Boys. Localized orbitals and localized adjustment functions. *Quantum Theory At., Mol., Solid State*, page 253, 1966.

[288] K Ruedenberg and G J Atchity. A quantum chemical determination of diabatic states. *J. Chem. Phys.*, 99:3799, 1993.

[289] R Sarkar, M Boggio-Pasqua, P F Loos, and D Jacquemin. Benchmarking TD-DFT and wave function methods for oscillator strengths and Excited-State dipole moments. *J. Chem. Theory Comput.*, 17:1117, 2021.

[290] D Cremer, M Filatov, V Polo, E Kraka, and S Shaik. Implicit and explicit coverage of multi-reference effects by density functional theory. *Int. J. Mol. Sci.*, 3:604, 2002.

[291] J Grafenstein and D Cremer. Development of a CAS-DFT method covering non-dynamical and dynamical electron correlation in a balanced way. *Mol. Phys.*, 103:279, 2005.

[292] M Merchan, B O Roos, R McDiarmid, and X Xing. A combined theoretical and experimental determination of the electronic spectrum of acetone. *J. Chem. Phys.*, 104:1791, 1996.

[293] T Fueno and K Yamaguchi. Comparison of the electronic spectra of geometric isomers. II. 1,2-disubstituted ethylenes. *Bull. Chem. Soc. Jpn.*, 45:3290, 1972.

[294] B Milian, R Pou-Amerigo, M Merchan, and E Orti. Theoretical study of the electronic excited states of tetracyanoethylene and its radical anion. *ChemPhysChem*, 6:503, 2005.

[295] T Zeng, R Hoffmann, and N Ananth. The Low-Lying electronic states of pentacene and their roles in singlet fission. *J. Am. Chem. Soc.*, 136:5755, 2014.

[296] C Bulliard, M Allan, and S Grimme. Electron energy loss and dissociative electron attachment spectroscopy of methyl vinyl ether and related compounds. *Int. J. Mass Spectrom.*, 205:43, 2001.

[297] P Swiderek, M Michaud, G Hohlneicher, and L Sanche. Electron-Energy loss spectroscopy of solid naphthalene and acenaphthene - search for the Low-Lying Triplet-States. *Chem. Phys. Lett.*, 175:667, 1990.

[298] V K Thorsmolle, R D Averitt, J Demsar, D L Smith, S Tretiak, R L Martin, X Chi, B K Crone, A P Ramirez, and A J Taylor. Photoexcited carrier relaxation dynamics in pentacene probed by ultrafast optical spectroscopy: Influence of morphology on relaxation processes. *Phys. B - Cond. Matter*, 404:3127, 2009.

[299] K B Wiberg, R E Stratmann, and M J Frisch. A time-dependent density functional theory study of the electronically excited states of formaldehyde, acetaldehyde and acetone. *Chem. Phys. Lett.*, 297:60, 1998.

[300] M B Robin. *Higher excited states of polyatomic molecules.* 1974.

[301] N E Schore and N J Turro. Mechanism of interaction of n, Pi-Star excited alkanones with Electron-Rich ethylenes. *J. Am. Chem. Soc.*, 97:2482, 1975.

[302] A Ledwith and H J Woods. Reactivity and structure of alkyl vinyl ethers.4. conformational effects of Alkoxy-Groups in alkyl vinyl ethers and alkyl aryl ethers on Charge-Transfer spectra with tetracyanoethylene, and reactivity towards electrophiles. *J. Chem. Soc. B*, page 310, 1970.

[303] C Salez and A Veillard. A comparison of different contractions for molecular calculations with gaussian-type functions. *Theoretica chimica acta*, 11(5):441–451, January 1968.

[304] P.J. Hay, W.J. Hunt, and W.A. Goddard. Generalized valence bond wavefunctions for the low lying states of methylene. *Chemical Physics Letters*, 13(1):30–35, 1972.

[305] Richard Peer Wayne. *Chemistry of atmospheres.* New York, NY (United States); Oxford Univ. Press, 1993.

[306] H. Feuchtgruber, F. P. Helmich, E. F. van Dishoeck, and C. M. Wright. Detection of interstellar ch3*. *The Astrophysical Journal*, 535(2):L111, jun 2000.

[307] G. Herzberg. Evidence for the presence of ch_2 molecules in comets. *Rev. Mod. Phys.*, 14:195–197, Apr 1942.

[308] Gerhard Herzberg. The bakerian lecture, the spectra and structures of free methyl and free methylene. *Proceedings of the Royal Society of London. Series A. Mathematical and Physical Sciences*, 262(1310):291–317, 1961, https://royalsocietypublishing.org/doi/pdf/10.1098/rspa.1961.0120.

[309] A Monfils and B Rosen. New method of excitation of the cometary emission bands at 4050 a. *Nature*, 164(4173):713–713, October 1949.

[310] G. B. Kistiakowsky and P. H. Kydd. A mass spectrometric study of flash photochemical reactions. i. *Journal of the American Chemical Society*, 79(18):4825–4830, 1957, https://doi.org/10.1021/ja01575a001.

[311] A. Langer, J. A. Hipple, and D. P. Stevenson. Ionization and Dissociation by Electron Impact; Methylene, Methyl, and Methane. *The Journal of Chemical Physics*, 22(11):1836–1844, 11 1954, https://pubs.aip.org/aip/jcp/article-pdf/22/11/1836/18805907/1836_1_online.pdf.

[312] F. P. Lossing, K. U. Ingold, and I. H. S. Henderson. Free Radicals by Mass Spectrometry. V. The Ionization Potentials of Methyl, Allyl, and Benzyl Radicals. *The Journal of Chemical Physics*, 22(4):621–625, 04 1954, https://pubs.aip.org/aip/jcp/article-pdf/22/4/621/18805339/621_1_online.pdf.

[313] Stephen V. O'Neil, III Schaefer, Henry F., and Charles F. Bender. C2v Potential Energy Surfaces for Seven Low-Lying States of CH2. *The Journal of Chemical Physics*, 55(1):162–169, 07 1971, https://pubs.aip.org/aip/jcp/article-pdf/55/1/162/18873929/162_1_online.pdf.

[314] W. G. Penney. On the bond energies and valency angles in some simple carbon compounds. *Trans. Faraday Soc.*, 31:734–746, 1935.

[315] H. H. Voge. Relation of the States of the Carbon Atom to Its Valence in Methane. *The Journal of Chemical Physics*, 4(9):581–591, 09 1936, https://pubs.aip.org/aip/jcp/article-pdf/4/9/581/18789434/581_1_online.pdf.

[316] G. A. Gallup. Structure of CH2. *The Journal of Chemical Physics*, 26(3):716–716, 03 1957, https://pubs.aip.org/aip/jcp/article-pdf/26/3/716/18811450/716_1_online.pdf.

[317] J. M. Foster and S. F. Boys. Quantum variational calculations for a range of ch_2 configurations. *Rev. Mod. Phys.*, 32:305–307, Apr 1960.

[318] James F. Harrison and Leland C. Allen. Electronic structure of methylene. *Journal of the American Chemical Society*, 91(4):807–823, 1969, https://doi.org/10.1021/ja01032a004.

[319] G. Herzberg and J. W. C. Johns. On the Structure of CH2 in its Triplet Ground State. *The Journal of Chemical Physics*, 54(5):2276–2278, 03 1971, https://pubs.aip.org/aip/jcp/article-pdf/54/5/2276/18872940/2276_1_online.pdf.

[320] A. Zanchet, L. Bañares, M. L. Senent, and A. García-Vela. An ab initio study of the ground and excited electronic states of the methyl radical. *Phys. Chem. Chem. Phys.*, 18:33195–33203, 2016.

[321] Alberto Rodríguez-Fernández, Maykel Márquez-Mijares, Jesús Rubayo-Soneira, Alexandre Zanchet, Alberto García-Vela, and Luis Bañares. Trajectory surface hopping study of the photodissociation dynamics of methyl radical from the 3s and 3pz rydberg states. *Chemical Physics Letters*, 712:171–176, 2018.

[322] A. García-Vela. Photodissociation of the methyl radical: the role of nonadiabatic couplings in enhancing the variety of dissociation mechanisms. *Phys. Chem. Chem. Phys.*, 23:25911–25924, 2021.

[323] Garikoitz Balerdi, Joanne Woodhouse, Alexander Zanchet, Rebeca de Nalda, María L. Senent, Alberto García-Vela, and Luis Bañares. Femtosecond predissociation dynamics of the methyl radical from the 3pz rydberg state. *Phys. Chem. Chem. Phys.*, 18:110–118, 2016.

[324] Sonia Marggi Poullain, David V. Chicharro, Alexandre Zanchet, Marta G. González, Luis Rubio-Lago, María L. Senent, Alberto García-Vela, and Luis

Bañares. Imaging the photodissociation dynamics of the methyl radical from the 3s and 3pz rydberg states. *Phys. Chem. Chem. Phys.*, 18:17054–17061, 2016.

[325] Richard C. Raffenetti. General contraction of Gaussian atomic orbitals: Core, valence, polarization, and diffuse basis sets; Molecular integral evaluation. *The Journal of Chemical Physics*, 58(10):4452–4458, 05 1973, https://pubs.aip.org/aip/jcp/article-pdf/58/10/4452/18885052/4452_1_online.pdf.

[326] Jr. Dunning, Thom H. Gaussian basis sets for use in correlated molecular calculations. I. The atoms boron through neon and hydrogen. *The Journal of Chemical Physics*, 90(2):1007–1023, 01 1989, https://pubs.aip.org/aip/jcp/article-pdf/90/2/1007/18974738/1007_1_online.pdf.

[327] Benjamin P. Pritchard, Doaa Altarawy, Brett Didier, Tara D. Gibson, and Theresa L. Windus. A New Basis Set Exchange: An Open, Up-to-date Resource for the Molecular Sciences Community. *J. Chem. Inf. Model*, 59(11):4814–4820, 2019.

[328] A New Basis Set Exchange: An Open, Up-to-date Resource for the Molecular Sciences Community., 2019. Accessed on Oct 10, 2019.

[329] John P. Perdew, Matthias Ernzerhof, and Kieron Burke. Rationale for mixing exact exchange with density functional approximations. *The Journal of Chemical Physics*, 105(22):9982–9985, 12 1996, https://pubs.aip.org/aip/jcp/article-pdf/105/22/9982/19228856/9982_1_online.pdf.

[330] Carlo Adamo and Vincenzo Barone. Toward reliable density functional methods without adjustable parameters: The PBE0 model. *The Journal of Chemical Physics*, 110(13):6158–6170, 04 1999, https://pubs.aip.org/aip/jcp/article-pdf/110/13/6158/19068890/6158_1_online.pdf.

[331] NIST Chemistry WebBook, 2023. Accessed on Feb 02, 2024.

[332] NIST Chemistry WebBook, 2023. Accessed on Feb 02, 2024.

[333] D S Bernstein. *Matrix Mathematics: Theory, Facts, and Formulas*. 2009.

Appendix A

A Valence-Bond-like Treatment of Methylene Dissociation

The contents of this chapter are currently unpublished. All aspects of this chapter are my own work.

A.1 Introduction

MSDFT is a cost-effective multi-state method, which is intended to handle strongly correlated systems and to be (natively) applied to excited states. The latter feature is in contrast to KS-DFT or the coupled cluster (CC) method, where the additional td-dft or EOM-CC formulations are needed to extend the ground state theories into methods for excited states. The MSDFT method expands all adiabatic states in a basis comprised of dynamically correlated diabatic states. And this diabatic-at-construction design premise makes the results directly interpretable, without the additional diabatization step that is required after most other methods. The KS determinants that form the diabatic basis are generated by splitting the system into fragments (which are typically the individual molecules of a dimer/ molecule cluster), and constraining the occupation, spin and possibly excitation of each fragment. Benchmarking of MSDFT has mostly focused on systems with loosely bound (i.e. Van-Der-Waals bound) excimers and exciplexes. Less investigations have attempted to elucidate how applicable this method is in situations where the fragments are arbitrary parts of a single covalently bound molecule.

A suitable system to investigate the suitability of MSDFT for VB-like descriptions of excited states is CH_3 (photo-)dissociation. This denotes the non-BO process in which CH_3 dissociates into CH_2 and H by breaking one of the 3 $C-H$ bonds, starting from an excited electronic state that was reached via vertical excitation from the absorption of a photon. Dissociation of a bond changes the relation between the molecular fragments from "strongly bonded" via "lightly interacting" to "spatially separated" and allows results for states across this whole spectrum to be visualized in a single plot. And the fact that the process is initialized by photo-excitation targets the investigation's focus on excited states. CH_3 provides a richer set of challenges than NH_3, which has previously been used[52] as a benchmark for a VB-like treatment within MSDFT. Firstly, the open shell nature of the methyl radical and methylene forces the solution to be a fundamentally multi-determinant wave function, which prevents methods like td-dft or CIS from being applicable. Secondly, the potential energy curves along the dissociation pathway have 3 avoided crossings between it's lowest 5 excited states (along with a multitude of symmetry- and spin-enforced conical intersections). And finally, the high symmetry of the molecule provides further challenges and benefits. To describe all 3 bonds at the same level of detail, they should all be treated equivalently in the active space; this would require the active space to include determinants which are fragmented with respect to *each* bond (see Section A.4.2.2), at triple the computational expense of affording that treatment only to the bond which actually gets broken. The process that will be used to benchmark MSDFT in this chapter is the motion of the departing hydrogen along one of the (C_2 rotation) axes of symmetry of the molecule. This motion direction was in this investigation chosen to define the $+x$ axis, see Fig. A.1. (The

Figure A.1: Axis orientation, important symmetry operations and atom labels in the CH_3 system.

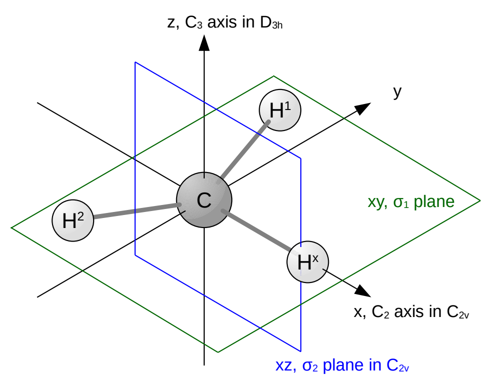

z axis was chosen to be perpendicular to the molecular plane, and therefore coincides with the C_3 axis in the full $D_{3\mathrm{h}}$ symmetry group. And thus the y axis is parallel to the line that connects the remaining two hydrogen atoms (with the $+y$ direction going from the third (H^2) to the second (H^1) hydrogen).) Along this reaction pathway the system keeps the largest possible subset of the molecule's symmetries (the $C_{2\mathrm{v}}$ symmetry group, whose symmetry operations include the C_2 rotation around the x axis, mirroring about the molecular plane (xy), and mirroring about the xz plane), while the remaining symmetries of the molecule's $D_{3\mathrm{h}}$ group are broken (most notably the 3-fold C_3 rotation symmetry around the z axis).

The potential of CH_3 and CH_2 to serve as a system for benchmarking newly developed methods has been recognized relatively early in the history of computational chemistry. It was for example used to benchmark contractions of gaussians into a Slater-like atomic orbital basis[303] and the Generalized Valence Bond (GVB) method.[304]

CH_3 and CH_2 have importance as (extremely short-lived) intermediates in organic reactions and they are detectable in the troposphere[305] and the interstellar medium[306].

The history of research on CH_3 and CH_2 is ripe with examples of researchers arriving at the wrong answers to the questions they set out to answer. The first observation which was (in 1942 [307]) wrongly assigned[308] to be signs of the existence of these molecules (CH_2 to be specific) was the $lambda4050$ emission band in the spectrum of the tail of comets. It took until 1949 for this to be disproved.[309] And it took until 1954 and 1954 (respectively) for the first *direct* proof (i.e., not via their reaction products) that CH_2 and CH_3 exist as a molecule that can be isolated in the laboratory. [310][311][312] The main complicating factor was the high reactivity of both molecules, compounded by the fact that many researchers relied on the wrongly assigned $lambda4050$ emission band for the detection of their desired product. Additionally, the planarity of CH_3 causes many of the transitions to be forbidden.

And in a turn of events that paralleled the experimentalists' struggles, when the emerging field of theoretical chemistry tried to use simulations instead of experiments to answer questions about these molecules, several of those questions again took decades to be concluded with a final answer. The first cause of these difficulties in simulations is that there are several examples where points of interest on the potential energy surfaces have unusually similar energies; Which causes the accuracy which is necessary in order to even make qualitative predictions to be escalated to a level that the usual computational methods of the time could not provide. The first example is the ordering (and order of magnitude of the separation) between the lowest 2 electronic states in CH_2 (the lowest singlet ($^1A_1$) and the lowest triplet ($^3B_1$) state). The profound difference between these states is that the $^1A_1$ state consists of a main determinant and significant contributions from a second determinant (while the $^3B_1$ state is a weakly correlated singe-determinant state). Therefore, a post-HF treatment is required to ensure that the calculations for both states are founded on a qualitatively correct wave function.[313] The second example where small energy differences slowed progress is the geometry of states like the $^1B_1$ ground state of CH_2 and $^2A_2''$ ground state of CH_3. In both of these states, the potential energy around the equilibrium geometry barely varies in the direction of their (out-of plane) bending vibrational mode and stays almost constant for a large range of angles. A common theme in both of these examples is the existence of singly occupied (sp^2 / sp^3) orbital lobes in the bent geometry of both molecules. When the molecule gets flattened or straightened out, these singly occupied orbital lobes are transformed into singly occupied p_z orbitals and the electron in that orbital gets partially shifted to the other side of the C atom. In molecules like NH_3 where the sp^3 orbital lobe (or the $2p_z$ orbital for flat NH_3) is doubly occupied, the electron-electron repulsion from that lobe exceeds the electron-electron repulsion between $C - H$ bond orbitals (which have their center of charge further out from the nucleus than the sp^3 orbital lobe). (Additionally, the average distance from the nucleus is minimally smaller for a sp^3 orbital lobe than for a $2p_z$ orbital, and the unbound electron pair is able to make better use of the gain in electron-nucleus potential than electrons in a bond orbital can.) But for CH_2 and CH_3, the single occupation in the sp^3 orbital lobe leads to a comparable decrease in the electron-electron repulsion as the further distance of the bond orbitals does.

Due to their small size (and relation to CH_4), attempts at simulating CH_3 and CH_2 started in the mid-1930's, during the infancy of theoretical chemistry.[314, 315] The methods used in those calculations are equivalent to a minimal-basis Hartree-Fock (HF) calculation in terms of the effects they take into account explicitly, but are relying on empirical parametrization of multiple parameters to reach a useful level of accuracy. HF is often regarded as adequate for getting close enough to the true molecular geometries. Not because it is especially sophisticated (in fact, its atomization energies are quite significantly off from reality), but because the influences on molecular energies that it neglects (especially dynamic correlation) vary only slowly with changes in geometry, and the sum of the energy terms it includes (or in other words, the total HF energy) almost always varies comparatively quickly with geometry changes. The problem arising for the bending of CH_3 and CH_2 is that the latter is not the case when the molecular geometry is inside the above mentioned large range of bending angles with near-constant total energy. And this "plateau" greatly amplifies the influence of small errors or inaccuracies in the energy gradients (due to neglected correlation) on the equilibrium geometry (compared to systems with typical bending force constants). The inability to reach the resulting accuracy requirements to resolve such small energy differences is why almost all early simulation attempts in which HF or equivalent methods were used gave the wrong answer for the ground state geometry of both molecules. And the bent geometry optimum only resulted from calculations that included more approximations than the state-of-the-art calculations of the time.[316] It took until the 1960s(/early 70s) for accurate post-HF methods to start being applied to this problem,[317] which shifted the narrative from the previous most accurate methods favoring the linear geometry to the most accurate methods from that time onward agreeing[318] [319] on the bent geometry of CH_2. This indicates that including correlation effects in the calculation was vital for arriving at the correct (bent) geometry. The second aggravating factor leading to the many difficulties in simulations is the reactivity and general instability of these molecules. This reactivity is exemplified by the processes that CH_3 or CH_2 can undergo even with only a singular molecule involved, which include: The fact that 3 of the 6 lowest electronic excitations of CH_2 are instable (and would instantaneously decompose into a C atom and a H_2 molecule)[313] on one hand, and on the other hand the photo-decomposition process investigated in this very chapter.

To date, experimental studies of CH_3 dissociation are plentiful. Computational studies are slightly rarer, and highly accurate computational results are much rarer still. The groups of Bañares and García-Vela have published a significant share of them. [320] [321] [322] Further references can be found in their publications. Two of their papers [323] [324] will be used to validate our high-level WFT reference calculations against.

Section A.2 will motivate the need to handle static correlation in a computationally cheap DFT-based method. This will be followed in Section A.3 by a quick overview of how MSDFT (separately) handles static correlation on one hand and dynamic correlation on the other; leading over into detailed explanation of the MSDFT method. The calculations that we performed and their setup and parameters are covered in Section A.4. The results start with an accurate MRCI calculation in Section A.5.1.2. This WFT reference is then used to benchmark MSDFT calculations with two different active space sizes in Section A.5.3 and Section A.5.4. And finally, excitation energies at the CH_3 and CH_2 equilibrium geometries are compared quantitatively in Section A.5.5.

A.2 Multistate Density Functional Theory

A.2.1 Motivation and Comparison to Wave Function Theory Methods

A.2.1.1 Motivation for MSDFT

MSDFT is a dynamic-then-static [11] method. In this type of method, dynamic correlation is treated in the first phase of any calculation in an independent-electron approximation for each diabatic state separately. And static correlation in the second, multi-determinant, phase by a configuration interaction method. MSDFT uses 2 existing concepts. Firstly, dynamic correlation is treated on a DFT level (or in other words, by an exchange correlation functional). The definition of that functional (for use within a single determinant) is deferred to established XC functionals. The second concept, used in order to be able to solve for specific determinants, is a block localization procedure that restricts electrons to certain sets of orbitals. The single-electron phase of the MSDFT method that uses these concepts is described in more detail in the first part of Section A.3. The main novel feature to the MSDFT method is a formalized approximation for how to use the DFT determinants/states as basis functions in a multi-state Hamiltonian. (See the second part of Section A.3.) This allows the second phase to accurately approximate static correlation and to solve for excited states. The main goal of the MSDFT method is to provide accuracy comparable to Kohn-Sham DFT, but at a much lower computational cost than most other methods that are suitable for treating strong correlation.

A.2.1.2 WFT/DFT Methods

Kohn-Sham DFT is very popular, mainly because (for the systems it is applicable to) it provides generally satisfactory accuracy for a well-scaling and generally low computational cost. In Kohn-Sham DFT, dynamic correlation is handled to within moderate to good accuracy by a large selection of exchange-correlation functionals. Although in td-DFT there exists a popular extension capable of handling excited states, the main problem is that neither standard DFT nor td-DFT (the latter on account of only handling single-electron excitations) can be used to solve for qualitatively correct statically correlated states. The most famous case where this is a problem is the dissociation of a $\mathrm{H}-\mathrm{H}$ bond, for which Kohn-Sham DFT can not describe the dissociated state qualitatively correctly. Most methods in the WFT method category are designed to handle static correlation, including the following ones. Most WFT methods and all of the below fall into what Liu[11] calls the static-then-dynamic category, in which the method first obtains a reasonable approximation to the true solution that treats static correlation between the most important determinants in an accurate but computationally expensive way. And then in a second step many more determinants are added, usually with a computationally cheaper treatment (most often perturbatively), in order to handle dynamic correlation. MCSCF is the most simple WFT method that handles static correlation. It can be used with a minimal set of determinants. In this method, all determinants use the same set of MOs, which are optimized for the resulting multi-determinant state. This leads to the problem that the orbitals can not be optimal for each determinant at the same time. CASSCF and NOCI fix this by extending the MCSCF method in two different ways. In CASSCF all determinants (still) use the same set of MOs, which are optimized for the resulting multi-determinant state. In order to be able to handle excited states, all occupation combinations in the active space are included in the set of determinants. The added degrees of freedom in describing the states (in terms of determinants) does also function as a workaround to MCSCF's constraints to the orbitals (them being common to all of the determinants). The downside of this solution is that including more determinants has one of the worst scaling computational costs in molecular simulations. NOCI on the other hand keeps the MCSCF strategy of using a minimal set of determinants. But the orbitals are optimized independently for each determinant. A slight disadvantage is that orbitals of different determinants are non-orthogonal. As an ab-initio method, the quality to within which WFT can treat dynamic correlation is only limited by how many excited determinants are taken into account explicitly. Although the achievable quality can thus theoretically be improved without limit; this is in practice only possible with configuration interaction, whose computational cost scales quite unfavorably, or with exceedingly high orders of perturbation theory, since this method converges very slowly. In conclusion, in WFT the treatment of dynamic correlation is very expensive, but static correlation is often being handled with just a few determinants. In contrast, Kohn-Sham DFT is cheap, comparable in cost to the HF or MP2 levels of WFT. With the outlined capabilities and downsides of DFT and WFT methods there is definitely a capability gap that could be filled by a cheap DFT-based method which is able to handle static correlation and reaches levels of accuracy close to that of WFT methods. There are a few multi-determinant DFT methods[166, 165, 172, 171] that have been proposed which try to fill this gap by handling dynamic correlation through approximate functionals and static correlation with a minimal set of determinants. Since these can get away with using minimal active spaces, the runtime will scale polynomially with that number, instead of with the number of all determinants involved in the dynamic correlation.

A.2.1.3 Treatment of Correlation in MSDFT

In practice, one of the most accurate WFT methods that accounts for both static and dynamic correlation is the CASSCF/MRCI combination. Here, the static correlation is treated first in CASSCF and at the same time, the orbitals are optimized for the only statically correlated states. After that, MRCI takes care of the majority of dynamic correlation by adding, on top of the determinants from CASSCF, certain excitations to and from orbitals outside its active space (usually singles and doubles from all reference determinants). This is therefore classified[11] as a static-then-dynamic type method. In contrast, MSDFT first obtains single-determinant Kohn-Sham DFT states which by their very nature are dynamically correlated. After that, MSDFT treats those Kohn-Sham DFT states as diabatic states and combines them into multi-determinant adiabatic states. This step takes care of static correlation. MSDFT is therefore classified[11] as a dynamic-then-static type of method.

A.3 Theory: The MSDFT Method in Detail

A.3.1 Overview

Solving for a wavefunction always involves finding the eigenfunctions of a Hamiltonian energy operator. In practice that problem is almost always formulated as an optimization in terms of a limited set of basis functions, which reduces it to the diagonalization of a Hamilton matrix. As its result this diagonalization yields energies and coefficient vectors for the description of the wave function. This can apply generally to wave functions on the single-electron or multi-electron level, or both, with basis functions being either orbitals, determinants or multi-determinant states. (Classical) DFT is somewhat of an exception because it theoretically solves for a density instead of a wave function. The determinant that in practice is optimized in Kohn-Sham DFT (which is often called its solution) is the optimal determinant under the assumption that this density is produced by a single-determinant wave function. This assumption is at best approximately true for the real wave function (the one that is the solution to the true ab-initio Hamilton operator). Therefore the Kohn-Sham determinants can in the postulation of the transition density functional (TDF) in MSDFT only be treated as a stand-in for explicitly dynamically correlated diabatic states which are dominated by a single determinant.

MSDFT follows this scheme (in spirit) twice in its two-phase optimization, in a manner similar to NOCI. In the first phase, a set of user-defined states (with implicitly included dynamic correlation) is obtained by diagonalizing a Kohn-Sham Hamiltonian (on the single-electron level). To be specific, a version of Kohn-Sham DFT is used which applies user-defined block-localization constraints to arrive at those different states, as explained in Section A.3.2. In the second phase, the resulting DFT states are used as basis functions for an optimization on the multi-electron level to take care of static correlation, as explained in Section A.3.3. Since only approximations to the wave functions that are the basis functions of this optimization are known, the Hamilton (and overlap) matrix elements in this phase have to be defined as approximations as well. This can be remedied by correction terms - inspired by Kohn-Sham DFT's exchange correlation functional - for which 3 approximations have been proposed so far.[52, 8, 96] These approximations are explained in more detail in Section A.3.3.

A.3.2 Basis Functions: BLW-DFT

In the first phase of a MSDFT calculation, single-determinant diabatic states are obtained in independent-electron approximation. This is similar to the Hartree-Fock phase that is prerequisite to MCSCF, or the independent-electron phase of a NOCI calculation, except that MSDFT uses Kohn-Sham DFT instead of Hartree-Fock. To overcome the restriction that standard DFT only yields the ground state, block-localization is used to constrain the wave function in order to force it to convergence to a non-ground-state solution. The full set of basis functions is partitioned into subsets called blocks. The determinant is still an (anti-symmetrized) product of orbitals that are linear combinations of atomic orbitals. But instead of being molecular orbitals that use all basis functions in the system, these orbitals now belong to a single block each and are formed from only the AO basis functions belonging to that block. These "block localized molecular orbitals" (BMOs) are as usual subject to optimization of the coefficients in the linear combination. But instead of the work boiling down to diagonalizing the full Kohn-Sham Hamilton matrix, the diagonalization is instead performed for each block individually - which is equivalent to ignoring any off-diagonal elements in the Hamilton matrix (and overlap matrix) linking the blocks, as if the matrices were block-diagonal. (Neglecting these off-diagonal overlap matrix elements leads directly to non-orthogonality between BMOs and ultimately to the need to explicitly normalize the determinants.) The only influence that the blocks exert on each other thus stems from the SCF procedure, which still applies to the system as a whole.

In the block-localization scheme used in this chapter, building up the Kohn-Sham determinant and density from those single-electron MOs proceeds mostly as in conventional Kohn-sham DFT (or Hartree-Fock), with the only exception that the electron occupation is not defined for the system as a whole but for each block individually. And a different choice for the occupation of the blocks (and sometimes also a different definition for the blocks themselves) is used for each of the various determinants. In the MSDFT implementation used in this chapter, only the occupation (of up and down electrons) on each of these blocks can be specified, and the block is filled up in the energetic order of its block molecular orbitals. A newer MSDFT program version[9] allows for ΔSCF-style excitations to higher block-localized molecular orbitals within any block, but that version is not used in the calculations in this chapter. The aim in this investigation was to determine whether a valence-bond like treatment of a molecule would allow the MSDFT method to yield correct excited states. A ΔSCF treatment of either of the two fragments runs counter to the spirit of a valence bond treatment. Furthermore, wherever it is suitable to access excited states through a ΔSCF treatment, it would make much more sense to apply that treatment to the molecule as a whole (or a reasonably self-contained subset of a large enough molecule) rather than individual fragments containing as few as a single atom.

In the simplest case, the definitions for the blocks in a determinant simply follow the typical definition of (spatially distinct) molecular fragments (such a block would be comprised of all AO basis functions centered on atoms belonging to that fragment). When used on a system where a bond is broken, this naturally leads to a VB description of the wave function. A block may also encompass *all* basis functions on a molecule (for a MO-based description) - especially if the system contains more than one molecule, but even if the system contains only one molecule. And the determinants are not limited to all using the same blocks. For example, determinants that are intended to make major contributions to a certain excited adiabatic state might very well contain a block of one of the following kinds (and exist alongside determinants of the above two types that do not include it): A block can contain only a specific single AO, a specific sub-shell on an atom, a block can contain all AOs with the same rotational symmetry around one nucleus which thus use the same spherical harmonic, which will in the following be called a "slice" of AOs, or any other sub-Hilbert-space of the system that can be expressed in terms of basis functions. The actual selection of determinants used in my calculations are explained in Section A.4.2.1.

The blocks can not only be used to localize electrons to specific regions, but sometimes also to constrain them to orbitals with specific symmetry representations, provided there exists a symmetry group for which every basis function transforms as one of the symmetry representations. If only basis functions with the same symmetry representation are combined in any block, then every MO formed in that block will transform as that representation. Therefore the determinant as a whole will transform as the product representation of all of the single electron wave functions (which is then also transforming as one of the symmetry group's representations). In the current implementation, where blocks can only be defined in terms of conventional gaussian contractions (centered on a single atom), this only works for a symmetry operator which all *basis functions* are eigenfunctions of. In CH_3, the only symmetry operation this applies to is mirroring about the molecular plane.

A.3.3 Hamiltonian: Hamilton Matrix Approximations

The second phase in the MSDFT method consists of solving for the multi-state wave function(s). Ideally, it would be possible to formulate the multi-electron wave function in the basis of the DFT states and optimize it by diagonalizing the resulting Hamilton matrix. But recall that the Kohn-Sham determinants that are commonly called the solutions of the calculations in this step are only approximations to the unknown true wave functions (without any guarantee that it has any resemblance of the true ground-state wave function with that density). Therefore the Hamilton and overlap matrix elements for the actual DFT states have to be guessed. However, since Kohn-Sham DFT is only intended for states which are dominated by a single determinant, matrix elements based on the Kohn-Sham determinant can be expected to be a reasonable first order approximation to the actual matrix elements (wherever the Kohn-Sham DFT method itself can be expected to be reasonably accurate).

The most straightforward approximation for the overlap matrix elements of the diabatic states is to use the overlap of the Kohn-Sham determinants. For the Hamilton matrix, the diagonal elements H_{II} should be the exact energy of the DFT states, and the best known approximation for that is their energies, as provided by BLW-DFT:

$$H_{II} = E^{\mathrm{DFT}}\left[\psi_I\right] \ . \tag{A.1}$$

According to the Lu-Gao theorems [4], the non-diagonal elements of the Hamilton matrix $H_{I \neq J}$ are theoretically expressable as a functional of only the transition density

n_{IJ}, which is therefore called a “transition density functional” (TDF):

$$H_{I\neq J} = E^{\mathrm{TDF}}[n_{IJ}] \ , \tag{A.2}$$

where the transition density is (canonically, i.e. for a WFT state) defined as $n_{IJ} = \langle \Phi_I^{\mathrm{WFT}} | \hat{\rho} | \Phi_I^{\mathrm{WFT}} \rangle$. Akin to the energy functional $E[n]$ in Kohn-Sham DFT, the functional for the off-diagonal Hamilton matrix elements is unknown and has to be approximated. In WFT, the off-diagonal matrix elements would be the matrix element of the electronic Hamiltonian $\hat{H}$ with the full wave function of the diabatic states Φ_I and Φ_J:

$$H_{I\neq J} = \langle \Phi_I | \hat{H} | \Phi_J \rangle \ . \tag{A.3}$$

This suggests the largest contribution to the approximation for $E^{\mathrm{TDF}}[n_{IJ}]$ to be given by the same (WFT-level) interaction, but applied to the Kohn-Sham determinants ($\psi^{\text{Kohn-Sham}}$):

$$H_{I\neq J} = E^{\mathrm{TDF}}[n_{IJ}] \approx \langle \psi_I^{\text{Kohn-Sham}} | \hat{H}^{\mathrm{WFT}} | \psi_J^{\text{Kohn-Sham}} \rangle = H_{IJ}^{\mathrm{WFT}} \ ; \tag{A.4}$$

Or in other words, the matrix element of the electronic Hamiltonian $\hat{H}^{\mathrm{WFT}}$ with the two Kohn-Sham determinants. The required corrections to this term are combined into a correlation correction F^{C}:

$$H_{I\neq J} = H_{IJ}^{\mathrm{WFT}} + F^{\mathrm{C}} \ . \tag{A.5}$$

Just like the XC functional in Kohn-Sham DFT, Eq. A.5 is effectively the definition for the correcting transition density functional F^{C}. This remaining (correlation-related) contribution to the TDF needs to be approximated using some educated guess. Note that despite $H_{I\neq J} = E^{\mathrm{TDF}}[n_{IJ}]$ being a function of the transition density, it is valid for for F^{C} and its approximations to depend on other parameters (like the individual densities n_I, n_J or Kohn-Sham determinants $\psi_{,}^{\text{Kohn-Sham}} I \psi_J^{\text{Kohn-Sham}}$), similar to how hybrid an meta XC functionals depend on other properties of the Kohn-Sham determinant than just its density. The approximation used in this chapter is the arithmetic average of the correlation energy of each state, scaled by their overlap:

$$F^{\mathrm{C}}[n_{IJ}, n_I, n_J, \psi_I^{\text{Kohn-Sham}}, \psi_J^{\text{Kohn-Sham}}, ...] = S_{IJ}\frac{1}{2}(E^{\mathrm{C}}[n_I] + E^{\mathrm{C}}[n_J]) , \tag{A.6}$$

where $E^{\mathrm{C}}[n]$ is given either by the correlation contribution to the xc functional (when those are separable); or by the difference between the exchange-correlation energy from DFT E^{XC} and the Hartree-Fock exchange energy determined using the Kohn-Sham orbitals $E^{\mathrm{HFx,KS}}$:[52]

$$E^{\mathrm{C}}[n_I] = E^{\mathrm{XC}}[n_I] - E^{\mathrm{HFx,KS}} . \tag{A.7}$$

To date, one approximation scheme with a different philosophy has been used. That scheme uses the fact that a high-spin (triplet or quartet) quartet state is a single-determinant state whose energy can be calculated in standard Kohn-Sham DFT, and that the low-spin (triplet or quartet) counterpart has to be energetically degenerate with it. This condition allows the unknown correlation interaction between the two $M_S = 0$ (low-spin) determinants that combine to form a $S = 0$ singlet and a $S = 1$ triplet state (or two $M_S = 1/2$ determinants that combine to form a $S = 1/2$ doublet and a $S = 3/2$ quartet state) to be determined exactly.[8]

A.4 Calculation Details

This section explains the setup and all relevant parameters for the MRCI and MSDFT calculations that were performed for the purpose of benchmarking the use of MSDFT for excited states.

A.4.1 Details for MRCI and MSDFT

A.4.1.1 Basis Size

All calculations shown have been carried out using the aug-cc-pVTZ basis set. MRCI calculations with basis sets ranging in size from cc-pVDZ to aug-cc-pVQZ (which preceded those shown) suggest that the aug-cc-pVTZ basis set offers the best balance of quality and computational cost (in MRCI). It is worth noting that these basis set comparisons also showed the outstanding importance of diffuse functions in the augmented basis sets. This same basis set that proved optimal in MRCI is also used for the MSDFT calculations, which ensures that they are directly comparable.

A.4.1.2 Basis Contractions

As explained in Section A.3.2, the DFT determinants in MSDFT are defined by the user in terms of occupations of blocks (user-defined sets of basis functions). One of the two main goals in the definitions of the diabatic determinants is to minimize the number of determinants needed to describe the adiabatic states. The diabatic determinants should therefore ideally be as similar to energy eigen-functions as possible. The second main goal is to define determinants that allow the user/ researcher to interpret the composition of the adiabatic states in terms of the diabatic determinants. Therefore the diabatic states should ideally carry a distinct meaning for a human. One factor that impedes the interpretation in terms of the diabatic states is if those diabatic states are too non-orthogonal, or even almost linearly dependent. This can technically be solved by orthogonalizing the set of determinants before diagonalizing it, as has been done in [26]. However, this significantly changes the meaning/interpretation of the diabatic states. Non-orthogonality between determinants can be caused or exacerbated if there are non-orthogonal AO basis functions in different blocks - assuming that the determinants differ in electronic occupation on those AOs/blocks. Neither type of non-orthogonality (between determinants or AOs) is an issue for obtaining the correct results, but especially the non-orthogonality between diabatic states makes interpreting the results very difficult. Both of these requirements on the diabatic determinants are easiest to fulfill if the orbitals that they are constructed from are also at least similar to energy eigen-functions (either MOs, fragment molecular orbitals "FMOs", or at least AOs, as opposed to primitive gaussians).

There are theoretically different ways to set up the contractions that define the basis functions in the aug-cc-pVTZ basis set. For most use cases they are all equally valid as long as they span the same degrees of freedom in the Hilbert space. Importantly, many programs allow non-orthogonality between basis functions on the same atom (in addition to the unavoidable non-orthogonality between basis functions on different atoms.) Basis set contractions are therefore often defined using the smallest possible number of gaussians for each contraction. Specifically, the aug-cc-pVTZ contractions that gamess uses by default (in the following called the "gamess basis") is constructed to span the same degrees of freedom as the general contraction scheme of Raffenetti[325] (used in Dunning's' aug-cc-pVTZ basis set[326]), but the gamess basis includes one computational optimization (with no effect on the result in most use cases). The difference is in how the "gamess basis" handles the gaussian primitives with the most diffuse exponents. The contraction scheme as envisioned by Raffenetti (see table 5 in [325]) has them contribute to both the occupied AOs and the virtual "contractions", while in the "gamess basis" these gaussians that are the sole components of the virtual basis functions are removed (coefficients of zero) from the contractions that form the occupied AOs. As a result, the occupied contractions in the "gamess basis" have their long-range tail suppressed and therefore do not directly correspond to atomic orbitals. In MSDFT however, for excitations into a virtual AO (say for example a C 3s orbital), it would cause difficulties if those virtual orbitals would exhibit significant similarities to occupied orbitals (C 1s or C 2s in this example). The virtual basis functions (all remaining basis functions) should be orthogonal to the core and valence basis functions (be composed of higher energy eigen-functions and diffuse functions). The basis used in this investigation therefore differs from both the gamess basis and Dunning's aug-cc-pVTZ basis using the contraction scheme of Raffenetti. The contractions used for the *core and valence* basis functions are taken unchanged from the basis set exchange (aug-cc-pVTZ.us.1.dat, version 0.8.9 [326, 327, 328]). All *virtual* basis functions were taken from the basis set exchange definition (which is identical to the gamess default) and (where necessary) were Gram-Schmidt orthogonalized to any occupied (core & valence) basis functions on the same atom. The virtual basis functions with higher angular momentum (p and d type AOs on H and the d and f type AOs on C) do not need to be orthogonalized, since they are already naturally orthogonal to the angular wave function component of all occupied basis functions. The virtual basis functions with low angular momentum (H 2 + +s and C 3 + +s and C 3 + +p contractions) do need to be orthogonalized to all core and valence basis functions with the same angular momentum. However, they do not need to be orthogonalized to each other, because any set of virtual AOs with the same angular wave function component (and thus possibly nonzero overlap) was always grouped into the same blocks in all calculations in this chapter.

A.4.2 MSDFT Details

The TDF in all MSDFT calculations of this investigation uses the "overlap-weighted average of the correlation energy" approximation. The PBE0 hybrid functional [329, 330] is used both in the evaluation of the diagonal elements of the multi-electron Hamilton matrix, and as a basis for the correlation energy in the TDF approximation. As described in Section A.3.2 above, the second phase of a MSDFT calculation uses user-specified determinants as the basis functions to construct ground and excited states. As described in Section A.4.2.2, these determinants are defined in terms of blocks, which in turn are defined as non-intersecting collections of basis functions. A.4.2.2 introduces some considerations that have to be made when defining these blocks. There is a lot of freedom in which determinants to choose, and in how to define the determinants and their blocks. The active space in this chapter contains both diabatic states of a localized (VB) and delocalized (MO) type, as explained below.

A.4.2.1 Delocalized vs. Localized States

Possibly the best known example where DFT (and HF) fails is $\mathrm{H-H}$ dissociation. This process can be described naturally in the valence bond picture. At an infinite separation of the nuclei, the ground state is a superposition of the 2 covalent states (with 1 electron on each atom). Around the equilibrium distance, however, the forming covalent bond is described qualitatively correctly as a roughly equal mixture of the above 2 states plus 2 ionic states. At intermediate distances the ground state is a linear combination of those 4 determinants that falls somewhere between the 2 extremes. Therefore the most straightforward way to model this dissociation (and bond breaking in general) in MSDFT is to use a VB-picture based minimal active space.

In the case of CH_3 dissociation, the equivalent set of determinants to the 4 determinants (2 covalent and 2 ionic) from the $\mathrm{H-H}$ dissociation example consists of 5 states (3 covalent and 2 ionic). In the CH_3 VB state that does not have an equivalent in the $\mathrm{H-H}$ dissociation example, both electrons from the broken bond have the same (e.g., up) spin, while the $\mathrm{C\,2p}_z$ electron has the opposite spin (e.g., down). This state is not negligible in this system because the two unpaired spins in the covalent determinants not only interact with each other, but also with the extra unpaired spin of the $\mathrm{C\,2p}_z$

electron. Most importantly, this state contributes one half of the qualitatively correct description for the singlet (and triplet) states that the CH_2 segment converges to when the interaction with the departing H atom vanishes. However, including only the 5 valence bond states with respect to the H^x-CH_2 bond (while using CH_2 fragment orbitals to treat the other two bonds) treats the 3 bonds which are equivalent at the equilibrium geometry in different levels of detail. Mitigating this requires one of the fixes described in Section A.4.2.2 below.

MSDFT, in the edge case of a single basis state with no constraints on the electrons, turns into Kohn-Sham DFT and perfectly reproduces the DFT results. In fact, as experience with DFT shows this is a good approximation (at least a qualitatively correct one) for the ground state of many molecular systems, and only fails to be a good approximation for strongly correlated systems. Since xc functionals (and xc potentials) are optimized for unmodified Kohn-Sham DFT, it stands to reason that they are best at yielding the most optimal orbital shape for the MOs of such unconstrained determinants. Since MSDFT (with any other active space) is using standard xc potentials to obtain fragment molecular orbitals (FMOs), it is using them slightly outside their intended application and determinants other than the ground state one will have slightly non-optimal orbital shapes. Even though describing a molecule entirely in the valence bond picture would be qualitatively correct, my experience has shown that for CH_2-H dissociation, adding the single unconstrained DFT determinant to an active space that already allows for a qualitatively correct description will indeed slightly lower the energy of the ground state, even at the CH_3 equilibrium geometry. And in the case of calculations which preceded the ones shown here, with active spaces which I wrongly assumed to be sufficient to model all relevant states, adding the delocalized determinant has revealed those deficiencies (through an unexpected lowering of adiabatic energies).

A.4.2.2 Blocks

Although the dissociation process breaks only one bond, all 3 bonds are identical at the equilibrium geometry. Splitting up only the 1 bond to treat it in the VB picture leaves the other 2 bonds with a description in the MO picture. This failure to treat the 3 equivalent bonds equivalently would lead to an asymmetrical equilibrium geometry. Treating the 3 bonds equivalently can be done in the following 2 ways.

For a systematic coverage of the whole Hilbert space that states in the VB picture can cover, there would need to be splits between blocks along all 3 $C-H$ bonds of the CH_3 molecule in every determinant, limiting each block to contain only basis functions centered on a single atom. And the complete active space would include all ways to distribute both electrons from each of the 3 bonds to the two blocks that cover it. Defining many of these determinants would also require placing the electrons on the C atom into 3 separate sp^2 hybridized orbitals, but the program only allows blocks to be defined in terms of conventional AOs ($2s$, $2p_x$, $2p_y$), not sp^2 hybridized orbitals. It is possible to let MSDFT construct states defined in terms of hybrid orbitals from conventional AOs, but this would further increase the number of required determinants. All in all this would exponentially inflate the number of required determinants.

The second possibility to symmetrize the treatment of the 3 bonds involves only splitting one bond in each determinant, but triplicating the above described 5 determinants (2 ionic + 3 covalent). For each of the 3 split bonds (even for the 2 hydrogen atoms that physically stay with the CH_2 fragment), the active space includes all 5 different determinants for 3×5 states total (the first 15 individual determinants in the list of B_1 states below). There is theoretically some overlap between the space that each of the 3 sets of differently split determinants spans, but this does not lead to any numerical problems in this system. Apparently the sigma orbitals that the determinants for each split bond combine to form have different enough shapes from the sigma orbitals within the CH_2 block.

A.4.2.3 Symmetry (and Representations)

In addition to localizing electrons to specific molecular fragments, atoms, and/or (sub-)shells, the block localization also makes it possible to take advantage of symmetries of molecules, as explained in more detail in Section A.3.2. In CH_3, the arrangement of the nuclei conforms to the $D_{3\mathrm{h}}$ symmetry at the equilibrium geometry and the $C_{2\mathrm{v}}$ symmetry group along the specific dissociation pathway. All MOs, determinants and states should transform as the representations in these symmetry groups. Gamess, which our group modified to implement the MSDFT method, uses AOs (contractions of gaussians) as the basis functions. And the fact that they are centered on a single nucleus breaks the mirror symmetry with respect to mirroring about the xz plane perpendicular to the molecular plane. Since mirroring about the molecular plane (xy) is the only symmetry operation that applies to each individual basis function, the highest symmetry that all of the basis functions can be categorized by is thus the C_{s} symmetry (sub-)group, for which each basis function transforms as one of these two representations: even symmetry functions on one hand (which include functions of A_1 and B_2 representations in the $C_{2\mathrm{v}}$ symmetry group; as well as E', A_1' and A_2' representations in the $D_{3\mathrm{h}}$ symmetry group); and mirror anti-symmetric (which includes B_1 and A_2 representations in $C_{2\mathrm{v}}$; as well as E'', A_1'' and a_2'' in the $D_{3\mathrm{h}}$ symmetry group). Luckily, none of the lower energy states or determinants transform as the A_2 representation of the $C_{2\mathrm{v}}$ group, so that only the A' representation of the C_{s} group has to yield solutions of two (A_1 and B_2) representations of the $C_{2\mathrm{v}}$ group. The used block definition scheme in combination with an AO basis does not allow to define blocks and determinants that obey the remaining symmetries of the system in the same way. Programs which are intended to utilize molecular symmetries would solve this by using basis functions which are linear combinations of AOs on atoms at equivalent sites and use those as basis functions for separate a_1 and b_2 representation calculations. In this system this would apply to the AOs of H^1 and H^2 with flipped +y and -y coordinates, for example $(H^1\,1s) + (H^2\,1s)$ and $(H^1\,1s) - (H^2\,1s)$.

In the MSDFT variant that allows local excitations within each block, the localization to the H^1 and H^2 atoms could be defined as excitations in the MO picture. But since that description of the localization would differ from the localization to the departing hydrogen atom, the 3 $C-H$ bonds would still not be treated equivalently.

For all of these reasons it is not possible to take advantage of the full symmetry of the system (neither the $C_{2\mathrm{v}}$ symmetry along the dissociation pathway nor the $D_{3\mathrm{h}}$ symmetry of the equilibrium geometry). For the mirror symmetry plane perpendicular to the molecular plane and rotation about the C_2 axis (which was oriented along the x axis) the correct symmetry can not be enforced and relies on the consistent and stable convergence of the DFT determinants. Specifically, each pair of A′ determinants that define the same state with respect to the H^1 and H^2 atom have to converge to the same results in order for them to cleanly combine to form A_1 and B_2 states.

While the breaking bond gives the blocks in the a′ representation a major influence on the results (and necessitates the complexity in their definitions), the a″ blocks are comparatively trivial. The only occupied MO of the a″ (b_1 and a_2 in $C_{2\mathrm{v}}$) MOs is the lowest "$C\,2p_z$" MO (see Fig. A.2f below). And even though the occupation of this MO changes between the A′ and A″ states, the VB picture does not describe it as a bond that gets broken by the dissociation. In the limit of infinite $C-H$ separation, the "$C\,2p_z$" MO naturally becomes fully localized to the CH_2 fragment, which means that the block definition for the a″ MOs does not have to achieve this fragment localization (which would have been possible by separating the leaving hydrogen's AOs from the other a″ AOs). The $C\,2p_z$ MO therefore remains very similar in shape to the $C\,2p_z$ AO along the whole dissociation pathway. Furthermore, the only initially empty a″ MO that electrons are excited into is the C 3p$_z$ AO, while none of the anti-bonding a$''$ MOs play any role in the relevant PEC's/ PES's. As a result, all a$''$ AOs can be kept in a single group strictly separate from the a$'$ AOs. This separation of the orbitals of the C_s representations was the foremost priority in the block definitions used in this chapter.

Another fact that can be exploited to enforce symmetries is that the a$_2$ MOs will be unoccupied in all of the resulting states. This would theoretically mean that no basis function that transforms as this a$_2$ symmetry representation would need to be included in any occupied block. However, some states are combinations of basis determinants where the blocks and their occupations are not themselves symmetric with respect to the σ_2 plane (and rotation about the C_2 axis) and follow/obey only C_s symmetry. In these basis determinants, including the a$_2$ basis functions should allow a more optimized shape for the C 2p$_z$ MO and thus probably a lower energy for each determinant. However, this is energetic lowering might very well be canceled out or over-compensated by the act of combining two symmetry-equivalent determinants into a symmetric and anti-symmetric combination. Any combination of the two symmetry-equivalent determinants in the VB picture will lead (in the MO picture) to a two-determinant state as well, with the main determinant which has the expected symmetries of the MOs, and a minor determinant whose contribution to the state is given by the amount of contribution that the a$_2$ basis functions have to the a$''$ MO. In the case where the a$''$ MO is singly occupied and the symmetric (/ antisymmetric) combination of the determinants, the major determinant contains a a$''$ MO that is symmetric with respect to the σ_2 plane (transforming as b$_1$, usually the C 2p$_z$ MO), while the combination of all electrons in the a$'$ MOs transforms as A$_1$ (/ B$_2$). And the minor determinant contains a a$''$ MO that is anti-symmetric with respect to the σ_2 plane (transforms as a$_2$), with an overall b$_2$ symmetry from the electrons in the a$'$ MOs.

To construct the simplest possible example it is instructive to assume that the a$'$

symmetry basis functions include only the $\mathrm{H^a}\,1\mathrm{s}$ (the 1s AO on $\mathrm{H^a}$) and $\mathrm{H^b}\,1\mathrm{s}$ AOs, and call them χ^{a} and χ^{b} - which means ignoring any C 2s or C $2\mathrm{p}_x$ basis functions on the central carbon atom. Their combinations will be called $\sqrt{\frac{1}{2}}[\chi^{\mathrm{a}} + \chi^{\mathrm{b}}] = \chi_{\mathrm{s}}$ and $\sqrt{\frac{1}{2}}[\chi^{\mathrm{a}} - \chi^{\mathrm{b}}] = \chi_y$. The b_1 basis function will be called χ_z, and the a_2 one χ_{yz}. A determinant localized along the $\mathrm{C}-\mathrm{H^a}$ bond (assuming an occupation of 1 electron on the H^a block and an otherwise unoccupied a′ block for simplicity) will be

$$\psi^{\mathrm{a}} = \hat{A}\left(\chi^{\mathrm{a}}(1)[\sqrt{1-r^2}\chi_z(2) + r\chi_{yz}(2)]\right) \ , \tag{A.8}$$

with $\hat{A}()$ being the anti-symmetrization operator and $r \ll 1$. Similarly, the symmetry-equivalent determinant localized along the $\mathrm{C}-\mathrm{H^b}$ bond is:

$$\psi^{\mathrm{b}} = \hat{A}\left(\chi^{\mathrm{b}}(1)[\sqrt{1-r^2}\chi_z(2) - r\chi_{yz}(2)]\right) \ . \tag{A.9}$$

The coefficient of $\sqrt{1-r^2}$ will be ignored in the following, as it does not contribute any insight and is close to unity. The symmetric (ψ_{s}) and antisymmetric (D_{a}) combinations of the two are

$$\psi_{\mathrm{sym}} = \sqrt{\frac{1}{2}}\psi^{\mathrm{a}} + \psi^{\mathrm{b}}] = \sqrt{\frac{1}{2}}\hat{A}\left(\chi^{\mathrm{a}}(1)[\chi_z(2) + r\chi_{yz}(2)] + \chi^{\mathrm{b}}(1)[\chi_z(2) - r\chi_{yz}(2)]\right) \tag{A.10a}$$

$$\psi_{\mathrm{ant}} = \sqrt{\frac{1}{2}}[\psi^{\mathrm{a}} + \psi^{\mathrm{b}}] = \sqrt{\frac{1}{2}}\hat{A}\left(\chi^{\mathrm{a}}(1)[\chi_z(2) + r\chi_{yz}(2)] - \chi^{\mathrm{b}}(1)[\chi_z(2) - r\chi_{yz}(2)]\right) \ , \tag{A.10b}$$

and re-arranging terms yields

$$\begin{aligned}\psi_{\text{sym}} &= \sqrt{\frac{1}{2}}\hat{A}\left([\chi^{\text{a}}(1)+\chi^{\text{b}}(1)]\chi_z(2)+r[\chi^{\text{a}}(1)-\chi^{\text{b}}(1)]\chi_{yz}(2)\right)\\ &= \hat{A}\left(\chi_{\text{s}}(1)\chi_z(2)+r\chi_y(1)\chi_{yz}(2)\right)\end{aligned} \tag{A.11a}$$

$$\begin{aligned}\psi_{\text{ant}} &= \sqrt{\frac{1}{2}}\hat{A}\left([\chi^{\text{a}}(1)-\chi^{\text{b}}(1)]\chi_z(2)+r[\chi^{\text{a}}(1)+\chi^{\text{b}}(1)]\chi_{yz}(2)\right)\\ &= \hat{A}\left(\chi_y(1)\chi_z(2)+r\chi_{\text{s}}(1)\chi_{yz}(2)\right)\ .\end{aligned} \tag{A.11b}$$

Equation A.11 shows that this specific type of orbital relaxation in the VB picture changes its appearance to dynamic correlation in the MO picture (with the associated concern that avoiding double counting of dynamic correlation in MSDFT is currently an open question). Cases where the A$''$ MOs are doubly occupied instead of singly occupied will result in a similarly mixed determinant; Here the addition of the (3-electron) determinants (where χ' and r' may or may not be the same orbital and coefficient as χ and r) yields in a similar manner:

$$\begin{aligned}\psi_{\text{sym}} = \sqrt{\frac{1}{2}}\hat{A}\Big(&\chi_{\text{a}}(1)[\chi_z(2)+r\chi_{yz}(2)][\chi'_z(3)+r'\chi'_{yz}(3)]\\ &+\chi_{\text{b}}(1)[\chi_z(2)-r\chi_{yz}(2)][\chi'_z(3)-r'\chi'_{yz}(3)]\Big)\end{aligned}\ , \tag{A.12}$$

which simplifies to:

$$\begin{aligned}= \hat{A}\Big(&\chi_{\text{s}}(1)[\chi_z(2)\chi'_z(3)+rr'\chi_{yz}(2)\chi'_{yz}(3)]\\ &+\chi_y(1)[r\chi_{yz}(2)\chi'_z(3)+r'\chi_z(2)\chi'_{yz}(3)]\Big)\end{aligned}\ , \tag{A.13}$$

Note that (assuming that χ and χ' are the same orbital, which implies that all of their constituing components are identical: $r = r', \chi_z = \chi'_z, \chi_{yz} = \chi'_{yz}$), the action of the anti-symmetrization operator will cancel the content of the square brackets with the $\chi_y(1)$ prefactor, and zero out that whole last line of the expression. Simply forcing any

a_2 *basis functions* to be unoccupied would not fully eliminate the problem of dynamic correlation, since some of the basis functions (H $2p_z$ AOs on the H^a and H^b hydrogen atoms) transform as neither the a_2 representation (thus they are required for relaxation in b_1 states and can not be forced to be unoccupied) nor as the b_1 representation (thus they can still lead to a *slight* relaxation away from pure b_1 MOs when included). Since it is unknown how much dynamical correlation would be double counted and how much of it is not already included in the xc functional, we made the choice to allow "proper" relaxation of these determinants in the VB picture, instead of using an ad-hoc half-measure restriction. And furthermore, not applying this restriction to determinants with non-symmetric block definitions has been the chosen strategy since the beginnings of the method, before we considered the potential benefits of applying it. And finally, even though this should not make any difference, it might be worth mentioning that some determinants which could utilize this a_2 block solely for convergence acceleration were originally defined without it in mind. And because the only benefits of splitting off this block could be faster calculations or negligibly better accuracy, these determinants have not been re-defined but are used as-is.

A.4.2.4 Excited States

Excited states are straightforward extensions of the above described states (either the delocalized states or the states with electron localized with respect to one of the $C-H$ bonds). Excitations are defined by moving an electron (a single one in all included determinants) from one specific AO (or block) to a "slice", a sub-shell or a similar group of AOs on a specific atom. Although the explicit excitations in the diabatic states are limited to only single excitations, the adiabatic states can form multiply excited states due to the splitting of bond orbitals into two separate blocks.

A.5 Calculation Results

MSDFT calculations were performed for the doublet and quartet states with a magnetic spin quantum number of $M_S = +1/2$. For comparison, we also carried out multi-reference configuration-interaction (MRCI) studies on these states.

A.5.1 MRCI

A.5.1.1 Calculations

[323] and [324] only reported potential energy curves (and excitation energies) that are relevant to the CH_3 photo-dissociation process (exclusively of $^2B_1$ and $^2A_1$ representations). However, the MSDFT results have doublet and quartet states ($S \in \{1/2, 3/2\}, M_S = +1/2$) - and both of all symmetry representations - intermixed. In order to obtain references for all MSDFT states, it was necessary to perform high-accuracy WFT calculations for all low-lying states. The results from [324] can be used to verify the $^2B_1$ and $^2A_1$ results of my MRCI calculations. As mentioned above, the aug-cc-pVTZ basis was used because MRCI calculations with smaller and larger basis sets (but otherwise similar to the one reported here) indicated that it provides adequate accuracy. As described in more detail further below, the geometry was optimized in CASPT2, and then the energies were obtained using MRCI. In both CASPT2 and MRCI the CASSCF active space consists of all excitations in the following orbital selections (inclusive):

- 3rd to 7th a_1 MO ($\mathrm{s}, \mathrm{p}_x, \mathrm{d}_{??}, \mathrm{f}_{??x}$ type orbitals) [1]
- 1st to 2nd b_1 MO ($\mathrm{p}_z, \mathrm{d}_{xz}, \mathrm{f}_{??z}$ type orbitals)
- 1st to 2nd b_2 MO ($\mathrm{p}_y, \mathrm{d}_{xy}, \mathrm{f}_{??y}$ type orbitals)

[1] The notation "??" stands for two repetitions of the same cardinal direction, i.e., "xx", "yy" and "zz".

Figure A.2: Active space MOs in MRCI at a $C-H$ distance of 1.70 Å, plotted at the specified iso-value.

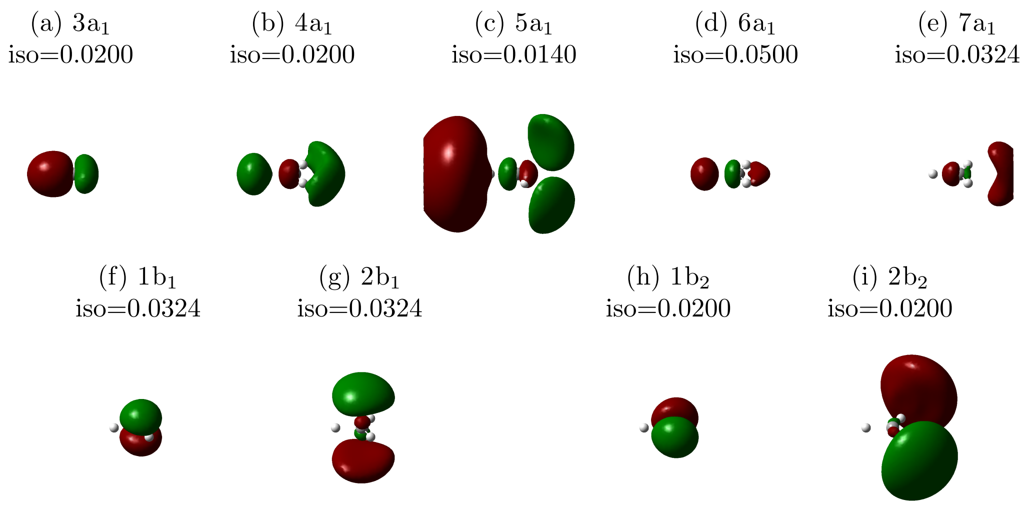

(for a total of 5 electrons and 13 holes in 9 orbitals). The active space MOs are plotted in Fig. A.2 for an (intermediate) $C-H$ separation of 1.70 Å. This is a smaller active space than the (5,15) CASSCF active space used in Ref. [323] and slightly smaller than the (5,10) CASSCF active space used in Ref. [324](or the (5,11) CASSCF active space used in Ref. [320]). But as will be shown in Section A.5.1.2, the MRCI results from the smaller active space are sufficiently similar, suggesting that this choice of active space is adequate.

The MRCI energies were obtained at ground state geometries along the $C-H$ dissociation pathway, which were obtained as follows. For each $C-H$ distance, the remaining 2 geometrical parameters in C_{2v} symmetry were optimized ($C-H_i$ distance and H_x-C-H_i angle where $i \in \{1,2\}$). This was done using CASPT2 only on the ground state (no state averaging). None of the orbitals are frozen during the CASSCF step, but the 1st a_1 MO was excluded from being correlated in the perturbation theory step of the first phase.

In the second phase, MRCI was used to solve for the wave functions for 17 of the lowest states. During the CASSCF step of this phase, the lowest a_1 MO is kept frozen (not optimized). Furthermore, the wave functions of all representations are obtained from the same CASSCF calculation, in order to ensure that the same MOs are included in the MRCI step. CASSCF yields 6 wave functions for each combination of representation and spin (although 1 to 5 of the 6 with the highest energy have a state-averaging weight of zero). The relative weights of the states in CASSCF for optimizing the common MOs are summarized below:

C_{2v} rep'	D_{3h} rep'	weights					MRCI states
$^2B_1$	$^2A_2''$& $^2E''$	60	55	35	15	(1)	4
$^4B_1$	$^4A_2''$& $^4E''$	40	15	(1)			2
$^2A_2$	$^2E''$(& $^2A_1''$)	1					1
$^4A_2$	$^4E''$(& $^2A_1''$)	40	1				2
$^2A_1$	$^2A_1'$& $^2E'$	60	55	45	35	(15)	4
$^4A_1$	$^4A_1'$& $^4E'$	1					1
$^2B_2$	$^2E'$(& $^2A_2'$)	40	25	(10)			2
$^4B_2$	$^4E'$(& $^2A_2'$)	1					1

Empty cells denote a weight of zero in CASSCF. Empty cells and values in parentheses are not included in the states that the subsequent MRCI step solves for. State for values in parentheses are nonetheless given a nonzero weight in the MO optimization CASSCF, because they are anti-crossing or could be anti-crossing with states of interest (which would cause the importance of MOs to change rapidly across those regions). For the same reason, the weight of states was chosen to gradually decrease depending on what they are being used for. States that can be both directly compared to MSDFT results (and to the Poullain et al./ balerdi et al. references) have weights around 60, while states that are only indirectly compared to MSDFT states have weights around 20. (Almost all) states with a weight of 1 are omitted from all plots, as their energy stays at least 11 eV above the equilibrium ground state.

Once the CASSCF MOs are obtained, the MRCI sub-steps themselves can be run separately for each representation and spin multiplicity (because the MOs are fixed at this point). Using all 6 of the CASSCF states as references for the CI excitations, each MRCI sub-step solves for 1-4 adiabatic states in the energy region of interest. The number of MRCI states being solved for is given in the last column of the above table.

A.5.1.2 MRCI Results

Figure A.3 shows the 14 most relevant states that were obtained in the MRCI calculation. The A$''$ states (anti-symmetric with respect to mirroring about the xy plane) are shown with red squares and the A$'$ states with blue diamonds. The ^{2}B$_1$ and ^{2}A$_1$ states are shown solid grey symbol fill and red or blue symbol outline and line. All quartet states are shown with black symbol outline and colored, hatched symbol fill. All states of B$_2$ and A$_2$ symmetry (anti-symmetric with respect to mirroring about the xz plane) are shown with thick symbol outlines and hatched symbol fill. Except for the fact that Fig. A.3 shows adiabatic states, the present MRCI results agree to within 0.5 eV with all potential energy curves obtained by Balerdi et.al. using the MRCI method[324] (See Fig. A.4). Two noteworthy observations on the states above the energy range accessible during the dissociation:

- The 4th ^{2}A$_1$ state (excitation to 3d$_{x^2-y^2}$) is "wavy" in the vicinity of 1.07 Å. This is an artifact of the CASSCF method and it only happens for certain combinations of included states and their weights. This specific combination of states and their weights was chosen nonetheless, as the state being supposed to be degenerate with the 3d$_{xy}$ state for symmetric geometries makes it clear what the correct shape of the PEC would be; and the "wrong" shape shows a curious parallel to one of the states in MSDFT.
- The 3rd and 4th ^{2}B$_1$ states have an avoided crossing at 1.7 Å (and 11.5 eV). The

Figure A.3: Potential energy curves in MRCI, classified by their C_{2v} representations (and spin).

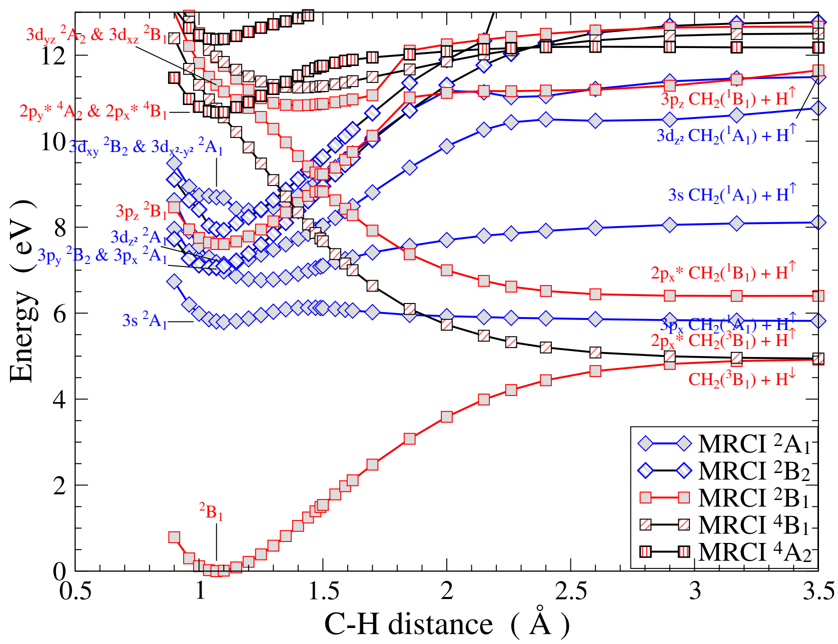

Figure A.4: MRCI potential energy curves, classified by their C_{2v} representations (at the CH_2 geometry) and (transverse) C_s representation (at the CH_3 geometry). From [324].

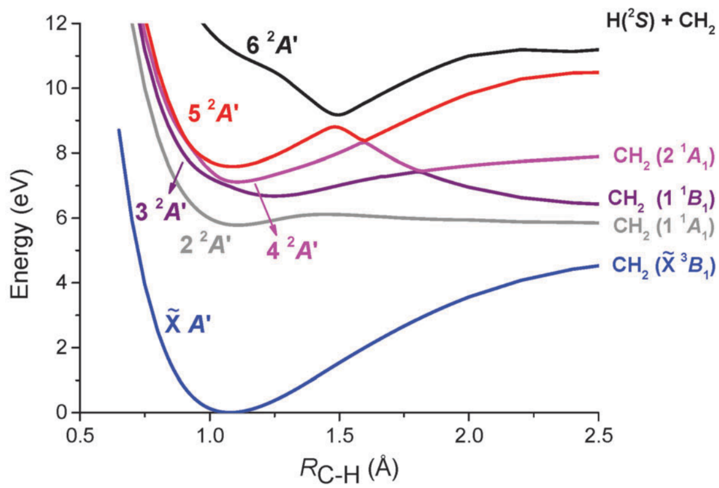

$C-H$ distance at which this feature appears (and to a lesser extent its shape) is also highly dependent on the weights. Its shape is either an artifact of the MRCI method caused by rapidly changing weights in this region, or alludes to the 4th $^2B_1$ state having an avoided crossing with the 5th $^2B_1$ in that region. Which one it is is irrelevant for the purposes of comparison, since none of the other calculations produces a state that the 4th or even 5th $^2B_1$ MRCI PEC could be compared to. (Something that 3 different A' states in this very crowded part of the PEC plot do as well.)

Key energies of CH_3 and CH_2 in MRCI are listed in Section A.5.5 where they are compared to MSDFT energies.

A.5.2 General Remarks on MSDFT Calculations

Although the terms "constrained" and "localized" can in general have interchangeable meanings, their use is deliberately differentiated between two different uses in this chapter. The term "localized" is used whenever electrons are being forced into orbitals centered on one fragment of the molecule (a single atom or a group of atoms) - and thereby excluded from the inverse set of atoms; especially in situations where they would otherwise occupy those other atoms to a significant degree. The main application where this is relevant is in generating valence bond configurations. In contrast, the term "constrained" is used for cases where electrons are placed into orbitals, sub-shells or "slices" with specific rotational symmetries.

A.5.2.1 Representation Split-up

As described in Section A.4.2.3 above, by utilizing the block partition for orbital occupation it is possible to define determinants which have a specific character with respect to mirroring about the molecular plane. Since the determinants of the A′ and A″ representations (in the C_s group) do not interact, they can be separated into two independent MSDFT calculations. The A′ calculation solves for only A′ adiabatic states using only A′ determinants, which include the A_1 representation determinants in the $C_{2\mathrm{v}}$ symmetry group (A_1' and E′ in $D_{3\mathrm{h}}$) and B_2 in the $C_{2\mathrm{v}}$ group (A_2' and E′ in $D_{3\mathrm{h}}$). The A″ representation includes the B_1 representations in the $C_{2\mathrm{v}}$ group (A_2'' and E″ in $D_{3\mathrm{h}}$) and A_2 in $C_{2\mathrm{v}}$ (A_1'' and E″ in $D_{3\mathrm{h}}$).

A.5.2.2 Spin Split-up

Similarly, MSDFT's current block definition scheme naturally produces single-determinant states with a well-defined difference between the number of up and down electrons, making them eigen-functions of the z-component of the spin operator $\hat{S}_z$. Determinants with one such magnetic spin quantum number M_S do not interact with states that have any other M_S value.

In contrast to the magnetic spin operator $\hat{S}_z$, only some determinants are eigen-functions of the absolute spin operator $\hat{S}^2$. With 3 unpaired electrons as in this system, the high-spin quartet states ($S = 3/2, M_S = \pm 3/2$) consist of a single determinant and can be separated into an independent calculation. On the other hand, doublet states ($S = 1/2, M_S = \pm 1/2$) and low-spin quartet multiplet states ($S = 3/2$, $M_S = \pm 1/2$) are of multi-determinant character. CSFs, which should be described by these configurations, can not be used as basis functions for the multi-determinant phase in MSDFT. Conversely, the single-determinant states with $M_S = \pm 1/2$ that can be used are not eigen-functions of the absolute spin operator. Thus, both doublet and low-spin quartet multiplet states will be the result of joint calculations, even though it should in theory be possible to utilize the fact that there is no interaction between them.

A.5.2.3 (Broken) Spin Multiplet Equivalence

States with negative M_S values would yield the same results as their positive counterparts due to the absence of (external) magnetic fields. Low-spin and high-spin projections of the same quartet state should theoretically yield the same energy, but the block definition scheme that was used in this chapter does not allow to define the $M_S = \pm 1/2$ and $M_S = \pm 3/2$ states in this system in an identical way. Furthermore, most Kohn-Sham exchange-correlation functionals are not specifically created to yield identical energies for high-spin and low-spin determinants. The subject of the MSDFT calculations in this chapter are states with magnetic spin quantum number $M_S = +1/2$ (doublet and quartet states with absolute spin quantum number $S = +1/2$ or $S = +3/2$).

Our group has devised a scheme for defining the TDF (interaction energy) in a singlet-triplet system between the two $M_S = 0$ determinants by enforcing the degeneracy between the low-spin ($S = 1$, $M_S = 0$) CSF and the high-spin ($S = 1$, $M_S = \pm 1$) determinant of a triplet - which then also determines the energy of the remaining $S = 1/2, M_S = \pm 1/2$ singlet energy.[8] The same scheme could also be adapted to utilize the degeneracy of high-spin ($M_S = \pm 3/2$) and low-spin ($S = 3/2$, $M_S = \pm 1/2$) triplet states to define the interaction between that low-spin quartet state and the respective (two) doublet states ($S = 1/2$, $M_S = \pm 1/2$). But that scheme is not used in this chapter for two reasons. Firstly, creating the respective low-spin counterpart determinants to a high-spin determinant is not always possible without use of block-excitations (including in this system). This made it seem valuable to determine if accurate results could be obtained with a more generally applicable TDF. And secondly, the energetic quality of the high-spin states is significantly worse than that of the low-spin doublet and quartet determinants. Since we suspect that this is due to some mistakes on our part or numerical problems (which we could not identify), we will refrain from showing the high-spin results at this time.Thus using those energies as references for the low-spin quartet states would definitely lead to worse results for the low-spin quartet energy, and probably also for the doublet energies.

A.5.2.4 Block Considerations

There are 3 effects that the block definition may be required to provide when defining a determinant. Since it is possible in this system, the highest priority task is to keep each block limited to basis functions of one symmetry representation (either a$'$ or a$''$). If AOs from the a$'$ and a$''$ representations are never grouped into common blocks, then any formed MOs and thus the determinant as a whole will also respect the symmetry of the system and transform as one of the representations of the C_s group. Since the DFT determinants of different representations do not interact, they can be treated in separate diagonalizations of the independent parts of the multi-electron Hamiltonian.

The other two things the block definition is responsible for are to localize and constrain electrons. All determinants that were used can be understood in terms of starting from the the DFT determinant and applying none, one or both of these modifications. Which of these 2 measures have to be employed depends on the type of determinant. Obtaining the determinant with neither localization nor excitation applied the is equivalent to using classical Kohn-Sham DFT.

To facilitate the breaking of the $\mathrm{C} - \mathrm{H}^x$ bond (the bond to the leaving hydrogen, reminder: aligned along the +x direction) in the ground state, at least that one sigma (VB) orbital has to be modeled by VB configurations that include covalent and ionic states. Or, according to the terms defined in Section A.5.2 above, the electrons in that orbital have to be localized. Most determinants in the active space include such a localization, where the AOs forming this orbital have to be separated into two different blocks on the respective H atom and the remaining CH_2 fragment. The electrons that should occupy that orbital are localized to either of the two blocks, with a different determinant covering each of the possible ways to assign those electrons to two blocks and all possible ways to assign spin orientations to these electrons and any other unpaired electrons (usually the $2p_z$ electron). Obviously the orbital treated in this way will always be an orbital in the a' representation as all sigma orbitals transform as this symmetry representation.

The VB basis states already include some excited basis configurations. The remaining types of excitation are covered by localizing individual electrons into specific AOs, and are generated as follows. Starting from one of the localized (VB picture) determinants or a fully delocalized determinant, an electron is removed from one of the occupied blocks and placed into a specific unoccupied AO (or a "slice" of AOs with the same spherical harmonic) on a specific atom. In the determinants used in the shown MSDFT calculations the atom is always the central carbon. Either that electron is placed into the only pre-existing singly occupied block (the one that produces the $2p_z$ MO), or the respective AOs that should contain it are grouped into an additional block.

In some cases, some of these different determinants corresponding to certain ways to assign the electrons and spins to the blocks will be omitted, specifically for minimal active space calculations. For example, if a state is modeled for which the active space includes a delocalized determinant, then not all localized determinants might be needed for that state. Especially if the resulting state is very similar to the delocalized determinant and only needs to have the contribution from the covalent or ionic determinants increased or decreased slightly with respect to a delocalized composition. This is used throughout the minimal active space calculation of the A_1 symmetry representation.

A.5.2.5 Spins, Determinants and CSFs

In several of the $M_S = 1/2$ determinants, the total spin is contributed by 3 unpaired electron spins (2 up spins and 1 down spin). All such A'' determinants that were employed feature are a single $2p_z$ (or $3p_z$) electron plus 2 electrons in the 2 VB fragment orbitals for the H_2C group and a hydrogen atom (one hydrogen 1s orbital and one orbital on the remaining CH fragment). Determinants with different combinations of spins in the same set of orbitals in reality interact via Hamiltonian exchange terms. Including only part of such a set of determinants with mutual interactions will lead to errors in the states' energy on the order of that interaction strength. Since magnetic fields and spin-orbit coupling are not included in the calculation, the Hamiltonian, the absolute spin operator and the projection of the spin operator in one direction commute, which means they have a common spectrum of eigen-functions. Or in other words, every eigenfunction of the Hamiltonian (unless degenerate) has to also be an eigenfunction of the absolute spin operator ($\hat{S^2}$) and the magnetic spin operator ($\hat{S_z}$). The consequence for MSDFT is that the determinants have to be chosen in such a way as to make sure that they can form CSFs (configuration state functions) that are eigen-functions of both the absolute spin operator and one selected component of the spin operator. In the case of 2 up and 1 down electron spin distributed among 3 orbitals there are 3 possible spin combinations, similar to the case in [176]. When all 3 determinants corresponding to these combinations interfere constructively, they form a single low-spin quartet state. Two different doublet states can be formed by linearly combining 3 (or in special cases 2) of these determinants such that the combination is orthogonal to the quartet state. In practice, there are two states of interest in this chapter which *could* be constructed from only 2 of these 3 determinants. In the example of the ground state, at sufficiently large CH_2-H separations one of the 3 states will have a vanishing contribution from the determinant with the down spin on the leaving H atom; And close to the equilibrium geometry one of the doublet states has a negligible contribution from the determinant with the down spin on the "C $2p_z$" MO (as evident from the fact that DFT can treat that state with a single determinant). Since these can not be guaranteed to be energy eigen-states in that 3-dimensional Hilbert space (especially since the energy eigen-states change along the reaction pathway), all 3 determinants of any such set will have to be included in the active space. The determinant in which the $2p_z$ electron's spin is aligned in the down direction can not be excluded.

A.5.2.6 Active Spaces Used in the Featured MSDFT Calculations

Of the many MSDFT calculations that were required to arrive at a suitable set of determinants for a minimal active space, the majority of the early attempts are not particularly interesting. Only calculations with two final types of active spaces are shown here: A minimal active space ("MAS" for "minimal active space") and a slightly larger active space ("MED" for "medium-sized"). The latter was generated by including complete "groups" of determinants, which firstly includes all 3 determinants whenever there is a triple of equivalent determinants split along the 3 bond directions. But it also includes determinants with all spin orientations that may be required to create configuration state functions that are eigen-functions of the absolute spin operator $\hat{S}^2$; as well as treating the C $3p_x$ and C $3p_y$ AOs equivalently. These groups of determinants can contain up to 9 determinants each and there is in total a handful of them (see A.5.3.1 "MED calculation" below). As a result, affording identical treatment to 3 $C-H$ bonds and all spin orientations (and the in-plane C 3p orbitals) in this very *systematic* active space construction comes at the cost of a rather large size (62 determinants total) of the "MED" active spaces for both a' and a'' representations.

The minimal active space ("MAS") was generated from the more systematic "MED" active space by removing any determinant that did not contribute to the accuracy of the lowest-energy potential energy curves. This active space construction strategy minimizes its size (to 30 determinants total) at the cost of making the active space construction less systematic and intuitive - and also at the cost of loosing some accuracy, especially in higher energy excited states, as will be shown in Sections A.5.3.2 and A.5.4.2.

A.5.3 MSDFT, Medium Sized Active Space (MED)

A.5.3.1 MED Calculation

This systematically constructed, medium-sized ("MED") active space was one of the first successful replications of the MRCI reference. The largest of the numerous problems in these attempts was (as mentioned in Section A.4.1.2 above) that the default basis function definition was not suited for defining excitations into specific AOs, atomic sub-shells, or "slices".

Table A.1 lists the diabatic states (DFT determinants and DFT configuration state functions) that are part of the "MED" active space. The two separate calculations handling states of the two non-interacting C_s symmetry representations are arranged vertically, while the two symmetry representations for blocks (and thus orbitals) are arranged left to right. An empty cell always denotes the case where the type of AO corresponding to that column is not separated out into its own block in the determinant that is described by that row.

The last column for each block symmetry denotes the block for constraining electrons to "slices" of AOs with specific angular wave function components. Since the a$'$ representation offers several possible sub-shells or "slices" that electrons could possibly be constrained to, this last column on the "a$'$ blocks" side denotes which of these is used (if at all). In the a$''$ representation it would make sense to excite or constrain electrons to a single "slice", namely the C $3 + \mathrm{p}_z$ one (which includes the C $3\mathrm{p}_z$ AO itself, plus C $4\mathrm{p}_z$ and higher AOs). For this representation, its occupation completely describes the block (and the absence of a separate block for this AO is denoted by an empty cell in this column). The first column is related to a possible numerical optimization involving basis functions of the a_2 symmetry representation (C d_{yz}, C f_{xyz}. The first factor that enables this is that there are no occupied a_2 or a_2-like MOs (in any of the determinants that are needed to describe the lowest lying states). The second factor is that determinants usually have to be eigenfunctions of the mirroring operator about the xz plane, unless they treat the symmetry-related Hydrogen atoms (#1 and #2) differently, in which case those determinants can break this symmetry slightly. In the symmetry broken case, the a_2 basis functions can make minor contributions to b_2-like MOs. But in determinants where this symmetry is unbroken, no basis functions of a_2 nature can contribute to any occupied MOs, neither to the relaxation of b_1 MOs nor do any occupied a_2 MOs exist. These AOs that are known to not contribute to any occupied orbitals can be separated out from (or included in) the a'' block without affecting the results (except for guaranteeing a lower numerical error in the a'' MO shapes, as the block then contains almost exclusively b_1 basis functions). The first column states whether this block was actually used for the determinant in question. Localization along one of the bonds is given by the "localized H" column, denoting along which of the bonds the blocks are split and the occupation of the respective hydrogen atom that is singled out by the block split. The blocks described by the remaining two columns ("$2p_z$MO" and "CH_2/CH_3") contain all remaining basis functions of the respective symmetry representation in C_s. Each cell contains the total electronic occupation and number of excess up electrons for the respective block in the respective DFT determinant. Empty cells denote that all respective basis functions are included in the block they usually belong to (as opposed to cells with the content "0 0", which denotes that the AOs are split out into their own block, in order to enforce an occupation of zero electrons on those AOs.)

The first section of the table contains determinants that are localized along the bond to one of the 3 hydrogen atoms. All 15 possible combinations of bond direction, occupations and spins are used in this calculation. (The 5 of these that localize along the x axis could have used the a_2 block.) The second section is the (for all intents and purposes) fully unconstrained B_1 determinant (using only the system's symmetry to inform its block definition). The third section (last B_1 section) contains determinants that constrain an electron to the $\mathrm{C}\,3+\mathrm{p}_z$ AO along with localization along any of the 3 bonds. Determinants with all 15 combinations are again used in this calculation.

The first four A_1 sections list determinants where an a' electron is excited to the $\mathrm{C}\,2\mathrm{p}_z$ MO or vice versa. The sections with the variants that are also localized along one of the bond contain all 6 possible combinations of occupation and spin for that occupation of the $\mathrm{C}\,2\mathrm{p}_z$ MO, and the sections without localization naturally contain only a single determinant each. (Again, the 4 of these that localize along the x axis could have used the a_2 block.) The last two sections cover the cases where an electron is excited to the 3rd shell a_1 AOs of carbon. For the excitation to $\mathrm{C}\,3+\mathrm{s}$ the calculation uses determinants with localization of the remaining electrons along one of the 3 bonds. All 15 such bond direction, occupation and spin combinations that are possible are used. For the $\mathrm{C}\,3+\mathrm{p}_x$ and $\mathrm{C}\,3+\mathrm{p}_y$ excitations only the respective single delocalized determinant is used.

Table A.1: All determinants in the MSDFT calculation with medium sized active space ("MED")

$M_S = +1/2$ A″ determinants, MED

a″ blocks			a′ blocks					n_{Dets}
a_2 block used? [b]	$2p_z$MO occ	$3p_z$AO [a] occ	localized H [a] id [c]	occ	CH_2/CH_3 occ [d]	C 3* AO [a] type	occ	
A″ determinants with only localization								
	1 +1		x	0 0	8 0			
	1 +1		1	0 0	8 0			
	1 +1		2	0 0	8 0			
	1 +1		x	2 0	6 0			
	1 +1		1	2 0	6 0			
	1 +1		2	2 0	6 0			
	1 +1		x	1 -1	7 +1			
	1 +1		1	1 -1	7 +1			15
	1 +1		2	1 -1	7 +1			
	1 +1		x	1 +1	7 -1			
	1 +1		1	1 +1	7 -1			
	1 +1		2	1 +1	7 -1			
	1 -1		x	1 +1	7 +1			
	1 -1		1	1 +1	7 +1			
	1 -1		2	1 +1	7 +1			
delocalized, unconstrained Kohn-Sham A″ determinant								
yes	1 +1				8 0			1

Table A.1: $M_S = +1/2$ A″ determinants, MED (continued)

a_2 [b]	$2p_z$ MO	$3p_z$ AO [a]	localized H [a]	CH_2/CH_3	C 3* AO [a]	n_{Dets}
A″ determinants with localization and C $2p_z \rightarrow$ C $3p_z$ excitation						
yes	0 0	1 +1	x 0 0	8 0		15
	0 0	1 +1	1 0 0	8 0		
	0 0	1 +1	2 0 0	8 0		
yes	0 0	1 +1	x 2 0	6 0		
	0 0	1 +1	1 2 0	6 0		
	0 0	1 +1	2 2 0	6 0		
yes	0 0	1 +1	x 1 -1	7 +1		
	0 0	1 +1	1 1 -1	7 +1		
	0 0	1 +1	2 1 -1	7 +1		
yes	0 0	1 +1	x 1 +1	7 -1		
	0 0	1 +1	1 1 +1	7 -1		
	0 0	1 +1	2 1 +1	7 -1		
yes	0 0	1 -1	x 1 +1	7 +1		
	0 0	1 -1	1 1 +1	7 +1		
	0 0	1 -1	2 1 +1	7 +1		
delocalized A″ determinant with only C $2p_z \rightarrow$ C $3p_z$ excitation						0 of 1

$M_S = +1/2$ A′ determinants, MED

a_2 [b]	$2p_z$ MO	$3p_z$ AO [a]	localized H [a]	CH_2/CH_3	C 3* AO [a]	n_{Dets}
A′ determinants with localization and C $2p_z$ constrained to 0 electrons occupation						
	0 0		x 2 0	7 +1		6
	0 0		1 2 0	7 +1		
	0 0		2 2 0	7 +1		
	0 0		x 1 +1	8 0		
	0 0		1 1 +1	8 0		
	0 0		2 1 +1	8 0		
delocalized A′ determinant with only C $2p_z$ constrained to 0 electrons occupation						
yes	0 0			9 +1		1

Table A.1: $M_S = +1/2$ A′ determinants, MED (continued)

a_2 [b]	$2p_z$ MO	$3p_z$ AO [a]	localized H [a]	CH_2/CH_3	C 3* AO [a]	n_{Dets}
A′ determinants with localization and C $2p_z$ constrained to 2 electrons occupation						
	2 0		x 0 0	7 +1		6
	2 0		1 0 0	7 +1		
	2 0		2 0 0	7 +1		
	2 0		x 1 +1	6 0		
	2 0		1 1 +1	6 0		
	2 0		2 1 +1	6 0		
delocalized A′ determinant with only C $2p_z$ constrained to 2 electrons occupation						
yes	2 0			7 +1		1
A′ determinants with localization and C $2p_z \rightarrow$ C 3s excitation						
yes	0 0		x 0 0	8 0	3s 1 +1	15
	0 0		1 0 0	8 0	3s 1 +1	
	0 0		2 0 0	8 0	3s 1 +1	
yes	0 0		x 2 0	6 0	3s 1 +1	
	0 0		1 2 0	6 0	3s 1 +1	
	0 0		2 2 0	6 0	3s 1 +1	
yes	0 0		x 1 -1	7 +1	3s 1 +1	
	0 0		1 1 -1	7 +1	3s 1 +1	
	0 0		2 1 -1	7 +1	3s 1 +1	
yes	0 0		x 1 +1	7 -1	3s 1 +1	
	0 0		1 1 +1	7 -1	3s 1 +1	
	0 0		2 1 +1	7 -1	3s 1 +1	
yes	0 0		x 1 +1	7 +1	3s 1 -1	
	0 0		1 1 +1	7 +1	3s 1 -1	
	0 0		2 1 +1	7 +1	3s 1 -1	
delocalized A′ determinant with C $2p_z \rightarrow$ C 3s excitation						0 of 1

Table A.1: $M_S = +1/2$ A′ determinants, MED (continued)

a_2 [b]	$2p_z$ MO	$3p_z$ AO [a]	localized H [a]	CH_2/CH_3	C 3* AO [a]	n_{Dets}
delocalized A′ determinants with C $2p_z \to$ C $3p_{x/y}$ excitation						
yes	0 0			8 0	$3p_x$ 1 +1	1
yes	0 0			8 0	$3p_y$ 1 +1	1

The "occ" columns describe the occupation (and spin excess) of the respective blocks; The "type" column specifies the type of sub-shell(s) that the respective electron is being excited into; The "id" column defines the singled out hydrogen; The "n_{Dets}" column lists the number of determinants used in a specific group of rows. The cells in the "occ" columns contain 2 values: The first is $N_{\text{e}} = N_{e\uparrow} + N_{e\downarrow}$, the nr. of electrons that occupy the block; and the second value (and it's sign) is $N_{e\uparrow} - N_{e\downarrow} = 2 * M_S$, the (signed) difference between up and down spins occupying the block, or equivalently the projection of the spin (counted in multiples of half atomic units, i.e., multiples of fermionic spin units).

[a] This block, when present, includes all AOs of that type regardless of shell. (For example, the $3p_x$ block additionally contains $4p_x$, $5p_x$ and 'aug' p_x; and localized blocks for singular hydrogen atoms contain in addition to the H 1s basis function all other a′ functions on that H.) An empty cell means that the respective basis functions are included in the main block of the same symmetry representation.

[b] See Section A.4.2.3. An empty cell again means that the respective basis functions are included in the main block of the a″ symmetry representation.

[c] An id of "x" denotes that the leaving hydrogen makes up the localized block, "1" and "2" are the two symmetry-equivalent hyrogen atoms.

[d] This occupation includes 2 electrons in the core C 1s MO, and 2 electrons each in the VB MOs along the 2 bonds that are not split.

Figure A.5: Potential energy curves in MSDFT with medium-sized active space, classified by C_s representations, compared to MRCI.

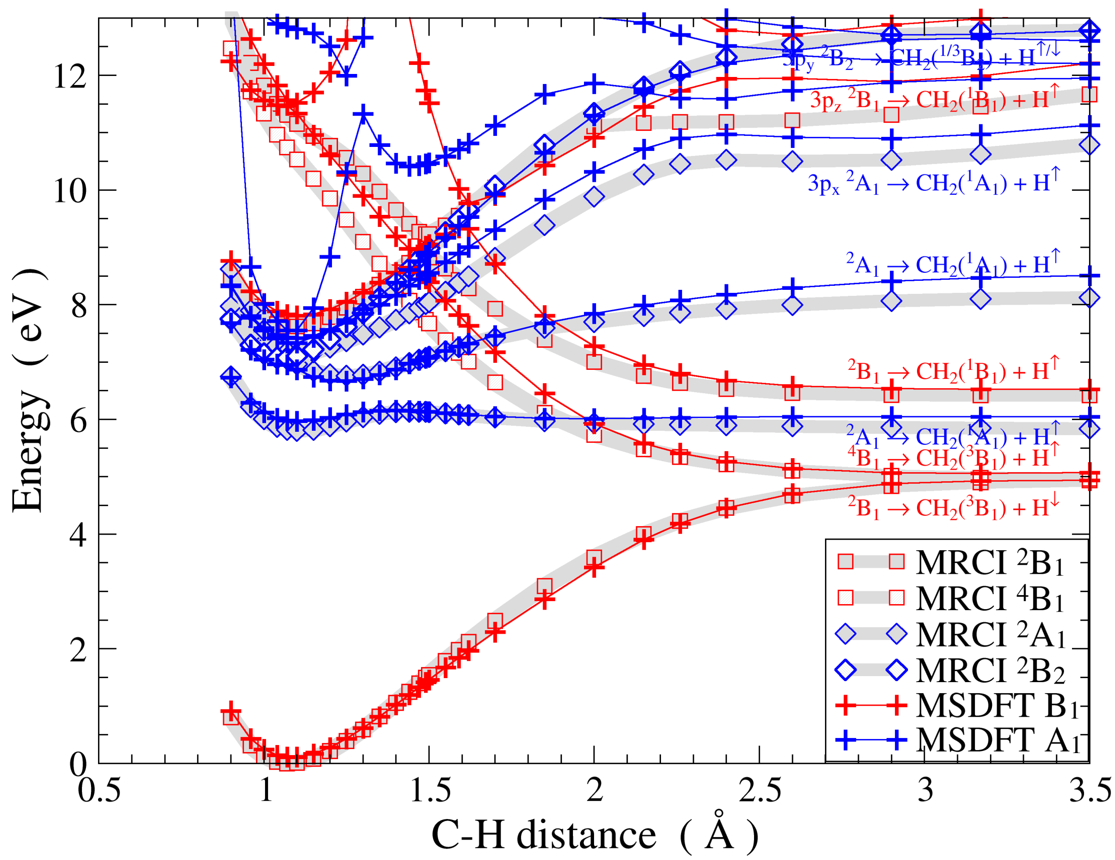

A.5.3.2 MED Results

Figure A.5 shows the MSDFT potential energy curves (thin colored lines) compared to the MRCI reference (thick grey lines). The (arbitrary) zero point of the energy scale is set to the MRCI ground state at the CH_3 equilibrium geometry, in order to keep the scale consistent with the previous figures. But the energies in either method are actually measured relative to the CH_2 doublet ground state in the respective method. This is the most accessible and energy-stable point on the potential energy curves to align the MRCI and MSDFT energy scales; and it keeps MSDFT from yielding energies that are noticeably below MRCI energies. The A$''$ states are shown in red and the A$'$ states in blue. For the results from MRCI (which distinguishes between doublet and quartet states and all 4 symmetry representations of $C_{2\mathrm{v}}$), all states of A_2 and B_2 representation are shown with a hatched line, thicker symbol outline and hatched symbol fill while all quartet states are shown with a hatched line, black symbol outline and colored (hatched) symbol fill. All MSDFT potential energy curves that fall within the energy range of the plot are shown. Of the 17 states that the MRCI calculation has yielded, only the 8 relevant ones are shown, in order to avoid clutter in the high-energy part of the graph. For the omitted MRCI potential energy curves, see Fig. A.3.

Generally, the lowest part of the ground state potential energy curve agrees to within 0.2 eV and the discrepancy generally increases with increasing energy. Most parts of potential energy curves with energies more than 0.75 eV above the ground state (and below the cutoff of the graph area at 13 eV) agree with MRCI to within 0.5 eV, with a few exceptions:

1. MSDFT's lowest $^4B_1$ state starts out very similar in energy to the MRCI reference at large separations, but as the energy rises towards closer separations their energetic discrepancy also gets larger, reaching about 0.9 eV in the left half of the graph.

2. Similarly, the anti-bonding $^2B_1$ state agrees with the MRCI reference to within 0.15 eV at large separations, but as the energy increases towards smaller separations, the error increases sharply (exceeding 1.0 eV at around 1.6 Å).

3. The $3p_z$ $^2B_1$ state is supposed to have an avoided crossing at 2.0 Å with a 4th state that is omitted from the plotted MRCI PEC's, but in MSDFT the next closest states at that separation are found at 14.0 eV and 14.2 eV, over 4 eV above the $3p_z$ $^2B_1$ state's energy. This leads to the energy of this state at separations above 2 Å to rise to 0.75 eV above the MRCI reference.

4. The $3p_x$ $^2A_1$ state is 0.2 to 0.5 eV too high in energy throughout.

5. The $3p_y$ $^2B_2$ state stays untypically close to the MRCI reference (0.2 eV), except at separations below 1.2 Å.

At 1 Å and 8 to 12 eV, the 5th and 6th A' states (the 4th $^2A_1$ state and 2nd $^2B_2$ state) are not reproduced correctly in MSDFT. The MED active space produces a A' state with an unreasonably steep parabolic shape that dips all the way down to within 0.1 eV of the $3p_y$ $^2B_2$ (and $3p_x$ $^2A_1$) states at 7.6 eV. This is not a feature that shows up in the MRCI results; the most similar state there being the second $^2B_2$ state (the 5th lowest A' state), which MRCI shows to only dip to around 8.0 eV. At 11.5 eV this state crosses a second incorrectly reproduced state, which stays above 10.5 eV. If these were compared to the $3d_{x^2-y^2}$ and $3d_{xy}$ states with the correct shape in MRCI, it would not be immediately obvious that and how these two "MED" active space MSDFT states are related. But comparison to the "MAS" active space MSDFT results and the MRCI states obtained with the state averaging weights that lead to the artifacts shown in the figures, makes it quite obvious. The higher state from the "MED" active space has a similar shape to the single state in that region that the MAS active space produces, which in turn is almost identical in shape to the $3d_{x^2-y^2}$ state in MRCI, although about

2 eV higher in energy. Via this comparison, the MSDFT states with this shape can be identified as $3d_{x^2-y^2}$ states, and the parabolic state would be the $3d_{xy}$ state (and it's symmetry would also explain how it can be almost degenerate with the $3p_{z^2}$ state).

The steep parabolic state could theoretically be a (low-spin) sextett state, which the MRCI calculation does not cover. This seems highly unlikely since any hextet that is symmetric with respect to the molecular plane would involve a triple excitation (or excitation into the $3p_z$ MO), which would easily exceed the energy scale of the graph. These facts and the suspiciously steep potential energy well of the PEC makes it seem exceedingly more likely that the shape of this PEC is an artifact caused by a shortcoming of the MSDFT method or the PBE0 functional.

A.5.4 MSDFT, Minimal Active Space (MAS)

A.5.4.1 MAS Calculation

The goal of this calculation was to reduce the size of the active spaces compared to the "MED" calculation as much as possible. In the case of the A'' (B_1) symmetry representation, removing from the "MED" active space any group of determinants that did not appear strictly necessary immediately led to a smaller active space with similar quality potential energy curves for the lowest energy states. Finding a minimal A' (A_1 & B_2) active space was less straightforward. The reduction of the active space size (starting from the one of the above calculation) required successively identifying the least important determinant(s) and removing them, until doing so was no longer possible without a significant impact on the potential energy curves. This was achieved by successively alternating the following three steps. First, any individual single determinant (or pair of symmetry related determinants) was removed and the change on the potential energy curves of the relevant states were evaluated. Secondly, a set of potential energy curves was calculated after removing the 3 of the determinants (or pairs thereof) with the smallest impact. Thirdly, each of the 3 combinations with only 2 of those candidates removed was calculated and compared to the above in order to ensure that the removal of the respective third determinant (or determinant pair) had not become more impactfull after the removal of the other two. In case one of the determinants failed this final check, these steps were restarted with only the 2 other determinants (or pairs) removed, otherwise the next iteration started with all 3 determinants removed. A fact that deserves emphasizing here is that arriving at these minimal active spaces was only possible *after* finding the larger ("MED") active space (especially for the A' representation).

Table A.2 lists the diabatic states (DFT determinants and DFT configuration state functions) that are part of the "MAS" active space. For a description of the table (column) format, see Section A.5.3.1.

The first section of the table contains determinants that are localized along the bond to one of the 3 Hydrogens. Of the 15 possible combinations of bond direction, occupations and spins, only 13 are used in this calculation. The combinations with the down spin on the $\mathrm{C}\,2\mathrm{p}_z$ MO and localization along the bonds to the remaining hydrogen atoms are clearly not needed; they are listed in the second section. (The 5 of these that localize along the x axis could (again) have used the a_2 block.) The (for all intents and purposes) fully unconstrained B_1 determinant (using only the system's symmetry to inform its block definition) is still used. The last B_1 section contains determinants that constrain an electron to the $\mathrm{C}\,3+\mathrm{p}_z$ AO along with localization along any of the 3 bonds. Only the 3 determinants that localize along the x axis, with exactly one electron on the H^x hydrogen, are used in this calculation. (9 such determinants would be needed to make the treatment symmetrical with respect to the 3 hydrogen atoms.)

Table A.2: All determinants in the MSDFT calculation with minimum active space ("MAS").

$M_S = +1/2$ A″ determinants, MAS

a″ blocks			a′ blocks					
a_2 block used? [b]	$2p_z$MO occ	$3p_z$AO [a] occ	localized H [a] id [c]	localized H [a] occ	CH_2/CH_3 occ [d]	C3⋆ AO [a] type	C3⋆ AO [a] occ	n_{Dets}
A″ determinants with only localization								
	1 +1		x	0 0	8 0			13 of 15
	1 +1		1	0 0	8 0			
	1 +1		2	0 0	8 0			
	1 +1		x	2 0	6 0			
	1 +1		1	2 0	6 0			
	1 +1		2	2 0	6 0			
	1 +1		x	1 -1	7 +1			
	1 +1		1	1 -1	7 +1			
	1 +1		2	1 -1	7 +1			
	1 +1		x	1 +1	7 -1			
	1 +1		1	1 +1	7 -1			
	1 +1		2	1 +1	7 -1			
	1 -1		x	1 +1	7 +1			
	1 -1		1	1 +1	7 +1			2 of 15 missing
	1 -1		2	1 +1	7 +1			
delocalized, unconstrained Kohn-Sham A″ determinant								0 of 1
A″ determinants with localization (H^x bond only) and C $2p_z \rightarrow$ C $3p_z$ excitation								
yes	0 0	1 +1	x	1 -1	7 +1			3 (of 9)
yes	0 0	1 +1	x	1 +1	7 -1			
yes	0 0	1 -1	x	1 +1	7 +1			
delocalized A″ determinant with only C $2p_z \rightarrow$ C $3p_z$ excitation								
yes	0 0	1 +1			8 0			1 [e]

$M_S = +1/2$ A′ determinants, MAS

a_2 [b]	$2p_z$ MO	$3p_z$ AO [a]	localized H [a]	CH_2/CH_3	C 3* AO [a]	n_{Dets}
A′ determinants with localization and C $2p_z$ constrained to 0 electrons occupation						
	0 0		x 2 0	7 +1		3 (of 6)
	0 0		1 2 0	7 +1		
	0 0		2 2 0	7 +1		
delocalized A′ determinant with only C $2p_z$ constrained to 0 electrons occupation						
yes	0 0			9 +1		1
A′ determinants with localization and C $2p_z$ constrained to doubly occupied						
						0 of 6
delocalized A′ determinant with only C $2p_z$ constrained to 2 electrons occupation						
	2 0			7 +1		1
A′ determinants with localization and C $2p_z \to$ C 3s excitation						
yes	0 0		x 0 0	8 0	3s 1 +1	5 of 15
yes	0 0		x 1 -1	7 +1	3s 1 +1	
	0 0		1 1 -1	7 +1	3s 1 +1	
	0 0		2 1 -1	7 +1	3s 1 +1	
yes	0 0		x 1 +1	7 -1	3s 1 +1	
delocalized A′ determinant with C $2p_z \to$ C 3s excitation						
yes	0 0			8 0	3s 1 +1	1 [e]
delocalized A′ determinants with C $2p_z \to$ C $3p_{x/y}$ excitation						
yes	0 0			8 0	$3p_x$ 1 +1	1
yes	0 0			8 0	$3p_y$ 1 +1	1

The "occ" columns describe the occupation (and spin excess) of the respective blocks; The "type" column specifies the type of sub-shell(s) that the respective electron is being excited into; The "id" column defines the singled out hydrogen; The "n_{Dets}" column lists the number of determinants used in a specific group of rows. The cells in the "occ" columns contain 2 values: The first is N_{e}, the nr. of electrons that occupy the block; and the second value (and it's sign) is $N_{e\uparrow} - N_{e\downarrow} = 2 * M_S$, the (signed) difference between up and down spins occupying the block, or equivalently the projection of the spin (counted in multiples of half atomic units, i.e., multiples of fermionic spin units).

[a] This block, when present, includes all AOs of that type regardless of shell. (For example, the $3\mathrm{p}_x$ block additionally contains $4\mathrm{p}_x$, $5\mathrm{p}_x$ and 'aug' p_x; and blocks for singular hydrogen atoms contain in addition to the H 1s basis function all other a′ functions on that H.) An empty cell means that the respective basis functions are included in the main block of the same symmetry representation.

[b] See Section A.4.2.3.

[c] "x" is the leaving hydrogen, "1" and "2" are the two symmetry-equivalent ones.

[d] This occupation includes 2 electrons in the core C 1s MO, and 2 electrons each in the VB MOs along the 2 bonds that are not split.

[e] This determinant is not part of the "MED" active space.

The first three A_1 sections list determinants where an a′ electron is excited to the C $2\mathrm{p}_z$ MO or vice versa. Both delocalized determinants are used, but out of the 6+6 possible variants with localization along one of the bonds, only the variation with excitation from the C $2\mathrm{p}_z$ MO onto the hydrogen are used (for all 3 bond directions). (The one of these that localizes along the x axis could (again) have used the a_2 block.) The last three sections cover the cases where an electron is excited to the 3rd shell a′ AOs

Figure A.6: B_1 potential energy curves in MSDFT with minimum active space (“MAS”), compared to “MED” MSDFT and MRCI.

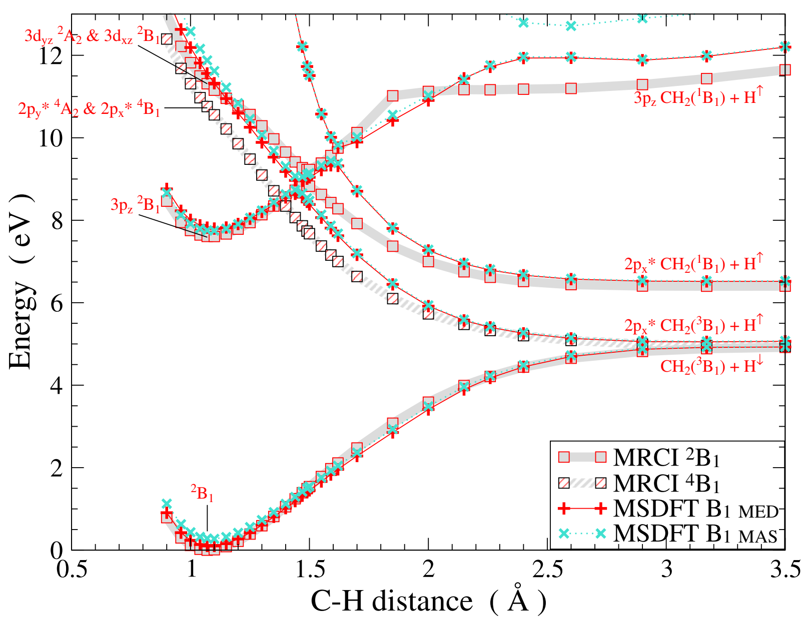

of carbon. For the excitation to C 3 + s the calculation now includes the delocalized determinant, but in return only 5 of the localized bond direction, occupation and spin combinations that are possible are needed. For the C 3 + p_x and C 3 + p_y excitations only the respective single delocalized determinant is used.

A.5.4.2 MAS Results

Figures A.6, Fig. A.7 and Fig. A.8 categorize the states into their spatial symmetries (with Fig. A.8 combining A_2 and B_2 symmetry states). The (arbitrary) zero point of the energy scale is again set to the MRCI ground state at the CH_3 equilibrium geometry. And the energies scale of MSDFT is still aligned to that of MRCI via the lowest CH_2 doublet ground state in the respective method (which for both MSDFT calculations is the MED energy at 3.5 Å, although the energetic difference to aligning them separately is negligible). Both sub-figures compare the systematic active space (MED) (pluses and

Figure A.7: A_1 potential energy curves in MSDFT with minimum active space ("MAS"), compared to "MED" MSDFT and MRCI. Note that the energy axis starts at 5.5 eV.

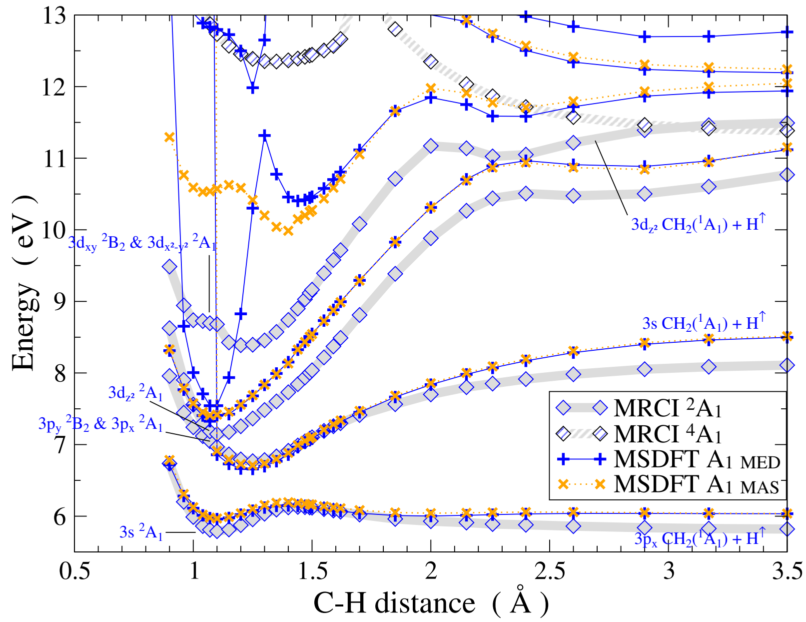

Figure A.8: A_2 and B_2 potential energy curves in MSDFT with minimum active space ("MAS"), compared to "MED" MSDFT and MRCI. Note that the energy axis starts at 6.5 eV.

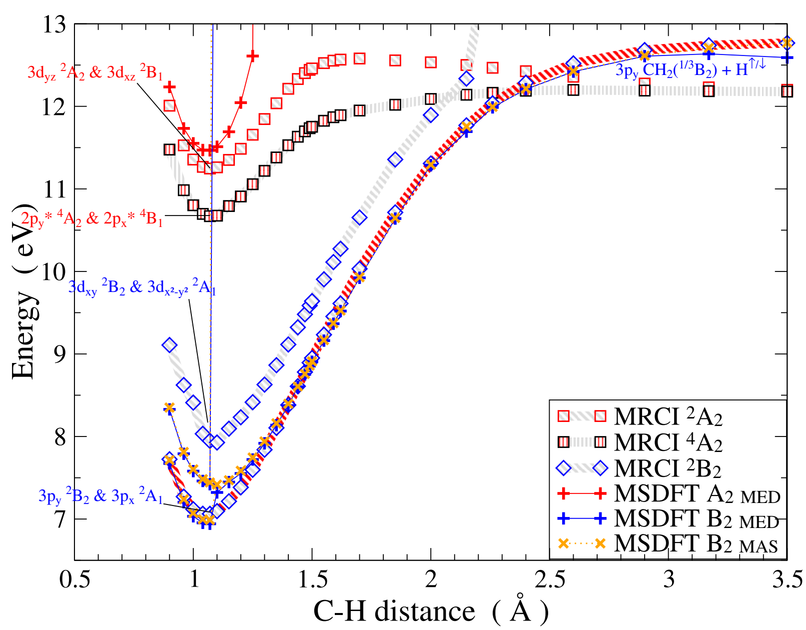

dashed/dotted lines in red/blue) to both the minimal active space (MAS) (crosses and solid lines in teal/orange), and to the MRCI reference (which uses the same styles as in Figures A.3 and A.5). For the results from MRCI (which distinguishes between doublet and quartet states and all 4 symmetry representations of C_{2v}), the $^2B_1$ and $^2A_1$states are shown with solid gray line and symbol fill and colored symbol outlines; all quartet states are shown with a hatched line, black symbol outline and colored (hatched) symbol fill, while all states of A_2 and B_2 representation are shown with a hatched line, thicker symbol outline and hatched symbol fill. Again, all MSDFT potential energy curves that fall within the energy range of the plot are shown. Of the 9 A'' and 8 A' states that the MRCI calculation has yielded, only the 6 and 7 relevant ones are shown in order to minimize the clutter in the high-energy part of the graphs. For the omitted MRCI potential energy curves, see Fig. A.3.

Splitting the symmetry representations further than in the figures of Section A.5.3.1 reveals that the potential energy curves for the $3p_x$ and $3p_y$ state abruptly stop being resolvable by either MSDFT active space; which shows in these plots as vertical line artifacts at the equilibrium geometry (the distance where the order of these two states flips). The reason is that the active spaces are lacking the basis determinants needed to describe both states for all distances, and the single basis determinant that describes them converges to wave functions with $^2B_2$ and $^2A_1$ symmetry on the shortened and lengthened side of the symmetric geometry, respectively.

In comparison of the two active spaces, and considering that the active spaces differ by an approximate halving of their sizes, the effect on the low lying states is remarkably small. The ground state is up to 0.2 eV higher than for the larger active space, especially at separations shorter than the equilibrium distance. The quantitative agreement of the other low lying states to the "MED" active space is to within 0.14 eV at worst, usually much better. One quantitative result both MSDFT active spaces agree on very precisely is the relatively small energy gap of the avoided crossing between the 2nd and 3rd lowest $^2B_1$ states; 0.40 ± 0.02 eV in MRCI, 0.33 ± 0.03 eV with the larger active space in MSDFT and 0.33 ± 0.03 eV with the MAS in MSDFT. The avoided crossing in MRCI is located at 1.50 ± 0.02 Å while in MSDFT they are located consistently at 1.45 ± 0.03 Å but at energies that differ slightly (by 0.095 ± 0.005 eV). Any severe changes are limited to the higher energy states (which were not monitored in the optimization of the A′ active space). The (bound) $2p_y^*$ $^4A_2$ state crossing the (anti-bonding) $2p_x^*$ $^4B_1$ state at 1.08 ± 0.03 Å and 11.49 ± 0.05 eV is missing with the MAS active space (though present with the MED active space). The MAS active space reproduces only the $3d_{x^2-y^2}$ state out of the two $3d_{xy}$ and $3d_{x^2-y^2}$ states (of which the MED active space qualitatively reproduces both, although with wrong energies). The only way a state in the smaller active space can realistically have a lower energy is if there is a DFT determinant among it that is more suited to describing this state than the ones in the MED active space. The delocalized 3s determinant in the "MAS" active space is the only change that would offer this advantage over the "MED" calculation, which instead has to combine 15 localized 3s determinants to describe the 3s excitation. These states also have the same (A_1) symmetry as the $3d_{x^2-y^2}$ state.

A.5.5 State Energy Comparison

Key excitation energies of CH_3 and CH_2 are listed in Table A.3. The values from the MSDFT, MRCI and Ref. [323] calculations are vertical excitation energies from the equilibrium geometry. The experimental values given in Table A.3 are excitations between the $\nu = 0$ vibrational states of the excited and electronic ground state. The excitation in the photo-dissociation experiment is also a vertical excitation process, but in the photo-dissociation experiment the excitation of of CH_3 originates from a mixture of vibrational states.[322] Since the MSDFT active spaces are only applicable to a

CH_3 system, the excitation energies of CH_2 had to be taken at the largest separation (3.5 Å) for both the MSDFT and MRCI calculations. A MSDFT calculation of an isolated CH_2 system would need a completely different active space, which would lack comparability to the calculations of the potential energy curves. The "shape" column describes if the states are bonding (with normal, strong or weak curvature around 1.07 Å) or repulsive/anti-bonding. For CH_2, the symmetry column is in the following format: $^{[2S+1]}([2S_{\mathrm{CH_2}}+1][G],^{[2S_{\mathrm{H}}+1]}\mathrm{H})_{([M_S])}$ Where $2S+1$ is the multiplicity of the whole system, $[2S_{\mathrm{CH_2}}+1]$ is the multiplicity of the CH_2 fragment, $[G]$ is the symmetry representation of the wave function, $[2S_{\mathrm{H}}+1]$ is the multiplicity of the H atom, and $[M_S]$ is the magnetic spin quantum number of the whole system.

Table A.3: Excitation energies of the electronic excitations in CH_3 and CH_2.

orbital (symmetry rep's)			CH_3 excitation energies (eV)				
MO	D_{3h}	C_{2v}	MAS	MED	MRCI	Balerdi[323]	Exp[331]
$\tilde{X}$	$^2A_2''$	$^2B_1$	0	0	0	0	0
3s	$^2A_1'$	$^2A_1$	5.87	5.70	5.82	5.84	5.73
$3p_y$ &	$^2E'$	$^2B_2$	6.71 [g]	6.71 [g]	7.07	6.87	7.44
$3p_x$	$^2E'$	$^2A_1$	7.14 [g]	7.13 [g]	7.05	"	"
$3d_{z^2}$	$^2A_1'$	$^2A_1$	7.17	7.22	7.18	8.47	8.28
$3p_z$	$^2A_2''$	$^2B_1$	7.55	7.65	7.62	7.65	7.44
$3d_{xy}$ &	$^2E'$	$^2B_2$		7.44 [h]	7.93 [i]	7.14	8.25
$3d_{x^2-y^2}$	$^2E'$	$^2A_1$	10.25 [h]	12.78 [h]	8.68 [h,j]	"	"
$2pi_x^\star$	$^4E''$	$^4B_1$ $\lvert M_S\rvert=\frac{1}{2}$	11.56	11.45	10.76		
		$^4B_1$ $\lvert M_S\rvert=\frac{3}{2}$	11.40 [k]	10.70 [l]	"		
$2p_y^\star$	$^4E''$	$^4A_2$		11.35	10.67		
$3d_{yz}$	$^2E''$	$^2A_2$			11.25		
$3d_{xz}$	$^2E''$	$^2B_1$			11.31	11.08	
	$^2A_2''$/ $^2E''$	$^2B_1$			11.95	11.60	

Table A.3: Excitation energies of the electronic excitations in CH_3 and CH_2.

orbital (symmetry rep's)		CH_2 excitation energies (eV)				
nr	C_{2v} state(s) [n]	MAS	MED	MRCI	Balerdi[323]	Exp[332]
$\tilde{X}$	$^2(^3B_1,{}^2H)$	0	0	0	0	0
$\tilde{X}$	$^4(^3B_1,{}^2H)_{\|M_S\|=1/2}$	0.14	0.14	0.03	"	"
$\tilde{X}$	$^4(^3B_1,{}^2H)_{\|M_S\|=3/2}$	0.02 [k]	0.02 [l]	"	"	"
1	$^2(^1A_1,{}^2H)$	1.10	1.11	0.90	0.98	0.39
1	$^2(^1B_1,{}^2H)$	1.59	1.59	1.48	1.48	1.43
2	$^2(^1A_1,{}^2H)$	3.58	3.57	3.19	3.16	
1	$^4(^3A_2,{}^2H)$	8.18	8.12	7.26	7.34	
1	$^2(^3A_2,{}^2H)$	8.24	8.24	7.28	"	
1	$^2(^3B_1,{}^2H)$	7.28	7.27	6.73	7.45	
2	$^4(^3B_1,{}^2H)$	8.45	8.44	7.58	"	
2	$^2(^1B_1,{}^2H)$	9.71 [o]	9.73 [o]		7.72	
2	$^4(^3A_2,{}^2H)$	16.49 [o]	12.98 [o]	11.01		
1	$^2(^3A_1,{}^2H)$	6.22	6.19	5.85	6.35	
1	$^4(^3A_1,{}^2H)$	7.11	7.01	6.46	"	
3	$^2(^1A_1,{}^2H)$	7.31	7.27	6.57	6.60	
2	$^2(^3B_2,{}^2H)$	7.84	7.84	7.85	7.57	
2	$^4(^3B_2,{}^2H)$		7.66	7.87	"	
3	$^2(^3B_2,{}^2H)$	9.43	9.32	8.98	7.93	
3	$^4(^3B_2,{}^2H)$				"	

Table A.3: Excitation energies of the electronic excitations in CH_3 and CH_2.

Listed for this chapter's calculations in MSDFT (with minimal active space "MAS" and medium size active space "MED"), our MRCI values, the MRCI values from reference [323], as well as experimental excitation energies.[332, 331]

[g] The character of the $3\mathrm{p}_{x,y}$ ${}^2\mathrm{E}'$ states is highly mixed in MSDFT, therefore any ordering is arbitrary.

[h] Potential energy curve shape is unrealistic. Energy should be treated as unreliable.

[i] Despite lower weight, energy is below $3\mathrm{d}_{x^2-y^2}$ state; active space may be unbalanced.

[j] Jumps in PEC, energy depends on state weights; active space may be too small.

[k] From localized single-determinant high-spin DFT calculation.

[l] From delocalized single-determinant high-spin DFT calculation.

[m] Too high in energy to resolve at CH_3 geometry, but state found at intermediate distances.

[n] In the format $^{<2S_{\mathrm{total}}+1>}(^{<2S_{\mathrm{CH_2}}+1>} < C_{2\mathrm{v}}$ representation $>$, $^{<2S_{\mathrm{H}}>}$H).

[o] Assignment unclear.

For CH_3 in MSDFT, the $2\mathrm{p}_x \rightarrow 2\mathrm{p}_x^{\star}\,{}^2\mathrm{B}_1$ state is too high in energy (at least 22 eV) to be distinguishable from other states at that energy. In CH_3, the 2nd ${}^2\mathrm{B}_2$ state is part of a pair of degenerate ${}^2\mathrm{E}'$ states. MRCI returns a too large energy for this potential energy curve and fails to capture its degeneracy with the corresponding 3rd ${}^2\mathrm{A}_1$ state. This issue may be due to the 3rd b_2 orbital not being included in this chapter's MRCI active space. At that energy (7.32 and 7.44 eV), the larger MSDFT active space produces two A' states (B_2 and A_1 in $C_{2\mathrm{v}}$) which are close to degenerate. Interestingly, the MAS fails to produce the ${}^2\mathrm{A}_1$ state of that degenerate pair.

The failure to correctly represent the degeneracy of E'/E'' states at the CH_3 geometry is a sign that the results for these states in MSDFT (and to a lesser extent in MRCI) are not converged with respect to the active space size. In MRCI, any discrepancy between the included a_1 vs. b_2 orbitals will affect the results. However, these states are above the energy range accessible during the dissociation, and any states of interest for the dissociation are reproduced reasonably well.

A prominent quantitative finding is that MSDFT overestimates the CH_2 excitation energies below +5 eV (among the lowest 4 states that are reachable though the photo-dissociation process), typically by 0.1 to 0.4 eV (with respect to this chapter's MRCI results). The higher CH_2 excitation energies which the active space has not been optimized for are off by up to 0.9 eV for both active spaces (ignoring 2 outliers: the $3d_{x^2-y^2}$ state of CH_3 and the 2nd $^4(^3A_2, ^2H)$ state of CH_2). Some part of this discrepancy may be caused by using the PBE0 functional on block-localized determinant. But it is also worth emphasizing that in both active spaces the number of determinants specifically dedicated to modelling the ground state (and the excitations into anti-bonding orbitals) is (due to the rigorous treatment in the VB picture) larger than the number of determinants for excitations into several of the 3rd shell AOs of the carbon atom. This would be expected to lead to more double-counting of dynamic correlation in the ground state than in the higher adiabatic states.

A.6 Summary

The goal of this investigation was to determine if it was possible to accurately resolve at least the 4 lowest states using valence bond-style determinants, and to do so using the smallest required number of them. Section A.4 presented advanced considerations and strategies that were used in these calculations to define both the set(s) of determinants in MSDFT multi-state calculations as well as the blocks in single-determinant optimizations.

The first problem that this investigation has shown arises when the basis states are not orthogonal enough to each other, or even nearly identical. As mentioned in A.4.1.2, this translates to a need for the AO basis functions (at least on the same atom) to be orthogonal to each other. (Or, as has been done in [26], the need to explicitly orthogonalize the set of determinants before diagonalizing it.)

Another (technically solved) complication is related to the fact that it can often aid interpretability (in systems with more than one unpaired electron spin) if the diabatic states are not just (spin-contaminated) single determinants but instead CSFs which are eigenfunctions of the spin magnitude operator. This can be and has been done.[26] But although being a solvable problem, it requires a diagonalization of a small sub-set of the basis determinants (of size 3x3 in this case, and of size 2x2 in the more common case with singlet and triplet states) for each determinant type with 2 or more unpaired spins. And setting up all of these required sub-diagonalizations is a manual procedure. Furthermore, some of the determinants that form the CSFs may require the use of the ΔSCF formulation.

Another known but unaddressed problem with the currently available MSDFT program versions is that the currently used block definition scheme in terms of the basis functions themselves does not allow for any theoretically possible block to be specified. The ability to define determinants/blocks in terms of any linear combinations of basis functions would (at least in some systems) improve interpret-ability of the resulting diabatic states. For example, if it was not for the symmetry of the CH_3 system, it would possibly have made sense to define the blocks on the C atom in terms of sp^2 hybridized AOs, instead of s and p AOs. This capability might (in systems where it is applicable) also lower the energies of diabatic states (and consequently of the adiabatic states), or reduce the required active space size. And it could even be used to define blocks in excited state determinants in terms of (fully optimized ground state) MOs - which would offer an alternative to the ΔSCF scheme and might potentially lead to a fully orthonormal or at least more orthogonal set of diabatic states.

The requirement for the lowest adiabatic state energy (or most similar energy to high quality WFT) can potentially conflict with the requirement of having the determinants interpretable as diabatic states. Especially when the active space (to improve the adiabatic state's energy) has a delocalized determinant added to describe an adiabatic state in the MO picture which is also described by localized states, then that delocalized determinant will obviously always be near collinear to the Hilbert space spanned by the full set of bond-localized determinants. If interpretability of the results is required, then this can be overcome by Gram-Schmidt orthogonalizing the delocalized diabatic state to all localized diabatic states. (Alternatively, all localized diabatic states can be orthogonalized to the delocalized one, which will contaminate their localization.)

The last and largest hurdle for applying MSDFT to bond breaking investigations like this one that this investigation has shown is that the freedoms in choosing determinants and defining them (that are listed in Section A.4.2) also make it labor intensive to find a truly minimal (and qualitatively sufficient) active space. The third Lu-Gao theorem[4] suggests that a minimal active space for the 3 lowest A$''$ and 4 lowest A$'$ states that are of interest to the photo-dissociation should require no more than $(3 + 4)^2 = 49$ basis determinants. The "MED" active space used $31 + 31 = 62$ determinants. And on one hand, in accordance with the fact that the Lu-Gao theorems give an *upper bound* for the lowest achievable active space size, the "MAS" active space was able to cut that down to $17 + 13 = 30$ determinants without noteworthy deterioration of the energies of those 7 adiabatic states. And on the other hand the 4th lowest A$''$ and 5th lowest A$'$ states are absolutely not well reproduced, even in the MED active space.

Systematically choosing all determinants that might be essential for low-energy states produced the MSDFT active space "MED" (Section A.5.3), which is in pretty good agreement to MRCI overall, at the cost of $31+31 = 62$ determinants. The MSDFT calculation with the "MAS" active space (Section A.5.4) demonstrated that carefully selecting the determinants makes it possible to halve the size of the active space to $17 + 13 = 30$ determinants without significantly deteriorating the energies of the states of interest. This came at the cost of the quality of some of the states immediately above the energetic region of interest, though. With both active spaces, the (low-spin) MSDFT potential energy curves are reasonably well reproduced (to within 1 eV of the reference for the higher energy state of interest and better for states with lower energies). This is also reflected in Table A.3 where the same trend is observable for the CH_3 and CH_2 states that were identifiable.

However, the high-spin quartet states energies are reproduced incorrectly in all multi-determinant MSDFT calculations. The reasons for this are unknown.

Appendix B

Calculation of the Block-Localized Ground and Excited State Energy Gradients

The operator form of the ground state energy gradient for RHF is given using [53]

$$\frac{\partial E}{\partial \langle \varphi_A |} = 4(1-\rho) f |\tilde{\varphi}_A\rangle \tag{B.1}$$

where the reciprocal orbitals $|\tilde{\varphi}_A\rangle$ are

$$\begin{aligned}
|\tilde{\varphi}_A\rangle &= |\varphi_A \varphi_{\notin A}\rangle \langle \varphi_A \varphi_{\notin A} | \varphi_A \varphi_{\notin A}\rangle^{-1} \\
&= |\varphi_A \varphi_{\notin A}\rangle \begin{pmatrix} \langle \varphi_A | \varphi_A\rangle & \langle \varphi_A | \varphi_{\notin A}\rangle \\ \langle \varphi_{\notin A} | \varphi_A\rangle & \langle \varphi_{\notin A} | \varphi_{\notin A}\rangle \end{pmatrix}^{-1}
\end{aligned} \tag{B.2}$$

here in Eq. B.2, $\langle\varphi_A|\varphi_A\rangle$ is the overlap matrix of the molecular orbitals, not an integral value. By using the method of block-wise matrix inversion[333]

$$\begin{pmatrix} A & B \\ C & D \end{pmatrix}^{-1} = \begin{pmatrix} (A - BD^{-1}C)^{-1} & -(A - BD^{-1}C)^{-1}BD^{-1} \\ -D^{-1}C(A - BD^{-1}C)^{-1} & D^{-1}C(A - BD^{-1}C)^{-1}BD^{-1} + D^{-1} \end{pmatrix} \tag{B.3}$$

we set

$$\begin{aligned} &(\langle\varphi_A|\varphi_A\rangle - \langle\varphi_A|\varphi_{\notin A}\rangle\langle\varphi_{\notin A}|\varphi_A\rangle)^{-1} \\ &= \langle\varphi_{\notin A}|(1 - \rho_{\notin A})|\varphi_{\notin A}\rangle^{-1} \\ &= \alpha \end{aligned} \tag{B.4}$$

After transformations, the following expressions are obtained

$$|\tilde{\varphi}_A\rangle = |(1 - \rho_{\notin A})|\varphi_A\rangle\alpha, (1 - (1 - \rho_{\notin A})|\varphi_A\rangle\alpha\langle\varphi_A|)\langle\varphi_{\notin A}|\varphi_{\notin A}\rangle^{-1}\rangle \tag{B.5}$$

$$\rho = |\tilde{\varphi}_A\rangle\langle\varphi_A\varphi_{\notin A}| = (1 - \rho_{\notin A})|\varphi_A\rangle\alpha\langle\varphi_A|(1 - \rho_{\notin A}) + \rho_{\notin A} \tag{B.6}$$

$$\begin{aligned} \frac{\partial E}{\partial\langle\varphi_A|} &= 4(1 - \rho)f|\tilde{\varphi}_A\rangle \\ &= (1 - (1 - \rho_{\notin A})|\varphi_A\rangle\alpha\langle\varphi_A|)(1 - \rho_{\notin A})f(1 - \rho_{\notin A})|\varphi_A\rangle\alpha \end{aligned} \tag{B.7}$$

We can further set α as a unit matrix to make $(1 - \rho_{\notin A})|\varphi_A\rangle$ ortho-normalized

$$\alpha = \langle\varphi_{\notin A}|(1 - \rho_{\notin A})(1 - \rho_{\notin A})|\varphi_{\notin A}\rangle^{-1} = \langle\Phi_A|\Phi_A\rangle^{-1} = \mathbf{1} \tag{B.8}$$

and obtain the energy gradient for block A

$$\frac{\partial E}{\partial\langle\varphi_A|} = 4(1 - (1 - \rho_{\notin A})|\varphi_A\rangle\langle\varphi_A|)(1 - \rho_{\notin A})f(1 - \rho_{\notin A})|\varphi_A\rangle \tag{B.9}$$

At the point of the lowest energy, the energy gradient is zero. We obtain the SCF equation with

$$\langle \varphi_i^A | (1 - \rho_{\notin A}) f (1 - \rho_{\notin A}) | \varphi_i^A \rangle = \epsilon_i^A \tag{B.10}$$

The SCF equation (in refs [40] and [44]) can then be obtained by putting Eq. B.11 into the above SCF equation. Because α is a unit matrix, Eq. B.6 now becomes

$$\rho = (1 - \rho_{\notin A}) \rho_A (1 - \rho_{\notin A}) + \rho_{\notin A} = \rho_A^x + \rho_{\notin A} \tag{B.11}$$

We have the property

$$(1 - \rho_{\notin A}) | \varphi_{\notin A} \rangle = | \varphi_{\notin A} \rangle - \rho_{\notin A} | \varphi_{\notin A} \rangle = 0 \tag{B.12}$$

If we set $|\Phi_i^A\rangle = (1 - \rho_{\notin A})|\varphi_i^A\rangle$, then $\langle \varphi_{\notin A} | \Phi_i^A \rangle = 0$. By multiplying $\langle \varphi_i^A |$ on the left of Eq. 2.8, using the idempotency relation $(1 - \rho_{\notin A})(1 - \rho_{\notin A}) = (1 - \rho_{\notin A})$, and keeping Φ_A orthogonal, we obtain

$$\langle \Phi_i^A | f | \Phi_i^A \rangle = \langle \Phi_i^A | \Phi_i^A \rangle \epsilon_i^A = \epsilon_i^A \tag{B.13}$$

$$f | \Phi_i^A \rangle = \epsilon_i^A | \Phi_{\notin A} \rangle \tag{B.14}$$

The above derivation from eqs B.12-B.14 is a reversed process of the generalized Phillips-Kleiman pseudopotential derivation in ref [83]. This means that the projected wavefunction of block A orthogonalized to all other blocks is the eigenfunction of the whole system.

To constrain the excited state particle orbitals φ_A orthogonal to the ground state occupied orbitals φ_A^0, we need $\langle \varphi_A | (1 - \rho_{\notin A}^0) | \varphi_A^0 \rangle = 0$. The following equation is solved with a Lagrange multiplier λ

$$\begin{aligned}\frac{\partial L}{\partial\langle\varphi_A|} =&(1-(1-\rho_{\notin A})|\varphi_A\rangle\langle\varphi_A|)(1-\rho_{\notin_A})f(1-\rho_{\notin_A})|\varphi_A\rangle-\lambda(1-\rho^0_{\notin_A})|\varphi^0_A\rangle\\ =&0\end{aligned} \tag{B.15}$$

By multiplying $|\varphi^0_A\rangle$ on the left, the Lagrange multiplier λ can be obtained

$$\lambda=\langle\varphi^0_A|(1-(1-\rho_{\notin A})|\varphi_A\rangle\langle\varphi_A|)(1-\rho_{\notin_A})f(1-\rho_{\notin_A})|\varphi_A\rangle \tag{B.16}$$

The equation then becomes

$$(1-(1-\rho^0_{\notin A})|\varphi^0_A\rangle\langle\varphi^0_A|)(1-(1-\rho_{\notin A})|\varphi_A\rangle\langle\varphi_A|)(1-\rho_{\notin_A})f(1-\rho_{\notin_A})|\varphi_A\rangle=0 \tag{B.17}$$

We can further rewrite the above equation into a symmetric form

$$\rho'(1-\rho_{\notin A})f(1-\rho_{\notin A})\rho'|\varphi^A_i\rangle=\rho'(1-\rho_{\notin A})|\varphi^A_i\rangle\epsilon^A_i \tag{B.18}$$

where $\rho'=1-(1-\rho^0_{\notin A})|\varphi^0_A\rangle\langle\varphi^0_A|=(1-\rho^0_{\notin A})|\varphi^0_{A\nu}\rangle\langle\varphi^0_{A\nu}|$ by using normalization property of complete nonorthogonal basis, $|\varphi^0_{A\nu}\rangle$ is ground state unoccupied orbitals. To solve this eigen-equation, we multiply $\langle\varphi^0_{A\nu}|=(\chi T^0_{A\nu})^\dagger$ on the left and set $|\varphi_A\rangle=\chi T_A=\chi T^0_{A\nu}T_A$ to project the equation to ground state unoccupied orbital space. The following equation is then obtained

$$(T^{0\dagger}_{A\nu}F'_AT^0_{A\nu})T'_A=(T^{0\dagger}_{A\nu}S'_AT^0_{A\nu})T'_AE_A \tag{B.19}$$

After the diagonalization, the particle orbitals will be selected according to the order of ground state unoccupied orbitals.

Appendix C

Glossary and Acronyms

Care has been taken in this thesis to minimize the use of jargon and acronyms, but this cannot always be achieved. This appendix defines jargon terms in a glossary, and contains a table of acronyms and their meaning.

C.1 Glossary

- **adiabatic states** – A set of states with zero stationary (velocity-independent) interaction, which keep their energetic ordering but may vary their character abruptly. (See also "state".)

- **branch** – A set of AO basis functions with the same angular momentum magnitude quantum number l (or the same angular momentum magnitude and magnetic angular momentum quantum numbers l and m_l)

- **Born-Oppenheimer approximation** – A ubiquitous approximation that takes the full (electronic *and* nuclear) Schrödinger equation of the system and solves it only for the electronic wave function (and energies of the electronic states), while keeping this result a function of the nuclear coordinates (to be solved either as its own Schrödinger equation or in a classical mechanics approximation).

- **charge transfer state, Charge transfer process (CT)** – A state of a system where significant charge (at least a large fraction of an electron) is moved between two separate (or separable) parts of a system. Or the process of moving charges in this manner.
- **configuration** – Many-body wave function that describes a certain arrangement of the electrons. Typically a single or only a few determinants.
- **contraction (Gaussian basis function contraction)** – A pre-optimization specifically for Gaussian type functions, using a linear combination to "contract" several ("primitive") Gaussians into a single (AO) basis function.
- **correlation** – Any deviation from the assumption that one electron's behavior only depends on what the other electrons are doing *in a time-averaged manner*. I.e. any effects that take into account that the probability of finding two electrons in specific places is not simply equal to the combination of the probabilities of finding each at one of the positions, including especially energetic effects. Causes states (when obtained with a method of sufficiently high quality to resolve this effect) to consist of a multitude of determinants.
- **density** – Usually means "electron probability density", unless noted otherwise.
- **Determinant** – Abbreviation for "Slater determinant". See "Slater determinant"
- **diabatic states** – A set of states with small or minimal velocity-dependent interaction, that keep (or only slowly and smoothly vary) their character, but may swap their energetic ordering. (See also "state".)
- **doubles** – 2-electron excitations (usually with respect to the base determinant)

- **dynamic (or weak) correlation** – Interaction with the one (or few) main determinant(s) where none of the contributions from each of the many additional determinants is noteworthy on its own. Typically attributed to electrons avoiding each other's presence on very short length scales. (See also "correlation".)

- **Gaussian/ Gaussian orbital** – Gaussian-type basis function (of the form $\exp(-r^2/r_0^2)$)

- **Hamiltonian** – Abbreviation for "Hamilton operator".

- **potential energy curve (PEC)** – Potential energy of an electronic state as a function of one nuclear coordinate (implies Born-Oppenheimer approximation)

- **potential energy surface (PES)** – Potential energy of an electronic state as a function of all or several nuclear coordinates (implies Born-Oppenheimer approximation)

- **singles** – 1-electron excitations (usually with respect to the base determinant)

- **Slater determinant** – Anti-symmetrized product of all occupied orbitals; $\psi(\{x_j\}) = \hat{A}\big(\prod_i \chi_i(x_j)\big) = \det(\{\chi_i(x_j)\})$ with $\hat{A}$ being the anti-symmetrization operator. (This either implies being a solution of an approximation like Hartree-Fock or Kohn-Sham DFT, or being a basis function for a correlated method, often both.)

- **Slater function/ Slater orbital** – Slater-type basis function (of the form $\exp(-r/r_0)$)

- **state** – Many-body and multi-configurational wave function which usually includes dynamic correlation. Therefore typically comprised of a large number of determinants.

- **static (or strong) correlation** – Interaction between determinants that results in an energy eigenfunction with similar magnitudes for the two (or more) largest coefficients (or largest few coefficients) of its determinants. Usually through an interaction between determinants with unusually close energies. Wave functions *without* static correlation have one main determinant whose coefficient exceeds all other coefficients by a large margin. (See also "correlation".)

- **super-exchange** – A superposition state made from charge transfer states in *both* directions. ... the same spherical harmonics ...

- **triples** – 3-electron excitations (usually with respect to the base determinant)

- **(valence) double zeta** – Basis set with two contractions of Gaussians for covering the (valence) AOs

- **(valence) quadruple zeta** – Basis set with four contractions of Gaussians for covering the (valence) AOs

- **(valence) triple zeta** – Basis set with three contractions of Gaussians for covering the (valence) AOs

- **wave function** – Usually refers to the multi-electron wave function of only the electrons (in Born-Oppenheimer approximation), unless noted otherwise.

C.2 Acronyms

Table C.1: Acronyms

Acronym	Meaning
Qbics	Quantum Biology, Informatics and Chemical Science (program)
	Acronyms containing ...cc... and ...aug...
aug	(prefix for) augmentation (basis functions)/ augmented (basis set)
cc	(prefix for) (Dunning's) correlation consistent (type basis set)
cc-pVDZ	correlation consistent polarization valence double zeta
aug-cc-pVDZ	augmented cc-pVDZ
ccpvtz	abbreviation for "cc-pVTZ"
cc-pVTZ	correlation consistent polarization valence triple zeta
aug-cc-pVTZ	augmented cc-pVTZ
cc-pVQZ	correlation consistent polarization valence quadruple zeta
aug-cc-pVQZ	augmented cc-pVQZ
	Acronyms containing ...CC... and ...EOM...
CC	coupled cluster (method)
CC2	second-order approximate coupled cluster singles and doubles
CC3	third-order approximate coupled cluster singles doubles and triples
EOM	equation-of-motion (formulation for excitations in the coupled cluster method)
EOM-CC	equation-of-motion coupled cluster (method for excited states)

Continued on next page

Table C.1 – Continued from previous page

Acronym	Meaning
CCSD	coupled cluster (method) with single and double excitations
EOM-CCSD	equation-of-motion coupled cluster (method) with single and double excitations
CCSDT	coupled cluster (method) with single, double and triple excitations
EOM-CCSDT	equation-of-motion coupled cluster (method) with single, double and triple excitations
CCSD(T)	coupled cluster (method) with single and double excitations and approximate triples
EOM-CCSD(T)(a)*	equation of motion coupled cluster theory at the singles and doubles level with perturbative triples computed via the (a)* formalism
CCSDT-3	coupled cluster method with singles, doubles and Bartlett et.al.'s 3rd level of approximate triples
EOM-CCSDT-3	equation-of-motion coupled cluster method with singles, doubles and Bartlett et.al.'s 3rd level of approximate triples
	Acronyms containing ...CI...
CI	configuration interaction (method) (with unspecified exitation order)
CDFT-CI	constrained density functional theory - configuration interaction
CIS	configuration interaction (method) with single excitations

Continued on next page

Table C.1 – Continued from previous page

Acronym	Meaning
SOS-CIS(D_0)	scaled opposite spin single excitation configuration interaction with quasidegenerate second order perturbation corrections
FCI	full configuration interaction
MR-CI	multi-reference configuration interaction
MRSDCI	multi-reference configuration interaction with single and double excitations
SAC-CI	symmetry-adapted cluster - configuration interaction (method)
	Acronyms containing ...DFT... and ...KS...
DFT	density functional theory
BLW-DFT	density functional theory with block localized wavefunction
CDFT-CI	constrained density functional theory - configuration interaction
EDFT	ensemble density functional theory
HKS-DFT	Hohenberg-Kohn-Sham density functional theory
KS	Kohn-Sham
BLKS (-DFT)	block localized Kohn-Sham (DFT)
KS-DFT	Kohn-Sham density functional theory
KS-DFT	Kohn-Sham (formulation for the most commonly used method within) density functional theory
MC-DFT	multi-configuration density functional theory
MSDFT	multi-state density functional theory (method)

Continued on next page

Table C.1 – Continued from previous page

Acronym	Meaning
TSO-DFT	target state optimized density functional theory
td-dft/ td-DFT/ TDDFT	time-dependent (formulation for) DFT
	Molecular formulas and acronyms for molecule names
CH_2	methyl (radical)/ carbene
CH_3	methylene (radical)
F_2	fluorine molecule
CF_2	difluorocarbene (radical)
$CH_2 = CH_2$	ethene/ ethylene
$CF_2 = CH_2$	vinylidene fluoride
$CF_2 = CF_2$	tetrafluoroethylene
OF_2	oxygen difluoride
CH_3NO_2	nitromethane
LiH	lithium hydride
NH_3	ammonia
$Me_2C = O$	$(CH_3)_2C = O$, acetone
$MeOCH = CH_2$	methyl vinyl ether/ methoxyethene
MVE	methyl vinyl ether/ methoxyethene
DME	1,2-dimethoxyethene (1,2-dimethoxy ethylene)
c-DME	cis- 1,2-dimethoxyethene (cis- 1,2-dimethoxy ethylene)
t-DME	trans- 1,2-dimethoxyethene (trans- 1,2-dimethoxy ethylene)
Naph	abbreviation for ”naphtalene”

Continued on next page

Table C.1 – Continued from previous page

Acronym	Meaning
PCA	para-chloromethyl anisole
TCNE	tetracyanoethylene
TFE	tetrafluoroethene/ tetrafluoroethylene
	Other acronyms
$\Delta\Delta E_{\text{Res}}$	exciton resonance energy
ΔE_{dist}	geometrical distortion energy
$\Delta E^{\star}_{\text{int}}$	interaction energy in an exiplex
ΔE_{Lint}	called local interaction energy
$\Delta E^{K_X}_{\text{Lpol}}(X^{\star} \cdot Y)$	polarization energy arising from local excitation
$\mathbf{T}_{\text{ms}}$	multi-state (kinetic energy)
n_{Dets}	abbreviation for ”number of determinants”
ν_{ad}	adiabatic excitation energies
ν_{em}	vertical emission energy
v_{ext}	potential from sources ”external” to the arrangement of the electrons (interaction of the electrons with the nuculeus, electrons with electromagnetic fields from outside the molecular system, ...)
ADC(2)	algebraic diagrammatic construction (second order)
Ang	abbreviation for ”angstrom” (a non-standard SI distance unit, 10^{-10} meters)
AO/ AOs	atomic orbital(s)
AS	active space

Continued on next page

Table C.1 – Continued from previous page

Acronym	Meaning
a.u.	arbitrary units
au	atomic unit(s) (a non-SI unit system)
B3LYP	Becke's 3-parameter (hybrid xc) functional based on Lee-Yang-Parr
BCT	backwards charge transfer (state/ process)
BLE	block localized excitation
BLMO/ BLMOs	block localized molecular orbital(s)
BLO/ BLOs	block-localized orbital(s)
BLW	block localized wave function
BLW-ED	block localized wavefunction (based) energy decomposition (analysis)
BNL(γopt)	optimized version of the range-separated Baer-Neuhauser-Livshits functional
BNL	range-separated Baer-Neuhauser-Livshits functional
BSSE	basis set superposition error
CAM-QTP	cambridge quantum theory project (XC functional)
CAS	complete active space
CASPT2	complete active space self consistent field with 2nd order perturbation theory
CASSCF	complete active space self consistent field
CR	charge transfer resonance
CSF/ CSFs	configuration state function(s)

Continued on next page

Table C.1 – Continued from previous page

Acronym	Meaning
CSOV	constrained space orbital variations
CT	charge transfer (state/ process)
D3	Grimme's empirical dispersion correction (up to 3-dipole-interaction order)
DIIS	(iterative matrix diagonalization method via) direct inversion of the iterative subspace
DM	geometry of the monomers in the optimized dimeric excimer
DMRG-CASPT2	density matrix renormalization group - complete active space with second order purturbation theory
DTS	dynamic-then-static (class of method)
EA	electron affinity
EC	exciplex complex
EDA	energy decomposition analysis
EET	excitation energy transfer (state/ process)
ER	exciton-resonance
ET	electron transfer (state/ process)
ETS	extended transition state (method)
ETS-NOCV	extended transition-state method with natural orbitals for chemical valencee
Ex	exciton/ excited
FCT	forward charge transfer (state/ process)
FMO/ FMOs	fragment molecular orbital(s)

Continued on next page

Table C.1 – Continued from previous page

Acronym	Meaning
froz	abbreviation for ”frozen”
GDAC	generalized diabatic at construction (class of methods)
GS	ground state
GSIE	ground-state interaction energy/ local interaction energy in the ground state
GVB	generalized valence bond (method)
HF	Hartree-Fock (method/ Hamilton operator)
HMDF	Hamiltonian matrix density functional
HOMO	highest occupied molecular orbital
HT	hole transfer (state/ process)
Hx	Hartree-exchange
IC-EIG	ionic configuration(s) determined by solving an eigenvalue equation
IC/ ICs	ionic configuration(s)
IC-PT	ionic configuration(s) determined by perturbation theory
int	interaction
IP	ionization potential
IQA	interacting quantum atom (method)
kcal	kilo-calorie(s) (a non-SI energy unit)
Lex	local excitation (state/ process)
LUMO	lowest unoccupied molecular orbital

Continued on next page

Table C.1 – Continued from previous page

Acronym	Meaning
M06-2X	Minnesota 06 (hybrid xc) functional with 2x the Hartree-type exchange
MAS	minimumactive space/ minimal active space
MAS-SE	minimal active space for super-exchange
MCSCF (MC-SCF)	multiconfiguration self-consistent-field
MED	abbreviation for ”medium sized active space”
MOM	maximum overlap method
MO/ MOs	molecular orbital(s)
MOVB	mixed molecular orbital and valence bond
MOW	maximum overlap of wave function
MP2	2nd order Möller-Plesset (perturbation theory method)
MSA	mean-signed-average (deviation)
MS-EDA	multi-state energy decomposition analysis
MSE	mean signed error
MS	multi-state
MS-SCF	multi-state self consistent field (method)
MUE	mean unsigned error
NEDA	natural energy decomposition analysis
nm	nanometer (a SI distance unit, 10^{-9} meters)
NOCI	non-orthogonal configuration interaction
NOCV	natural orbitals for chemical valence (theory)

Continued on next page

Table C.1 – Continued from previous page

Acronym	Meaning
NOSI	non-orthogonal state interaction
occ	abbreviation for ”occupation”
OCD	orbital and configuration-state delocalization
OLED/ OLEDs	organic light-emitting diode(s)
PBE0	parameter free Perdew-Burke-Enzerhof hybrid xc functional
PCET	proton- coupled electron transfer (process)
PEC	potential energy curve
PES	potential energy surface
pol	abbreviation for ”polarization”
post-HF	post hartree-fock (family of methods)
post-SCF	post self-consistent field (family of methods)
QM/MM	(mixed) quantum mechanical and molecular mechanical (method) (a method with different treatment for different atoms)
RMSD	root-mean-square deviation
RVS-SCF	reduced variational space self-consistent-field
SAPT	symmetry-adapted perturbation theory
SCF-CV-DFT	self consistent field constricted variational density functional theory
SCF-MI	self-consistent field for molecular interactions
SCF	self-consistent field
SCS	spin-component-scaled (CC2 and ADC(2) method)

Continued on next page

Table C.1 – Continued from previous page

Acronym	Meaning
SEET	singlet excitation energy transfer
SE	super-exchange
SGM	square gradient minimization
SOS	scaled-opposite-spin (approximation/ method)
SVD	singular value (matrix) decomposition
TADF	thermally activated delayed fluorescence
TDF	transition density functional
TEET	triplet excitation energy transfer
ΔSCF	delta self consistent field (method)
T-SF	state generated from orbitals optimized in the triplet state ($M_S = 1$) followed by an $\alpha \rightarrow \beta$ spin flip
TSO	targeted state optimization (approach)
eV	(a non-SI energy unit)
UV	ultraviolet (light/ electromagnetic radiation)
VB	valence-bond (theory/ method)
WFT	wave function theory (family of methods)
xc	exchange correlation (functional in Kohn-Sham DFT)